UNICAMP

UNIVERSIDADE ESTADUAL DE CAMPINAS
Faculdade de Engenharia Química

ROSILENE ANDREA WELTER

DESENVOLVIMENTO E OTIMIZAÇÃO DA SÍNTESE DE ÉSTER DE ÁCIDO GRAXO POR ROTA ENZIMÁTICA E TiO_2-FOTOCATALISADO

DEVELOPMENT AND OPTIMISATION OF FATTY ACID ESTER SYNTHESIS BY ENZYMATIC AND TIO_2-PHOTOCATALYSIS

Campinas
2022

ROSILENE ANDREA WELTER

DEVELOPMENT AND OPTIMISATION OF FATTY ACID ESTER SYNTHESIS BY ENZYMATIC AND TIO_2-PHOTOCATALYSIS

DESENVOLVIMENTO E OTIMIZAÇÃO DA SÍNTESE DE ÉSTER DE ÁCIDO GRAXO POR ROTA ENZIMÁTICA E TiO_2-FOTOCATALISADO

Thesis presented to the Faculty of Chemical Engineering of the University of Campinas in partial fulfilment of the requirements for the degree of Doctor, in Chemical Engineering in the area of Chemical engineering within the scope of the Cotutela Agreement signed between Unicamp and James Cook University.

Unicamp:
Supervisor/Orientador: Osvaldir Pereira Taranto
Co-supervisor/Coorientador: Lucimara Gaziola de la Torre

James Cook University:
Supervisor/Orientador: Michael Oelgemöller
Co-supervisor/Coorientador: Mark Robertson
Co-supervisor/Coorientador: Mark C. Barnes

ESTE TRABALHO CORRESPONDE À VERSAO FINAL DA TESE DEFENDIDA PELA ALUNA ROSILENE ANDREA WELTER GABAS E ORIENTADA PELO PROF. DR. OSVALDIR PEREIRA TARANTO

Campinas
2022

Ficha catalográfica
Universidade Estadual de Campinas
Biblioteca da Área de Engenharia e Arquitetura
Rose Meire da Silva - CRB 8/5974

W467d
Welter, Rosilene Andrea, 1983-
Development and optimisation of fatty acid ester synthesis by enzymatic and TiO2-photocatalysis / Rosilene Andrea Welter Gabas. – Campinas, SP : [s.n.], 2022.

Orientadores: Osvaldir Pereira Taranto e Michael Oelgemöller.
Coorientador: Lucimara Gaziola de la Torre.
Tese (doutorado) – Universidade Estadual de Campinas, Faculdade de Engenharia Química.
Em cotutela com: James Cook University.

1. Biodiesel. 2. Fotocatálise. 3. Catálise enzimática. 4. Óleos e gorduras - Reúso. I. Taranto, Osvaldir Pereira, 1963-. II. Oelgemöller, Michael. III. Torre, Lucimara Gaziola de La, 1971-. IV. Universidade Estadual de Campinas. Faculdade de Engenharia Química. VI. Título.

Informações Complementares

Título em outro idioma: Desenvolvimento e otimização da síntese de éster de ácido graxo por rota enzimática e TiO2-fotocatalisado
Palavras-chave em inglês:
Biodiesel
Photocatalysis
Enzymatic catalysis
Oils and greases - reuse
Área de concentração: Engenharia Química
Titulação: Doutora em Engenharia Química
Banca examinadora:
Osvaldir Pereira Taranto [Orientador]
Raphael Soeiro Suppino
Elias Basile Tambourgi
João Lameu da Silva Junior
Juliana Martins Teixeira de Abreu Pietrobelli
Data de defesa: 08-11-2022
Programa de Pós-Graduação: Engenharia Química

Identificação e informações acadêmicas do(a) aluno(a)
- ORCID do autor: https://orcid.org/0000-0002-8901-3814
- Currículo Lattes do autor: http://lattes.cnpq.br/1572367807587848

Folha de aprovação da defesa de tese de doutorado defendida por ***ROSILENE ANDRÉA WELTER GABAS*** aprovada em 08 de novembro de 2022 pela banca examinadora constituída pelos professores doutores:

Prof. Dr. Osvaldir Pereira Taranto - Presidente e Orientador
FEQ / UNICAMP
Videoconferência

Prof. Dr. Elias Basile Tambourgi
FEQ / UNICAMP
Videoconferência

Prof. Dr. Raphael Soeiro Suppino
FEQ/ UNICAMP
Videoconferência

Prof. Dr. João Lameu da Silva Júnior
Universidade Federal do ABC
Videoconferência

Profa. Dra. Juliana Martins Teixeira de Abreu Pietrobelli
Universidade Tecnológica Federal do Paraná - Campus de Ponta Grossa
Videoconferência

A ATA da defesa com as respectivas assinaturas dos membros encontra-se no SIGA/Sistema de Fluxo de Dissertação/Tese e na Secretaria do Programa da Unidade.

I dedicate this work to my sons: Henry and Thomas.

ACKNOWLEDGEMENTS

Firstly, I wish to thank my supervisors Professor Dr. Osvaldir Pereira Taranto, Professor Dr. Michael Oelgemöller, Professor Dra. Lucimara Gaziola de la Torre, Professor Dr. Mark Robertson, and Professor Dr. Mark Barnes for supporting my research during this period. Secondly, I would like to thank Dr. Harrison Santana for his help, support and encouragement during all the moments.

Moreover, I would like to thank my research groups in Brazil: Laboratory of thermofluidic dynamic process (LPTF), Nano&Bio Technology Laboratory for advanced development (Landba), and in Australia: Oelgemöller Group.

I would like to express sincere gratitude to Francisco Gabas and our sons: Henry and Thomas, for accompanying me on this journey, my family in Brazil, and especially my mother, who always believed in me and my dreams. Moreover, I would like to thank my friends in Brazil, who supported me emotionally and whom I miss so much; and our Brazilian friends in Australia, who welcomed us and supported us as our new family.

Finally, I would like to thank Unicamp (Brazil) and JCU (Australia) for allowing me and providing the necessary support for my research development. This work was developed with financial support in part by the Coordenação de Aperfeiçoamento de Pessoal de Nível Superior - Brasil (CAPES) Finance Code 001 and by the Competitive Research Training Grant (2021 and 2022) from the College of Science and Engineering at James Cook University.

RESUMO

O biodiesel tem ganhado cada vez mais importância em substituiçao ao combustíveis fósseis. O uso de óleo de cozinha residual (WCO) e de outras matérias-primas com alto teor de ácidos graxos livres para producao de biodiesel vêm aumentando devido à necessidade de materia prima alternativa aos oleos utilizados no setor alimentício, e também por se tratar de um problema ambiental. Entretanto, novas tecnologias são necessárias para contornar algumas lacunas no processo tradicional usando ácido ou base forte como catalisador e atender a demanda do uso de WCO como materia prima. Assim, este trabalho busca analisar catalisadores sólidos ecologicamente corretos (Lipase duplamente imobilizada e óxido metálico fotoativado) através de condições operacionais amenas, menor volume de reagentes e resíduos, menor custo e facilidade de manuseio, recuperação do catalisador e purificação do produto. Primeiramente, o uso da lipase foi estudado avaliando sua atividade enzimática após uma dupla imobilização. *C. antarctica lipase* B (CALB) foi inicialmente imobilizada na superfície de nanopartículas de TiO_2 e depois aprisionada em microesferas de alginato de cálcio pela técnica de microfluídica de gota. O microbiocatalisador obtido, $(CALB_{TiO_2})_{EDTA\text{-}Ca}$, manteve alta atividade enzimática ($REA_{t=0}$=232%) e estabilidade ($REA_{t=30\ dias}$=263%) em um tamanho (diâmetro, Ø=8,9·104 nm) que permitiu recuperação do que $CALB_{TiO_2}$ (Ø=2,3·102 nm) ou $CALB_{Free}$ (Ø=5,0 nm), e mostrou uma porosidade favorável para difusão sem liberar $CALB_{TiO_2}$. Um segundo processo foi avaliado utilizando TiO_2 fotocatalisado para esterificação e transesterificação. As seguintes etapas foram desenvolvidas para obter um processo otimizado: pré-tratamento do catalisador, recuperação, reutilização e caracterização físico-química, otimização do processo por planejamento experimental rotacional composto central (CCR) avaliando a razão molar dos reagentes (1:3 a 1:55) e fração de catalisador (1-30% p/p), avaliação da temperatura (25-65°C), irradiação de luz (UVA, luz solar), matéria-prima (esterificação de ácido oleico, transesterificação de óleo de canola e esterificação/transesterificação simultânea de WCO), caracterização físico-química do produto (Biodiesel), análise dos parâmetros por metodologia quadrática de superfície de resposta (RSM), uso de diferentes álcoois (metanol, etanol e n-propanol), determinação das curvas cinéticas para diferentes temperaturas, desenvolvimento de modelos matemáticos para determinar os parâmetros cinéticos (Sistema homogêneo: 1. Primeira ordem para reaçao direta/primeira ordem inversa; 2. Primeira ordem para reaçao direte/segunda ordem para inversa; 3. Segunda ordem para reaçao direta/segundo ordem para inversa; 4. Primeira ordem para reaçao direta/terceira ordem para inversa; 5. Segunda ordem para reaçao direta/quarta ordem para inversa; Sistema heterogéneo: 6. Langmuir-Hinshelwood), e determinação dos parâmetros termodinâmicos. Como resultado, o éster metílico de ácido graxo (FAME) foi

obtido pela conversão de 98% (±0,8) de ácido oleico, 73% (±1,41) de óleo de canola e 82% (±1,24) de WCO (65°C, 20% TiO_2 (w/w), irradiação de luz UVA). A reutilização do catalisador foi analisada após cinco ciclos de recuperação e reutilização. A conversão foi de 71% para ácido oleico, 36% para óleo de canola e 59% para WCO. A caracterização do catalisador indica que o material orgânico foi retido nos poros do catalisador. O processo de recuperação foi eficiente e removeu cerca de 90% da matéria orgânica; porém, tende a aumentar a cada ciclo. Esse incremento resultou em um catalisador com menor área superficial, agregação de partículas, menor acesso aos sítios ativos e impedimento do acesso à luz. Consequentemente, aumentando o bandgap. Todos esses aspectos reduziram a eficiência do catalisador. A caracterização do FAME indica que o processo resulta em um produto altamente puro. Assim, desenvolver um processo eco-friendly através de um catalisador heterogêneo que opere em condições operacionais amenas é uma opção promissora para complementar ou substituir os métodos tradicionais por ácidos fortes ou álcalis como catalisadores.

ABSTRACT

Biodiesel has gained increased importance as a substitute for fossil fuels. The use of waste cooking oil (WCO) and other feedstock with high free fatty acid contents is increasing. New technologies are required to supply this demand and circumvent some gaps in the traditional process, using strong acids or bases as catalysts. Thus, this work tries to analyse solid eco-friendly catalysts (Lipase double immobilised and photoactivated metal oxide) by mild operational conditions, small volumes of reagents and waste, lower cost and easy handle, catalyst recovery and product purification. First, lipase was studied by evaluating its enzymatic activity after a double immobilisation. *C. antarctica lipase B* (CALB) was first immobilised onto the TiO_2 nanoparticle surface and entrapped into calcium alginate microbeads using a microfluidic droplet technique. The microbiocatalyst obtained, $(CALB_{TiO2})_{EDTA\text{-}Ca}$, retained high enzymatic activity ($REA_{t=0}$=232%) and stability ($REA_{t=30days}$=263%) at a size (diameter, Ø=$8.9\cdot10^4$ nm) that enabled easier recovery than $CALB_{TiO2}$ (Ø=$2.3\cdot10^2$ nm) or $CALB_{Free}$ (Ø=5.0 nm), and showed a favourable porosity for diffusion without releasing $CALB_{TiO2}$. A second process was evaluated by photocatalised TiO_2 for esterification and transesterification. The following steps were developed to obtain an optimised process: catalyst pretreatment, recovery, reuse, and physicochemical characterisation, process optimisation by central composite rotational (CCR) experimental design evaluating reactants molar ratio (1:3 to 1:55) and catalyst content (1–30% w/wt), evaluation of temperature (25–65°C), light irradiation (UVA, sunlight), feedstock (esterification of oleic acid, transesterification of canola oil and simultaneous esterification/transesterification of WCO), physicochemical characterisation of the product (Biodiesel), analysis of the parameters by response surface quadratic methodology (RSM), use of different alcohols (methanol, ethanol, and n-propanol), determination of the kinetic curves for different temperatures, development of mathematical models to determine the kinetic parameters (Homogeneous system: 1. First order forward/first order backward; 2. First order forward/second order backward; 3. Second order forward/second order backward; 4. First order forward/third order backward; 5. Second order forward/fourth order backward; Heterogeneous system: 6. Langmuir-Hinshelwood), and determination of the thermodynamic parameters. As a result, fatty acid methyl ester (FAME) was obtained by the conversion of 98% (±0.8) oleic acid, 73% (±1.41) canola oil, and 82% (±1.24) WCO (65°C, 20% TiO_2 (w/w), UVA light irradiation). The catalyst reusability was analysed after five cycles of recovery and reuse. The conversion was 71% for oleic acid, 36% for canola oil, and 59% for WCO. Catalyst characterisation revealed organic material retained in the catalyst pores. The recovery process was efficient and removed about 90% of the organic material; however, it tends to increase in each cycle. This increment resulted in a catalyst with a lower surface area, particle

aggregation, less access to the active sites, and prevention of light access. Consequently, the bandgap was increased. These aspects reduced the catalyst efficiency. FAME characterisation indicated that the process resulted in a highly pure product. Thus, an eco-friend process using a heterogeneous catalyst that operates under mild operational conditions is a promising option to complement or substitute for traditional methods that use strong acid or alkali catalysts.

PUBLICATIONS

- Patent (2019): Process to obtaining microbiocatalysts with metallic nanoparticles, and their use. Process n. BR 10 2019 027652 5.
- Congress (2020): C. *antarctica* enzyme catalytic capacity increases due to immobilization in nanometallic matrix. 1st Digital Congress on Nanobiotechnology and Bioengineering (I CDNB). 01 – 04 June, 2020. Embrapa (Brazil).
- Grant presentation (2021): Esterification of fatty acid by photocalytic route. James Cook University.
- Chapter book (2021): Welter, R., Silva Jr., J., de Souza, M., Lopes, M., Taranto, O., & Santana, H. (2022). Chapter II - *Are Microreactors the Future of Biodiesel Synthesis?* (1st ed., Vol. 1). Book: The future of biodiesel, Novapublishers, ISSN: 979-8-88697-166-8.
- Conference (2022): Photocatalytic biodiesel production from feedstocks with high fatty acid content. Journées Annuelles SP2P'2022. 7 – 8 Junte, 2022, Paris, France.
- **Thesis - Chapter II:** In preparation (2022): Welter, R. A., Santana, H. S., de la Torre, L., Barnes, M. C., Taranto, O. P., & Oelgemöller, M. (2022). Biodiesel production focusing on heterogenous catalysts and eco-friendly routes. *ChemBio Eng Rev.*
- **Thesis - Chapter III:** Journal article (2022): Welter, R. A., Santana, H. S., Carvalho, B. G., Melani, N., Oelgemöller, M., de la Torre, L. G., & Taranto, O. P. (2022). Droplet microfluidics for double lipase immobilisation using TiO_2 and alginate microbeads. *Journal of Industrial and Engineering Chemistry*, *110*, 576–586. https://doi.org/10.1016/j.jiec.2022.03.028.
- **Thesis - Chapter IV:** Journal article (2022): Welter, R. A., Santana, H. S., de la Torre, L. G., Robertson, M., Taranto, O. P., & Oelgemöller, M. (2022). Methyl oleate synthesis by TiO_2 photocatalytic esterification of oleic acid: optimisation by response surface quadratic methodology, reaction kinetics and thermodynamics. *ChemPhotoChem*, *6*(7), e202200007. https://doi.org/10.1002/cptc.202200007.
- **Thesis - Chapter V:** Submited (2022): Welter, R. A., Santana, H. S., de la Torre, L., Barnes, M. C., Taranto, O. P., & Oelgemöller, M. (2022). Biodiesel production from canola oil photocatalysed by TiO_2. *Fuel Journal.* Available at SSRN: https://dx.doi.org/10.2139/ssrn.4201382.
- **Thesis - Chapter VI:** In preparation (2022): Welter, R. A., Santana, H. S., de la Torre, L., Barnes, M. C., Taranto, O. P., & Oelgemöller, M. (2022). TiO_2 photocatalysed for biodiesel production from the simultaneous esterification and transesterification of waste cooking oil. *Journal of Environmental Chemical Engineering.*

TABLE OF CONTENTS

LIST OF TABLES

Chapter II

Chapter III

Chapter IV

Chapter V

Chapter VI

APPENDIX B – SI of Chapter III

APPENDIX C – SI of Chapter IV

APPENDIX D – SI of Chapter V

APPENDIX E – SI of Chapter VI

LIST OF FIGURES

Chapter II

Chapter III

Chapter IV

Chapter V

Chapter VI

APPENDIX A – SI of Chapter II

APPENDIX B – SI of Chapter III

APPENDIX C – SI of Chapter IV

APPENDIX D – SI of Chapter V

APPEDNIX E – SI of Chapter VI

Chapter I

Introduction

Biodiesel is currently the most promising renewable fuel to replace diesel (Borugadda & Goud, 2012; Ong et al., 2021), and new technologies have been evaluated to improve the efficiency and quality of the process and product. As a result, global biodiesel production since 2005 has increased more than sevenfold (Ogunkunle & Ahmed, 2019). In 2018, biodiesel production equalled 29% of petroleum-derived diesel production (IEA, 2020). In 2019, 41 billion litres were produced (IEA, 2020). The US, Brazil, and Europe are the biggest biodiesel market. In 2016, this market moved USD 34.1 billion and was projected to reach USD 41.2 billion in 2021 (Biodiesel Market, 2017). Although the biofuel market has been increasing, it has some issues, mainly with feedstock, industrial processes, and biofuel prices. Currently, biofuel feedstock originates from edible oil (D. Singh, Sharma, Soni, Sharma, & Kumari, 2019), which has been competing with the food sector and represents almost 8% of grain consumption. Although grain production has been increasing, the increment has mostly been to the feed and food sector. Two raw materials have been frequently considered: non-edible oils and reused oils. The use of non-edible oils indirectly competes with edible oils, considering both require land for planting. The use of reused oils, such as WCO, appears to be the best option that would also help solve an environmental issue. WCO reduces the feedstock price, resulting in biodiesel with a more competitive price. Considering that biodiesel costs 40% more than petrodiesel (Y. Zhang, Dubé, McLean, & Kates, 2003), and the biodiesel process is 1.5 to 3 times more expensive (Mardhiah, Ong, Masjuki, Lim, & Lee, 2017a), an efficient process with low-cost feedstock is an important gap to overcome.

Biodiesel is a mixture of long-chain fatty acid alkyl esters (FAAE) produced mainly by esterification, transesterification, or both. Transesterification, the most common reaction, occurs between triglycerides (TGL) and alcohol in the presence of a catalyst, such as strong acid or alkali, producing FAAE and glycerol. However, these conventional homogeneous catalysts demand extensive separation and reaction product purification processes that generate large amounts of waste (G. Berrebi, P. Dufresne, & Y. Jacquier, 1993). These issues may be resolved by solid eco-friendly catalysts, such as metal oxides, enzymes, zeolites, alumina, and waste material (Alsharifi, Znad, Hena, & Ang, 2017; Arzamendi et al., 2007; Calero et al., 2014; Corro, Pal, & Tellez, 2013; Wan Omar & Saidina Amin, 2011; Rosilene Andrea Welter, Santana, Carvalho, Melani, Oelgemöller, de la Torre, et al., 2022). Heterogeneous catalysts are easily separated and regenerated, safer, and less corrosive (Chouhan & Sarma, 2011; De & Boxi, 2020; Granados et al., 2007; Ma & Hanna, 1999).

The use of enzymes, frequently lipases, is an alternative to traditional processes. However, the free enzyme tends to lose the catalytic capacity easily; it is less stable and harder to recover. The use of immobilised lipases helps overcome these issues. On the other hand, the development of an efficient immobilisation method represents a fundamental challenge for the adaptation of lipase catalysis in chemical processes. Recently, double immobilisation techniques, e.g., adsorption followed by entrapment, have been studied to overcome these deficiencies. Following this approach, CALB was immobilised onto lignin nanospheres and confined into calcium alginate hydrogel beads. The enzymatic activity remained at 70% compared to the free CALB (Sipponen et al., 2018). Silva et al. (2011) obtained a high thermal and chemical stability for lipase from *Burkholderia cepacia* double immobilised by SiO_2/Chitosan. Porcine pancreatic lipase was double immobilised on TiO_2/Chitosan and resulted in an REA of 84% with high thermal and chemical stability (Deveci, Doğaç, Teke, & Mercimek, 2015).

The use of double immobilisation involving magnetic nanoparticles has been explored for easy recovery (Netto, Toma, & Andrade, 2013; Xie & Zang, 2018). However, these nanoparticles form aggregates due to magnetic dipole–dipole attractions (Baharfar & Mohajer, 2016). The application of a second polymer support may improve the chemical stability and hence decrease aggregation. CALB maintained an enzymatic activity of 94% when immobilised onto cellulose acetate coated Fe_2O_3 nanoparticles (N. Singh, Raj Kumar, & Sachan, 2013), and 95% when immobilised onto Fe_3O_4/chitosan (Hosseini et al., 2019), respectively. Other examples include *Candida rugose* lipase fixed on Fe_3O_4/silica (Xie & Zang, 2018), Fe_3O_4/poly(styrene-methacrylic acid) microspheres (Xie & Wang, 2014), Fe_3O_4/graphene (Xie & Ma, 2009), or hydroxyapatite-encapsulated γ-Fe_2O_3 (Xie & Zang, 2017), respectively. The simultaneous entrapment of different lipases has also been studied. *Pseudomonas cepacia* lipase and *Candida antarctica* lipase were immobilised together in Fe_3O_4/hydrophobic sol-gel materials derived from $CH_3Si(OCH_3)_3$ (MTMOS), achieving REA values of 330% and 210%, respectively (Reetz, Zonta, Vijayakrishnan, & Schimossek, 1998). These studies indicate that double immobilisation processes result in sufficiently small microbeads to increase the surface area and hence access to the catalyst, while at the same time being large enough to allow their recovery and handling.

The use of photocatalised oxide metals is a second alternative to the traditional process. Photocatalysis has been studied extensively for organic product degradation (Carp, Huisman, & Reller, 2004; Rajeshwar et al., 2008) [e.g. dyes, pesticides, and pharmaceuticals (Kanakaraju, Glass, & Oelgemöller, 2014; Konstantinou & Albanis, 2003; Rajeshwar et al., 2008)], but not for organic synthesis (N. Hoffmann, 2015). However, it has recently been evaluated as an alternative for biodiesel synthesis by esterification and transesterification. For example, oleic acid and methanol esterification was achieved using a TiO_2 catalyst and light irradiation, resulting in 98% conversion (R. A. Welter, Santana, Torre, Robertson, Taranto, et al., 2022). TiO_2 nanotubes as the catalyst and sunlight irradiation for WCO transesterification gave 91% conversion (Khaligh et al., 2021). TiO_2/g-C_3N_4 under sunlight irradiation resulted in 89.5% conversion for TGL from WCO (M. Khan et al., 2021). The advantage of photoreactions is their development under mild temperatures (up to the alcohol boiling point) and pH, resulting in a high-purity product that can be recovered easily with easy catalyst reuse.

Thus, based on this context, this thesis contributes to the development of technologies that can improve and facilitate biodiesel production, as described below in the main and specific objectives.

1.1 Main objective

The main objective of this study is the development of eco-friendly methods to produce biodiesel by optimising two different catalysts: enzymes and photocatalised oxides (Detailed scheme in APPENDIX A).

1.2 Specific objectives

- Development of an optimised catalyst using double immobilised lipase.
- Development of an optimised catalyst using photocatalised oxide.
- Evaluate the esterification and transesterification process and determine the best operational conditions.
- Determine the kinetic parameters by mathematical modelling.
- Determine the thermodynamic parameters.

1.3 Thesis organisation

This thesis reports alternative and eco-friendly catalysis applied to biodiesel production by esterification and transesterification. After this introductory chapter, a literature survey is shown in Chapter II. The literature survey reviews the different technologies to produce biodiesel and introduces relevant data to show the importance of this research. Chapter III shows the development of a new microbiocatalyst consisting of a double-immobilised lipase. The *Candida antarctica* lipase B was immobilised on TiO_2 nanoparticles and then into calcium alginate microbeads. The final microbiocatalyst resulted in high enzymatic activity, no leaching and stability, indicating that it could be a good alternative to producing biodiesel by the enzymatic route.

The following chapters are on the use of photocatalysis to produce biodiesel. Chapter IV establishes the operational conditions and the kinetic and thermodynamic parameters for biodiesel produced by oleic acid and methanol esterification using photoirradiated TiO_2 as the catalyst. The experimental tests included the analysis of the catalyst pretreatment, its recovery, and reuse. In addition to its physicochemical characterisation, optimisation of the experimental conditions for the esterification reaction was developed using a response surface quadratic methodology obtained by central composite rotational design (RSM-CCRD). The kinetic data were used to determine the kinetic parameters by mathematical modelling using Matlab®, and the thermodynamic parameters were established.

Chapter V examines the use of canola oil to produce biodiesel. The transesterification of canola oil and alcohol (methanol or ethanol) using photoirradiated TiO_2 was evaluated at different temperatures. The experimental data, kinetic mathematical modelling and thermodynamic parameters indicated that a temperature increment is relevant to increasing the system energy and allowing better mass transfer. Moreover, the irradiation using UVA light and sunlight and the reuse of the catalyst were evaluated. The final product was characterised and compared with biodiesel obtained by transesterification catalysed using acid or alkali. The biodiesel obtained using photocatalysed TiO_2 had high purity. However, canola oil transesterification resulted in lower conversion than oleic acid esterification.

Chapter VI reports the simultaneous esterification and transesterification of waste cooking oil (WCO) and alcohol using photocatalysed TiO_2. The WCO was chosen because it is currently considered an environmental issue to be solved; it is a cheaper feedstock, and contrary to edible oil, WCO does not compete with the food and agricultural markets. The highest free fatty acid content indicated that esterification occurred more easily than transesterification, even though both occurred. Similar to the previous chapter, the experimental kinetic data at different temperatures were obtained, the kinetic parameters were obtained by mathematical modelling, and afterward, the thermodynamic properties were determined. Chapter VII summarises the conclusions of this thesis with suggestions for future studies.

Chapter II

Literature review

Submission (12/2022): Rosilene Andrea Welter[1,2], Harrson Silva Santana[2], Lucimara Gaziola de la Torre[2], Mark C. Barnes[1], Osvaldir Pereira Taranto[2], Michael Oelgemöller[1,3]. Biodiesel production focusing on heterogenous catalysts and eco-friendly routes, *ChemBioEng Rev*.

Filiation: (1) College of Science and Engineering, James Cook University, Postcode Qld 4811, Townsville, Queensland, Australia. (2) School of Chemical Engineering, University of Campinas, Postcode 13083-852, Campinas, SP, Brazil. (3) Faculty of Chemistry and Biology, Hochschule Fresenius gGmbH-University of Applied Sciences, Limburger Straße 2, Postcode D-65510, Idstein, Germany.

Highlights

- Current and future biodiesel markets are discussed.
- Advantages and disadvantages of heterogeneous vs. homogenous catalysis are compared.
- Microscale processes are analysed.
- Challenges and obstacles of each technology are debate.

Abstract

Biodiesel is produced on large scales as an eco-friendly substitute and additive to fossil fuels. Catalytic homogeneous processes using strong acids and alkalis and natural oils have been realised in industry. However, these traditional routes have several disadvantages such as the generation of large volumes of waste, high water and reagent needs, use of hazardous reagents, high operation costs, and utilisation of valuable feedstocks and catalysts, respectively. Different solutions have been subsequently investigated such as cheap alternative feedstocks, co-solvents and catalysts, sustainable operational conditions, advanced reactor designs and scales, and advantageous pre- and post-reaction treatments. This review explores and analyses the main aspects of biodiesel technologies and opportunities. It also describes some advanced improvement strategies.

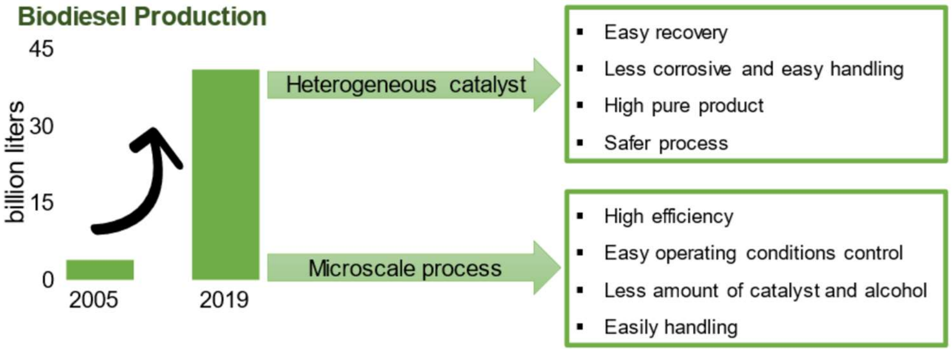

Figure 2. 1. Graphical abstract: Biodiesel production focusing on heterogenous catalysts and eco-friendly routes.

Keywords:

Biodiesel, heterogeneous catalyst, microfluidic, sustainable technology, waste cooking oil.

2.1 Introduction

Biodiesel is currently the most promising renewable fuel for the replacement of diesel (Borugadda & Goud, 2012; Ong et al., 2021). New technologies have constantly evolved to further improve the efficiency and quality of production processes and products. Although the biofuel market has been steadily increasing, it has experienced some major challenges with feedstock, industrial operation processes, and biofuel prices. Current biofuel feedstocks comprise largely of edible vegetable oils from the food sector. Alternative, non-competing feedstocks for the production of biodiesel have thus been proposed, in particular non-edible and recovered (waste) oils.

Biodiesel is a mixture of long-chain fatty acid alkyl esters (FAAE) produced mainly by esterification, transesterification or both processes simultaneously. The most common reaction, transesterification, occurs between triglycerides (TGL) and alcohols in the presence of a catalyst such as strong acid or alkali, producing FAAE and glycerol. Manufacturing processes are frequently developed using batch or continuous large-scale reactors and homogeneous catalysts, but these methods demand extensive separation and reaction product purification processes that generate large amounts of waste (G. Berrebi et al., 1993). Likewise, they require many unit operations and specialised equipment suitable for operations under corrosive and hazardous conditions. Some of these disadvantageous process parameters may be overcome by solid eco-friendly catalysts or continuous-flow operation.

Different solid eco-friendly catalysts such as metal oxides, enzymes, zeolites, alumina, and modified waste materials have been studied (Alsharifi et al., 2017; Arzamendi et al., 2007; Calero et al., 2014; Corro et al., 2013; Wan Omar & Saidina Amin, 2011; Rosilene Andrea

Welter, Santana, Carvalho, Melani, Oelgemöller, de la Torre, et al., 2022). Heterogeneous catalysts are easily removed and regenerated, safer to use, and commonly less corrosive (Chouhan & Sarma, 2011; De & Boxi, 2020; Granados et al., 2007; Ma & Hanna, 1999). The use of bifunctional catalysts for simultaneous esterification and transesterification represents a promising approach as it enables mild operational conditions, lower equipment and operation costs. For example, sulfonated metals such as $Al(HSO_4)_3$ enabled esterification and transesterification of feedstocks with high FFA and water contents (e.g. WCO) without saponification, but with easy catalyst recovery and reuse (Ramachandran, Sivakumar, Suganya, & Renganathan, 2011). However, heterogeneous catalysts may leach and deactivate easily (Santacesaria, Vicente, di Serio, & Tesser, 2012; Thanh, Okitsu, Boi, & Maeda, 2012; van Gerpen, 2005). A different approach employs heterogeneous photocatalysis, which has been effectively applied to esterification processes (Corro, Tellez, Bañuelos, & Mendoza, 2012; Manique, Silva, Alves, & Bergmann, 2016; Suthar & Verma, 2018; Rosilene A. Welter, Santana, Torre, Robertson, Taranto, & Oelgemöller, 2022). The advantages of photocatalytic materials are their generally low costs, high stability, easy handling, post-reaction recovery, and reusability (Alsharifi et al., 2017; Brito, 2008; Xie & Ma, 2009). Photocatalysis also does not involve saponification or catalyst leaching. Catalyst-free processes represent another eco-friendly option. For example, supercritical conditions can be applied for esterification and transesterification, but necessitate extreme operational conditions and equipment. As the water content can furthermore interfere with the esterification process, favouring hydrolysis, a feedstock of high purity is desired.

The implementation of microscale plants is an alternative to traditional batch operations. Microplants naturally require smaller amounts of catalyst, enable shorter residence times, and provide higher heat and mass transfer, easier management, maintenance, and operational control (Bannatham et al., 2021). Scale-up is typically achieved by serial or parallel operation of microdevices (Roberge, Ducry, Bieler, Cretton, & Zimmermann, 2005; Terry, Jerman, & Angell, 1979; R. Welter, Silva Jr., de Souza, Lopes, Taranto, & Santana, 2022). The inner structures of these devices promote turbulent mixing that increasing mass transfer and hence reduce residence times, the amount of alcohol and catalyst. Although microscale processes commonly employ homogeneous catalysts to avoid clogging, heterogeneous operations have been developed. For example, heterogeneous conditions were compared for a semi-industrial pilot microreactor and a conventional batch reactor. The microscale process required a residence time of 15 minutes against 50 minutes for the traditional system (Mohadesi, Aghel, Maleki, & Ansari, 2019).

Other important operation parameters include catalyst immobilization and reuse, process efficiency and product quality. This review intends to analyse some of the most important aspects of biodiesel production, comparing and discussing conventional and recent technologies.

2.2 Current status and challenges

2.2.1 The biodiesel market

Since 2005, global biodiesel production has increased by more than 7 times (Ogunkunle & Ahmed, 2019). In 2018, biodiesel production equalled 29% of the petroleum-derived diesel production (IEA, 2020). Similarly, 41 billion litres were produced (IEA, 2020) in 2019, with the US, Brazil and Europe as the biggest biodiesel markets (Figure 2. 2). In 2016, its market value reached USD 34.1 billion, and was projected to grow to USD 41.2 billion in 2021 (Biodiesel Market, 2017). While biodiesel production saw a decline of approximately 10% in 2020 due to the Covid-19 pandemic, it is expected to reach 46 billion litres between 2023 and 2025 (IEA, 2020). Prices for biofuels and their feedstocks have developed similarly over the last decade, but have overall seen a sharp decline with a further decline expected for biodiesel (‘Biofuels’, 2019).

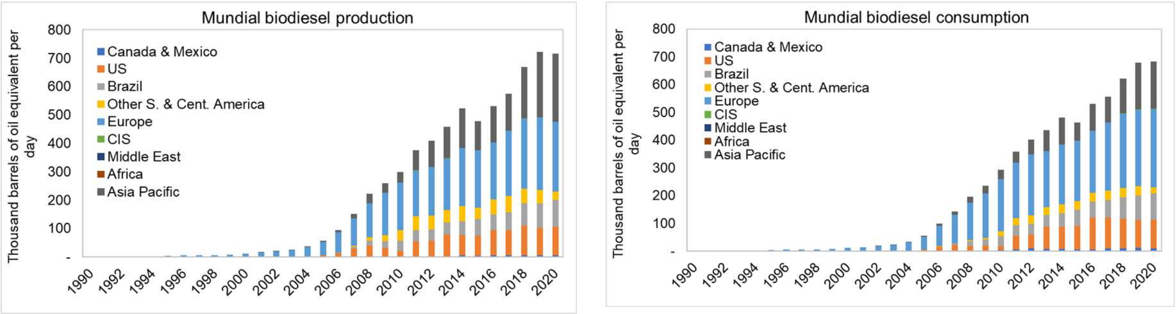

Figure 2. 2. Mundial biodiesel production and consumption between 1990 and 2020. (a) Biodiesel production, and (b) biodiesel consumption (Reprinted with permission from “Statistical Review of World Energy 2021” - Statistical Review of World Energy 2021, 2021).

Currently, biofuel feedstocks derive mainly from edible oils with almost 8% of total grain consumption (D. Singh et al., 2019), and has thus been competing with the food sector. While grain production has seen a steady increase in the last decade, this was mainly driven by feed and food sectors (Figure 2. 3). Since biodiesel costs about 40% more than petrodiesel (Y. Zhang et al., 2003), and since the biodiesel process is between 1.5 and 3 times more expensive (Mardhiah, Ong, Masjuki, Lim, & Lee, 2017), low-cost feedstocks for its production are highly desirable. Two raw materials are frequently proposed as alternative, cheap, non-competing feedstocks for biodiesel production: non-edible oils and waste oils. While the use of non-edible oils still competes indirectly with edible oils due to the need for its planting, hence also contributing to deforestation, the utilization of used and recovered waste oils represents a more sustainable option. Waste cooking oil (WCO), for example, represents a significant environmental burden that demands urgent solutions. In addition, the implementation of WCO as feedstocks will produce biodiesel at a more competitive price.

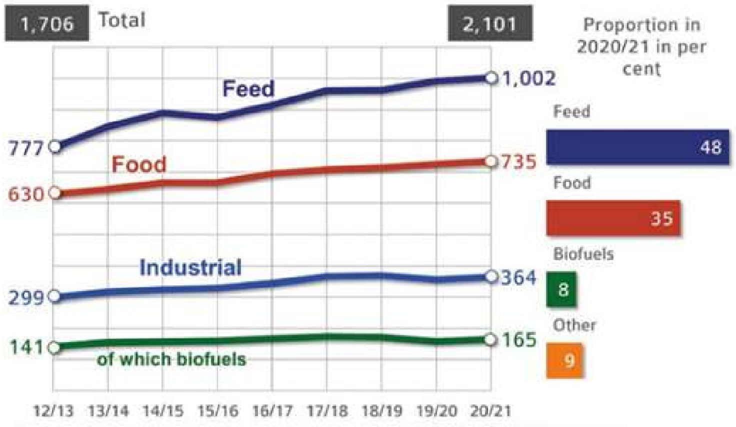

Figure 2. 3. Global grain consumption, 2020 and 2021 estimated in million tonnes. Grains considered barley, maize, millet, oat, rye, and wheat. Industrial production of starch, beer, alcohol and bioethanol. Other industrial uses, seed and losses (Reprinted with permission from (UFOP, 2020), Copyright: © AMI 2021 | Source: IGC).

The growing importance of biodiesel has naturally led to significant research and technology development efforts over the last years (Figure 2. 4). As part of this, the interest in the utilization of WCOs and alternative feedstocks with high content of FFA has increased, while the use of edible oils such as soybean has decreased. Moreover, new technologies exploiting raw materials with high FFA content, which cannot be converted using conventional alkaline conditions, have been successfully developed.

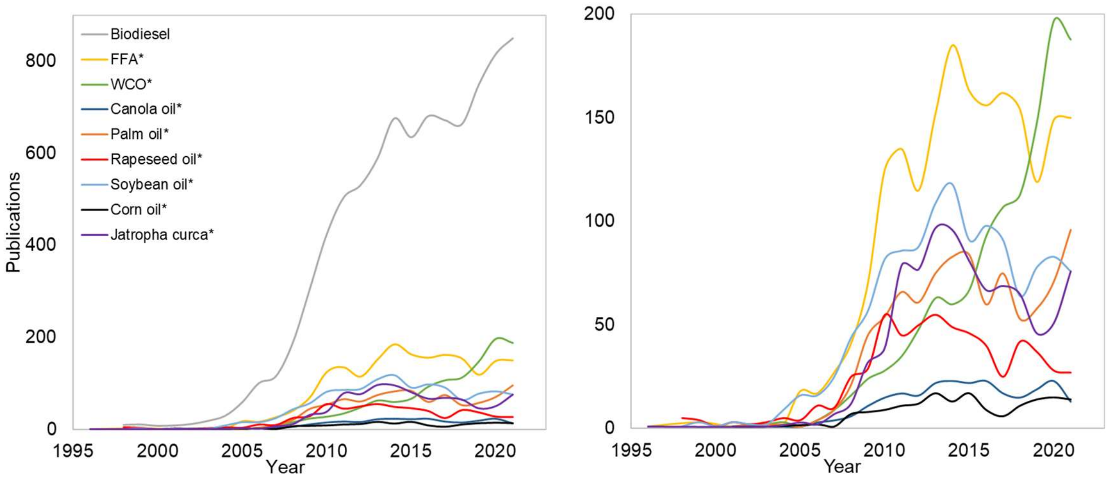

Figure 2. 4. Scientific publications based on biodiesel production. *Considers publication with the “respective subject + Biodiesel”.

The usage of biodiesel has a number of advantages over conventional fuels (as defined by ASTM D6751, EN 14214, and IS 15607):

- Complement or replacement of fossil fuels without modification of current engines (van Gerpen, 2005).
- Availability from renewable sources, e.g. vegetable oils, waste cooking oil, and animal fat (Anastopoulos, Zannikou, Stournas, & Kalligeros, 2009; B. Freedman, Pryde, & Mounts, 1984; Ogunkunle & Ahmed, 2019; Veljković, Stamenković, Todorović, Lazić, & Skala, 2009).
- A much higher biodegradability of 90% for biodiesel (30 days), compared to 24.5% for petrodiesel (Ayhan Demirbaş, 2002).
- Lower greenhouse gas emissions by as much as 86% during production and use (lifecycle) (Shu et al., 2010; Ternel, Bouter, & Melgar, 2021)(Erin Voegele, 2020).
- Zero-sulfur content, which reduces atmospheric pollution. In contrast, petrodiesel fuels contribute up to 80% of the SO_2 in the atmosphere due to incomplete combustion (eCycle, 2014; Shu et al., 2010).
- Lower greenhouse gas (GHG) emissions, with the US biodiesel industry expected to achieve annual GHG reductions of more than 35 million tons by 2022 (Erin Voegele, 2020; Shu et al., 2010).
- Flash point (>130°C) is higher than diesel (60-80°C). A higher flash point makes it more difficult for the vapours to ignite, allowing safe handling (ASTM D975, 2021).

These characteristics are especially important in a context of rising global energy consumption. By 2050, the global energy demand is expected to increase by 53% (Anwar, 2021; Bilen et al., 2008; IEA, 2020) and the fuel requirement by 59% (Anwar, 2021), respectively. Without further intervention, GHG emissions are consequently expected to rise by 39% by 2030 (Anwar, 2021; Mofijur et al., 2017). For the transportation sector, which is responsible for 58% of fossil fuel consumption (Escobar et al., 2009), electric cars have been proposed as alternative vehicles. However, these require high-capacity batteries and their manufacturing show unfavourable GHG emissions. Nevertheless, electrification and biofuels have been proposed as complementary technologies to reach Green Deal targets (Ternel et al., 2021).

Moreover, biodiesel is an alternative fuel for trucks, trains, boats and barges, construction equipment, diesel generators (hospitals and remote areas) and other industrial facilities. The U.S. military uses large quantities of diesel fuel for its vehicles due to its lower flammability and explosivity, which could subsequently be substituted by biodiesel (EIA, 2021).

2.3 Feedstock

Triglycerides (TGL) and free fatty acid (FFA) can be used as biodiesel feedstock. Vegetable oils are the most common raw material, and the content of TGL and FFA are variable, as described in Table 2. 1 . Edible oils, such as canola and palm oil, have been used in biodiesel production (Figure 2. 5) , with palm oil currently the most common worldwide, while Europe uses more rapeseed/canola. However, the consumption of edible oils has decreased (animal fats, canola oil, and soybean oil), except for palm oil, and the use of WCO has increased. Reusing waste oils can improve the cost efficiency of biodiesel production because raw materials account for approximately 60–80% of the total costs (Zahan & Kano, 2018). Another option to reduce the price of raw materials could be the use of distilled fatty acids obtained as a by-product from the oil refining process, which are currently used in the production of alkyl resins for paints, lubricant formulation, and animal feed (Dumont & Narine, 2007).

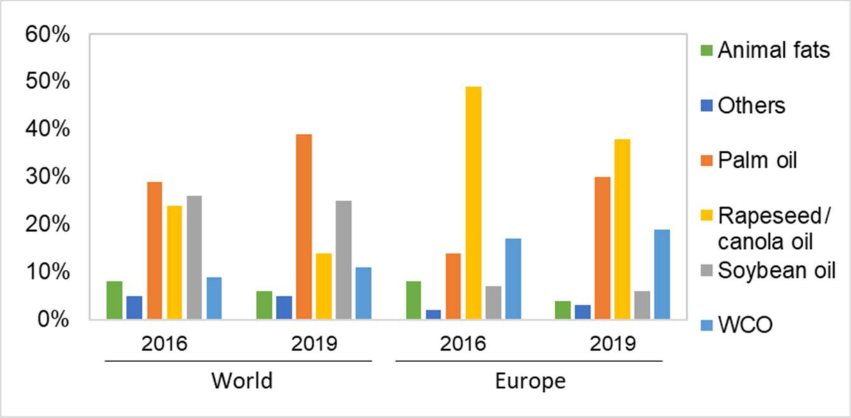

Figure 2. 5. Biodiesel production feedstock. (Compilated data from: UFOP, 2016, 2020).

2.3.1 Waste cooking oil (WCO)

Waste cooking oil is a non-edible resource with a high FFA content (Ma & Hanna, 1999; Mardhiah, Ong, Masjuki, Lim, & Pang, 2017). During the frying process, the oil is heated in the presence of water from food and air at high temperatures (160–200°C). This process causes hydrolytic, oxidative, and thermolytic changes. The water and FFA contents in WCO are thus higher than in crude edible oil. Consequently, some differences are notable: an increase in viscosity and specific heat, a change in surface tension, colour, and a higher tendency of fat to foam (Kulkarni & Dalai, 2006; Leung, Wu, & Leung, 2010). WCO with FFA content <15% is called yellow grease, and >15% brown grease (Sandesh Suresh, Suresh, & Kudre, 2019).

WCO is considered an environmental problem because of its necessary disposal (Y. Zhang et al., 2003). Currently, the WCO ends up reaching natural water reserves, polluting water bodies and raising the Biochemical Oxigen Demand (DBO) (Dimple Sharma, n.d.). The European Union collected 0.7 to 1 million tonnes/year (Supple, Howard-Hildige, Gonzalez-Gomez, & Leahy, 2002). Canada produces 120.000 tonnes/year of yellow grease (FFA<15%) (M. Canakci & J. Van Gerpen, 2001). Consequently, it has been proposed as a cheap and abundant feedstock to produce biodiesel (Supple et al., 2002). For this, a pretreatment is required: filtration, water content removal, and FFA reduction. The FFA content can be converted to biodiesel by an esterification process. Esterification and transesterification can occur in series or simultaneously. The order of the reactions depends on the catalyst and operational conditions. Biodiesel from WCO is frequently darker. Although ASTM D 6751 does not specify colouration, it can be removed easily using an activated carbon bed (Pruszko, 2020).

2.4 Mechanisms of biodiesel generation

Esterification and transesterification are the most common routes to produce biodiesel. However, interesterification has been considered as a third option to produce fatty acid ethyl ester (FAEE) (Sootchiewcharn, Attanatho, & Reubroycharoen, 2015). Fischer-esterification describes the reaction between a free fatty acid and alcohol in the presence of a catalyst, generating biodiesel and water (Figure 2.6). The esterification reaction of FFA occurs preferably in the presence of a short-chain alcohol (methanol, ethanol or propanol) (Guo et al., 2021; Moradi, Saidi, & Najafabadi, 2021; S. M. Silva, Peixoto, & Freire, 2020; M. v.d. Silva, Hori, & Reis, 2015; Stacy, Melick, & Cairncross, 2014). A high volume of alcohol is frequently used to prevent the backward reaction (hydrolysis). The most common catalyst is a strong acid such as sulfuric acid (G. Berrebi et al., 1993). Esterification is frequently used as a first step (pretreatment) for oils with a high FFA content such as WCO.

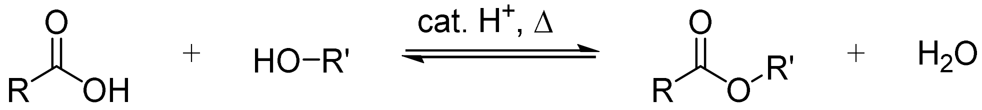

Figure 2. 6. Esterification mechanism by acid catalyst.

Transesterification is the main reaction applied on large scales industrially and utilises either strong acids or alkalis as catalysts. Under acidic conditions, the reaction generates biodiesel and glycerine (Figure 2. 7). In contrast, base-catalysis (saponification) furnishes the corresponding fatty acid salts instead.

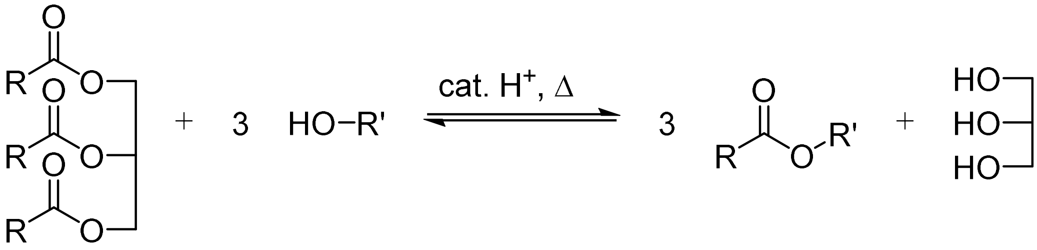

Figure 2. 7. Transesterification mechanism by acid catalyst.

Both reactions require high temperatures up to 120°C (Stacy et al., 2014), and consequently demand considerable energy and specific unit operations when working with short-chain alcohol at temperatures greater than their boiling point. Different technologies have been explored to optimize biodiesel production (Table 2. 2), with a wide range of operation conditions, catalysts, reactors, and efficiency, respectively.

Table 2. 1: *FFA content in biodiesel feedstock.*

		Fatty acid					
Feedstock	**FFA content**	**Oleic** ($C_{18}H_{34}O_2$)	**Linoleic** ($C_{18}H_{32}O_2$)	**Linolenic** ($C_{18}H_{30}O_2$)	**Palmitic** ($C_{16}H_{32}O_2$)	**Stearic** ($C_{18}H_{36}O_2$)	**Ref.**
Animal fat[a]	7-50%	38%	-	-	19%	3%	(Wan Ghazali, Mamat, Masjuki, & Najafi, 2015)
Brown grease[b]	>15%	29 - 46%	28 - 43%	0.8%	18 - 23%	7 - 13%	(Kolet, Zerbib, Nakonechny, & Nisnevitch, 2020; Sandesh Suresh et al., 2019; Wan Ghazali et al., 2015)
***Jatropha* oil**	15%	43%	15%	-	15%	7%	(Corro et al., 2013; Huang & Chang, 2010; Laura Cassiday, 2018; Wan Ghazali et al., 2015)
Palm oil	3 – 10%	40%	10%	-	43%	5%	(Hayyan et al., 2011; Yebo, 2016)
Rapeseed/ Canola oil	10 – 18%	61%	21%	10%	-	-	(M. A. Ali, Nouruddeen, Muhamad, Latip, & Othman, 2013; Laura Cassiday, 2018)
Soybean oil	<1%	23%	54%	8%	7%	3%	(Huang & Chang, 2010; Laura Cassiday, 2018; Wan Ghazali et al., 2015)
WCO	>10%	38 - 44%	26 - 32%	0.2%	4-26%	1-10%	(Corro et al., 2011; Verma & Sharma, 2016)
Yellow grease[c]	<15%	22 - 48%	21 - 38%	1 - 5%	10 - 23%	13%	(Sandesh Suresh et al., 2019; Verma & Sharma, 2016; H. Wu, Gong, Guo, Zhang, & Li, 2011)

[a]Chicken fat; [b]WCO with FFA content < 15%; [c]WCO with FFA content > 15%.

Table 2. 2: *Biodiesel production by different technologies.*

Reactional medium	Advantages	Disadvantages
Homogeneous		
Supercritical conditions	– Product with high purity, – Less or no catalyst (Cao, Han, & Zhang, 2005; Fernández, Fiori, Ramos, Pérez, & Rodríguez, 2015; Qadeer et al., 2021; Saka & Kusdiana, 2001; L. Wang & Yang, 2007)	– High temperature (>250°C), – High pressure (>10 MPa), – Requires pretreatment to remove water (Cao et al., 2005; Fernández et al., 2015; D. Kusdiana & Saka, 2001; Qadeer et al., 2021; Saka & Kusdiana, 2001; L. Wang & Yang, 2007).
Microwave	– High efficiency, fast reaction, – Mild operational conditions, – Less or no catalyst (M. A. Ali et al., 2013; Amore & Leadbeater, 2007; Kappe, 2004; Leadbeater & Stencel, 2006; Nguyen et al., 2020; Razzaq & Kappe, 2008).	– Selective heating, – Overheating of solvent, – Catalyst and medium hotspots, – Reagent diffusion limited (Antonio & Deam, 2007; Ferrari, Hunt, Stiegman, & Dudley, 2015; Hincapié, Valange, Barrault, Moreno, & López, 2014; Priecel & Lopez-Sanchez, 2019; Xu, Zhou, Su, Ou, & You, 2016; X. Zhang, Hayward, & Mingos, 1999).
Strong bases (KOH, NaOH)	– Fast reaction (Thanh et al., 2012; van Gerpen, 2005), – Catalyst readily available (Mardhiah, Ong, Masjuki, Lim, & Lee, 2017).	– Soap formation, – Requires highly refined oil (Santacesaria et al., 2012; Thanh et al., 2012; van Gerpen, 2005), – FFA content <0.5% (Bernard Freedman, Butterfield, & Pryde, 1986; Thanh et al., 2012; van Gerpen, 2005), – Product difficult to purify, – Catalyst difficult to recover (Konwar, Boro, & Deka, 2014; Long, Fang, Su, & Yang, 2014), – High volumes of wastewater (Mardhiah, Ong, Masjuki, Lim, & Lee, 2017).
Strong acid (H_2SO_4)	– Applicable to FFA (Konwar et al., 2014; Long et al., 2014; Santacesaria et al., 2012; Thanh et al., 2012; van Gerpen, 2005), Catalyst readily available (Mardhiah, Ong, Masjuki, Lim, & Lee, 2017).	– Product difficult to purify, – Catalyst difficult to recover (Konwar et al., 2014; Long et al., 2014), Biodiesel with sulfur content higher than 100 ppm (standard limit) (Mardhiah, Ong, Masjuki, Lim, & Lee, 2017).

Reactional medium	**Pros**	**Cons**
Heterogeneous		
Bases (CaO)	– Ease of recovery (Santacesaria et al., 2012; Thanh et al., 2012; van Gerpen, 2005), – Reduced corrosion (Mardhiah, Ong, Masjuki, Lim, & Lee, 2017), – Reduced toxicity (Mardhiah, Ong, Masjuki, Lim, & Lee, 2017).	– Low activity, – Requires high temperature and alcohol content, – Water poisonous to active sites, – Easy leaching and active site deactivation (Konwar et al., 2014; Long et al., 2014; Santacesaria et al., 2012; Thanh et al., 2012; van Gerpen, 2005).
Acid $Al(HSO_4)_3$	– Simultaneous esterification and transesterification, – Applicable to FFA content (Santacesaria et al., 2012; Thanh et al., 2012; van Gerpen, 2005), – Reduced corrosion, – Reduced toxicity (Mardhiah, Ong, Masjuki, Lim, & Lee, 2017).	– Requires high temperature and alcohol content, – Water poisonous to active sites, – Easy leaching and active site deactivation (Santacesaria et al., 2012; Thanh et al., 2012; van Gerpen, 2005).
Metal Oxides ($Cr.SiO_2$)	– Esterification and/or transesterification (Wan Omar & Amin, 2011; R. A. Welter, Santana, de la Torre, Barns, Taranto, & Oelgemöller, 2022), – Reduced toxicity, – Easy recovery (Boro, Konwar, & Deka, 2014; Ramachandran et al., 2011).	– Limited reuse (Nigam & Singh, 2011), – Easy leaching and active site deactivation (Santacesaria et al., 2012; Thanh et al., 2012; van Gerpen, 2005), – High temperatures (di Serio, Tesser, Pengmei, & Santacesaria, 2008; Santacesaria et al., 2012), – Water poisonous to active sites (Santacesaria et al., 2012).
Photocatalysts (TiO_2+UVA)	– Simultaneous esterification and transesterification (R. A. Welter, Santana, de la Torre, Barns, Taranto, & Oelgemöller, 2022), – High physical and chemical stability, – Easy handling, – Easy recovery, – High product purity (Alsharifi et al., 2017; Brito, 2008; Xie & Ma, 2009).	– Slow reaction, – Parallel and non-desirable reaction, – Deactivation by impregnation of organic material (R. A. Welter, Santana, de la Torre, Barnes, Taranto, & Oelgemöller, 2022; R. A. Welter, Santana, de la Torre, Barns, Taranto, & Oelgemöller, 2022; Rosilene A. Welter, Santana, Torre, Robertson, Taranto, & Oelgemöller, 2022).
Biocatalysts (Lipases)	– Mild operational conditions (Macrae & Hammond, 1985; Oliveira, Bastos, & de la Torre, 2019; Peirce et al., 2016; Zdarta et al., 2016; S. Zhang et al., 2013) – Esterification and transesterification, – High product purity, – Low wastewater generation (Alnoch, Santos, de Almeida, Krieger, & Mateo, 2020; Hosseini et al., 2019; Macrae & Hammond, 1985; Tamalampudi et al., 2008).	– Low reaction efficiency, – Easy leaching and deactivation of active sites (Alnoch et al., 2020; Hosseini et al., 2019; Macrae & Hammond, 1985; Tamalampudi et al., 2008).

2.5 Non-catalytic routes

2.5.1 Supercritical conditions

Processes under supercritical conditions can be applied for esterification and transesterification (Table 2. 3), but requires high temperatures (>250°C) and high pressures (>10 MPa) (Cao et al., 2005; Fernández et al., 2015; D. Kusdiana & Saka, 2001; Qadeer et al., 2021; Saka & Kusdiana, 2001; L. Wang & Yang, 2007). The properties of the alcohol employed, such as dielectric constant, viscosity, specific gravity, and polarity, must be considered for supercritical processes (Ayhan Demirbaş, 2002; Dadan Kusdiana & Saka, 2004; Narayan & Madras, 2017; Patil, Gude, & Deng, 2010; Saka & Kusdiana, 2001). The water content can interfere with the esterification process, favouring hydrolysis. Likewise, transesterification of feedstocks such as TGLs with a high water content can produce FFA and glycerol (Qadeer et al., 2021). The process can be conducted in the presence of an acid catalyst, subsequently improving the reaction efficiency.

Methanol is the most common alcohol used for biodiesel production under supercritical conditions (Qadeer et al., 2021). It is a polar solvent with hydrogen bonding between molecules. Under supercritical conditions, the degree of hydrogen bonding decreases, reducing the polarity and increasing the solubility (Alenezi, Leeke, Winterbottom, Santos, & Khan, 2010; Qadeer et al., 2021). Moreover, nonpolar TGL is solvated by methanol. This feature results in a one-phase mixture with optimized mass transfer, which consequently improves yields of FAME production (dos Santos, Voll, Ramos, & Corazza, 2017; Goembira, Matsuura, & Saka, 2012; Dadan Kusdiana & Saka, 2004; Saka & Kusdiana, 2001). Unsaturated fatty acids (oleic, linoleic, and linolenic) as feedstocks react easier than saturated fatty acids (palmitic and stearic) (Aboelazayem, Gadalla, & Saha, 2018; Alenezi et al., 2010; Ayhan Demirbaş, 2002; Dadan Kusdiana & Saka, 2004; Narayan & Madras, 2017; Patil et al., 2010; Saka & Kusdiana, 2001; Serrano, Corazza, Mitchell, & Krieger, 2021). Different reactor designs have been considered, of which the batch process is the most commonly applied.

Table 2. 3: *Biodiesel production by supercritical conditions.*

Reactor	Reaction	System	Feedstock	Alcohol	Oil: Alcohol	T (°C)	Pressure (MPa)	t (min)	Biodiesel (%)	Ref.
Batch	Est	Hom	FFA[a]	MeOH	1:1.6	270	10	30	97	(Alenezi et al., 2010)
Batch	Est	Hom	Levulinic acid	EtOH	1:09	280	15	10	80	(Kothe, Melfi, dos Santos, Corazza, & Ramos, 2020)
Batch	Est	Hom	Oleic acid	MeOH	1:20	260	20	60	95	(Jin et al., 2015)
Batch	Est/Trans	Hom	Palm fatty acid distillate	MeOH	1:6	290	40	30	78	(Lokman, Goto, Rashid, & Taufiq-Yap, 2016)
Batch	Est/Trans	Het	Palm fatty acid distillate	MeOH	1:6	290	40	30	98	(Lokman et al., 2016)
Batch	Est/Trans	Hom	Rapeseed oil	MeOH	1:14	270	15	17	97	(Sert & Atalay, 2017)
Batch	Est/Trans	Hom	Rapessed oil	MeOH	1:09	270	30	20	94	(Saka & Kusdiana, 2001)
Batch	Est/Trans	Hom	WCO+Crambe oil	EtOH	1:02	300	30	20	70	(dos Santos et al., 2017)
Batch	Trans	Hom	Jojoba oil	MeOH	1:30	287	12.3	23	96	(N. K. Singh, Singh, & Sharma, 2022)
Batch	Trans	Hom	Chicken fat	MeOH	1:6	400	41.1	6	88	(Marulanda, Anitescu, & Tavlarides, 2010b)
Cont. flow	Est/Trans	Hom	Chicken fat	MeOH	1:20	280	110	60	97	(Manuale, Torres, Vera, & Yori, 2015)
Conti. flow	Trans	Hom	Chicken fat	MeOH	1:9	375	20	10	84	(Marulanda, Anitescu, & Tavlarides, 2010a)
Microbatchreactor	Interest	Hom	Refined palm oil	ethyl acetate	1:50	350	200	20	52	(Sootchiewcharn et al., 2015)
Microbatchreactor	Trans	Hom	Rice bran oil	EtOH	1:5	300	8.5	24	75	(Akkarawatkhoosith, Tongtummachat, Kaewchada, & Jaree, 2021)

[a] Mixture of FFA: 88% Oleic acid, 4.5% linoleic acid, 3.5% palmitic acid and 4% others.

2.5.2 Microwave-assisted conditions

Activation with microwave has been applied for esterification and transesterification (Table 2. 4) (Amore & Leadbeater, 2007; Azcan & Danisman, 2008; Azcan & Yilmaz, 2013; D. Kim, Choi, Kim, Seol, Ha, et al., 2011; D. Kim, Choi, Kim, Seol, & Jung, 2011). Through this process, friction and collision occur between molecules, which subsequently generates heat. Consequently, reaction is achieved quickly under mild operational conditions and with smaller amounts of catalyst (M. A. Ali et al., 2013; Amore & Leadbeater, 2007; Kappe, 2004; Leadbeater & Stencel, 2006; Nguyen et al., 2020; Razzaq & Kappe, 2008). Irradiation can be conducted continuously or pulsed (Azcan & Danisman, 2008; D. Kim, Choi, Kim, Seol, Ha, et al., 2011) and has been applied for different feedstock. The limitations of this process are caused mainly by the catalyst (Azcan & Danisman, 2008; Bölük & Sönmez, 2020; Hernando, Leton, Matia, Novella, & Alvarez-Builla, 2007; D. Kim, Choi, Kim, Seol, Ha, et al., 2011; Taghvaei, Jafari, Assadpoor, Nowrouzieh, & Alishah, 2014). Additional drawbacks include selective heating, overheating of polar solvents, hotspots around solid catalysts and limitations of reagent diffusion (Antonio & Deam, 2007; Ferrari et al., 2015; Hincapié et al., 2014; Priecel & Lopez-Sanchez, 2019; Xu et al., 2016; X. Zhang et al., 1999).

2.5.3 Miscellaneous methods

Other methods for esterification and transesterification have been explored (Table 2.5), such as electrolysis, reactive distillation, and assisted plasma (Cubas, Machado, Pinto, Moecke, & Dutra, 2016; Fereidooni, Abbaspourrad, & Enayati, 2021; Helmi, Tahvildari, Hemmati, Aberoomand azar, & Safekordi, 2021; Korkut & Bayramoglu, 2018; Oliveira Palm et al., 2022; Rachman, Komariah, Andwikaputra, & Umbara, 2018; Rafati, Tahvildari, & Nozari, 2019). These investigations were prompted by the need for mild operational conditions and utilization of feedstocks with high FFA contents. The procedures developed commonly operate with reduced amounts of catalyst or even without.

Table 2. 4: *Biodiesel production by microwave-assisted radiation.*

Reactor	Reaction	Sist.	Feedstock	Alcohol	Oil: Alcohol	Power (W)	Catalyst	% wt	t (min)	Biodiesel (%)	Ref.
Batch	Est	Het	Silk-cotton seed oil	MeOH	1:18	270	CaO	0.3	114s	98	(Rahul Soosai, Moorthy, Varalakshmi, & Yonas, 2022)
Batch	Est	Het	PFAD	MeOH	1:9	-	TiO_2-GO	4	20	93	(Soltani, Khanian, Shean Yaw Choong, Asim, & Zhao, 2021)
Batch	Trans	Hom	WCO	MeOH	[a]	-	KOH	0.8	7	98	(Milano et al., 2018)
Batch	Trans	Hom	*Jatropha Curcas* oil	MeOH	7:11	500	H_2SO_4	2	90	61	(Athar et al., 2022)
Batch	Trans	Hom	WCO	MeOH	1:8	600	KOH	1.2	6	98	(I. K. Hong, Jeon, Kim, & Lee, 2016)
Batch	Trans	Hom	WCO	MeOH	1:6	750	$NaOCH_3$	0.8	10	98	(K. S. Chen, Lin, Hsu, & Wang, 2012)
Batch	Trans	Hom	Camelina oil	MeOH	1:6.91	800	KOH	1.26	5.85	95	(Rokni, Mostafaei, Dehghani Soufi, & Kahrizi, 2022)
Batch	Trans	Het	*Spirulina platensis*	EtOH	1:8	800	PEG/MgO/ZSM-5	2	40	96	(Qu et al., 2021)
Cont. Packed bed	Trans	Het	Waste cotton seed cooking oil	MeOH	1:9.6	180	CaO	-	9.7	90	(A. Sharma, Kodgire, & Kachhwaha, 2019)

[a]59% v methanol / v oil %

Table 2. 5: *Biodiesel production by miscellaneous methods.*

Method	Reaction	Feedstock	Alcohol	Oil: Alcohol	Catalyst	% wt	T (°C)	t (min)	Biodiesel (%)	Ref.
Corona discharge plasma	Ester	WCO	Methanol	1:6	-	-	2	110	78[a]	(Cubas et al., 2016)
Electrolysis	Transest	WCO	Methanol	1:12	KOH	-	120	120	99	(Rachman et al., 2018)
Electrolysis	Transest	WCO	Methanol	1:8	Na^+/zeolite-chitosan	1	25	30	97	(Fereidooni, Abbaspourrad, & Enayati, 2021)
Electrolysis	Transest	WCO	Methanol	1:6	HPMo/support graphene oxide	0.85	25	900	91	(Helmi et al., 2021)
Plasma assisted	Transest	Ethyl acetate	Methanol	1:6	$H_3(PMo_3O_{10})_4.H_2O$ (H_3PMo)	10	25	90	77	(Oliveira Palm et al., 2022)
Plasma assisted	Transest	Soybean oil	Methanol	1:15	Active carbon	-	65	30	92	(Buchori, Istadi, Purwanto, Kurniawan, & Maulana, 2016)
Plasma assisted	Transest	Soybean oil	Methanol	1:15	Active carbon+H_2SO_4	-	65	30	74	(Buchori, Istadi, Purwanto, Kurniawan, & Maulana, 2016)
Plasma assisted	Transest.	Ethyl acetate	Methanol	1:6	$NaOCH_3$	0.1	25	30	90	(Oliveira Palm et al., 2022)
Reactive destilation	Est	Dodecanoic acid	2-ethylhexano	1:1	-	-	130	120	40	(Kiss, Dimian, & Rothenberg, 2008)
Reactive destilation	Est	Dodecanoic acid	2-ethylhexano	1:1	sulfated zirconia-	-	130	120	75	(Kiss et al., 2008)
Ultrasound assisted	Transest	Canola oil	Methanol	1:7.5	CaO	5.35	60	150	99	(Korkut & Bayramoglu, 2018)
Ultrasound assisted	Transest	Canola oil	Methanol	1:7	calcium diglyceroxide	9.33	60	135	82	(Korkut & Bayramoglu, 2018)
Ultrasound assisted	Transest	WCO	Methanol	1:6	KOH	0.75	30	30	97	(Babajide, Petrik, Amigun, & Ameer, 2010)
Ultrasound assisted	Transest	Sunflower oil	Methanol	1:6	KOH	0.75	30	30	94	(Babajide et al., 2010)
Ultrasound assisted	Transest	Soybean oil	Methanol	1:6	KOH	0.75	30	30	98	(Babajide et al., 2010)

[a]Obtained by acid number.

2.6 Catalytic routes

Catalytic routes are the most common for the production of biodiesel. Homogeneous or heterogeneous systems were evaluated using acids, alkalis, oxides, and biocatalysts in free or immobilized forms. Based on the catalyst used, different operational conditions (e.g. temperature, molar ratio, mixing, catalyst loading and pH), feedstock (e.g. free fatty acid, crude edible oil and WCO), reaction types (e.g. esterification and transesterification), and reactor systems (e.g. batch, continuous flow and microdevices) have been explored.

Bifunctional catalysts have emerged to carry out esterification and transesterification reactions either separately or simultaneously. The implementation of bifunctional catalysts that operate in two subsequent steps increases the process cost. While these materials can be easily adapted to exciting conventional plants, their complexity naturally makes them expensive to produce. In addition, the implementation of such catalysts may result in low efficiency, poor reusability, or leaching. The use of bifunctional catalysts for simultaneous esterification and transesterification is considered more attractive. The coupled process occurs rapidly under mild operational conditions and with low equipment and operation’s costs. Heterogeneous catalysts are the most commonly employed with the catalytic surface comprising of acidic and basic sites (Avhad & Marchetti, 2015). However, one-step processes may still be expensive due to the high costs of these advanced catalytic materials, leaching and rapid deactivation. Their technical implementation also requires changes in the entire industrial plant. The reduction in the catalyst’s efficiency may affect both transformations, e.g. esterification and transesterification, differently. Consequently, the recovery and reactivation of these tandem-materials needs to be further investigated.

2.6.1 Homogeneous catalysis

Strong homogeneous bases or acids as catalysts are commonly used in industrial processes (Table 2. 6), but they are corrosive, hazardous, and not environmentally friendly (Anwar, 2021; Erin Voegele, 2020; Ogunkunle & Ahmed, 2019). The alkali-catalysed process is the most common for large scale operation (B. Freedman et al., 1984), is applied only for transesterification and requires pH ranges of 12 and 14 (Clark, Medeiros, Boyd, & Snell, 2013). However, the process is unsatisfactory for low-cost feedstocks such as WCO because of their high free fatty acid content. A FFA content of less than 0.5% is desirable (Bernard Freedman et al., 1986; Thanh et al., 2012; van Gerpen, 2005) to minimize soap formation (Figure 2. 8) (van Gerpen, 2005) which demands neutralization by acid and washing for product purification. This procedure may result in an aqueous emulsion that makes separation of the desired ester and glycerol challenging and subsequently necessitates high water contents. Consequently, the entire process results in a large volume of wastewater that requires further treatment (Mardhiah, Ong, Masjuki, Lim, & Lee, 2017).

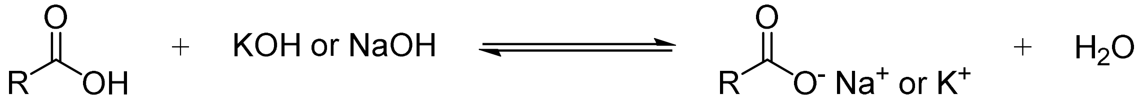

Figure 2. 8. FFA reaction with strong bases generating soap and water.

In contrast, the acid-catalysed process can be applied to feedstocks with high FFA contents as it operates by esterification and transesterification. However, the process is slower than the alkali-catalysed methodology (Thanh et al., 2012; van Gerpen, 2005), requires coating of stainless steel components due to corrosion, does not allow catalyst recovery, and requires large water contents for product treatment. The process is furthermore conducted under extreme temperature (70–120°C) and pH conditions. The usage of mineral acids such as H_2SO_4 for the esterification also leads to high sulfur contents in the biodiesel products, with the maximum allowed of up to 10 ppm according to the ASTM D975-21 (ASTM D975, 2021).

Industrially, the process involving high FFA content feedstock is frequently carried out in two steps: (1) esterification of FFA by concentrated sulfuric acid and (2) transesterification of triglycerides by strong alkali (Thanh et al., 2012). The reaction efficiency depends mainly on the feedstocks' purity, alcohol to oil molar ratio, catalyst, and temperature (B. Freedman et al., 1984). The most economical conventional process uses batch reactors and mechanical stirring, however, requires prolonged reaction times and high temperatures. These disadvantages have been overcome by using microplants (R. Welter, Silva Jr., de Souza, Lopes, Taranto, & Santana, 2022), ultrasonic irradiation, and co-solvent addition techniques, which reduce the reaction time and demand lower temperatures (Thanh et al., 2012).

Table 2. 6: *Biodiesel by homogeneous catalysts.*

Reactor	Reaction	Feedstock	Alcohol	Oil: Alcohol	T (°C)	Catalyst	% wt	t (min)	Biodiesel (%)	Ref.
Batch	Est	Palmitic acid	MeOH	1:10	65	$H_5BW_{12}O_{40}$	10.9mmol/L	180	99	(Z. Sun, Duan, Zhao, Wang, & Jiang, 2015)
Batch	Est/Trans	*Chrysophyllum albidum* oil	MeOH	1:9	65	H_2SO_4	1	40	99	(Kasirajan, 2021)
Batch	Trans	WCO	MeOH	1:8	65	KOH	1	90	90	(Sree, Chowdary, Kumar, Anbazhagan, & Subramanian, 2021)
Batch	Trans	WCO	MeOH	1:9	70	KOH	1	120	98	(Agarwal, Chauhan, Chaurasia, & Singh, 2012)
Batch	Trans	WCO	MeOH	1:3	60	KOH	1	60	94	(Sahar et al., 2018)
Batch	Trans	WCO	MeOH	1:6	60	$NaOCH_3$	0.8	60	92	(Dias, Alvim-Ferraz, & Almeida, 2008)
Batch	Trans	WCO	MeOH	1:6	60	KOH	1.2	60	96	(Dias et al., 2008)
Con	Trans	WCO	MeOH	1:6	50	KOH	1	480	96	(Unker et al., 2010)
Cont.	Est	Oleic acid	MeOH	1:3	120	H_2SO_4	1	120	95	(Stacy et al., 2014)
Micro Cont	Trans	Castor oil	EtOH	1:14	50	NaOH	1	10	97	(Martínez Arias, Fazzio Martins, Jardini Munhoz, Gutierrez-Rivera, & Maciel Filho, 2012)
Micro Cont	Trans	Palm oil	MeOH	1:21	60	KOH	4.5	180 s	95	(Azam, Uemura, Kusakabe, & Bustam, 2016)

2.6.2 Heterogeneous catalysis

The use of heterogeneous catalysts has seen a substantial growth. One important reason is their easier management and recovery. Different materials have been evaluated as summarized in Table 2. 7 and discussed below.

Metal oxides can act as a base or acid according to the metal's properties and catalyst's treatment such as doping with sulfuric acid. Alkalis are generally more active than acids (Arzamendi et al., 2007; Perego & Bosetti, 2011), but they can be applied only to transesterification. Acid catalysis occurs with Bronsted or Lewis acids (Lotero et al., 2005). The active sites of Bronsted acids are fewer than for homogeneous acids. Consequently, the biodiesel process requires more severe conditions (e.g. high temperatures and alcohol contents) (Mardhiah, Ong, Masjuki, Lim, & Lee, 2017). However, Bronsted acids can be used for esterification and transesterification simultaneously. Lewis acids are stronger than Bronsted acids, but they can only be used for feedstock without water and FFA content as these act as poisons.

Alkaline earth oxides (Be, Mg, Ca, Sr, Ba, and Ra) show base characteristics and can thus be used for transesterification. They are non-metallic, insoluble in water, silver-white in colour, and heat resistant. Alkaline earth metal oxides donate electrons to other substances; beryllium oxide is amphoteric, and barium oxide is the strongest base. Magnesium and calcium oxides are the most abundant ones (Courtenay Stanley Goss Phillips, 2021) and are therefore commonly applied (Conceição et al., 2007; Santacesaria et al., 2012). The activity of the solid catalyst is dependent on the active sites on the CaO or MgO surface (Thanh et al., 2012). The alkalinity of the active sites is responsible for the reaction, and many studies have improved this property by adding other chemicals and pretreatments or by using more than one metal oxide. Active sites can be reconstituted by washing with acetone (di Serio, Mallardo, Carotenuto, Tesser, & Santacesaria, 2012) and calcination to remove CO_2 and H_2O content (Thanh et al., 2012). However, heterogeneous base catalysts require high temperatures, long reaction times, large alcohol contents and high triglyceride purity, and the catalyst leaches rapidly (di Serio, Casale, Tesser, & Santacesaria, 2010; Santacesaria et al., 2012).

Materials such as natural waste shells and eggshells with high Ca contents can be used for transesterification. However, they frequently show good efficiency during their initial application (>90%) but much lower efficiencies after recovery and recycling (<30%) (Nigam & Singh, 2011). Subsequent doping has been investigated using alkali metals and has resulted in high conversions even for reused catalysts (Boro et al., 2014).

Transition metal oxides (e.g. Ti, Co, Cu, Cr, Zn, Pt, and Zr) provide a large variety of surface structures and energies. The metal oxide surface atoms can be acidic or alkaline based on the metal cation and oxygen anion coordination. These materials are used for esterification and transesterification reactions, in free or immobilized form and upon optional photoactivation (Corro et al., 2013; Corro, Sánchez, Pal, Cebada, & Fierro, 2017; Corro et al., 2012). The wet impregnation method is frequently used for zirconia immobilization (Zr) of metal nitrate salt. The final catalysts such as Mg/ZrO_2, Ca/ZrO_2, Sr/ZrO_2 or Ba/ZrO_2 can be used for simultaneous esterification and transesterification (Wan Omar & Amin, 2011).

Alkali metal oxides can be used for transesterification. These metal oxides (Li, Na, K, Rb, Cs, and Fr) are shiny, soft, of low density, and oxidize easily. In addition, they have high thermal and electrical conductivity. Sodium and potassium oxide are the most abundant.

Some metals can be sulfonated and hence become acidic such as $Al(HSO_4)_3$. Using this catalyst, it is possible to obtain high conversions by esterification and transesterification from feedstocks with high FFA and water contents (e.g. WCO) without saponification. The material can be also easily recovered and reused (Ramachandran et al., 2011). However, the catalyst can leach and deactivate rapidly (Santacesaria et al., 2012; Thanh et al., 2012; van Gerpen, 2005).

Heteropolyacids (HPA) supported on oxides can be applied to esterification and transesterification reactions. HPAs are soluble in methanol but gain higher activity and stability after immobilization on oxides. The most common oxides used are Zr, Ti, Sn, and Nb-based, or mixtures, such as TiO_2/SiO_2. However, the catalyst is susceptible to leaching and poisoning by water (Santacesaria et al., 2012).

Table 2. 7: *Biodiesel produced by heterogeneous catalyts.*

Reactor	React.	Feedstock	Alcohol	Oil:Alcohol Molar ratio	T (°C)	Catalyst	% wt	t (min)	Biod. (%)	N. cycles (Reuse)	Biod. (%) reuse	Ref.
Batch	Est	Oleic acid	MeOH	1:15	75	Biomass-based polymers	-	180	96	-	-	(A. Wang, Zhang, Li, & Yang, 2019)
Batch	Est	Oleic acid	MeOH	1:12	90	Fe_3O_4@PILPW	-	300	93	-	-	(Z. Wu, Chen, Wang, Wan, & Guan, 2016)
Batch	Est	Oleic acid	MeOH	1:15	110	[HMIM]HSO_4	-	480	95	-	-	(Roman et al., 2019)
Batch	Est	Oleic acid	MeOH	1:45	100	HZ zeolite/1.0/60	-	240	83	-	-	(Vieira et al., 2015)
Batch	Est	Oleic acid	MeOH	1:45	100	HZ zeolite/2.0/80	-	240	73	-	-	(Vieira et al., 2015)
Batch	Est	Oleic acid	MeOH	1:45	100	HZ zeolite/0.5/60	-	240	71	-	-	(Vieira et al., 2015)
Batch	Est	Oleic acid	MeOH	1:45	100	HZ zeolite	-	240	55	-	-	(Vieira et al., 2015)
Batch	Est	Oleic acid	MeOH	1:5	100	LO (lanthanum oxide)	-	420	63	-	-	(Vieira et al., 2013)
Batch	Est	Oleic acid	MeOH	1:10	60	M-MMT K10 acid	-	180	70	-	-	(Harun, Jihadi, Ramli, Hassan, & Zubir, 2018)
Batch	Est	Oleic acid	EtOH	1:10	60	M-MMT K10 acid	-	180	40	-	-	(Harun et al., 2018)
Batch	Est	Oleic acid	PropOH	1:10	60	M-MMT K10 acid	-	180	35	-	-	(Harun et al., 2018)
Batch	Est	Oleic acid	MeOH	1:5	100	SLO/HZSM-5	-	420	100	-	-	
Batch	Est	Oleic acid	MeOH	1:5	100	SLO (sulfated lanthanum oxide)	-	420	98	-	-	(Vieira et al., 2013)
Batch	Est	Oleic acid	MeOH	1:18	88	SO_3-HM-ZSM-5–3	-	600	100	-	-	(Mostafa Marzouk et al., 2021)
Batch	Est	Oleic acid	MeOH	1:20	50	Sugarcane bagasse - SO_3H	-	1440	85	-	-	(Flores et al., 2019)
Batch	Est	Oleic acid	MeOH	1:8	150	TiO_2/NP-800	-	480	87	-	-	(Essamlali, Larzek, Essaid, & Zahouily, 2017)
Batch	Est	Oleic acid	MeOH	1:40	60	TPA3/MCM-41	-	360	100	-	-	(Patel & Brahmkhatri, 2013)
Batch	Est	Oleic acid	MeOH	1:9	60	$Zr(SO_4)_2$	-	300	98	-	-	(Senoymak Tarakcı & Ilgen, 2018)
Batch	Est	Oleic acid	MeOH	1:20	100	300-Nb_2O_5/SO_4^{2-}	-	240	92	-	-	(Sturt, Vieira, & Moura, 2019)
Cont. microreactor	Trans	WCO	MeOH	3:1.7 v/v	62	Kettle limescale	8.9	15	93%	-	-	(Mohadesi, Aghel, Maleki, & Ansari, 2020a)

Cont.

Reactor	React.	Feedstock	Alcohol	Oil:Alcohol Molar ratio	T (°C)	Catalyst	% wt	t (min)	Biod. (%)	N. cycles (Reuse)	Biod. (%) reuse	Ref.
Cont. microreactor	Trans	WCO	MeOH	2.25:1 v/v	63	Cow bone	8.5	1	99	-	-	(Mohadesi, Gouran, & Dehghan Dehnavi, 2021)
Cont. microreactor	Trans	WCO	MeOH	2.25:1 v/v	65	KOH/Clinoptilolite	8.1	13	97	-	-	(Mohadesi, Aghel, Maleki, & Ansari, 2020b)
Cont. microreactor	Trans	Sunflower oil	MeOH	2.5:1 v/v	60	Chicken bone	10	10	51	-	-	(Pavlović et al., 2021)
Packed Cont. microreactor	Trans	Palm oil	MeOH	1:24	65	Calcium oxide	1g/cm^3	9	99	-	-	(Chueluecha, Kaewchada, & Jaree, 2017)
Batch	Trans	WCO	MeOH	1:0.25 v/v	63	$MnCO_3$/Na-silicate	1	120	95	-	-	(Kouzu, Fujimori, Suzuki, Koshi, & Moriyasu, 2017)
Batch	Trans	WCO	MeOH	1:15	65	CaO	7.5	360	90	-	-	(Maneerung, Kawi, Dai, & Wang, 2016)
Batch	Est/Trans	*Jatropha curcas oil*	MeOH	1:15	150	$5Bi_2O_3–La_2O_3$	2	240	93	3	87	(Rabiah Nizah et al., 2014)
Batch	Est/Trans	WPO[a]	MeOH	1:15	80	7WZC[d]	2	60	94	5	79.3	(Mansir, Teo, Mijan, & Taufiq-Yap, 2021)
Batch	Est/Trans	Soybean oil	MeOH	1:50	65	40% CaO–MoO3–SBA-15	6	480	83	5	77	(Xie & Zhao, 2014)
Batch	Est/Trans	*Jatropha curcas oil*	MeOH	1:30	160	Activated Mg–Al hydrotalcites	5	240	93	4	86	(Y. T. Wang, Fang, Zhang, & Xue, 2015)
Batch	Est/Trans	Palm oil	MeOH	1:20	85	$CaO–CeO_2$ (1:1)	5	180	95	18	90	(Thitsartarn & Kawi, 2011)
Batch	Est/Trans	*Jatropha curcas oil*	MeOH	1:6	60	$CaO\text{-}Fe_2(SO_4)_3$	5	180	100	3	80	(Endalew, Kiros, & Zanzi, 2011)
Batch	Est/Trans	*Jatropha curcas oil*	MeOH	1:25	160	CaO–La2O$_3$	3	180	99	5	80	(Lee, Juan, & Taufiq-Yap, 2015)
Batch	Est/Trans	WPO[a]	MeOH	1:9	65	CaO/Al_2O_3	4	240	89	2	80	(Elias, Rabiu, Okeleye, Okudoh, & Oyekola, 2020)
Batch	Est/Trans	WSO[b]	MeOH	1:9	65	CaO/Al_2O_3	4	240	98	2	77	(Elias et al., 2020)
Batch	Est/Trans	Palm fatty acid distillate	MeOH	1:15	80	CAWS-(7) SO_4	5	180	80	4	46	(Syazwani, Rashid, Mastuli, & Taufiq-Yap, 2019)

Cont.

Reactor	**React.**	**Feedstock**	**Alcohol**	**Oil:Alcohol Molar ratio**	**T (°C)**	**Catalyst**	**% wt**	**t (min)**	**Biod. (%)**	**N. cycles (Reuse)**	**Biod. (%) reuse**	**Ref.**
Batch	Est/Trans	WCO[c]	MeOH	1:15	205	[Fe $(HSO_4)_3$	1	240	94.5	5	91.2	(Alhassan et al., 2013)
Batch	Est/Trans	Rapeseed oil	MeOH	1:6	62	GO-to-NaOH-bentonite	6	270	96	2	80	(B. Ali et al., 2018)
Batch	Est/Trans	WCO[c]	MeOH	1:20	180	K-ITQ-6	5	1440	80	2	35	(Macario et al., 2010)
Batch	Est/Trans	WCO[c]	MeOH	1:11	182	MgZnO	3.32	360	92	5	87	(Olutoye & Hameed, 2011)
Batch	Est/Trans	WCO[c]	MeOH	1:27	100	Mo–Mn/γ-Al_2O_3-15 wt% MgO	5	240	91	10	70	(Farooq, Ramli, & Subbarao, 2013)
Batch	Est/Trans	*Jatropha curcas oil*	MeOH	1:40	160	Zn8@Fe-C400	7	240	100	10	94	(Y. T. Wang et al., 2018)
Packed bed	Trans	Palm oil	MeOH	1:70	1:1	KOH-TiO_2/Al_2O_3	157g//cm^3	60	96	3	89	(Baroutian, Aroua, Raman, & Sulaiman, 2011)
Packed bed	Trans	*Jatropha curca oil*	MeOH	1:40	240	Pellets	173m^2/g	17.54	99	5	80	(Sakthivel, Halder, & Gupta, 2013)

2.6.3 Photocatalysis

Heterogeneous photocatalysis is a widely applied to advanced oxidative process (AOP), and it is frequently used for the degradation of organic compounds. It can also be used to synthesize products such as esters (Corro et al., 2013, 2017, 2012; Manique et al., 2016). The process is based on irradiating an inorganic semiconductor such as TiO_2, ZnO, or CdS. Semiconductors are characterised by their valence band (BV), conduction band (BC) and band gap energies (BG). When the semiconductor is excited by photons (hν) with energy equal to or higher than the BG, electrons migrate from the BV to the BC. The electron-hole pair created can rapidly recombine or can initiate oxidative and reductive reactions as described in Figure 2. 9 (Alves, 2008; Espindola, 2010; Fox & Dulay, 1993; N. Hoffmann, 2015).

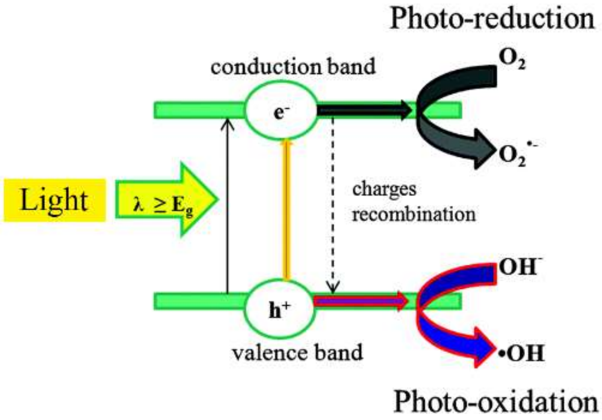

Figure 2. 9. Inorganic semiconductor's energy in the presence of light (Reprinted with permission from (Colmenares & Luque, 2014), Copyright Creative Commons Attribution 3.0.

The usage of inorganic semiconductors activated by either ultraviolet light or natural sunlight for esterification purposes has been investigated (Table 2. 8) (Corro et al., 2012; Manique et al., 2016; Suthar & Verma, 2018). The advantages of heterogeneous photocatalysts include their low costs, high chemical stability, easy handling, post-reaction recovery and reusability (Alsharifi et al., 2017; Brito, 2008; Xie & Ma, 2009).

Table 2. 8: *Biodiesel produced by photocatalysis.*

Reactor	Reaction	Feedstock	Alcohol	Oil: Alcohol Molar ratio	T (°C)	Catalyst	% wt	t (min)	Biod. (%)	Ref.
Batch	Est	Oleic acid	MeOH	1:55	55	TiO_2 + UVA	20	240	98	(Rosilene A. Welter, Santana, Torre, Robertson, Taranto, & Oelgemöller, 2022)
Batch	Est	Oleic acid	EtOH	1:55	55	TiO_2 + UVA	20	240	21	(Rosilene A. Welter, Santana, Torre, Robertson, Taranto, & Oelgemöller, 2022)
Batch	Est	Oleic acid	PropOH	1:55	55	TiO_2 + UVA	20	240	6	(Rosilene A. Welter, Santana, Torre, Robertson, Taranto, & Oelgemöller, 2022)
Batch	Est	Oleic acid	MeOH	1:9	40	Au/TiO_2 + Visible light	10	360	85	(Praneeth & Paria, 2020)
Batch	Est	Oleic acid	MeOH	1:12	30	TiO_2 + UVA	12	240	75	(Manique et al., 2016)
Batch	Trans	WCO	EtOH	1:9	65	CuO/ZnO + UVA	5	120	93	(Guo, Jiang, Ding, & Lu, 2022)
Batch	Trans	WCO	MeOH	1:9	60	TiO_2/g-C_3N_4 + sunlight	2	60	84	(M. Khan et al., 2021)
Batch	Trans	WCO	MeOH	1:8	60	TiO_2 + sunlight	nanotubes	240	91	(Khaligh et al., 2021)

Titanium dioxide (TiO_2) is the most frequently used metal oxide photocatalyst owing to its high photosensitivity, high thermal and chemical stability, corrosion resistance, and non-toxicity (Omo Ibhadon & Fitzpatrick, 2013; Suthar & Verma, 2018). Titanium dioxide is found in three modifications: anatase, brookite, and rutile, each with different physical and chemical characteristics (Table 2. 9) and different crystalline structures (Figure 2. 10). All require UVA light (wavelength: 315–400 nm) for the best catalyst activation, but the band gap is also reached in the presence of sunlight, which lowers the process cost. Tropical, subtropical and Mediterranean regions offer advantageous climatic conditions with high UV indices for several months of the year (ARPANSA, 2022), which makes them interesting locations for solar photocatalytic biodiesel production.

Table 2. 9: *Titanium dioxide characterization.*

	Anatase	**Brookite**	**Rutile**	**Ref.**
BG (eV)	3.26	3.13	3.05	(Reyes-Coronado et al., 2008)
Refractive index	2.488	2.583	2.609	(Hanaor & Sorrell, 2011)
Density (g/cm³)	3.83	4.17	4.24	(Koelsch, Cassaignon, Guillemoles, & Jolivet, 2002)
Unit cell volume (nm³)	0.1363	-	0.0624	(Hanaor & Sorrell, 2011)
Crystal size	< 11	11 – 35	> 35	(Hanaor & Sorrell, 2011)
Mohs scale	5.5 - 6.0	5.5 – 6	6.0 - 6.5	(Koelsch et al., 2002)
Occurrence	Common	Rare	Common	(M. R. Hoffmann, Martin, Choi, & Bahnemann, 1995)

The different crystal structures of titanium dioxide can be combined such as in the commercial Aeroxide® TiO_2 P25 with 80% anatase and 20% rutile (Aeroxide, 2020). TiO_2 can be modified by doping with nitrogen ions or metal oxides such as tungsten trioxide that improve its absorption in the visible range (Kurtoglu, Longenbach, & Gogotsi, 2011), or can be immobilized, e.g., in biopolymers such as calcium alginate. This immobilization technique has been successfully applied for Triclosan degradation, and the same efficiency was observed for TiO_2 in both its free and immobilized form (Kosera, Cruz, Chaves, & Tiburtius, 2017).

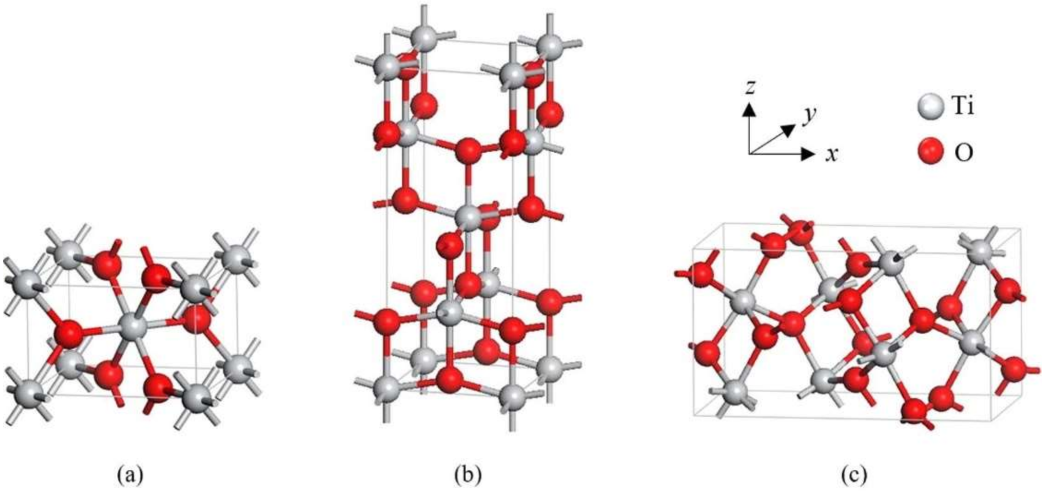

Figure 2. 10. TiO_2 crystalline forms (a) rutile, (b) anatase and (c) brookite. (Reprinted with permission from (Samat, Ali, Taib, Hassan, & Yahya, 2016), Copyright: Creative Commons CC-BY).

2.6.4 Biocatalysts

Biocatalytic reactions frequently occur under mild operational conditions, thus reducing energy needs, process hazards, product purification requirements, and wastewater volumes (Aransiola, Ojumu, Oyekola, Madzimbamuto, & Ikhu-Omoregbe, 2014; Chang, Liao, Lee, & Shieh, 2005; Hosseini et al., 2019; Macrae & Hammond, 1985; Meher, Churamani, Arif, Ahmed, & Naik, 2013). The most common biocatalysts utilized are yeast and enzymes (Table 2. 10), which can be applied in their free or in immobilized form.

Yeasts can catalyse esterification and transesterification reactions. Therefore, they are considered a green material for reducing the requirement of feedstock pretreatment, e.g. removal of water and FFA, and product purification treatment. Reactions occur under mild operational conditions (25-45°C and pH of 5.5 – 7.0, Devanesan et al., 2007), but the catalyst requires an incubation period as a pretreatment step.

Likewise, esterification and transesterification can be catalysed by enzymes, most commonly lipases, which can be derived from animals (dairy and pancreatic), vegetables (soy, cotton and rye) or microbials (yeasts, fungi and bacteria) (Arpigny & Jaeger, 1999; Dalla-Vecchia, Nascimento, & Soldi, 2004; Kapoor & Gupta, 2012). Lipases achieve high selectivity, high purity, a reduction in wastewater, and do not cause saponification (Al-Zuhair, 2007; Severson, Martín, & Grossmann, 2013). Vegetable oils, WCO or animal fat, have been used as feedstock (Macrae & Hammond, 1985; Otero, Ballesteros, & Guisán, 1988; Rosset et al., 2019; Tamalampudi et al., 2008; Wancura et al., 2019; Xie & Ma, 2009).

The application of enzymes has a number of disadvantages. In their free form, they show low stability and recoverability, which causes significant process costs and requires strict operational control (Chiou & Wu, 2004; Severson et al., 2013). The most common free lipases used are *Candida* (28%), *Thermomyces* (14%), *Burkholderia* (14%), *and Rhizopus* (12%) (Dutra et al., 2022). Lipase from *Candida antarctica subtillis,* CALB (EC 3.1.1.3), is one of the most common lipases studied (Dutra et al., 2022). These lipases are hydrolytic enzymes capable of acting over a wide range of pH (6.0-8.0) and temperatures (30–70°C) (Dalla-Vecchia et al., 2004; Ghanem & Aboul-Enein, 2005; Macrae & Hammond, 1985). Immobilization of lipases tends to reduce their enzymatic activity, but at the same time increases their chemical stability and facilitates their recovery (Table 2. 11) (Alnoch et al., 2020; Sipponen et al., 2018).

Double immobilization, e.g., adsorption followed by entrapment, can improve the performances of biocatalytic processes. Following this approach, CALB maintained its enzymatic activity of 70% after immobilization onto lignin nanospheres confined into calcium alginate hydrogel beads (Sipponen et al., 2018), of 94% when immobilized onto cellulose acetate-coated Fe_2O_3 nanoparticles (N. Singh et al., 2013), and of 95% when immobilized onto Fe_3O_4 magnetic nanoparticles entrapped into chitosan (Hosseini et al., 2019), respectively. These studies revealed that double immobilization results in microbead shapes that are small enough to increase the surface area and allow access to the catalyst, but large enough to allow recovery and handling of the microbeads.

Table 2. 10: *Biodiesel produced by biocatalyst.*

Reactor	Reaction[a]	Feedstock	Alcohol	Oil: Alcohol	T (°C)	Catalyst	Support	Wt	t (min)	Biodiesel (%)	N. Cycles (Reuse)	Biodiesel (%) reuse	Ref.
Batch	Est/Trans	WCO	MeOH	1:4	40	CALB	Fe_3O_4 MNPs@TEOS-TSD	1 g	1800	96	6 (10)	70 (15)	(Parandi et al., 2022)
Batch	Trans	WCO	MeOH	1:6	35	B. *cepacia*	SPION[b]	25/10/10[c]	2100	91	5	54	(Karimi, 2016)
Batch	Trans	Soybean oil	MeOH	1:4	35	C. *rugosa*	Magnetic chitosan microspheres		1800	87	4	72	(Xie & Wang, 2012)
Batch	Trans	*Jatropha curcas* oil	MeOH	1:6	37	Lipase from *Aspergillus niger*	PDA-TiO_2 NPs	10	1800	92	8	[d]	(Zulfiqar et al., 2021)
Microreactor	Trans	Sunflower oil	MeOH	1:2.5	30	lipase from *Thermomyces lanuginous*	-	4%	-	-	-	-	(Abdulla Yusuf et al., 2020)
Microreactor cont	Trans	Soybean oil	MeOH	1:7	50	CALB	-	-	53	95	-	-	(Bi, Zhou, Jia, & Wei, 2017)
Microreactor cont	Trans	WCO	MeOH	1:90	40	Lipase from *Thermomyces lanuginosus*	γ-Fe_2O_3	-	20	92	-	-	(Gojun, Šalić, & Zelić, 2021)
MFBR[d]	Trans	WCO	MeOH	1:4	35	*Bacillus subtillis* cells	*Fe_3O_4-PVA*	12%	2880	89	10	82	(J. Liu, Chen, Yan, Yi, & Yao, 2022)

[a]Alcohol: Methanol.[b]Superparamagnetic iron oxide nanoparticles; [c]25 wt. %, water content of 10 wt. % and n-hexane content of 10 wt. %; [d]Residual activity: ~9 U.mg^{-1}.min^{-1} (1 cycle) and ~2.5 U.mg^{-1}.min^{-1} (8 cycles); [d]magnetically fluidized bed reactor.

Table 2. 11: *Lipase immobilization efficiency comparison by REA analysis.*

Enzyme	Support 1	Support 2	REA (%)	Ref.
CALB	Calcium alginate microbeads	-	100%	(Rosilene Andrea Welter, Santana, Carvalho, Melani, Oelgemöller, de la Torre, et al., 2022)
CALB	Octyl agarose	-	100%	(Peirce et al., 2016)
CALB	Silica-lignin matrix	-	92%	(Zdarta et al., 2016)
CALB	Calcium alginate beads		88%	(S. Zhang et al., 2013)
CALB	AuNPs	-	80%	(Barros, Santos, Barbosa, Piovan, & Riegel-Vidotti, 2019)
CALB	TiO_2	-	289%	(Rosilene Andrea Welter, Santana, Carvalho, Melani, Oelgemöller, de la Torre, et al., 2022)
CALB	TiO_2	Calcium alginate microbeads	232%	(Rosilene Andrea Welter, Santana, Carvalho, Melani, Oelgemöller, de la Torre, et al., 2022)
CALB	Fe_3O_4	Chitosan nanoparticles	95%	(Hosseini et al., 2019)
CALB	Fe_2O_3	Cellulose acetate-coated	94%	(N. Singh et al., 2013)
CALB	Lignin nanoparticles	Alginate beads	70%	(Sipponen et al., 2018)
Lipase from porcine pancreas	$Zn_3(PO_4)_2$	-	147%	(B. Zhang et al., 2016)
Candida rugosa lipase	Glyoxyl agarose	-	50%	(Otero et al., 1988)
Lipase from porcine pancreas	$Cu_3(PO_4)_2$	-	460%	(Cui, Zhao, Liu, Zhong, & Jia, 2016)
Candida rugosa lipase	Fe_3O_4	-	60%	(Xie, Hu, & Yang, 2015)
Lipase from porcine pancreas	TiO_2	Chitosan	100%	(Deveci et al., 2015)
Candida rugosa lipase	Fe_3O_4	alginate polyaldheyde	60%	(Hou, Qi, & Zhu, 2015)

2.7 Microscale plant for biodiesel production

Microscale plants integrate microfluidic concepts, a technology used to manipulate fluids in microscale processes. Generally, microdevices have a volume between 10 and 1000 µL (Balbino et al., 2016; Dimov et al., 2008; Santana, Lopes, Silva, & Taranto, 2018). This technology has been investigated experimentally and numerically in several areas such as biological systems, liquid-liquid extraction, food and pharmaceuticals industries, chemical waste degradation, and biodiesel synthesis (Balbino et al., 2016; Dimov et al., 2008; Farra et al., 2012; Feng et al., 2012; Ho, Ng, Li, & Yoon, 2015; Neethirajan et al., 2011).

Microchannels reactors, compared with conventional industrial plants, have advantages such as shorter residence times, higher heat and mass transfers, and easier management, maintenance and operational control (Bannatham et al., 2021). Mass transfer tends to be 30-times higher than on traditional scales (Bannatham et al., 2021). Moreover, the better physical and energetic homogeneity increases the process viability without mass and heat spots that can damage the process system.

The use of micromodules facilitates process maintenance. In the case of saponification, for example, microplants can reduce the volumes of water and reactants. When operated in parallel, only the modules where process problems occur require exchange. In contrast, traditional batch system demand shut-down of the whole plant. Biodiesel purification by traditional processes includes distillation, filtration, liquid-liquid extraction, or, more often, gravitational separation (Fonseca, Teleken, de Cinque Almeida, & da Silva, 2019). When performed in microreactors, gravitational separation is not possible, but other effective separation methods based on liquid-liquid extraction (Johnson, Zawadzka, Deobald, Crawford, & Paszczynski, 2008; Kralj, Sahoo, & Jensen, 2007), centrifugal forces (Nasiri et al., 2020), and micro-heat exchanger (Santana, Sanchez, & Taranto, 2017) have been developed instead.

Flexible scale-up is achieved in serial or parallel microdevices (numbering up), although this requires substantial investment costs (Roberge et al., 2005; Terry et al., 1979; R. Welter, Silva Jr., de Souza, Lopes, Taranto, & Santana, 2022). Microdevices can be produced by numerous 3D printing techniques (photolithography, soft lithography, moulding microfabrication, and laser ablation) using a range of suitable materials (glass, polymers, metals, ceramics) (Bishop et al., 2015; Coltro et al., 2007; M. G. C. da Silva, Canevesi, Welter, Vieira, & da Silva, 2015; de Carvalho, Taketa, Garcia, Han, & de la Torre, 2021; Santana et al., 2018). For example, Billo and co-workers constructed a microplant capable of producing 2.8 L.min^{-1} of biodiesel (Billo et al., 2015). The microplant comprised of 35 manifolds with eight modules of 50 devices each, totalling 14.000 microreactors.

The knowledge of fluid flow behaviour and microdevice design is essential to develop optimal systems. Computational fluid dynamics (CFD) techniques are thus linked to process design approaches. CFD generates process information based on different parameters (e.g. density, viscosity, temperature, molarity, concentration, and experimental data) and generates information to optimize the process (Lax, 2007).

An analysis of microdevice design is fundamental to improve the system efficiency by promoting turbulent mixing spots and increasing the contact area between the reagents. The reactants are pumped into the microchannels in small, interspersed segments, and the mass transfer, which facilitates the reaction, occurs across the borders of the reactants (M. Lukić & Vrsaljko, 2021). To achieve better transfer mass, the design of microdevices can be optimized by reducing the channel diameter, using a complex channel geometry, or implementing micromixers.

The relevance of the diameter of the channels was evaluated for biodiesel produced from sunflower oil. For a residence time of 252 s, microchannels of 0.96 mm and 0.46 mm in diameter resulted in similar conversions of 89% and 92%, respectively. The difference was more apparent with 43 % and 80%, respectively, when the residence time was reduced to 112 s (Guan et al., 2009). Thus, smaller cross-sections increase conversions by increasing the pressure drop, but this approach can cause leaks in the system and requires more energy.

Micromixers attached to the inlet of microreactors and microchannels with complex channel designs have been developed for biodiesel production with improved reagent mixing. The use of a T-shaped micromixer coupled to a microtube (Figure 2. 11) was compared with zigzag microchannels with a T-shape inlet (Figure 2. 12). Following the same operation conditions (1mol TGL:9mols MeOH, 1.2 w/w_t % KOH, 60ºC), the micromixer coupled to the microchannel resulted in a conversion of 89% (residence time of 180 s) (Rahimi, Aghel, Alitabar, Sepahvand, & Ghasempour, 2014), while the complex zigzag design resulted in a conversion of 99.5% (residence time of 28 s) instead (Wen, Yu, Tu, Yan, & Dahlquist, 2009). Likewise, laminar versus turbulent flow patterns were evaluated for biodiesel produced from castor oil (1TGL:9 EtOH, 1 w/w_t% NaOH, 50ºC, Figure 2. 13). In turbulent flow mode (Tesla-microchannel design), a 93% conversion was achieved, compared to 76% by laminar flow (T-shape) and 87% by intermediary flow (Omega-shape). Subsequent experiments were conducted under the same operating conditions and with the same channel designs but using 1 mol TGL:24 mol EtOH instead of 9 mol EtOH, resulting in 97%, 93% and 95% conversion, respectively (Martínez Arias et al., 2012). Hence, the increase in mass transfer due to turbulent mixing caused lower alcohol content requirements.

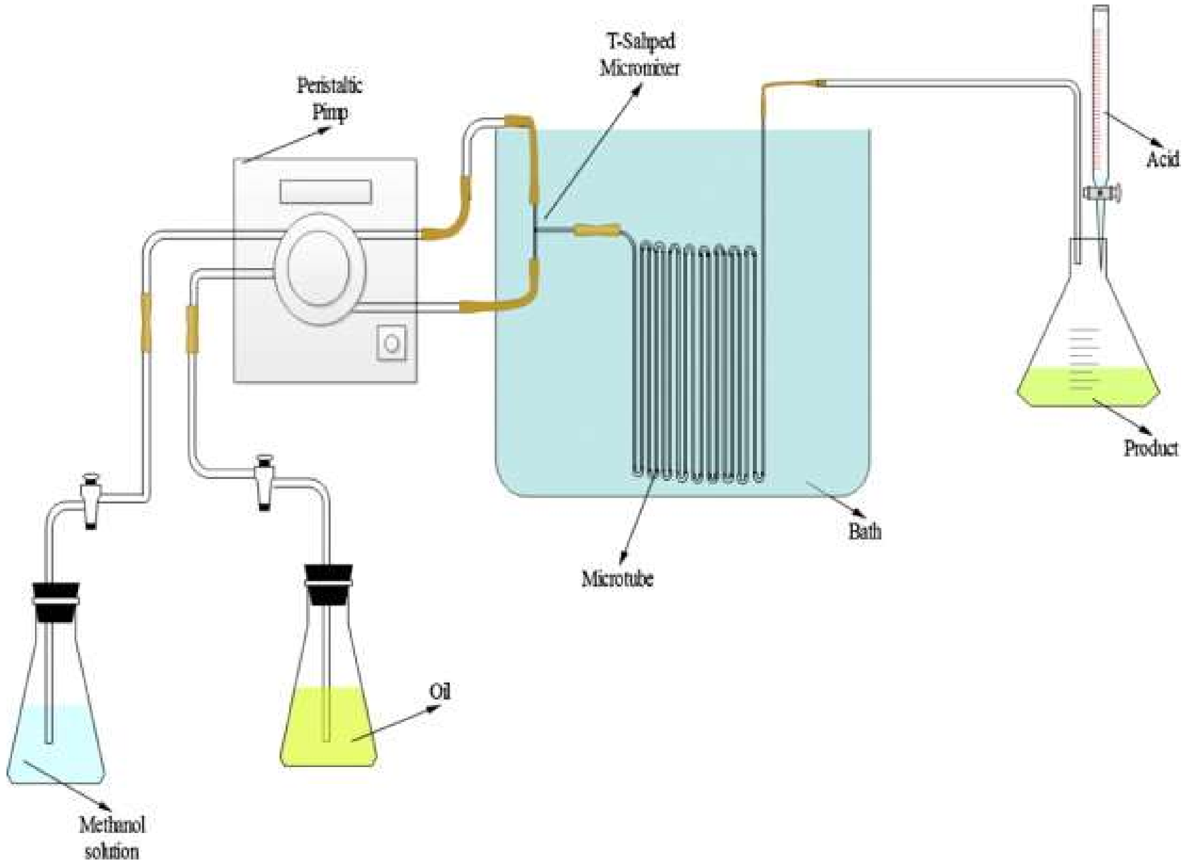

Figure 2. 11. T-shaped micromixer coupled to a microtube reactor to produce biodiesel. (Reprinted with permission from Rahimi et al., (2014) and Elsevier, Copyright (2014) license number: 5360540097272).

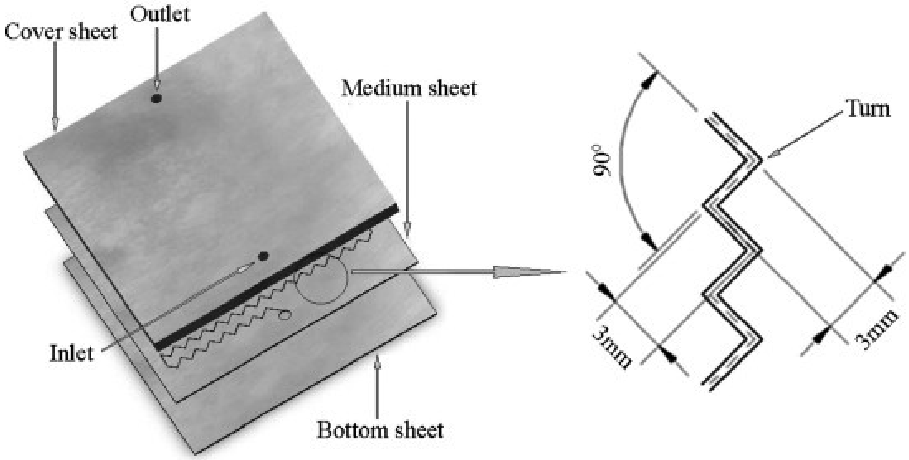

Figure 2. 12. Zigzag microchannel design reactor to produce biodiesel (Reprinted with permission from Wen et al., (2009). and Elsevier, Copyright (2009) license number: 5GB494627212).

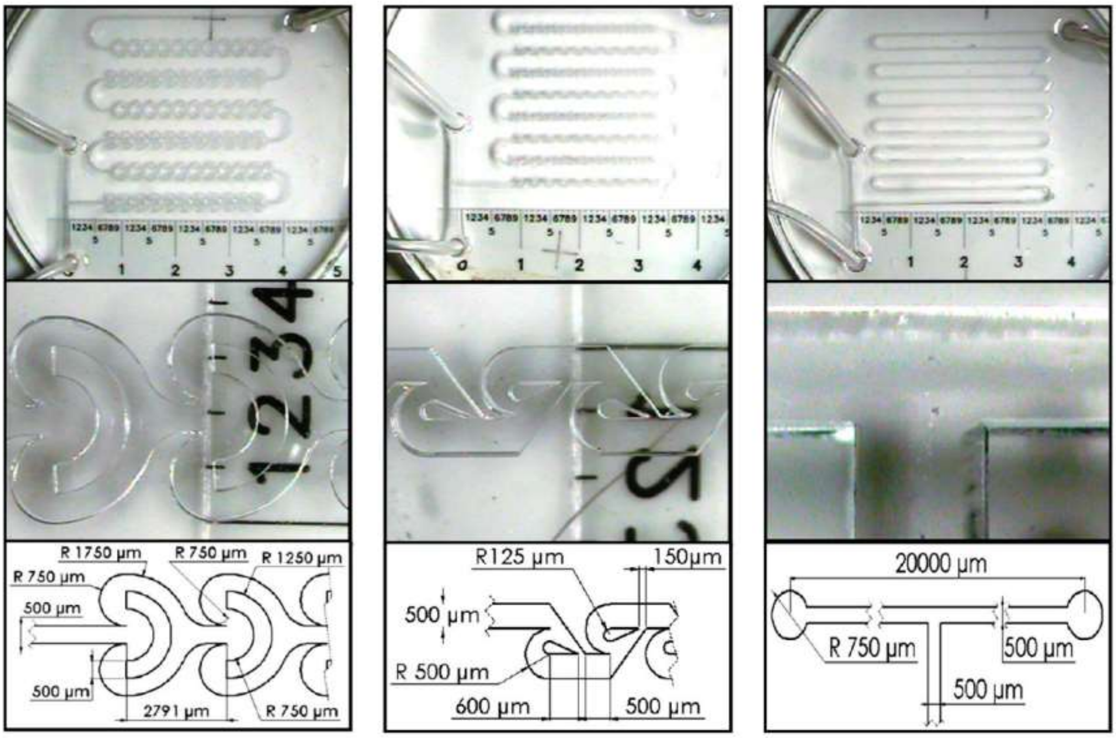

(a) (b) (c)

Figure 2. 13. Microchannels designs for microreactor used to produce biodiesel. (a) Omega-shaped, (b) Tesla-shaped, and (c) T-shaped (Reprinted with permission from Martínez Arias et al., (2012), Copyright (2012) American Chemical Society).

The microdevice design also impacts the system's temperature requirement. For microdevices that cannot achieve good mixing, operation at the boiling point of the alcohol may be considered. Hence, the mixture changes from a liquid–liquid interface to a gas–liquid interface, resulting in convective mixing and consequently improving conversion towards FAAE. However, these operation conditions demand more energy, and the reactor system becomes more susceptible to leaks and high-pressure points. Using optimized designs, however, the temperature requirements for optimal conversion may be lower.

Biodiesel obtained by homogeneous alkali transesterification (liquid-liquid interface) was generated in two microdevices (poor mixing *versus* turbulent spots) at 30, 50, and 70°C, respectively. The simple system resulted in 66%, 73%, and 88% conversion at these temperatures. In contrast, the device with turbulent spots resulted in 75%, 93%, and 93% conversion over the same temperature range (Martínez Arias et al., 2012). Hence, the reactor design with turbulent spots reduces the energy requirements as superior conversions were obtained if compared to the simple system with laminar flow.

The mass transfer increment by microdevice design optimization improves the efficiency and reduces the alcohol content requirement and the residence time. Thus, microchannels with a design that generate chaotic and turbulent spots of the reactants flow are desirable for an efficient microsystem.

While homogeneous catalysts have been studied most extensively for biodiesel production in microdevices, heterogeneous catalysts have likewise attracted attention. The use of low-cost heterogeneous catalysts (KOH/Clinoptilolite (Mohadesi et al., 2020b), kettle limescale (Mohadesi et al., 2019), and cow bone (Mohadesi et al., 2021) to produce biodiesel from WCO were evaluated in microdevices, and conversions of 97%, 93%, and 99% conversion were achieved. A semi-industrial pilot microreactor (200 mL, Figure 2.14) was used for WCO-methanol transesterification using kettle limescale as the catalyst (62°C, 8.9 wt. % catalyst, 1.7methanol:3oil volume ratio). Optimized process conditions were reached with a residence time of 15 minutes (93% conversion), compared to 50 minutes using the conventional batch reactor process (Mohadesi et al., 2019).

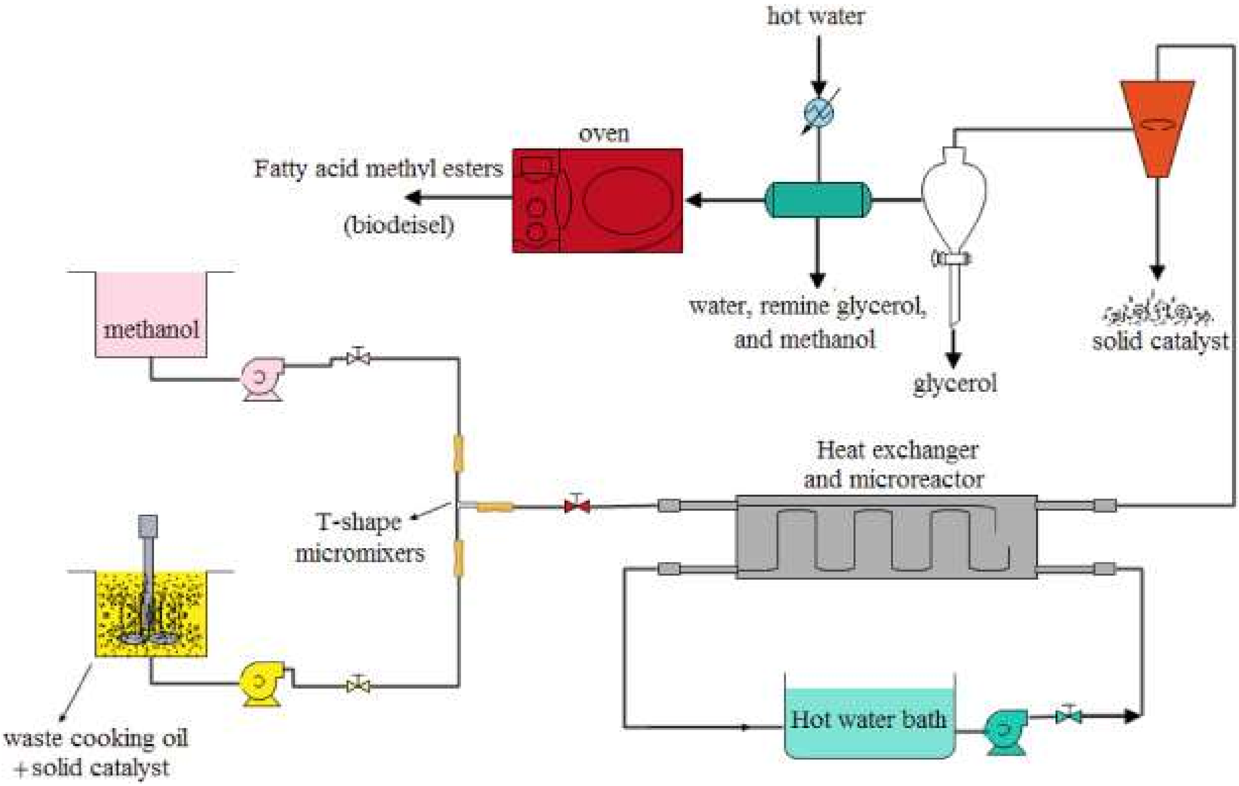

Figure 2. 14. Semi-industrial pilot microplant used for biodiesel productin by WCO and kettle limescale as the catalyst (Reprinted with permission from Aghel et al., (2019) and Elsevier, Copyright (2019) license number: 5360501088909).

Lipases are common heterogeneous catalysts applied to biodiesel production by esterification and transesterification. However, these enzymes are expensive, difficult to immobilise, retain and recover, easily leach, and require careful control of the operational conditions. The implementation of microdevices reduces catalyst leaching and maintenance, and enables a better control of the operation conditions. Lipases have consequently been studied in microreactors with edible and non-edible oils (Budžaki, Miljić, Tišma, Sundaram, & Hessel, 2017). Parallel microdevice modules furthermore minimize enzyme losses in the case of process complications, as only affected units would have to be stopped, while all remaining units would continue production. A microplant with a microreactor (catalyst: lipase from *Thermomyces lanuginosus* (723±19 U/mg) and microseparator (extraction by deep eutectic solvents – DES) in series resulted in 94% conversion using sunflower oil and ethanol (1:10 molar ratio, 40°C, 20 minutes residence time) (Gojun et al., 2021).

2.8 Microflow photochemistry

Photochemical processes have been successfully investigated in microreactors, for example, for the synthesis of steroids (Sugimoto, Fukuyama, Sumino, Takagi, & Ryu, 2009), L-pipecolinic acid (Takei, Kitamori, & Kim, 2005) and pinacol from benzophenone (H. Lu, Schmidt, & Jensen, 2001), as well as the degradation of pollutants (He, Li, Zhang, & Wang, 2010; Kanakaraju et al., 2014). The large surface area and narrow channel depth of microdevices promote better irradiation and hence improve the general photoreaction efficiency. Naturally, microdevices need to be transparent and are manufactured from materials with cut-wavelengths compatible with the irradiated light, e.g., glass, quartz, silicon, and fluoropolymers (Ahsan, Gumus, & Erickson, 2013; Lin, Ma, Fielitz, Obare, & Ofoli, 2012; H. Lu et al., 2001; Ramos, Ookawara, Matsushita, & Yoshikawa, 2014). Photocatalysts can be introduced as an externally mixed colloidal system, or can be coated (e.g. sol-gel (Domínguez et al., 2021), sputtering (Kestenbaum et al., 2002), spray coating (Deshlahra, Pfeifer, Bernstein, & Wolf, 2011), spin coating (Schimpf et al., 2002), or vapor+solvent depositing (Huesing et al., 2003) to the internal microchannel surface. In the latter case, the compatibility between the catalyst and the internal surface of the microchannels needs to be considered. Immobilization also frequently requires pretreatment of the channel material. Silver-coated TiO_2 (0.8 wt. % Ag/TiO_2) was immobilized in a microphotoreactor using a sol-gel method and this device was subsequently utilized for wastewater treatment (Figure 2. 15) (Domínguez et al., 2021). An efficiency of 99% was achieved under the optimised operational conditions (10.22 $\mu l.min^{-1}$ flow rate, 12.94 $mg.L^{-1}$ inlet concentration, 6.2 initial solution pH, and 7.53 $W.m^{-2}$ min UV-LEDs light intensity) (Eskandarloo, Badiei, Behnajady, & Ziarani, 2015). The use of TiO_2 nanotubes has also been evaluated for different processes such as phenol photoeletrocatalysis in fixed-bed microreactors with 80% efficiency (Suhadolnik, Pohar, Likozar, & Čeh, 2016) and biodiesel production from oleic acid and methanol with 86%

efficiency (Manique et al., 2016), respectively. The combination of photochemistry and microfluidics can improve a range of photocatalytic processes and enables efficient and economical processes.

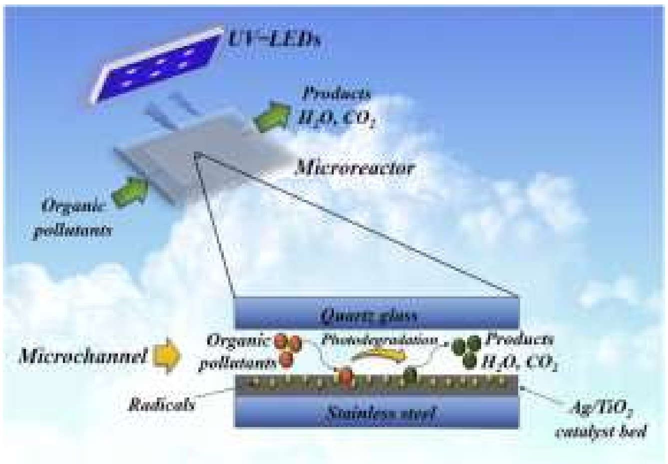

Figure 2. 15. Microphotoreactor coated by Ag/TiO_2 for organic products degradation (Reprinted with permission from Eskandarloo et al., (2015) and Elsevier, Copyright (2019) license number: 5360550205441).

2.9 Conclusion

Biodiesel production has seen a sharp increase to meet its growing demand as a fuel source. However, new technologies are needed to improve or replace current industrial processes. The use of microdevices and heterogeneous catalysts such as enzymes and photocatalysts represent interesting approaches as they overcome many of the issues encountered in traditional homogeneous processes using strong acids and alkalis. However, further research is urgently needed to reach scalability, obtain kinetic and thermodynamic parameters, and achieve process optimization. WCOs represent an eco-friendly alternative to edible oils, reducing the competition with food industries and solving the environmental burden caused by these waste materials.

Chapter III

Droplet microfluidics for double lipase immobilisation using TiO_2 and alginate microbeads

Permission: This article was published in Journal of Industrial and Engineering Chemistry, Vol 110, Rosilene Andrea Welter[1,2], Harrson Silva Santana[1], Bruna Gregatti Carvalho[1], Natalia Melani[1], Michael Oelgemöller[2,3], Lucimara Gaziola de la Torre[1], Osvaldir Pereira Taranto[1], Droplet microfluidics for double lipase immobilisation using TiO_2 and alginate microbeads, 576-586, Copyright Elsevier (2022) https://doi.org/10.1016/j.jiec.2022.03.028

Filiation: (1) School of Chemical Engineering, University of Campinas, Postcode 13083-852, Campinas, SP, Brazil. (2) College of Science and Engineering, James Cook University, Postcode Qld 4811, Townsville, Queensland, Australia. (3) Faculty of Chemistry and Biology, Hochschule Fresenius gGmbH-University of Applied Science, Postcode D-65510, Idstein, Germany.

Abstract

A double immobilisation technique was developed for *C. antarctica lipase* (CALB) that improved its enzymatic activity and solved difficulties frequently observed in reactions catalysed by lipases. The first immobilisation consisted of CALB adsorption onto a TiO_2 nanoparticle surface ($CALB_{TiO_2}$). The adsorption was carried out by an oriented monolayer formed by CALB's hydrophilic amino acids and the TiO_2 surface, leaving the CALB's active site accessible for reaction. As a result, an increase in enzymatic activity was achieved. The Relative Enzymatic Activity ((REA) obtained was 289%. The second immobilisation consisted of $CALB_{TiO_2}$ entrapment into calcium alginate microbeads $[(CALB_{TiO_2})_{EDTA-Ca}]$, obtained by an internal crosslinking ion-exchange mechanism and using microfluidic droplet technique. The microbiocatalyst obtained, $(CALB_{TiO_2})_{EDTA-Ca}$, retained a high enzymatic activity ($REA_{t=0}$=232%) and stability ($REA_{t=30days}$=263%) at a size (diameter, $Ø=8.9\cdot10^4$ nm) that enabled easier recovery than $CALB_{TiO_2}$ ($Ø=2.3\cdot10^2$ nm) or $CALB_{Free}$ ($Ø$=5.0 nm), and showed a favourable porosity for diffusion without releasing $CALB_{TiO_2}$. Although the microbeads showed $CALB_{Free}$ leaching, as demonstrated by the loss of REA after a mechanical resistant test, $(CALB_{TiO_2})_{EDTA-Ca}$ maintained an almost constant REA.

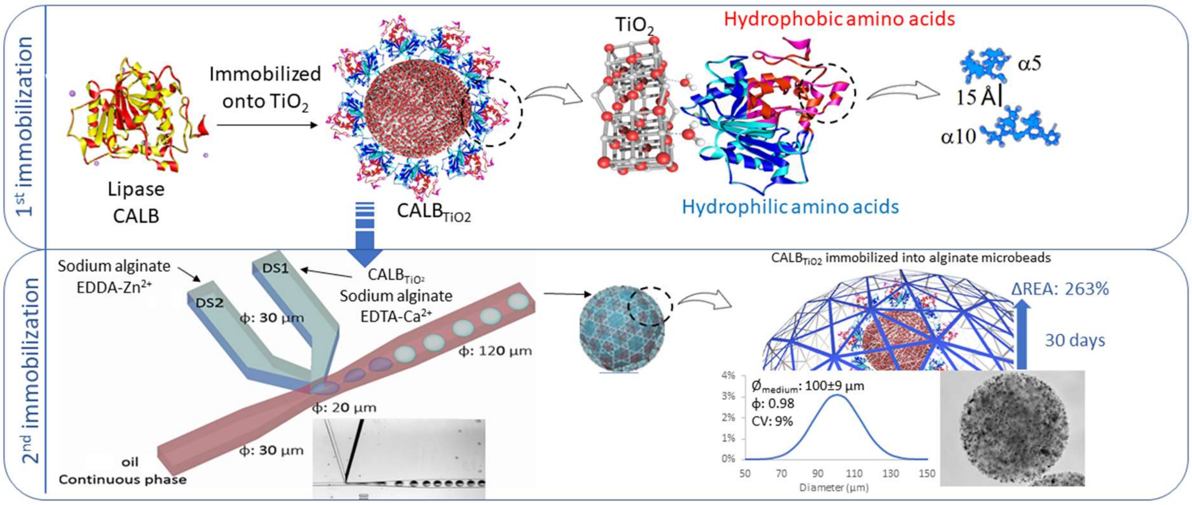

Figure 3. 1. Graphical abstract: Droplet microfluidics for double lipase immobilisation using TiO_2 and alginate microbeads.

Keywords

Lipase immobilisation, droplet microfluidic, titanium dioxide, *Candida antarctica* lipase B, enzymatic catalyst.

3.1 Introduction

The development of an efficient immobilisation method represents a fundamental challenge for the adaptation of lipases' catalysis in chemical processes. One of the most common lipases studied in this regard is from *C. antarctica (*CALB-EC 3.1.1.3). However, CALB is frequently used after immobilisation with acrylic resin or biopolymer matrices. These materials are known to favour catalyst recovery and enzyme stability but show reduced enzymatic activity (Joyce, Kempson, & Prestidge, 2016; Macrae & Hammond, 1985; Sipponen et al., 2018). For example, CALB holds only 51% of its enzymatic activity compared to free lipases when immobilised on acrylic resin (Sipponen et al., 2018), mainly due to changes of the enzyme's amino acids after the chemical immobilisation processes. Likewise, the lipase of *Yarrowia lipolytica* immobilised on calcium alginate biopolymer showed a 50% reduction in enzymatic capacity due to the loss of enzyme to the medium (da S. Pereira, Fraga, Diniz, Fontes-Sant'ana, & Amaral, 2018). Lipase immobilisation requires an understanding of the chemical and physical characteristics of the enzyme and its amino acids (Arana-Peña, Rios, Carballares, Gonçalves, & Fernandez-Lafuente, 2021).

Enzymes are flexible structures and their tertiary and quaternary structures can be altered according to the conditions of the environment, type of immobilisation and interactions with the support. The hydrophobicity of the surroundings, for example, causes the enzyme to reorganise its structures to achieve the lowest activation energy (van Santen, 2009). This behaviour is one of the main features that defines enzyme stability, retention on the support, and catalyst activity (Joyce et al., 2016; Uppenberg, Hansen, Patkar, & Jones, 1994; Zisis et al., 2015). In the presence of a hydrophobic support, lipases are linked in multiple layers to hydrophobic residues, but their active sites are no longer accessible for reaction. Consequently, the improved immobilisation results in lower catalyst activity (Joyce et al., 2016; Reis et al., 2009; Tan, Lim, Ong, & Pang, 2019) (Mechanism described in Section S3.1 and Figure S3.1.a. of SI - , APPENDIX B). In contrast, in the presence of hydrophilic support, the hydrophilic chain residues of lipase are linked by one layer around the support. This keeps the hydrophobic residues free and the active site accessible for reaction, resulting in a higher catalyst activity (Joyce et al., 2016; Laszlo & Evans, 2007; Zisis et al., 2015) (Section S3.1 and Figure S3.1.b of SI - APPENDIX B).

In addition, hydrophilic supports help to retain water content, which is essential for enzyme maintenance (Laane & Verhaert, 1987; Zaks & Klibanov, 1985). Cejudo-Sanches et al. (2020) immobilised *Rhizomucor miehei* lipase (RML) onto octyl-agarose and poly-allylamine (PAA). As a result, the immobilised lipase showed a 6-times higher catalytic activity, and it was found 44-times more stable. The hydrophilicity of the support was found crucial for this improvement. Badoei-dalfard et al. (2022) immobilised lipase KM12 on glutaraldehyde-activated graphene oxide/chitosan/cellulose acetate nanofibers. Subsequently, the immobilised lipase showed a 20% higher catalytic activity with a decrease of 20% after 10 reuse cycles. Hydrophilic elements surrounding the lipases generally tend to improve enzymatic activity; for example, hydrophilic solvents resulted in an increase of 4-8%, while hydrophobic solvents caused a reduction by 4-30% (Badoei-dalfard et al., 2022). Arana-Peña et al. (2021) immobilised different lipases on hydrophobic supports. According to their results, CALB maintained a REA (Relative enzymatic activity; considered a percentage ratio of free enzyme enzymatic activity) of about 100% after immobilisation with high stability. However, there is no general process for lipase immobilization that considers the lipase complexity and chemical/physical properties.

According to Zisis et al. (2015), CALB, different from other lipases, can act as an esterase in the presence of a hydrophilic solvent, or like a lipase in the presence of a hydrophobic solvent. Thus, it can be attached to hydrophilic supports such as TiO_2 through its hydrophilic amino acids, and still maintain a high enantio- and regioselectivity for hydrophobic substrates through its hydrophobic amino acids, where the active site and its respective lids (α5 and α10) are located. As hydrophilic materials for lipase chemical immobilisation, nanoscale supports like inorganic oxides (Fe_2O_3, SiO_2, CuO_2, Ti_8O_{15}, and TiO_2) with strong adsorption abilities (Mukhopadhyay, Dasgupta, Chattopadhyay, & Chakrabarti, 2012) and large surface areas have been studied (Foresti, Valle, Bonetto, Ferreira, & Briand, 2010; Hou et al., 2015; Viñambres, Filice, & Marciello, 2018). However, interactions with these inorganic oxides may induce modifications in the enzyme's conformation, which can subsequently impact on the response of the active site with the medium (Köhler & Wünsch, 2007). In the case of TiO_2 and CALB, this resulted in enzymatic activity increment (An et al., 2020) and chemical/thermal stability (Chronopoulou et al., 2011). Zhou et al. (2021) immobilised *Aspergillus oryzae* lipase on ethenyl triethoxy silane modified TiO_2, and the immobilised lipase showed an REA of 428%. Likewise, lipase from porcine pancreas showed an REA of 147% when immobilised on $Zn_3(PO_4)_2$ (B. Zhang et al., 2016) and REA of 460% when immobilised on $Cu_3(PO_4)_2$ (Cui et al., 2016), respectively. Nano-sized porous matrices increase the surface area and hence contact with substrates, which subsequently improves catalytic capacity (Shuai, Das, Naghdi, Brar, & Verma, 2017). Although lipases immobilised on inorganic oxides have shown satisfactory results, they have some disadvantages, such as the leaching of enzyme into the medium by desorption, and the nanoscale size that hinders convenient catalyst recovery.

Physical immobilisation usually takes place on supports larger than nanoscale, facilitating biocatalyst recovery. However, these favour enzyme leaching (Alnoch et al., 2020; Fundueanu, Nastruzzi, Carpov, Desbrieres, & Rinaudo, 1999). Hydrogels like alginate, agarose, chitin, chitosan, and cellulose are frequently used as a support for physical entrapment. They exhibit advantages such as their sustainability, abundance, non-toxicity, and biocompatibility. Gelation processes that result in microbeads provide shapes that, on the one hand, are small enough to increase the surface area, consequently the catalyst access, and on the other hand, are large enough to allow microbeads' recovery and handling (Bassett, Håti, Melø, Stokke, & Sikorski, 2016; de Carvalho et al., 2021; Håti et al., 2016).

One of the most promising gelation processes on microscale is the competitive internal crosslinking ion exchange (CLEX) develope. Bassett et al. (2016). It occurs under mild and reproducible operation conditions without interfering with the enzyme's characteristics (de Carvalho et al., 2021; Oliveira et al., 2019). The CLEX mechanism can also be conducted using microfluidic droplet techniques (DMT) (de Carvalho et al., 2021; Håti et al., 2016). Microfluidic technology has advantages, such as short residence times, process intensification, higher process safety and control, easy heat exchange, favourable reaction kinetics, and easy maintenance and repairs without completely stopping production. Scale-up to desired production scales is simply achieved through serial or parallel setup of microdevices (Roberge et al., 2005; Terry et al., 1979). Microbeads generated by DMT have been applied to the immobilization of different biocatalysts such as enzymes, bacteria or antibodies, as well as for drug encapsulation (Bassett et al., 2016; de Carvalho et al., 2021; Håti et al., 2016; Mazutis, Vasiliauskas, & Weitz, 2015; Oliveira et al., 2019). The degree of physical entrapment can be tuned to either release the material by diffusion or to strongly entrap it. In both cases, the relation between encapsulated material and pore size defines the material's diffusion/entrapment behaviour. When using lipases, efficient entrapment is desired, but with high diffusion of the subtrate. However, lipases frequently have diameters smaller than most pores of biopolymer matrices, which consequently results in their leaching.

Recently, double immobilisation techniques, e.g. adsorption followed by entrapment, have been studied to overcome these deficiencies. Following this approach, CALB was immobilised onto lignin nanospheres confined into calcium alginate hydrogel beads. The enzymatic activity remained at 70% compared to the free CALB (Sipponen et al., 2018). Silva et al. (2011) obtained a high thermal and chemical stability for lipase from *Burkholderia cepacia* double immobilised by SiO_2/Chitosan. Porcine pancreatic lipase was double immobilised by TiO_2/Chitosan and resulted in an REA of 84% with high thermal and chemical stability (Deveci et al., 2015). The use of double immobilisation involving magnetic nanoparticles has been explored for easy recovery (Netto et al., 2013; Xie & Zang, 2018). However, these nanoparticles form aggregates due to magnetic dipole-dipole attractions (Baharfar & Mohajer, 2016). The application of a second polymer support may improve the chemical stability and hence decrease aggregation. CALB maintained an enzymatic activity of 94% when immobilised onto cellulose acetate coated Fe_2O_3 nanoparticles (N. Singh et al., 2013), and 95% when immobilised onto Fe_3O_4/chitosan (G. S. Silva et al., 2011), respectively. Other examples are *Candida rugose* lipase fixed on Fe_3O_4/silica (Xie & Zang, 2018), Fe_3O_4/poly(styrene-methacrylic acid) microspheres (Xie & Wang, 2014), Fe_3O_4/graphene (Xie & Ma, 2009), or hydroxyapatite-encapsulated γ-Fe_2O_3 (Xie & Zang, 2017), respectively. The simultaneous entrapment of different lipases has also been studied. *Pseudomonas cepacia* lipase and *Candida antarctica* lipase were immobilised together in Fe_3O_4/hydrophobic sol-gel materials derived from $CH_3Si(OCH_3)_3$ (MTMOS), and REA values of 330% and 210%, respectively, were achieved (Reetz et al., 1998). These studies indicate that double immobilisation processes result in sufficiently small microbeads to increase the surface area and hence access to the catalyst, while at the same time being large enough to allow their recovery and handling.

This work explored a double immobilisation process of attaching the enzyme first by adsorption and subsequently by entrapment. As the initial support, TiO_2 was chosen, thereby improving enzymatic activity and turning the enzyme into a nanostructure. As the second support, alginate microbeads obtained by CLEX via DMT were selected, turning the material into a large structure for easy recovery and adaptation in different reactors including fixed beds. The present study contributes to the growing field of enzymatic catalysis applications and microfluidic techniques applied to catalyst immobilisation. This double immobilisation technology represents an effective method to fix lipases without leaching. Moreover, it may solve challenges that frequently occur in immobilisation processes such as reductions in enzymatic activity, low chemical stability of enzymes, leaching of enzyme into the medium, and poor practical catalyst recovery and reuse.

3.2 Experimental methodology

3.2.1 Materials

Materials and reagents were purchased from Sigma-Aldrich unless specified otherwise: Lipase of *C. antarctica,* CALB (EC 3.1.13) lyophilised powder, p-Nitrophenyl palmitate, titanium dioxide (TiO_2), Fluorinert™ oil FC-40, ethylenediaminetetraacetic acid (EDTA) (Merck), ethylenediamine-N, N′-diacetic acid (EDDA), 3-(N-morpholino) propanesulfonic acid (MOPS) (Merck), perfluorooctanol (PFO) 20% (v/v), sodium alginate, glutaraldehyde, paraformaldehyde (PFA), ethanol and hexamethyldisilane (HMDS). Purchased from Synth: monosodium phosphate, disodium phosphate, calcium chloride dihydrate ($CaCl_2.H_2O$), zinc acetate dihydrate ($Zn(CH_3COO)_2).2\ H_2O$), sodium carbonate (Nuclear), absolute ethanol (LS Chemical), Triton X-100 (Nuclear), dimethyl sulfoxide (Cristália), sodium tetraborate decahydrate (Neon), fluorosurfactant Pico-Surf® (2% v/v) (Sphere Fluidics), polydimethylsiloxane (PDMS) (SYLGARD™ 184 Silicone Elastomer, Brand: Dow Corning) and Aquapel® (Brand: Pittsburgh Glass Works, USA).

3.2.2 Enzymatic activity

Candida antarctica lipase B catalytic activity was measured by p-nitrophenyl palmitate (p-NPP) hydrolysis. The lipase was dissolved in a 0.05 M sodium phosphate buffer solution by using 7 $mg_{enzyme}/mL_{solution}$ ($8.6U/mL_{solution}$) mixed with 1 ml of 0.5% (w/v) p-NPP dissolved in ethanol as substrate and incubated for 5 min at 30°C. The reaction was stopped by adding 2 mL of 0.5 N Na_2CO_3 and centrifugation (10 minutes at 10,000 rpm). The supernatant was diluted to a 1:10 volume ratio and measured by UV/VIS spectrophotometer (410 nm, Micronal - AJX-1900). A standard p-NPP curve with a linear equation of $y = 56.518x - 0.0072$ (R^2=0.9984*)* was obtained*.* Analysis was conducted in triplicate, and the results were given as relative enzymatic activity (% REA). REAs were compared for the sample of interest and the control sample. As the control sample the enzymatic activity of the free enzyme was considered.

3.2.3 Zeta potential of CALB, TiO_2, $CALB_{TiO_2}$, and microbeads

The Zeta potential (ζ) of CALB (7 $mg_{enzyme}/mL_{solution}$), TiO_2 (50 mg/mL), and CALB immobilised onto TiO_2 (molar ratio of 0.3:1) were measured in water at 25°C in triplicate using Malvern Zetasizer Nano ZS equipment with a backscattering detection angle of 173° and 30 runs per measurement.

3.2.4 First immobilization: CALB onto TiO_2 nanoparticle ($CALB_{TiO_2}$)

The lipase was gently mixed with TiO_2 (CALB and TiO_2 molar ratio of 0.3:1) in an aqueous solution with pH 6.7 at 25°C to obtain $CALB_{TiO2}$ for 30 minutes.

3.2.5 Second immobilisation: CALB, TiO_2, and $CALB_{TiO_2}$ by CLEX via DMT

CLEX via DMT was used to produce calcium alginate microbeads, a gelation method successfully used for encapsulation in other works (Bassett et al., 2016; de Carvalho et al., 2021; Håti et al., 2016; Oliveira et al., 2019). This process was employed for three compounds: CALB, TiO_2 nanoparticles, and the first immobilisation product, $CALB_{TiO2}$. TiO_2 nanoparticles were immobilised to evaluate their influence on the gelling process by analysing their impact on the affinity of cations (Ca^{2+} and Zn^{2+}) and chelates (EDTA and EDDA) and consequently interferences in ion exchanges.

The CLEX methodology resulted in microbead formation by internal gelation mechanisms based on competitive ligand exchange crosslinking (Bassett et al., 2016), which depends on the relative ionic affinity between divalent cations and chelates. The CLEX process occurred in a microdevice, Figure 3. 2, via DMT, consisting of one inert continuous phase and two dispersant phases containing chelates and divalent cations. This study was performed with the following aims: (a) to obtain a general microdevice for optimal microbeads production, (b) to generate microbeads without catalyst, and (c) to immobilise enzyme and/or nanometal.

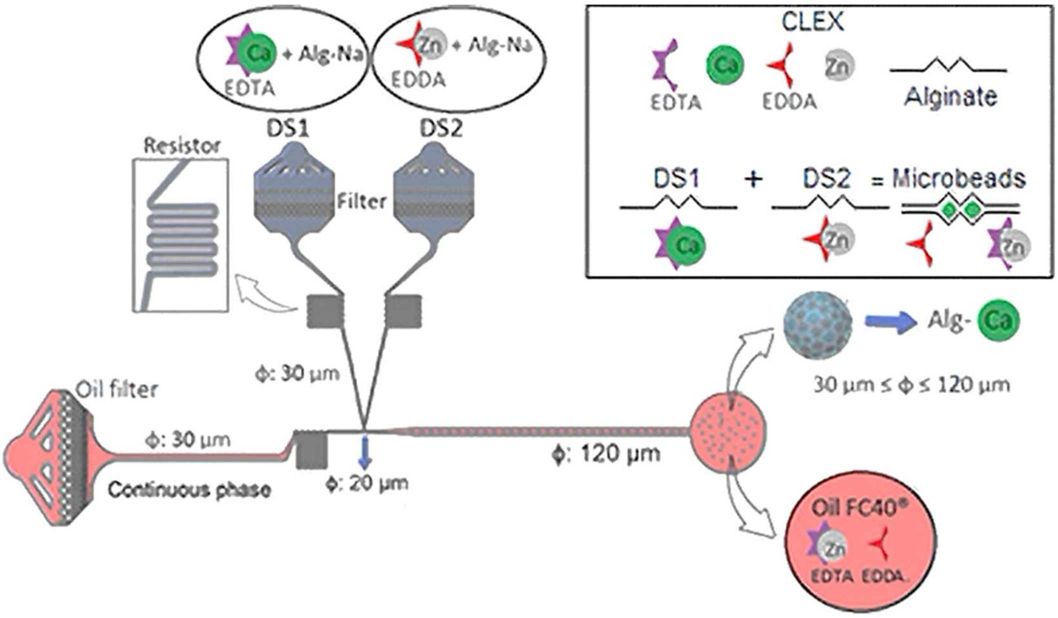

Figure 3. 2. Microdevice for biopolymer microbeads production by internal crosslinking ion exchange (CLEX) via droplet microfluidic technique (DMT). DS1 - Dispersant solution 1, containing EDTA and Ca^{2+}. DS2 - Dispersant solution 2, containing EDDA and Zn^{2+}.

The microdevice was manufactured using the soft lithography technique and made of PDMS and glass. The microdevice's microchannels were treated with Aquapel® to increase their hydrophobicity and improve the liquid flow behaviour (de Carvalho et al., 2021; Oliveira et al., 2019).

The microfluidic device had one continuous oil channel and two droplet dispersant phase channels; all channels had fluid resistors and solution filters. The contact between these three inlets resulted in dispersive emulsion droplets. The flows were fed by microfluidic tubing [PTFE tubing 0.56 mm ID and 1.07 mm OD (Adtech Polymer Engineering, UK)] connected to glass syringes (2.5 mL for the continuous phase and 1 mL for dispersant phases) (Hamilton, USA) and syringe pumps (Harvard Apparatus, PHD ULTRA, USA) (de Carvalho et al., 2021; Oliveira et al., 2019).

Calcium alginate microbeads by CLEX via DMT were produced at 25°C using one continuous phase and two dispersant phases (DS). The continuous phase, which consisted of Fluorinert™ oil FC-40 with fluorosurfactant Pico-Surf® (2% v/v), was pumped at flow rates of 4-10 µL/min. For the dispersant phases, sodium alginate was first dissolved in deionised water with a resistivity of 18 MΩ by vigorously mixing, resulting in a concentration of 2% (wt/vol.). The solutions containing ions and chelates were subsequently added to two different sodium alginate solutions, resulting in two distinct dispersant solutions (pH 6.7), DS1 (containing: 84 mM EDTA, 84 mM calcium chloride dihydrate ($CaCl_2.H_2O$), and 40 mM MOPS) and DS2 (containing: 84 mM EDDA, 84 mM zinc acetate dihydrate ($ZnCH_3CO_2$ H_2O), and 40 mM MOPS). Both dispersant phases were evaluated by using the same flow rate of 2-8 µL/min.

Microbead post-treatment: after microbead manufacturing, the emulsion was broken up using PFO 20% (v/v).

Microbead mechanical resistant tests: the microbeads were washed with MOPS buffer (pH 6.7) by mixing with a stirrer (600 rpm) and subsequent centrifugation (580G) for 1 minute. This process was repeated 3 times.

Microbead physical characteristics' analysis: Images of the microbeads were taken by optical microscopy (Inverted Research Microscope Eclipse Ti-U, Nikon, Japan) and analysed by ImageJ software (National Institutes of Health - NIH, USA). Microparticles' polydispersity was carried out using about 250 microbeads and the coefficient of variation (CV), standard deviation (SD), diameter, ratio, size distribution and sphericity by Feret diameter were determined.

Statistical analysis: All individual experiments were performed in triplicate unless specified otherwise. Data were presented as the means ± standard deviation (SD).

SEM-EDS: Scanning Electron Microscopy (SEM) was conducted using a Quatrro S (Thermo Fisher Scientific) equipped with an Energy Dispersive Spectroscopy (ANAX-60P-B, Termofisher Scientific). SEM images were manipulated by Photopad Professional v. 6.59® to highlight the most important results (Primary SEM images are shown in Section S3.4 of SI - APPENDIX B). For SEM and EDS analysis, the microbeads were dehydrated in four steps as described by Carvalho *et al.* (2001): (i) fixation with glutaraldehyde 2% and PFA 4%, (ii) dehydration with ethanol (ethanol concentration: 50, 70, 95, and 100%), (iii) chemical "critical point drying" using HMDS, and (iv) sample disposing on a glass slide and fixation in stubs with carbon tape.

The immobilisation was carried out for CALB, TiO_2 and $CALB_{TiO_2,}$ as described in Table 3.1. A concentration of 5 mg/mL of CALB and 50 mg/mL of TiO_2 nanoparticles were added to the dispersant solutions, DS1 and/or DS2 (Table 3. 1). After producing microbeads containing CALB, $TiO_{2,}$ or $CALB_{TiO_2}$, the same post-treatment processes, mechanical resistant tests, and physical characteristics were performed as mentioned above.

Table 3. 1: *CALB and TiO_2 immobilisation into calcium alginate microbeads: dispersant solution analysis.*

	DS1	DS2
Free$_{catalyst}$	-	-
(CALB)$_{EDTA-Ca}$	CALB$_{Free}$	-
(CALB)$_{EDDA-Zn}$	-	CALB$_{Free}$
(TiO_2)$_{EDTA-Ca}$	TiO_2	-
(TiO_2)$_{EDDA-Zn}$	-	TiO_2
(CALB$_{TiO_2}$)$_{EDTA-Ca}$	CALB$_{TiO_2}$	-
(CALB$_{TiO_2}$)$_{EDDA-Zn}$	-	CALB$_{TiO_2}$

3.3 Results and discussion

The double immobilisation technique was evaluated for CALB's catalyst efficiency enhancement. Firstly, the lipase immobilisation onto TiO_2 nanoparticles (CALB$_{TiO_2}$) was assessed. This strategy was explored to improve lipase activity and enzyme entrapment in different structures or microgels, and compared the catalytic performance to the free enzyme condition. Secondly, CALB$_{TiO_2}$ was entrapped in calcium alginate microbeads obtained by CLEX via DMT. This method was explored to improve the physical characteristics and to increase the immobilised enzyme dimensions from nanosize (first immobilisation) to microsize (second immobilisation). Consequently, easier handling and recovery was achieved while maintaining high porosity and substrate diffusion.

3.3.1 First immobilization: CALB onto TiO_2 nanoparticle (CALB$_{TiO_2}$)

The CALB binding behaviour onto TiO_2 nanoparticles was investigated in terms of the enzyme adsorption efficiency, catalyst capacity changes, and synergistic relationship between the enzyme's amino acids and the hygroscopic nanometal particles. Zeta potential, optical microscopy, enzymatic activity, SEM, and EDS were used as characterisation techniques. CALB immobilised onto TiO_2 (CALB$_{TiO_2}$) has a larger diameter (nanoscale) when compared with the free enzyme (angstrom-scale). The adsorption process eases handling and recovery and enables a second immobilisation.

According to the zeta potential values (Figure 3. 3), CALB$_{TiO_2}$ (ζ=-41 mV) showed a surface charge similar to CALB (ζ=-36 mV) but lower than TiO_2 (ζ=-25 mV), indicating that the lipase molecules adsorb on the TiO_2 surface (Figure 3. 3). The CALB adsorption is confirmed by SEM analysis (Figure 3. 4.c and Figure 3. 4.d), where enzyme structures can be found as clusters (highlighted in red) spread between titanium nanoparticles (highlighted in blue). However, the enzymes' clusters observed on the TiO_2 surface are smaller than that of free enzyme, indicating a lower agglomeration behaviour with probably an easier access to the enzyme's surface and active site. The CALB adsorption was also confirmed by EDS analysis (Figure 3. 4.a, Figure 3. 4.b, and Figure 3. 4.c), where Mg^{2+} ions are found in CALB and $CALB_{TiO_2}$, but not in TiO_2, indicating the presence of enzyme after the immobilisation process. Although Mg^{2+} is not found in the native CALB structure, it is a specific compound found in the $CALB_{Free}$ that we used, which may be an impurity, that helped to observe the enzyme presence with the support, considering that Mg^{2+} was not found connected to the other compounds.

The enzymatic activity was improved and maintained at a similar level for 30 days (REA of $[CALB_{TiO_2}]_{t=24h}$ =286% and $[CALB_{TiO_2}]_{t=30\ days}$ =263%) (Figure 3. 3; Section S3. 3 of SI - APPENDIX B). The enzymatic activity increase occurred possible because of the oriented adsorption by the hydrophilic amino acids and consequent exposure of hydrophobic residues in the active site (Section S3.3.1 of SI - APPENDIX B). The proposed mechanism for the immobilisation of CALB onto TiO_2 is described in Figure 3. 5. A similar improvement in enzymatic activity was observed in the literature for lipase from porcine pancreas immobilised on $Zn_3(PO_4)_2$ [REA= 147% (ZHANG, Shuang et al., 2013)] and immobilised on $Cu_3(PO_4)_2$ [REA of 460% (Cui et al., 2016)].

The enzymatic activity is also determined by the amino acid residues' expansion or retraction, especially for the active site's hydrophobic lids α5 (residues 139–150) and α10 (residues 266–289). However, the entire enzyme chain is flexible, and some amino acids are more impacted by the surrounding characteristics (Section S3. 1 of SI –APPENDIX B). For example, in the presence of a non-polar solvent such as cyclohexane (ε of 2.02 at 20°C), CALB tends to reduce the total surface area (Δ_{area}: -29 Å^2) and hydrophilic area (Δ_{area}: -361 Å^2). In contrast, the hydrophobic area tends to increase (Δ_{area}: 332 Å^2). Moreover, in water (ε of 80.1 at 20°C), CALB increases the total surface area (Δ_{area}: 616 Å^2), hydrophilic area (Δ_{area}: 339 Å^2), and hydrophobic area (Δ_{area}: 277 Å^2) (Trodler & Pleiss, 2008). Furthermore, in water the hydrophilic chains expand around the enzyme surface, increasing the hydrophilic area (Trodler & Pleiss, 2008; Zisis et al., 2015). Therefore, in the presence of hydrophilic support with a high dielectric constant such as TiO_2 [ε of 95.0 at 20°C (McPherson, Kim, Shanware, Mogul, & Rodriguez, 2003)], the hydrophilic residues may tend to scatter onto the TiO_2 surface, forcing the hydrophobic residues to be exposed, consequently opening the active site's lids (Ganjalikhany, Ranjbar, Taghavi, & Moghadam, 2012; Gruber & Pleiss, 2012; Trodler & Pleiss, 2008; Zisis et al., 2015).

Thus, the use of TiO_2 (Ø=$2.2\cdot10^2$ nm) as catalytic support for CALB (Ø=5.0 nm) results in an improved enzymatic catalyst, as observed by the REA increase (Figure 3. 3.a). However, the final structure remains nanoscale (Ø=$2.3 \cdot 10^2$ nm), which is difficult to handle and recover. Consequently, a second immobilisation using $CALB_{TiO_2}$ can improve the physical catalyst characteristics by increasing the support size. In this research, the second immobilisation method explored was the use of alginate microbeads obtained by CLEX via DMT.

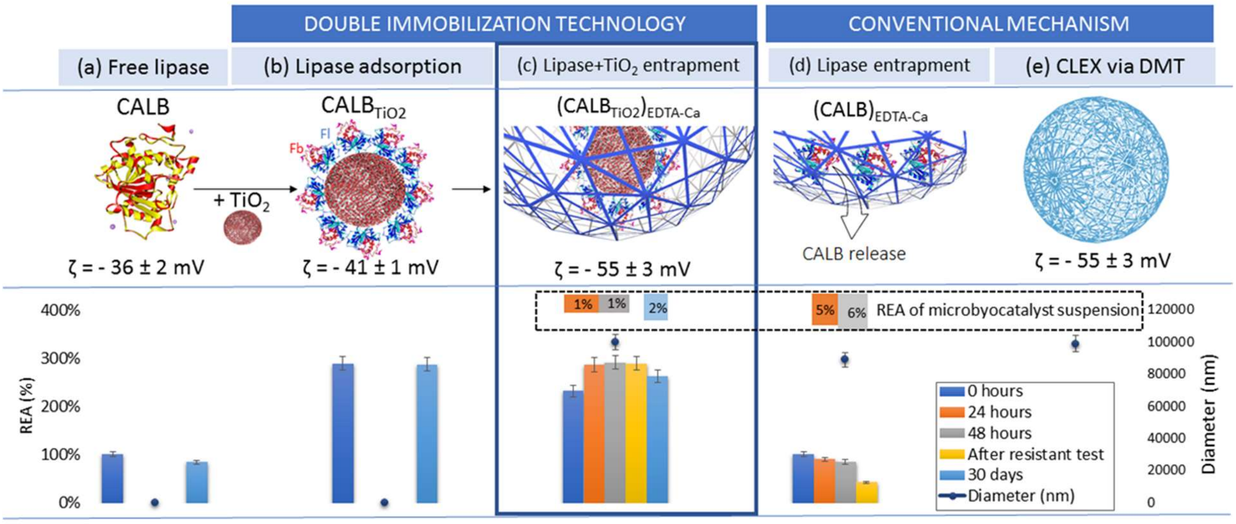

REA: Relative enzymatic activity is considered as a percentage of free enzyme
ζ: Zeta Potential
Fb: hydrophobic amino acids
Fl: hydrophilic amino acids

Figure 3. 3. CALB immobilisation comparison comparative chart: (a) Free enzyme; (b) CALB immobilised onto TiO_2 nanoparticles, (TiO_2 ζ=-25 mV); (c) Lipase immobilised onto TiO_2 by adsorption, followed by CALB+TiO_2 immobilised into calcium alginate microbeads obtained by CLEX via DMT; (d) CALB immobilised into calcium alginate microbeads obtained by CLEX via DMT; (e) Microbeads obtained by CLEX via DMT without CALB and/or TiO_2 [PDB ID: 5A71 (STAUCH et al., 2015)] Chemical structures developed by: Chemdoodle®. The design was developed by: Sketchup Pro 2021® and PhotoPad Professional v. 6.59®.

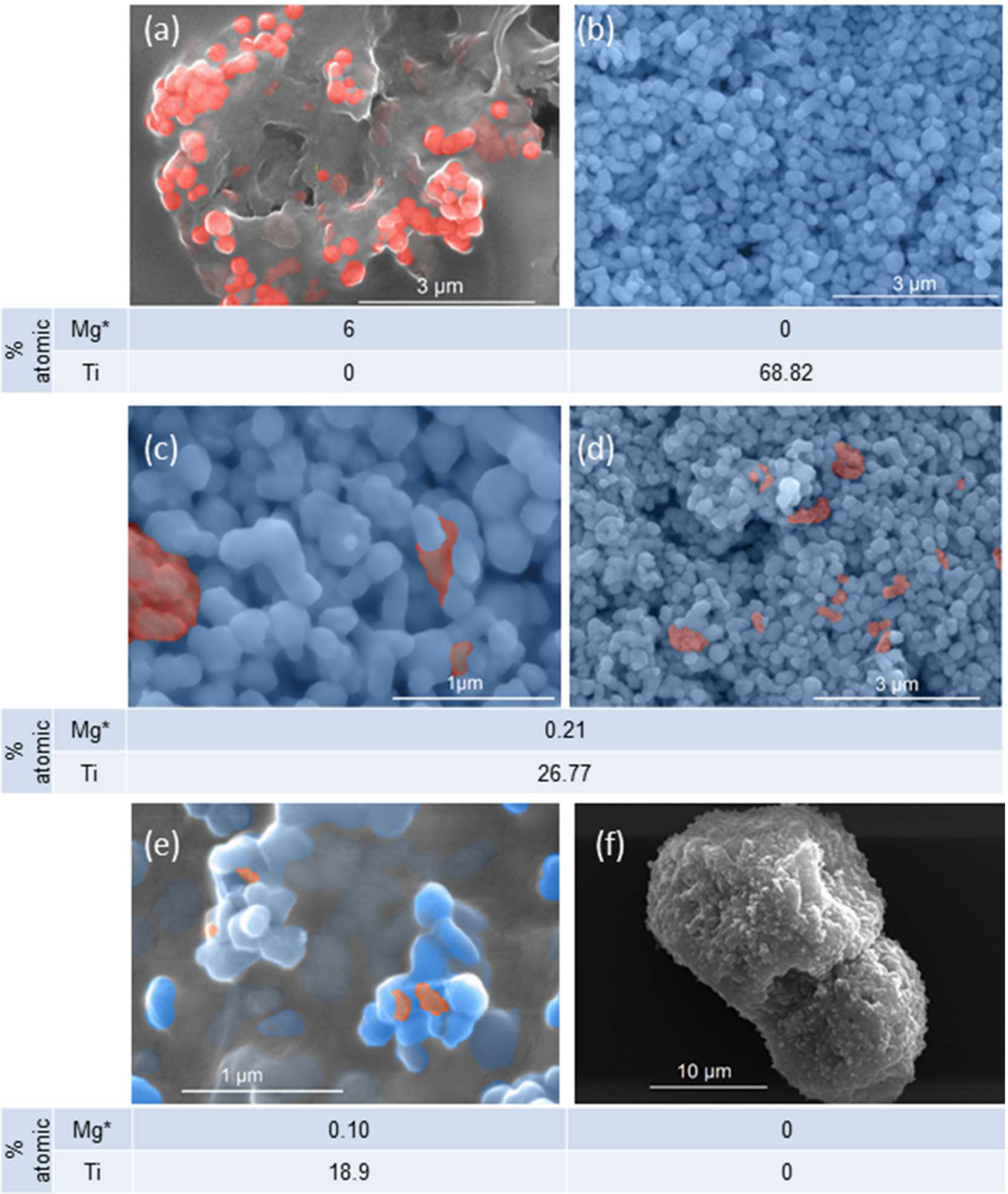

% atomic	Mg*	6	0
	Ti	0	68.82

% atomic	Mg*	0.21
	Ti	26.77

% atomic	Mg*	0.10	0
	Ti	18.9	0

Figure 3. 4. SEM images of (a) CALB (free) image (bar represents 3 µm); (b) TiO_2 image (bar represents 3 µm); (c and d) Image of CALB immobilised onto TiO_2 (bar represents 3 µm and 1 µm, respectively); (e and f) Image of CALB immobilised onto TiO_2 entrapped into calcium alginate microbeads (represents 10 µm and 1 µm, respectively). Images processed y PhotoPad Professional v. 6.59®. Highlighted in red: CALB, highlighted in blue: TiO_2 nanoparticles. Original SEM images are presented in Section S3.4 of SI - APPENDIX B: Figure S3. 6 (a – r). EDS results: Mg*: Although Mg^{2+} is not found in native CALB, it was detected in $CALB_{Free}$, being used as a “marker” to assess its presence in other structures as $CALB_{TiO2}$ and $(CALB_{TiO_2})_{EDTA\text{-}Ca}$.

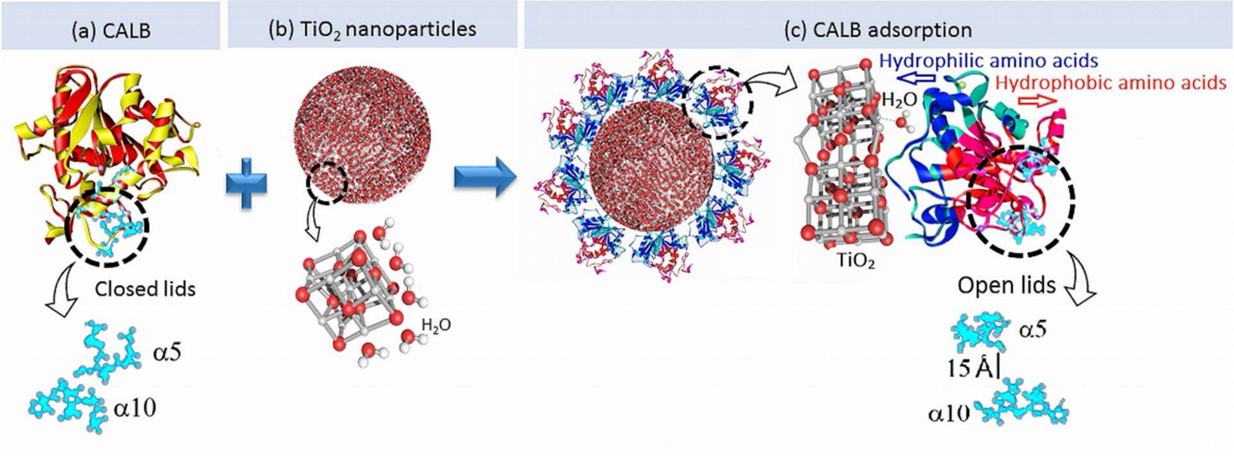

Figure 3. 5. Proposed mechanism of CALB immobilisation onto TiO_2 nanoparticles by hydrophilic amino acid oriented adsorption and hydrophobic amino acid exposure resulting in the opening of active site lids (α5 and α10). (a) Free enzyme with closed lids; (b) TiO_2 spherical nanoparticles; (c) CALB immobilised on TiO_2 by hydrophilic amino acids. This movement results in the exposure of hydrophobic amino acids and the opening of the lids. [PDB ID: 5A71 (STAUCH et al., 2015)], Chemical structures were developed by: Chemdoodle®, and the design was developed by: Sketchup Pro 2021® and PhotoPad Professional v. 6.59®.

3.3.2 Second immobilisation: catalyst into alginate microbeads

CLEX via DMT was explored to produce calcium alginate microbeads used as a second catalytic support. The immobilisation of $CALB_{Free}$, TiO_2, and $CALB_{TiO_2}$ was evaluated. The analysis of $CALB_{Free}$ and TiO_2 were expected to reveal synergic effects in the gelling process, while the $CALB_{TiO_2}$ immobilisation was the focus of this research.

3.3.3 Alginate microbeads production by CLEX via DMT

Internal ion exchange occurred in a microdevice (Figure 3. 6) containing two inlets for dispersant solutions and one for the continuous phase. The two dispersant solutions (DS1 and DS2) were sodium alginate containing divalent cations and chelates (Ca^{2+}-EDTA and Zn^{2+}-EDDA). Both were injected in a channel containing an inert hydrophobic (continuous phase), which caused drops to form (more details in Section S3. 2 of SI – APPENDIX B). The drop formation directly depended on the three flow rates (DS1, DS2, and continuous phase), which determined kinematic viscosity, superficial velocity, and tension between fluids (Joyce et al., 2016). The optimised flow rates, used as standard, were 8 µL/min for continuous phase and 2 µL/min for dispersant phases, and furnished microbeads with a diameter of 99±6 µm, sphericity of 0.90 and CV of 6%, respectively.

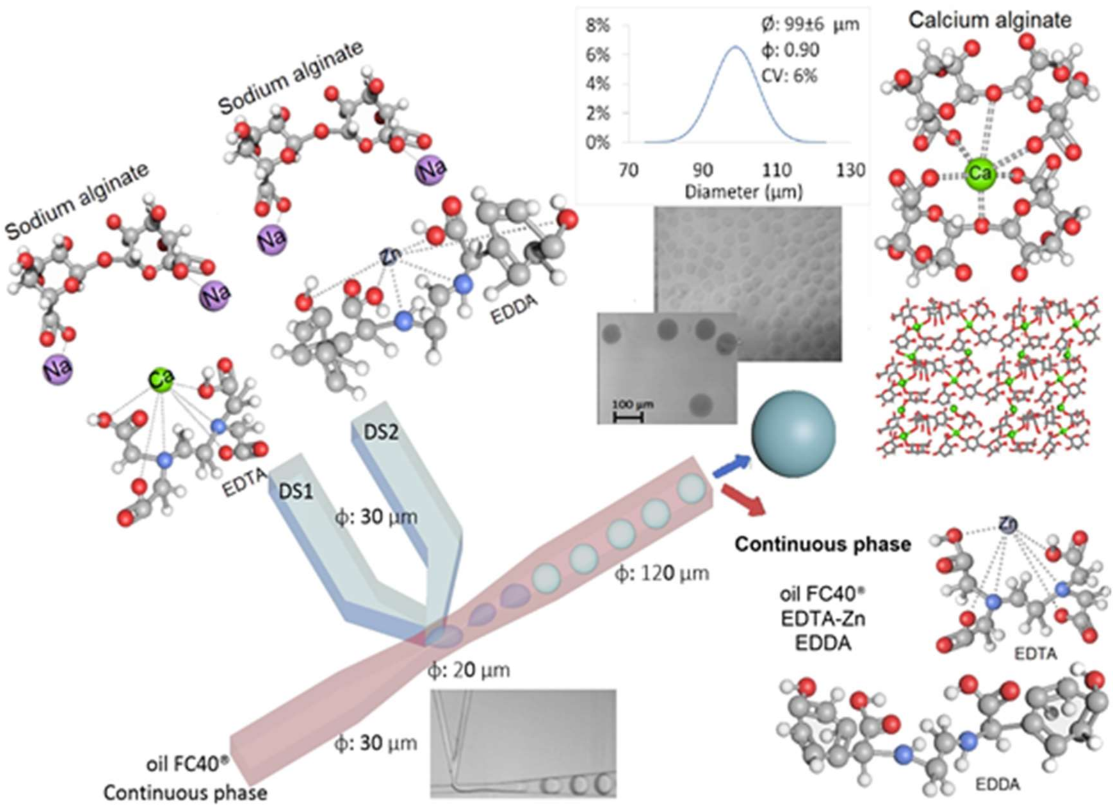

Figure 3. 6. Schematic diagram for the microfluidic droplet synthesis of alginate microbeads, Free$_{catalyst}$, obtained by internal Ion exchange crosslinking. Methylene blue was used to highlight the microbeads. Chemical structures were developed by: Chemdoodle®, and the design was developed by: Sketchup Pro 2021® and PhotoPad Professional v. 6.59®.

3.3.4 Influence of TiO_2 on alginate microbeads by CLEX via DMT

The influence of the metallic oxide on the alginate gelation process was examined as they compete with the divalent cations (Ca^{2+} and Zn^{2+}). The alginate gelation occurred only with titanium dioxide added to the EDTA-Ca stream, $(TiO_2)_{EDTA\text{-}Ca}$, with particles without aggregation. In this case, the average diameter was 99±9 µm, and sphericity 0.88. In $(TiO_2)_{EDTA\text{-}Ca}$ (Figure 3. 7.a), titanium dioxide nanoparticles remained free without interaction with the reagents present in this flowing liquid. Ionic calcium was linked to alginate due to its strong affinity to this material, while ionic zinc was strongly linked to EDTA.

In contrast, when TiO_2 was added into the EDDA-Zn stream $(TiO_2)_{EDDA\text{-}Zn}$ (Figure 3. 7.b), no alginate gelation was observed, probably because TiO_2 has a strong affinity to zinc ions. This affinity blocked the zinc ions from being linked to EDTA, consequently preventing calcium ions release. Since the gelation process requires free calcium ions to be linked to alginate, the alginate gelation did not occur. Even after mixing of the streams, ionic zinc was unavailable for ion exchange, and consequently, calcium ions coordinated to EDTA, preventing alginate gelation (mechanism described in Figure S3.5 of *S*I – APPENDIX B).

When TiO_2 was mixed in both alginate/EDTA-Ca and alginate/EDDA-Zn streams [$(TiO_2)_{EDTA\text{-}Ca/EDDA\text{-}Zn}$] (Figure 3. 7.c), partial alginate gelation was observed, probably due to a lower TiO_2 concentration in each stream with ionic zinc partially surrounded by TiO_2. Kaneko *et al.* (2010) compared the TiO_2 interference into calcium alginate microbeads by the traditional crosslinking method using $CaCl_2$. The TiO_2 nanoparticles were added to the sodium alginate solution. The authors obtained spherical particles. The particles' zeta potential changed from -1.3 to -73 mV, showing high chemical stability and non-aggregation behaviour.

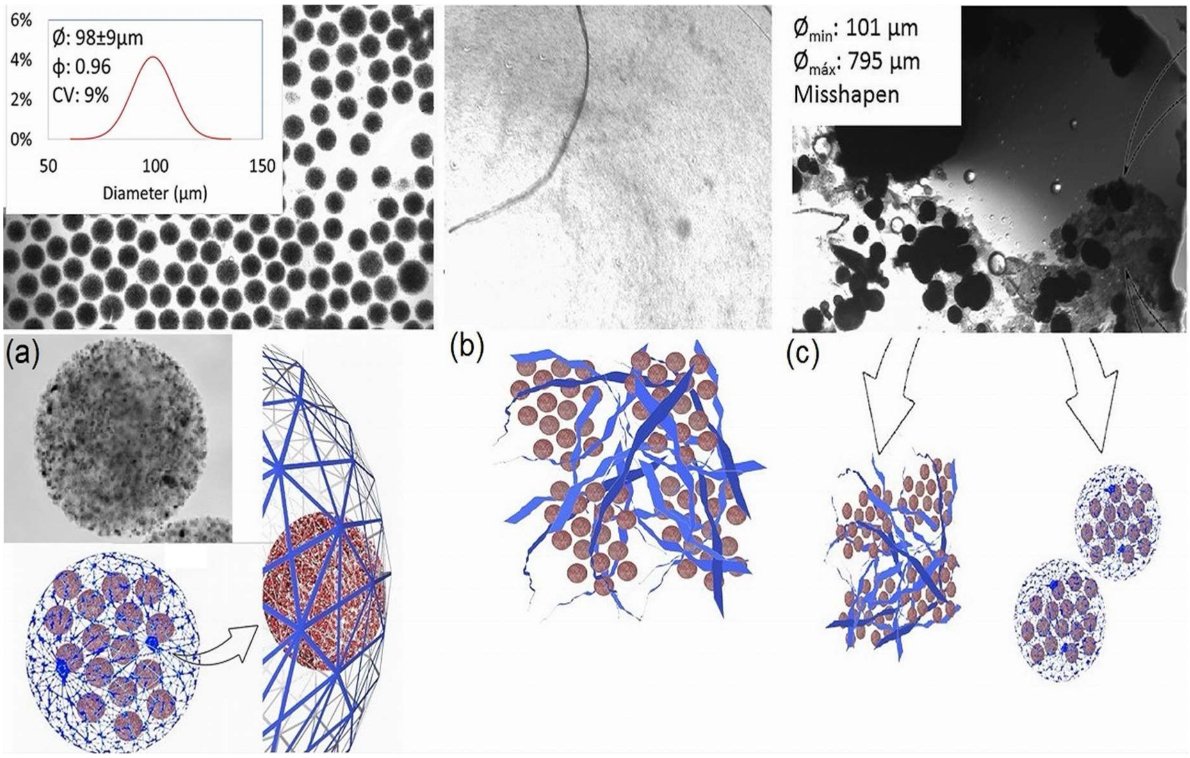

Figure 3. 7. TiO_2 entrapment. (a) $(TiO_2)_{EDTA\text{-}Ca}$ gelling: obtaining microbeads. (b) $(TiO_2)_{EDDA\text{-}Zn}$ gelling: without obtaining microbeads. (c) $(TiO_2)_{EDTA\text{-}Ca/EDDA\text{-}Zn}$ gelling: obtaining misshapen microparticles. Structures' design developed by: Sketchup Pro 2021® and PhotoPad Professional v. 6.59®. Microbeads images obtained by: Optical Microscope, Microbeads analysis by ImageJ software (National Institutes of Health, USA).

3.3.5 Influence of $CALB_{Free}$ on alginate microbeads by CLEX via DMT

The effect of the CLEX method's reagents on the enzymatic capacity and the impact of the enzyme in the gelling process was investigated to obtain an improved microbiocatalyst.

The enzymatic activity of CALB$_{Free}$ was analysed in the presence of CLEX reagents separately to verify the optimal stream (DS1 or DS2) composition for CALB immobilisation. For these analyses, the reagents' concentrations were the same as in the CLEX method, and CALB$_{Free}$ was kept in contact for 30 minutes before enzymatic activity was analysed. CALB$_{Free}$ enzymatic activity changes, shown in Figure 3. 8 (details in Section S3. 3 of SI – APPENDIX B), were similar to those described in the literature for other lipases. The presence of sodium alginate did not produce a notable change (Dharmsthiti & Kuhasuntisuk, 1998), calcium chloride increased enzymatic capacity (Dharmsthiti & Kuhasuntisuk, 1998; Snellman, Sullivan, & Colwell, 2002), and zinc acetate formed a white cloud, making the analysis inconclusive. However, lipases tend to reduce their enzymatic activity in the presence of salts (Dharmsthiti & Kuhasuntisuk, 1998; Snellman et al., 2002), in particular chelating ligands like EDTA and EDDA (Ghori, Iqbal, & Hameed, 2011; Handelsman & Shoham, 1994; Snellman et al., 2002). In this case, when analysing just the enzyme behaviour, the dispersant solution DS1 containing Ca^{2+}-EDTA is a better medium to add to CALB$_{Free}$, in contrast to Zn^{2+}-EDDA. However, it is still necessary to analyse its enzymatic activity when those reagents are mixed, and the gelation process is carried out. Moreover, the enzyme can interfere with those components' capacity to initiate the gelling process. Thus, CALB$_{Free}$ immobilisation into calcium microbeads was evaluated by different combinations of enzyme and dispersant solution streams.

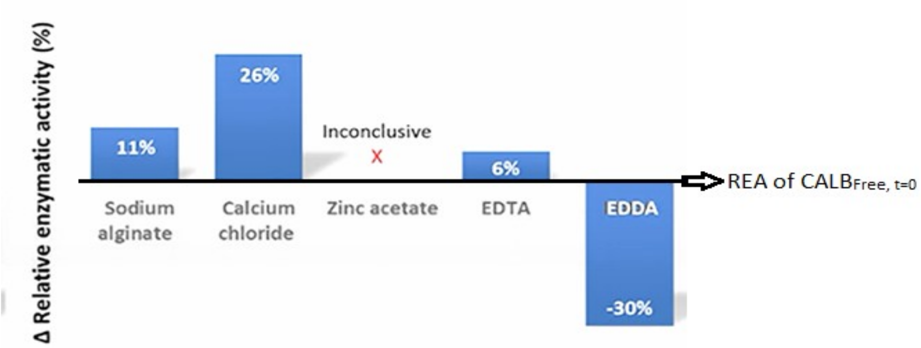

Figure 3. 8. Influence of different compounds used for alginate microbeads produced by CLEX via DMT on CALB enzymatic activity. ΔREA (%) represents the variation between the REA (%) obtained after 30 minutes of contact between the CALB and the respective compound and the REA (%) of CALB$_{Free}$. Details are shown in Section S3. 3 of SI – APPENDIX B.

The addition of CALB$_{Free}$ to the CLEX dispersant solutions can interfere with the ion exchange process and hence cause variations in its enzymatic capacity during and after the gelation process. This assumption was explored by promoting the alginate gelation process and evaluating the $CALB_{Free}$ presence in the DS1 reagents (Ca-EDTA), named $(CALB)_{EDTA\text{-}Ca}$, and $CALB_{Free}$ in the DS2 reagents (Zn-EDDA), named $(CALB)_{EDDA\text{-}Zn}$.

According to the enzymatic activity and physical characterisation (Figure 3. 9.a and Figure 3. 9.b), $(CALB)_{EDTA\text{-}Ca}$ is a better option for immobilisation than $(CALB)_{EDDA\text{-}Zn}$. $(CALB)_{EDTA\text{-}Ca}$ resulted in spherical microbeads (Ø=89±9µm, ϕ=0.93) and CV=9%, while $(CALB)_{EDDA\text{-}Zn}$, furnished distorted particles and a polydisperse system. Furthermore, the reagents impacted on the enzymatic activity of $CALB_{Free}$ during the gelling (t=0h, REA of $(CALB)_{EDTA\text{-}Ca}$=100±2% and REA of $(CALB)_{EDDA\text{-}Zn}$=82±6%, and reduced the stability (t=24h, REA of $(CALB)_{EDTA\text{-}Ca}$=90±3% and REA of $(CALB)_{EDDA\text{-}Zn}$=67±5% (details in S3.3 of SI -, APPENDIX B). Consequently, DS1 was considered the best option for lipase immobilisation. The results obtained for DS2 support the assumption that ionic zinc improves enzyme aggregation, as observed by cloud formation when free CALB was merged with a Zinc solution (Figure 3. 9.b).

The entrapment efficiency of free $(CALB)_{EDTA\text{-}Ca}$ in the microbeads showed that the alginate matrix could not retain the lipase. The enzyme's release was observed by enzymatic activity analysis of the microbeads and their suspension solutions. After 48 hours, a decrease in the microbeads' enzymatic activity (REA of $(CALB)_{EDTA\text{-}Ca}$=85±7%, details in S3.3 of SI - APPENDIX B) in combination with the enzymatic activity of the suspension solution (REA=5±4%, details in S3 of SI - APPENDIX B) was noted (Figure 3. 3.c). During the mechanical resistant test, the microbeads lost 51% of enzymatic activity (REA of $(CALB)_{EDTA\text{-}Ca}$=42±3% (details in S3.3 of SI - APPENDIX B, Figure 3. 3.c). A similar result has been reported with Lipase from *Yarrowia lipolytica* immobilised in calcium alginate microbeads, and the catalytic support released 50% of the enzyme to the surrounding (da S. Pereira et al., 2018). Therefore, because of $(CALB)_{EDTA\text{-}Ca}$ leaching, double immobilisation should be considered to improve entrapment immobilisation.

3.3.6 $CALB_{TiO_2}$ entrapment into microbeads by CLEX via DMT

$CALB_{TiO_2}$ was immobilised into calcium alginate microbeads using the gelling process CLEX via DMT, resulting in a microbiocatalyst with high enzymatic activity (REA=232±8 %, details in S3.3 of SI - APPENDIX B) after double immobilisation. Although $CALB_{Free}$ and TiO_2 showed better results immobilised in DS1 (EDTA-Ca) than DS2 (EDDA-Zn), synergistic effects may have resulted in a different interaction. Therefore, double immobilisation was explored by adding $CALB_{TiO_2}$ to DS1 and DS2. Based on the results obtained, $(CALB_{TiO_2})_{EDTA\text{-}Ca}$ (Figure 3. 9.d) is the best option to immobilise CALB, resulting in an improved enzymatic catalyst. For $(CALB_{TiO_2})_{EDDA\text{-}Zn}$ (Figure 3. 9.c), $CALB_{TiO_2}$ did not achieve good enzymatic activity and efficient gelation.

(CALB$_{TiO_2}$)$_{EDTA\text{-}Ca}$ resulted in spherical microbeads (ϕ=0.98 and Ø=89±9μm) and CV=9%, while (CALB$_{TiO_2}$)$_{EDDA\text{-}Zn}$ showed reduced gelling process efficiency and distorted particles. After double immobilisation, (CALB $_{TiO_2}$)$_{EDTA\text{-}Ca}$ (Figure 3. 3.c and Figure 3. 9.d) showed an enzymatic activity similar to CALB$_{TiO_2}$ (Figure 3. 3.b). The effect of CALB in the presence of the CLEX's reagents was analysed separately (Figure 3. 8), indicating that interactions observed before the gelling process are retained even after microbead generation (Figure 3. 10). Microbeads obtained by CALB$_{TiO_2}$ immobilised in DS1 (EDTA-Ca) resulted in an REA increase (REA of (CALB$_{TiO_2}$)$_{EDTA\text{-}Ca}$: 232±8%, and DS2 (EDDA-Zn) in an REA decrease (REA of (CALB$_{TiO_2}$)$_{EDDA\text{-}Zn}$: 96±6% (details in S3.3 of SI - APPENDIX B). However, there is a strong synergistic effect between CALB and TiO_2, resulting in an enzymatic activity improvement for both tests (t=24h, REA of (CALB$_{TiO_2}$)$_{EDTA\text{-}Ca}$: 286±4% and REA of CALB$_{TiO_2}$)$_{EDDA\text{-}Zn}$: 127±5% (details in S3.3 of SI - APPENDIX B). The lower REA variation of (CALB$_{TiO_2}$)$_{EDDA\text{-}Zn}$ is explained by a complexation mechanism that occurred in the presence of zinc ions, as independently observed for CALB$_{Free}$ in the presence of ionic zinc (Section 3. 2), and CALB and TiO_2 in the gelling process when added to DS2 (Section 3. 2).

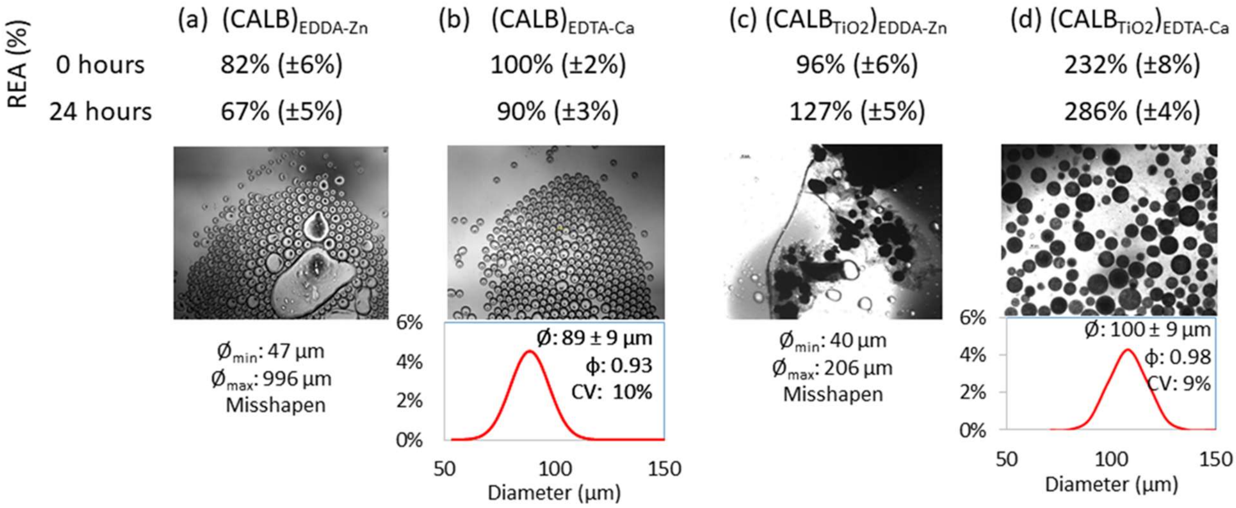

Figure 3. 9. CALB and CALB$_{TiO_2}$ immobilised into alginate microbeads obtained by CLEX via DMT. (a) CALB added into DS1 (Ca-EDTA); (b) CALB added into DS2 (Zn-EDDA); (c) CALB+TiO_2 added into DS1 (Ca-EDTA); (d) CALB+TiO_2 added into DS2 (Zn-EDDA). REA (%) details are in Table S3. 3 of SI. Structures' design developed by: Sketchup Pro 2021® and PhotoPad Professional v. 6.59®., Microbeads images obtained by: Optical Microscope, Microbeads analysis by ImageJ software (National Institutes of Health, USA). Microbeads images were obtained by: Optima Microscope, Microbeads analysis by ImageJ software (National Institutes of Health, USA).

3.3.7 ***($CALB_{TiO_2}$)$_{EDTA\text{-}Ca}$: improved enzyme catalyst***

The CALB double immobilisation resulted in an improved biocatalyst with high enzymatic activity, stability and non-leaching (Figure 3. 3 and Figure 3. 4). CALB adsorbed onto TiO_2 ($CALB_{TiO_2}$) and entrapped into calcium alginate microbeads via DMT [($CALB_{TiO_2}$)$_{EDTA\text{-}Ca}$] effectively prevents enzyme release (Figure 3. 3.c). Different behaviour was observed for CALB immobilised on TiO_2. In this last case, CALB could subsequently desorb (Figure 3. 3.b) or even leach if immobilised into alginate microbeads without being immobilised first onto TiO_2 (Figure 3. 3.d). The zeta potential value analysis supported this assumption. Considering that CALB and $CALB_{TiO_2}$ have similar surface charges, an almost complete oriented adsorption of CALB onto TiO_2 must have occurred. Likewise, considering that ($CALB_{TiO_2}$)$_{EDTA\text{-}Ca}$ and microbeads obtained by CLEX via DMT without catalyst (Figure 3. 3.e) had similar surface charges, it can be concluded that entrapment occurred successfully. The surface charge of -55mV also indicates a colloidal system without aggregation behaviour or high chemical stability. The SEM images (Figure 3. 5) showed that CALB is spread out on the TiO_2, and both were present on the microbeads' surface. However, according to the images and EDS results (Figure 3. 3), a small quantity of CALB was present in the final microbiocatalyst, indicating that further optimisation could improve its enzymatic capacity.

The chemical stability can also be confirmed through enzymatic activity, which was analysed over 30 days. ($CALB_{TiO_2}$)$_{EDTA\text{-}Ca}$ showed an increase in enzymatic capacity ($\Delta REA_{1day\text{-}30days}$=31% (details in S3 of SI - APPENDIX B), $CALB_{TiO_2}$ retained its enzymatic capacity ($\Delta REA_{1day\text{-}30days}$=-2%), and $CALB_{Free}$ reduced its enzymatic capacity ($\Delta REA_{1day\text{-}30days}$=-16%). The enzymatic activity decrease of immobilised CALB may also occur due to enzyme leaching. This was evaluated by testing the microbeads' liquid suspension and microbeads after the mechanical resistant test, in which the microbeads were washed and centrifugated vigorously. Both analyses revealed a tendency for (CALB)$_{EDTA\text{-}CA}$ leaching because of a CALB diameter similar to the microbeads' pores. Contrary, ($CALB_{TiO_2}$)$_{EDTA\text{-}Ca}$ did not leach because the lipase was strongly connected to $TiO_{2,}$ and together they most likely possess a size larger than the microbeads' pores.

Compared to other lipase immobilisation methods (Table 3. 2), the CALB adsorption onto TiO_2, followed by the alginate entrapment, is a promising strategy for lipase immobilisation. Using nanometal particles such as TiO_2, the enzyme improves the enzymatic capacity (Cui et al., 2016; S. Zhang et al., 2013). However, their nanoscale is challenging for catalyst recovery and handling. Thus, a second immobilisation is required to solve this limitation. One option is immobilisation by entrapment using polymers such as alginate, but this tends to reduce the enzymatic capacity. Firstly it reduces the enzyme's surface area contact' Hence, the smaller the particle (like microparticles), the better the immobilised enzyme's performance (Netto et al., 2013; Xie & Zang, 2018). Secondly, the pores of polymer chain tend to allow enzyme leaching, in contrast to the enzyme immobilised onto TiO_2, which results in a size larger than the polymer chains' pores. This results from this study complements similar findings reported in the literature (Hosseini et al., 2019; N. Singh et al., 2013; Sipponen et al., 2018).

The microbiocatalyst developed, $(CALB_{TiO_2})_{EDTA\text{-}CA}$, can overcome shortcomings often observed during immobilisation processes, and enables higher enzymatic activity and stability, easier retention, recovery, and handling.

Table 3. 2: *Lipase immobilisation efficiency comparison by REA analysis.*

Enzyme	Support 1	Support 2	REA (%)	Ref.
Aspergillus oryzae lipase	TiO_2+ETS[a]	-	428%	(Zhou et al., 2021)
CALB	Calcium alginate microbeads	-	100%[3]	This study
CALB	Octyl agarose	-	100%	(Peirce et al., 2016)
CALB	Silica-lignin matrix	-	92%	(Zdarta et al., 2016)
CALB	Calcium alginate beads		88%	(S. Zhang et al., 2013)
CALB	AuNPs	-	80%	(Barros et al., 2019)
CALB	TiO_2	-	289%[c]	This study
CALB	TiO_2	Calcium alginate microbeads	232%[3]	This study
CALB	Fe_3O_4	Chitosan nanoparticles	95%	(Hosseini et al., 2019)
CALB	Fe_2O_3	Cellulose acetate-coated	94%	(N. Singh et al., 2013)
CALB	Fe_3O_4	$CH_3Si(OCH_3)_3$ (MTMOS)	210%	(Reetz et al., 1998)
CALB	Lignin nanoparticles	Alginate beads	70%	(Sipponen et al., 2018)
Candida rugosa lipase	Glyoxyl agarose	-	50%	(Otero et al., 1988)
Candida rugosa lipase	Fe_3O_4	-	60%	(Xie et al., 2015)
Candida rugosa lipase	Fe_3O_4	alginate polyaldheyde	60%	(Lan, Zhao, Guo, Guan, & Zhang, 2015)
Candida rugosa lipase	Fe_3O_4	Graphene	65%	(Xie & Ma, 2009)
Candida rugosa lipase	Fe_3O_4	Chitosan	66%	(Hou, Wang, Zhu, & Wei, 2016)
Candida rugosa lipase	Fe_3O_4	MPP/Chitosan[b]	75%	(Hou et al., 2016)
Lipase from porcine pancreas	$Cu_3(PO_4)_2$	-	460%	(Cui et al., 2016)
Lipase from porcine pancreas	$Zn_3(PO_4)_2$	-	147%	(B. Zhang et al., 2016)
Lipase from porcine pancreas	TiO_2	Chitosan	84%	(Deveci et al., 2015)
Lipase KM12	Graphene oxide	Chitosan+cellulose acetate	120%	(Badoei-dalfard et al., 2022)
Pseudomona cepacia	Fe_3O_4	$CH_3Si(OCH_3)_3$ (MTMOS)	330%	(Reetz et al., 1998)

[a]Ethenyl triethoxy silane; [b]Metal-polyphenol film consolidated Fe_3O_4/chitosan hybrid microcapsules; [c]REA details are in S3.3 of SI – APPENDIX B.

3.4 Conclusion

A microbiocatalyst was developed through a double lipase immobilisation methodology. In a first immobilisation process, CALB was adsorbed onto TiO_2 nanoparticles ($CALB_{TiO_2}$), resulting in an enzymatic activity of 189%, higher than that of the free enzyme. It is assumed that CALB was immobilised onto TiO_2 nanoparticles in one layer through hydrophilic amino acids scattering, mainly found on the external enzyme structure. The CALB's hydrophilic amino acids attached to the TiO_2 nanoparticles' surface forces the exposure of hydrophobic residues. This whole process opens the active site's lids (residues α5 and α10), consequently improving the enzymatic activity. In a subsequent second immobilisation process, $CALB_{TiO_2}$ was entrapped into calcium alginate microbeads [$(CALB_{TiO_2})_{EDTA\text{-}Ca}$]. The $(CALB_{TiO_2})_{EDTA\text{-}Ca}$ showed $REA_{t=0}$ of 232%, $REA_{t=24h}$ of 286%, and $REA_{t=30days}$ of 255%, clearly demonstrating an improvement in the enzymatic activity and stability; and $REA_{after\ resistant\ test}$ of 289%, suggesting that that catalyst leaching did not occur. The Zeta Potential of 55 mV supports surface charge stability and non-aggregation behaviour. The final microparticles showed a diameter of 100 µm, and are thus easier to recover than CALB or $CALB_{TiO_2}$. Consequently, the improved microbiocatalyst obtained by double immobilisation offers a promising option for lipases immobilisation. It may overcome the limitations frequently observed for free enzymes (reuse and recovery difficulty and low enzymatic stability) and immobilised enzymes (decreased enzyme activity, enzyme loss, limitation in the use of continuous reactors). However, future research in this field should explore applications of these advanced microbiocatalyst, their economic evaluation and their large scale implementation.

Acknowledgements

The authors would like to thank the Thermo-Fluid Dynamics Process Laboratory of Unicamp (LPTF), Unicamp Microfluidic Laboratory (LaNBDA), and Biomass Characterization, Analytical Resources and Calibration Laboratory (LRAC) for providing their facilities to carry out this project. LGT thanks the National Council for Scientific and Technological Development (CNPq) (productivity grant 302212/2019-1).

Funding sources

This study was financed in part by the Coordenação de Aperfeiçoamento de Pessoal de Nível Superior - Brasil (CAPES) Finance Code 001.

Chapter IV

Methyl oleate synthesis by TiO_2-photocatalytic esterification of oleic acid: optimisation by response surface quadratic methodology, reaction kinetics and thermodynamics

Permission: This article was published in ChemPhotoChem, Vol 6(7), Rosilene Andrea Welter[1,2], Harrson Silva Santana[2], Lucimara Gaziola de la Torre[2], Mark Robertson[1], Osvaldir Pereira Taranto[2], Michael Oelgemöller[1,3]. Methyl oleate synthesis by TiO_2-photocatalytic esterification of oleic acid: optimisation by response surface quadratic methodology, reaction kinetics and thermodynamics, e202200007, Copyright: 2022 The Authors. ChemPhotoChem published by Wiley-VCH GmbH (Creative Commons — Attribution 4.0 International — CC BY 4.0) doi.org/10.1002/cptc.202200007.

Filiation: (1) College of Science and Engineering, James Cook University, Postcode Qld 4811, Townsville, Queensland, Australia; (2) School of Chemical Engineering, University of Campinas, Postcode 13083-852, Campinas, SP, Brazill; (3) Faculty of Chemistry and Biology, Hochschule Fresenius gGmbH-University of Applied Science, Postcode D-65510, Idstein, Germany.

Abstract

Methyl oleate, an example of a FAME (fatty acid methyl ester), was produced by oleic acid (OA) photoesterification with TiO_2 and UVA light. Different parameters were evaluated and optimised: catalyst pretreatment, temperature (25-65°C), catalyst loading (1-30% w/w_{OA}) and oleic acid:alcohol molar ratio (1:3-1:55). Response surface quadratic methodology obtained by central composite rotational design (RSM-CCRD) was used to evaluate the main operational conditions of the photoesterification process. A high conversion of 98% (±0.8) at 65°C, 20% TiO_2 (w/w_{OA}), and 1(OA):55(methanol) molar ratio was achieved. The photoesterification mechanism is furthermore proposed. The Langmuir-Hinshelwood kinetic model considered the forward and backward reaction as first-order fits with the best accuracy (R^2 of 0.997). The thermodynamic results ($\Delta G_{338.15K}$=-20.745 kJ/mol, ΔH=13.748 kJ/mol, and ΔS=0.471 kJ/mol.K) indicate that the operating conditions are important, both to supply the energy requirement of the reaction, but also to increase the miscibility of the reactants.

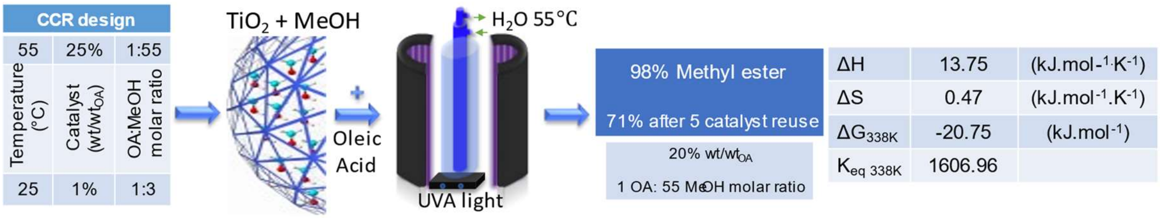

Figure 4. 1. Graphical abstract: Methyl oleate synthesis by TiO_2-photocatalytic esterification of oleic acid: optimisation by response surface quadratic methodology, reaction kinetics and thermodynamics.

4.1. Introduction

Biodiesel has gained increased importance as a substitute for fossil fuel. As a result, global biodiesel production increased from 6 billion litres per year in 2005 to 46 billion litres per year in 2020 (Ogunkunle & Ahmed, 2019). Biodiesel has several advantages over petrodiesel, most importantly, it is four times easier to degrade (A. Demirbaş, 2008) and emits 86% fewer greenhouses gases (Voegele, 2020). Biodiesel is preferentially obtained from renewable sources such as vegetable oils, and is frequently produced by transesterification catalysed by strong acids. However, the efficiency of biodiesel as a fuel source is commonly reduced due to its high free fatty acid (FFA) content (Corro et al., 2013), its production cost is high due to the need of advanced process technologies, and the large volumes of reagents and waste involved demand appropriate treatment (Zhen et al., 2012). Esterification is another method of producing biodiesel because of the easy availability of raw materials with high free fatty acid content (Corro et al., 2013; Guo et al., 2021; Manique et al., 2016; Zhen et al., 2012). Vegetable oils, such as canola oil and waste cooking oil (WCO), contain a high amount of free fatty acids, with their main component being oleic acid (Anwar, 2021; Ghazani, García-Llatas, & Marangoni, 2014). The use of WCO causes an about 60% reduction in the cost of biodiesel production (Mohadesi et al., 2019). Thus, the esterification of free fatty acid represents a promising option for biodiesel production.

The esterification reaction of free fatty acid occurs preferably in the presence of short-chain alcohols (methanol, ethanol or propanol) and requires a catalyst (Guo et al., 2021; Moradi et al., 2021; S. M. Silva et al., 2020; M. v.d. Silva et al., 2015; Stacy et al., 2014). The most common catalysts are strong acids such as sulfuric acid. However, the use of strong acids causes problems such as equipment corrosion, the difficult removal of the catalyst, and the large amounts of waste generated (G. Berrebi et al., 1993). These issues may be circumvented by a solid eco-friendly catalyst and photochemical activation. Photocatalysis using metal oxide and light is generally used to degrade organic compounds (Carlucci, Degennaro, & Luisi, 2019; Karan, Mukhopadhyay, & Chakraborty, 2020). However, this methodology is also promising for the esterification of free fatty acid (Carlucci et al., 2019; Karan et al., 2020). For example, UVC light-irradiated ZnO/SiO_2 resulted in a conversion of 96% for free fatty acid from *Jatropha curcas* (Corro et al., 2013), Cr/SiO_2 in the presence of solar light gave a conversion of 96% for free fatty acid from waste cooking oil (Corro et al., 2017), $La^{3+}/ZnO\text{-}TiO_2$ irradiated by UVC light produced a conversion of 96% for free fatty acid from waste cooking oil (Guo et al., 2021). Clay-supported anisotropic Au-modified N, S-doped TiO_2 nanoparticles in the presence of UV-Vis showed a conversion of 87% for oleic acid (Praneeth & Paria, 2020). The advantage of photoesterification is its high conversion under mild operational conditions (temperature and pH), the high purity of the photoproduct, and the easy recovery and reuse of the photocatalyst. However, photocatalysis frequently requires complex pretreatments to enhance FAME production.

Titanium dioxide is non-toxic, chemically stable, easy to handle, and recoverable (Carp et al., 2004). Therefore, it has been used for the degradation of organic pollutants such as dyes, pesticides and pharmaceuticals (Kanakaraju et al., 2014; Konstantinou & Albanis, 2003; Rajeshwar et al., 2008). In contrast, synthetic photocatalysis with TiO_2 has not been explored widely (N. Hoffmann, 2015). However, some authors successfully developed esterification protocols using titanium dioxide and light irradiation. For example, capric acid esterification in the presence of glycerol resulted in a conversion of 97% (Karan et al., 2020), crude palm oil with methanol of 96% (Wulandari, Adiwibowo, Redjeki, Ibadurrohman, & Slamet, 2019), and oleic acid with methanol of 86% (Manique et al., 2016) respectively. Despite these encouraging studies, the TiO_2-photoesterification process has not yet been optimised in terms of its operational conditions, synergic effects between reagents and catalyst, or catalyst reuse. The thermodynamic and kinetic reaction parameters have also not been established yet, and these parameters are crucial for the development of a scalable and cost-efficient process.

Scale-up of heterogeneous photocatalytic processes remains challenging due to significant photon and mass transfer limitations (van Gerven, Mul, Moulijn, & Stankiewicz, 2007). Continuous-flow conditions can generally improve the performances of photochemical transformations (Oelgemöller, Hoffmann, & Shvydkiv, 2014), and have subsequently become widespread in synthetic photochemistry (Fukuyama, Kasakado, Hyodo, & Ryu, 2022). Recently, heterogeneous photocatalysis has been realized in an advanced meso-scale flow reactor (Mo & Jensen, 2016). Numbering-up of smaller reactors has furthermore been demonstrated for photocatalytic water treatment (Motegh, van Ommen, Appel, & Kreutzer, 2014). Continuous-flow operation thus represents a promising strategy for photocatalytic biodiesel production. In fact, microreactors have been previously proposed for biodiesel production (R. Welter, Silva Jr., de Souza, Lopes, Taranto, & Santana, 2022) as they improve the crucial mass transfer between reagents (Rahimi, Mohammadi, Basiri, Parsamoghadam, &

Masahi, 2016).

Consequently, this study aimed to develop an optimised photoesterification protocol based on experimental, thermodynamic, and physicochemical parameters. TiO_2 activation by UVA light and oleic acid in the presence of different short-chain alcohols were chosen as model systems. In addition, catalyst pretreatment and recovery processes were investigated. Several operational conditions, such as the oleic acid:alcohol molar ratio, catalyst content, and temperature, were considered.

4.2. Methodology

4.2.1. Materials

Reagents and solvents were obtained from the following suppliers: TiO_2 (P25: Aeroxide®, Evonik), methanol (HPLC grade, Fisher Chemical), oleic acid 90% (Sigma-Aldrich), dichloromethane (DCM, AR, 99.5%, Univar), sodium hydroxide pellets (NaOH, Univar), acetone (AR, 99.5%, ChemSupply), diethyl ether (AR, 99.5%, Univar), ethanol (AR, 99.5%, Univar), 0.02 N potassium hydroxide in aqueous solution ($KOH_{aqueous}$, ±0.5%, Ace Chemical Company), 0.02 N potassium hydroxide in ethanol solution ($KOH_{ethanol}$, ±0.5%, Ace Chemical Company) and n-propanol (AR, 99.5%, ChemSupply). Samples were filtered through a Hydraflon 0.22μm, 35 mm syringe filter. Irradiations were conducted in a Rayonet RPR-200 photochemical reactor (Southern New England Ultraviolet Company) equipped with 16 F8T5/BL fluorescent tubes (Ushio, 8W Black Light UVA T-5 G5 Base). NMR spectra were recorded on a *Bruker Ascend™ 400 MHz* Spectrometer. Attenuated total reflectance-Fourier transform infrared spectroscopy (FTIR-ATR) was carried out using a Nicolet™ iS™ 5 FTIR Spectrometer, coupled with an iD7 ATR accessory (ThermoFisher Scientific). Particle analyses were conducted using the Quantacrome AsiQwin equipment. The surface morphology was analysed by scanning electron microscopy (SEM, JSM-5410LV SEM-EDS Oxford). Elemental chemical characterisation was obtained by energy dispersive spectrometer (EDS), using a JSM-5410LV SEM-EDS Oxford.

4.2.2. TiO_2 Catalyst

Pretreatment. TiO_2 was mixed with the reactants for a specific time before starting the photoreaction. Five tests were conducted: (1) OA (30 minutes); (2) OA+MeOH (30 minutes); (3) MeOH (5 minutes); (4) MeOH (30 minutes); and (5) MeOH (60 minutes) (Table S4.1 of SI – APPENDIX C). The catalyst was mixed with the respective reagent by magnetic stirring (300 rpm) at 55°C, the same temperature used in the following photoesterification tests. Catalyst and reactant were added according to the correct weight necessary for the reaction (Table S4.1 of SI - APPENDIX C). After pretreatment, the mixture (catalyst and reactant) was loaded into the reactor prior to photoesterification. The subsequent photoesterification experiments occurred at constant operational conditions, as indicated in Section 4. 1.

Recovery and reuse. At the end of each photoesterification experiment, the catalyst was filtered, washed with acetone (mixing vigorously with magnetic stirring at 500 rpm), allowed to settle for 20 hours, and the acetone layer was removed by decantation (1RP). After three repetitions (3RP), the catalyst was dried at 100ºC for 24 hours, crushed, and stored in a plastic vial at room temperature. The efficiency and reusability of the recovered TiO_2 were evaluated by characterisation and subsequent photoesterification tests. The photoesterification test followed by 3RP was considered as one complete cycle of catalyst reuse (C1). This process was performed five times (C1, C2, C3, C4, and C5) as tests 39 to 43, described in Table S4. 1 of SI - APPENDIX C.

Characterisation. TiO_2 characterisation analyses prior and after each photoesterification were performed as follows: chemical characterisation was conducted by FTIR-ATR at room temperature in the spectral range of 400-1000 cm^{-1}. Spectra analysis was carried out using OriginPro 2021® (Learning Edition, OriginLab Corporation). Peak deconvolution analysis was performed by PeakDeconvolution.opx from OriginLab® using the baseline model: Straight Line, Peak Resolution Enhancement Method: 2nd derivative Smooth Derivative Method:Quadratic Savitzki-Golay, 2nd order polynomial. Particle size, pores' volume, pore size, and total surface area were obtained by N_2 physisorption to perform isotherms: Brunauer, Emmet, and Teller (BET), and Barrett, Joyner and Halenda (BJH) (Quantachrome Instruments, 2009). Thermoanalyses were carried out to determine the presence of organic material inside the catalyst's pores. Thermal gravimetric analysis (TGA) and differential scanning calorimetric (DSC) were performed by adopting air and nitrogen at 10˚C/min in a range of room temperature to 800˚C. The SDT650 equipment was used, and the data was handled by Trios® software (TA instruments) and OriginPro 2021® (Learning Edition, OriginLab Corporation). Crystalline material characterisation was conducted by X-ray powder diffraction (XRD) using a Siemens D5000 Diffractometer under the irradiation of Cu K α (λ_{XRD} =0.154060 nm). Spectra analysis was carried out using OriginPro 2021® (Learning Edition, OriginLab Corporation). The average crystallite size was obtained by the Scherrer equation (Equation 4.

1), using K_{XRD}= 0.9 and λ_{XRD}=1.5406 Å, and considering the prominent peaks observed in the spectrum for anatase (25.23°) and rutile (27.43°).

$$D_C = \frac{K_{XRD} \cdot \lambda_{XRD}}{\beta_{XRD} \cdot \cos \theta_{XRD}} \qquad \text{Equation 4. 1}$$

4.2.3. Photoesterification process

Photocatalytic esterification of oleic acid with methanol. TiO_2 was added to methanol and mixed at the respective photoesterification test temperature. After 30 minutes, TiO_2+Methanol and oleic acid were loaded into the reactor (Figure 4. 2). The photoreactor and the reaction heating (water bath) were turned on 30 minutes prior to the photoesterification experiment. The cylindrical batch reaction vessel (100 mL) was manufactured of Pyrex glass (cut-off wavelength ≤290 nm) and was equipped with an inner 'cold' finger for heating. The reagents were mixed by magnetic stirring, and the reaction was stopped after 240 minutes. During kinetic studies, samples (<3 mL each) were withdrawn after set reaction times (15, 30, 45, 60, 120, 180, and 240 minutes). The samples were filtered by syringe, rota-evaporated at 40°C to remove the liquid phase (170 mbar for 15 minutes, 72 mbar for 30 minutes, and 30 mbar for 30 minutes), and the conversion was determined by ^{1}H-NMR spectroscopy based on the integration of baseline separated signals. The final sample taken after 240 minutes was furthermore characterised and stored in a glass vial at room temperature.

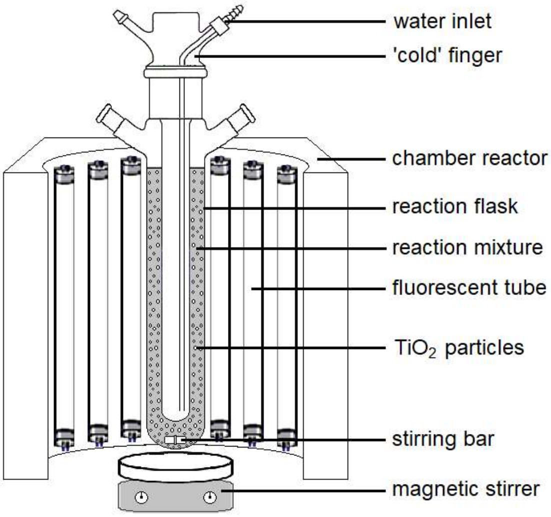

Figure 4. 2. Photoesterification reactor scheme.

Oleic acid conversion determination. Oleic acid conversions were determined by ^{1}H-NMR spectroscopy by correlating baseline separated FAME and oleic acid peak areas (Figure S4.6 of SI – APPENDIX D). The peak areas A_1 (CH_3O) and A_2 (CH=CH) were obtained using MestReNova® software (Version 6.0.2-5476, Mestrelab Research S.L.) and were used to determine the conversion rate as described in Equation 4. 2.

$$\mathrm{OA\ conversion\ (\%)} = 100 \cdot \left(\frac{\mathrm{A}_2}{3} \cdot \frac{2}{\mathrm{A}_1}\right) \quad \text{Equation 4. 2}$$

FTIR-ATR was alternatively used to determine oleic acid conversion rates (Details described in S4.3 of SI - APPENDIX C). Peak deconvolution analysis was carried out using PeakDeconvolution.opx (OriginLab®) by baseline model: Straight Line, Peak Resolution Enhancement Method: 2nd derivative Smooth Derivative Method:Quadratic Savitzki-Golay, 2nd order polynomial. The oleic acid conversion values were in agreement with those determined by NMR analysis.

Activation energies and enthalpies were determined using the Arrhenius (Equation 4. 3) and van‘t Hoff`s (Equation 4. 4) models.

Arrhenius model:

$$\ln(\mathrm{k}) = -\frac{\Delta \mathrm{E}}{\mathrm{R} \cdot \mathrm{T}} + \ln(A) \quad \text{Equation 4. 3}$$

van‘t Hoff`s model:

$$\ln(\mathrm{K}) = -\frac{\Delta \mathrm{H}}{\mathrm{R} \cdot \mathrm{T}} + \frac{\Delta \mathrm{S}}{\mathrm{R}} \quad \text{Equation 4. 4}$$

4.2.4. Optimisation study

The operational conditions (OA:MeOH molar ratio, TiO_2 loading and temperature) for photoesterification were evaluated to obtain an optimised reaction protocol. The Central Composite Rotational Design (CCRD) model for experimental development was followed, and the parameters’ effects were analysed by response surface quadratic methodology (RSM), both obtained through Statistica 7.0® software.

A total of 33 experiments were carried out. The CCR design for two independent variables (OA:MeOH molar ratio and catalyst loading) was investigated using 11 experiments (Table 4. 1), Entries 6 to 16 described in Table S4. 1 of SI - APPENDIX C). Three additional tests were conducted as a triplicate using operation conditions extracted from the literature (Entries 17 to 19 in Table S4.1 of SI - APPENDIX C, with 1OA:12MeOH molar ratio and 15% w/w_{OA} of TiO_2) (Manique et al., 2016). Two further test reactions were performed to extrapolate the CCRD model conditions (Entries 20 and 21 in Table S4. 1 of SI - APPENDIX C, with 1OA:55MeOH molar ratio, 25% and 30% w/w_{OA} of catalyst). Three experiments were conducted to confirm the best operational conditions (Entries 22 to 24, Table S4. 1 of SI - APPENDIX C triplicate of 1OA:55MeOH molar ratio and 20% w/w_{OA} of TiO_2). Two more experimental tests were subsequently conducted to validate the mathematical model obtained (Entries 25 and 26 in Table S4. 1 of SI - APPENDIX C). Three blank tests were furthermore performed by keeping the operational conditions constant [55°C, OA:MeOH as 1:55 and 20% of TiO_2 (w/w_{OA})]: Blank 1 (without catalyst), Blank 2 (without light with the reactor wrapped in aluminium foil), and Blank 3 (without catalyst and light with the reactor wrapped in aluminium foil) (Entries 27 to 29 in Table S4. 1 of SI -IV, APPENDIX C). The medium deviation was evaluated in triplicate [OA:MeOH as 1:29 and 10% of TiO_2 (w/w_{OA}), OA:MeOH as 1:12 and 15% of TiO_2 (w/w_{OA}), and OA:MeOH as 1:55 and 20% of TiO_2 (w/w_{OA})].

Table 4. 1: *Operation parameters for oleic acid photoesterification optimisation by CCR design.*

Parameter	**Unit**	**Factorial and centre level**			**Axial level**	
		Low (-1)	Centre (0)	High (+1)	Lowest ($-\sqrt{2}$)	Highest ($\sqrt{2}$)
OA:MeOH	molar ratio	1:16	1:29	1:42	1:3	1:55
Catalyst	(% w/w_{OA})	5	10	15	1	20

RSM was used to investigate the operational conditions' relationship and their impact on FAME yields. A second-order polynomial order was used for the independent variables' interactions, and the oleic acid conversion was chosen as the response. The results were evaluated by the coefficient of determination (R^2), standard deviation (SD), occasionality of the results by null hypothesis (p-value), and experimental data adaptability to the model (F-test). In addition, the influence of each individual variable was analysed by their correlation with the dependent variables (unstandardised β* and standardised β), their significance (t-test), and their capacity to predict the dependent variable (p-level).

The temperature influence was investigated through 12 experiments (Entries 29 to 38 in Table S4. 1 of SI - APPENDIX C). The temperatures selected were 25ºC, 35ºC, 45°C, 55°C, and 65°C, respectively. Two specific operational conditions were evaluated: (PC1), as described in the literature [1:12 of OA:MeOH and 15% TiO_2 (w/w_{OA})] (Manique et al., 2016) and (PC2), as obtained through this study [1:55 of OA:MeOH and 20% TiO_2 (w/w_{OA})].

Moreover, the use of different alcohols (ethanol and n-propanol) was investigated by performing two experiments (Entries 44 and 45 in Table S4. 1 of SI - APPENDIX C), keeping the operational conditions constant [55°C, OA:MeOH as 1:55 and 20% of TiO_2 (w/w_{OA})].

4.2.5. Kinetics and thermodynamic parameters

Kinetic parameters are essential to understanding the reaction's performance over time, and by that, equilibrium conditions can be reached. Furthermore, future process scale-up modelling and simulations rely on these data to achieve reliable and applicable results. The equilibrium's composition is required to determine the equilibrium constant and the thermodynamic properties. Ten experimental kinetics were evaluated at different temperatures (range between 25°C to 65°C) and under two operational conditions (PC1 and PC2, Entries 29 to 38 in Table S4. 1 of SI - APPENDIX C). Five kinetics models, along with the reaction conditions proposed, were evaluated, as described in Table 4. 2. Four models considered a homogeneous system with complete miscibility between reagents, and mass transfer effects were neglected. The difference between them is the order of the forward (esterification) and the backward reaction (hydrolysis). Based on literature findings, free fatty acid esterification by heterogeneous catalysis was satisfactorily described by the HSE1HN (Harun et al., 2018), HSE1H2 (Benyong Han et al., 2019), and HSE2H2 (Cho, Kim, Hong, & Yeo, 2012; Narenji-Sani, Tayebee, & Chahkandi, 2020), HSE1H2 (Hussain & Kumar, 2018), and HSE2H2 models (Prasanna Rani, Ramana Neeharika, Kumar, Satyavathi, & Sailu, 2016; Veillette, Giroir-Fendler, Faucheux, & Heitz, 2017), respectively. The Langmuir-Hinshelwood (L-H) kinetic model was chosen as the fifth model that considers a heterogeneous system with complete miscibility between reagents and a heterogeneous catalyst with active homogeneous sites. The L-H model is frequently used for photocatalysis with nanoparticles (Ameh, Jimoh, Abdulkareem, & Otaru, 2013; Chaemchuen, Heynderickx, & Verpoort, 2020; Choo, 2018; Ezzati, 2018; Karan et al., 2020; Ould Brahim, Belmedani, Hadoun, & Belgacem, 2021; Rajarshi Kar, Oindrila Gupta, Kunal Mandol, & Sangita Bhattacharjee, 2012; S Khezrianjoo & HD Revanasiddappa, 2012; Tang & Huren An, 1995).

Mathematical modelling was performed using the Matlab® software package and the results were evaluated by R^2, SD, p-value, and F-test. The parameters from the model with the best accuracy were subsequently used to obtain the thermodynamic properties. Using the

Arrhenius model (Equation 4. 3), the temperature (T) effect was evaluated to obtain the activation energy (ΔE_a) and frequency factor (A). By the van‘t Hoff’s model (Equation 4. 4), enthalpy (ΔH) and entropy (ΔS) were determined. Using Equation 4. 5, the Gibb’s free energy variation (ΔG) was obtained, which depended on T and an equilibrium constant (K_{eq}).

$$\Delta \mathrm{G} = -R \cdot T \cdot ln(K_{eq}) \qquad \text{Equation 4. 5}$$

Table 4. 2: *Kinetic models evaluated for oleic acid and methanol photoesterification, experimental kinetic data.*

Assumptions	**Model**	**Equation**
Homogeneous		
HSE1HN -FR: first order -BR: neglected	$\frac{dx_{FFA}}{dt} = -k_1 \cdot x_{FFA}$	Equation 4. 6
HSE1H1 -FR: first order -BR: first order	$\frac{dx_{FFA}}{dt} = k_{-1} \cdot (1 - x_{FFA}) - k_1 \cdot x_{FFA}$	Equation 4. 7
HSE1H2 -FR: pseudo-first order -BR: second order	$\frac{dx_{FFA}}{dt} = k_{-1} \cdot (1 - x_{FFA}) - k_1 \cdot C_{FFA_0} \cdot x_{FFA}^2$	Equation 4. 8
HSE2H2 -FR: second order -BR: second order	$\frac{dx_{FFA}}{dt} = k_{-1} \cdot C_{FFA_0} \cdot (1 - x_{FFA})^2 - k_1 \cdot C_{FFA_0} \cdot x_{FFA}^2$	Equation 4. 9
Heteroegenous		
L-H kinetic model[a] -FR: first order -BR: first order -FFA and FAME are bounding the catalyst capacity	$\frac{\mathrm{d}x_{FFA}}{\mathrm{dt}} = \mathrm{k}_{-1} \cdot \frac{\mathrm{K}'_2 \cdot x_{FFA}}{1 + \mathrm{K}'_2 \cdot \mathrm{C}_{\mathrm{FFA}_0} \cdot x_{FFA}} - \mathrm{k}_1 \cdot \frac{\mathrm{K}'_1 \cdot (1 - x_{FFA})}{1 + \mathrm{K}'_1 \cdot \mathrm{C}_{\mathrm{FFA}_0} \cdot (1 - x_{FFA})}$	Equation 4. 10

[a] Model’s detailed development can be found in Section S4.2 of SI - APPENDIX C; FR: forward reaction; BR: backward reaction.

4.3. Results and discussion

4.3.1. Catalyst: TiO_2 nanoparticles

Photocatalyst pretreatment. The impact of reagent absorption (oleic acid and alcohol) on the photoesterification efficiency was initially studied by evaluating oleic acid conversion rates after each individual pretreatment. The addition of oleic acid was found to decrease the photocatalyst’s efficiency (Figure 4. 3), possibly due to the formation of a film on TiO_2 that blocked its pores (Pettibone, Cwiertny, Scherer, & Grassian, 2008). Oleic acid may also reduce light access to the photocatalyst due to its higher refractive index compared to methanol [at 55°C, RI_{OA}: 1.4475 (Maser, 2001), RI_{MeOH}: 1.3165 (Craig, 1953)], especially at lower wavelengths such as UVA (Maser, 2001)The initial addition of methanol prevents oleic acid from covering the surface of TiO_2, and 30 minutes of contact prior to the addition of oleic acid was found sufficient to fill the catalyst's interstices. According to the BET model constant value (C_{BET} >1,Table 4. 3), coverage occurred in a monolayer. The methanol monolayer adsorption arises through the binding of its oxygen atom with the TiO_2 (anatase). Additionally, a weak hydrogen bond from methanol to TiO_2 has been described, resulting in a monodentate configuration (Setvin et al., 2017). The monolayer configuration results in a higher adsorption energy (0.7-0.74 eV) than the second layer (0.24 eV). In contrast, methanol and rutile result in a stronger interaction than anatase but still form a monolayer (Yang et al., 2018).

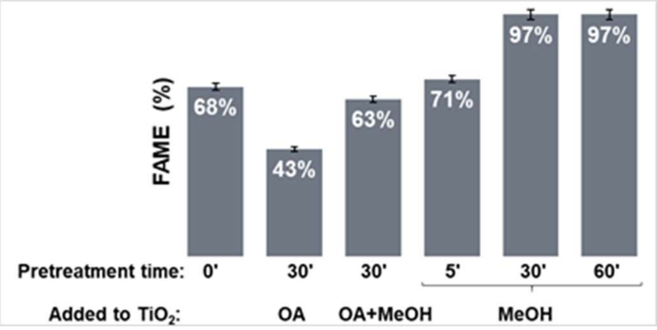

Figure 4. 3. Oleic acid (OA) conversion (%) during photoesterification after different catalyst pretreatments: OA for 30 minutes, OA+MeOH for 30 minutes, and MeOH for 5, 30, and 60 minutes, respectively. Standard deviation <1%. Photoesterification conditions: 55°C, 1OA mol:55MeOH moles, 20% TiO_2 (w/w_{OA}).

Physicochemical characterisation of TiO_2. TiO_2 was characterised qualitatively and quantitatively before and after photoesterification, recovery, and reuse. According to the data obtained by FTIR-ATR and TGA/DSC after photoesterification (Figure 4. 4 and S4. 3 of SI - APPENDIX C) the photocatalytic material retained 27% (w/w) of organic material (74% of FAME and 26% of oleic acid). FAME was removed easier than oleic acid during the recovery process, confirming that FAME adsorbed weaker than oleic acid. The complete recovery and washing process (3 RP) effectively removed 93% of organic material. The remaining 7% possibly consisted of oleic acid present in the internal interstices of the nanoparticles. After five complete cycles of photoesterification and subsequent recovery (C5), 9% (w/w) of organic material remained on TiO_2 (22% of FAME and 78% of oleic acid).

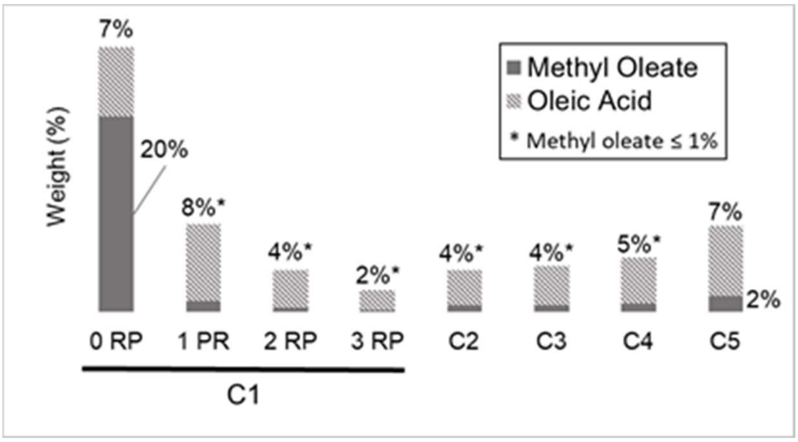

Figure 4. 4. Organic material present within TiO_2 after photoesterification operational conditions PC2. Values obtained by TGA and FTIR analysis (S4.3 of SI – APPENDIX C) considering 0 (0 RP) to 3 (3RP) washing procedure for the first use (C1), and up to 5 cycles of catalyst use.

The physical characteristics of TiO_2 changed due to the presence of organic material, as shown in Figure 4.5). Two effects were notable. The pores became obstructed, causing a reduction in pore volume and diameter, and a decrease in the catalyst surface area. In addition, the particles' agglomeration changed, causing their size to increase, hence reducing their surface area. After photoesterification, the high organic material content resulted in the obstruction of pores (a decrease of 28% in the surface area compared with pure TiO_2) and agglomeration of particles (an increase of 38% of particle size compared with pure TiO_2). After C1 (Photoesterification + 3 RP), the pores were accessible (a decrease of 9% in the surface area and 70% of the surface recovered compared with pure TiO_2) with less agglomeration (an increase of 9% of particle size compared with pure TiO_2). After 5 cycles of catalyst use and recovery, the organic material was more impregnated; however, particles were almost open (a decrease of 11% in the surface area compared with pure TiO_2) but showed higher particles agglomeration (an increase of 26% of particle size compared with TiO_2).

The XRD analysis (Table 4. 4, Section S4. 3 of SI - APPENDIX C) produced almost constant results for all samples. The crystallite size had an average of 21.65 nm (±0.65). The composition was 90% of anatase and 10% of rutile, similar to that obtained by EDS analysis (Figure 4. 5.d; Section S4. 3 of SI - APPENDIX C). The combination of different TiO_2 crystallite forms (anatase and rutile) improves the photocatalytic efficiency due to synergic effects. Consequently, the transfer of photo-excited electrons and positive holes in the crystallite forms can occur (Li et al., 2009).

SEM analyses (Figure 4. 5.a-c) showed variations in the catalyst's structure. After five cycles, the particles were slightly more agglomerated with sharper structures. This aggregation may block the active sites, reducing the catalytic activity and catalyst's stability (Li et al., 2009). In addition, the catalyst powder showed visible differences (Figure 4. 5.e). A higher content of organic matter resulted in a darker, heavier, and more clustered powder.

Table 4. 3: *TiO_2 characterisation by physisorption.*

	Pore vol. (cm^3/g)	**Pore diameter (nm)**	**Surface area (m^2/g)**	**Particle size (nm)**	C_{BET}
TiO_2 pure	0.737	3.524	51.851[a]	27.5515	61.326
TiO_2 0RP	0.610	3.034	37.565	38.0293	26.626
TiO_2 C1	0.671	3.181	47.393	30.1431	35.938
TiO_2 C5	0.620	3.016	41.203	34.6715	29.014

[a]Surface area standard value according to the manufacturer: 35-65 mg^2/g (Aeroxide, 2020).

Table 4. 4: *TiO_2 characterisation by XRD[a].*

	Crystallite size[d] (nm)	**Anastase (%)**	**Rutile (%)**
TiO_2 pure	22.25	91%	9%
TiO_2 PE[b]	21.95	91%	9%
TiO_2 C1[c]	20.58	91%	9%
TiO_2 C5	21.53	90%	10%

[a]XRD: spectra are shown in S 3; [b]TiO_2 after photoesterification reaction; [c]C1: after 1 cycle of photoesterification and 3RP; [d]Obtained by the Scherrer equation (Equation 4. 1).

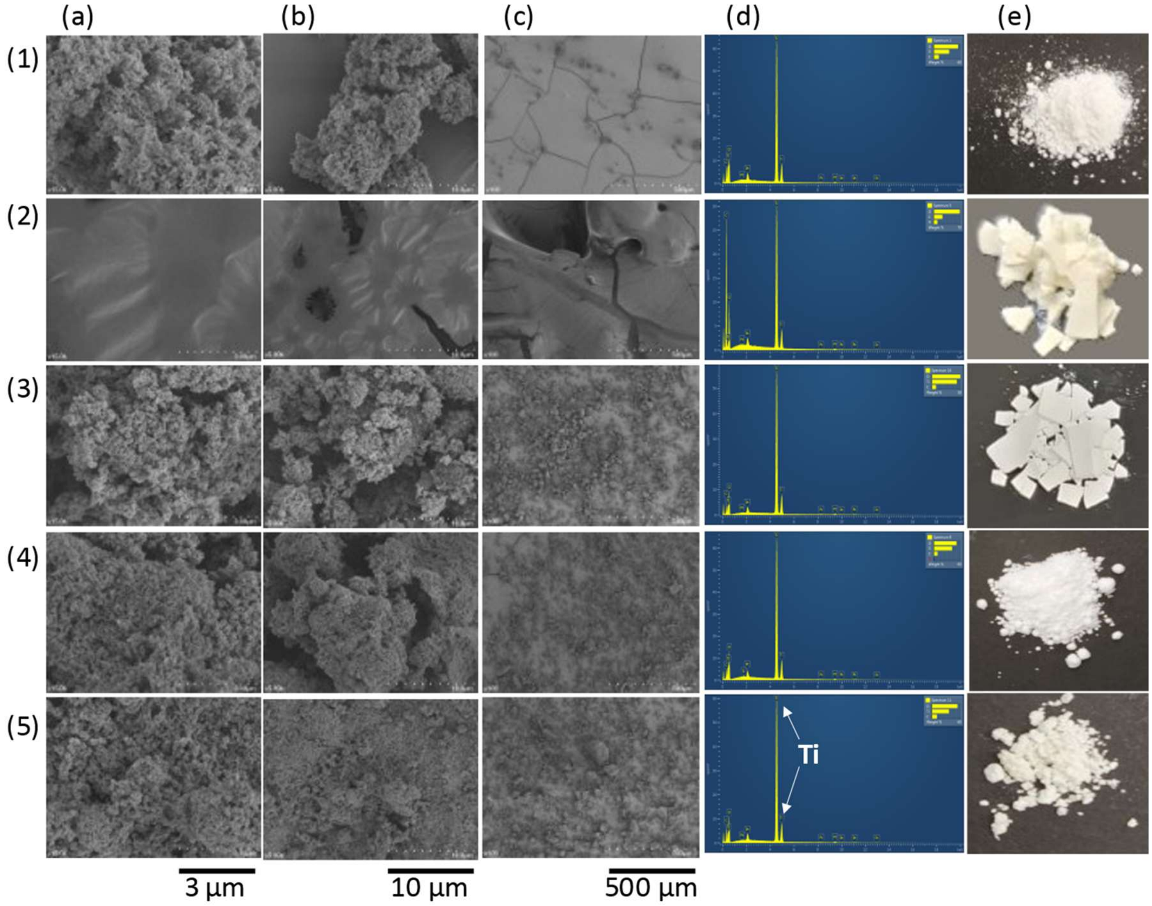

Figure 4. 5. (1) Pure, (2) After photoesterification by operational conditions PC1, (3) After photoesterification by operational conditions PC2, (4) After 1 use (C1), (5) After 5 cycles of catalyst use and recovery (C5). (a) SEM image: 3µm, (b) SEM image: 10 µm, (c) SEM image: 500 µm, (d) EDS, (e) Photographic Images.

4.3.2. Photoesterifications

Esterifications of oleic acid and short-chain alcohols (using TiO_2 irradiated by UVA as a catalyst) were evaluated in a batch reactor. The following operational conditions were assessed: temperature, catalyst loading, oleic acid:alcohol molar ratio, and alcohol type.

A high oleic acid conversion of 98% was obtained with a 1OA:55MeOH molar ratio and 20% w/w_{OA} at 55°C after 4 hours of irradiation. In comparison with other literature studies (Table 4. 5), this result demonstrates that TiO_2 without any further modification can effectively initiate photoesterification if pretreatment is carefully evaluated first.

Table 4. 5: *Oleic acid and methanol esterification obtained by different catalysts and operational conditions.*

Catalyst	% (w/w_{OA})	MeOH:1OA Molar ratio	T (°C)	Time (h)	FAME (%)	Ref.
TiO_2 + UVA	20	55	55	4	98	This study
Au/TiO_2 + Visible light	10	9	40	6	85	(Praneeth & Paria, 2020)
Biomass-based polymers	3	15	75	3	96	(A. Wang et al., 2019)
Fe_3O_4@PILPW	13	12	90	5	93	(Z. Wu et al., 2016)
[HMIM]HSO_4	15	15	110	8	95	(Roman et al., 2019)
HZ zeolite/1.0/60	10	45	100	4	83	(Vieira et al., 2015)
HZ zeolite/2.0/80	10	45	100	4	73	(Vieira et al., 2015)
HZ zeolite/0.5/60	10	45	100	4	71	(Vieira et al., 2015)
HZ zeolite	10	45	100	4	55	(Vieira et al., 2015)
LO (lanthanum oxide)	10	5	100	7	63	(Vieira et al., 2013)
M-MMT K10 acid	5	10	60	3	70	(Harun et al., 2018)
SLO/HZSM-5	10	5	100	7	100	(Vieira et al., 2013)
SLO (sulphated lanthanum oxide)	10	5	100	7	98	(Vieira et al., 2013)
SO_3-HM-ZSM-5–3	5	18	88	10	100	(Mostafa Marzouk et al., 2021)
Sugarcane bagasse -SO_3H	0.1	20	50	24	85	(Flores et al., 2019)
TiO_2 + UVA	15	12	30	4	75	(Manique et al., 2016)
TiO_2/NP-800	10	8	150	8	87	(Essamlali et al., 2017)
TPA3/MCM-41	3.7	40	60	6	100	(Patel & Brahmkhatri, 2013)
$Zr(SO_4)_2$	3	9	60	5	98	(Senoymak Tarakcı & Ilgen, 2018)
300-Nb_2O_5/SO_4^{2-}	5	20	100	4	92	(Sturt et al., 2019)

4.3.3. Optimisation study: alcohol and catalyst content

Initially, the effects of two process variables (oleic acid:methanol molar ratio and catalyst content) on oleic acid conversion using a CCR design was performed (as described in Table S4.1 of SI - APPENDIX C), and the results are summarised in Figure 4. 6 and Figure 4. 7. A clear correlation between these variables and the reaction performance was observed. The best values obtained were close to the CCR design's highest level of the content of catalyst (20% w/wOA) and methanol (1OA:55Me), suggesting further improvement potential of the experimental design (Figure 4. 8 and Figure 4. 9). Oleic acid conversions between 12% and 98% were achieved, clearly showing the importance of these two variables. The tests were conducted in triplicates and the experimental standard deviation (1OA:12Me / 15% TiO_2 and 1OA:55Me / 20% TiO_2, as described in Table S4.1 of SI - APPENDIX C) resulted in a value of ±0.00786, indicating excellent reproducibility of the experimental results. The elliptical contour of the response surface confirms that correlations between variables were significant (C. Hong & Haiyun, 2010) and the surface's shape reveals that the maximum efficiency for the process was obtained (Sidik et al., 2016) (OA conversion of 97% (±0.8%) for 20% (w/w_{OA}) TiO_2 and 1OA:55MeOH). Further increase in the catalyst content (25% and 30% (w/w_{OA}) TiO_2) produced a decrease in oleic acid conversion.

Based on the CCR design of the complementary tests (19 tests, as described in Table S4.1 of SI - APPENDIX C), a mathematical model (Equation 4.10) was developed. The experimental and model data convergence resulted in an R2 of 0.989 (Figure 4. 10). According to ANOVA analysis (Table 4. 6), it showed a p-value <0.0001 and an F-value of 173.51 (F-value $\gg F_{crit}$). These parameters clearly reflect the accuracy between the mathematical model and the experimental results.

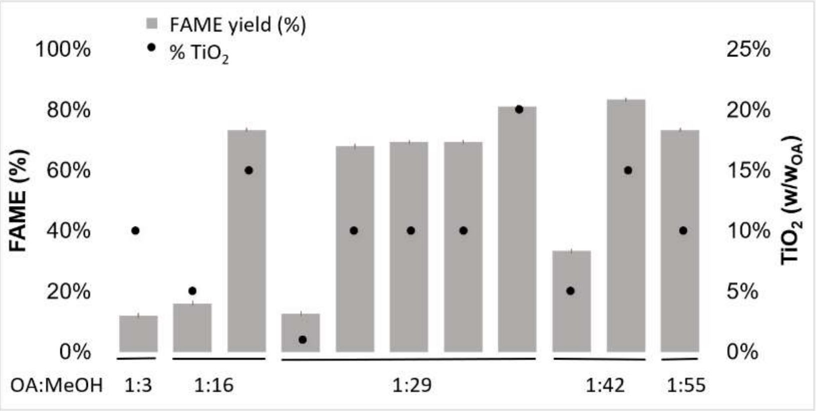

Figure 4. 6. Central composite rotational (CCR) experimental design of oleic acid conversion (%) with methanol to FAME using TiO_2 and UVA irradiation: Oleic acid conversion (%) at equilibrium. Temperature: 55°C, TiO_2 content range between 1% and 20% (w/w$_{OA}$) and OA:MeOH molar ratio range between: 1:3 and 1:55. Experimental standard deviation (σ) of ± 0.00786.

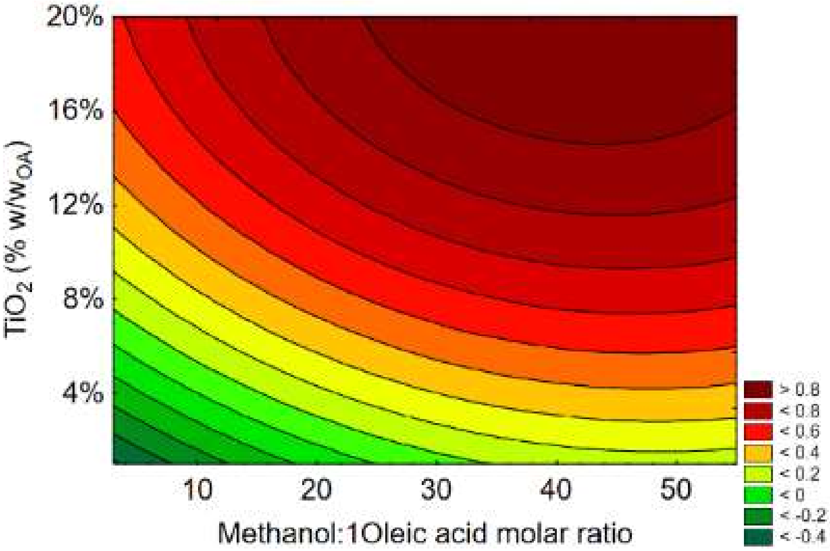

Figure 4. 7. Central composite rotational (CCR) experimental design of oleic acid conversion (%) with methanol to FAME using TiO_2 and UVA irradiation: Surface response contour plots of FAME (%) conversion for catalyst content – oleic acid:methanol molar ratio. Temperature: 55°C, TiO_2 content range between 1% and 20% (w/w$_{OA}$) and OA:MeOH molar ratio range between: 1:3 and 1:55. Experimental standard deviation (σ) of ± 0.00786.

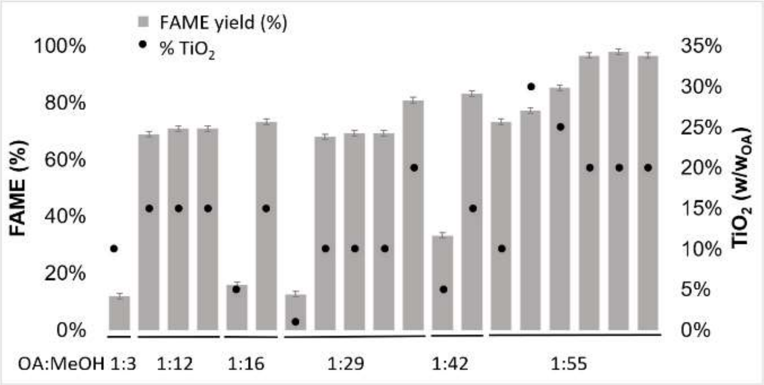

Figure 4. 8. Central composite rotational (CCR) experimental design of oleic acid conversion (%) with methanol to FAME using TiO_2 and UVA irradiation: Oleic acid conversion (%) at equilibrium. Temperature: 55°C, TiO_2 content range between 1% and 30% (w/w_{OA}) and OA:MeOH molar ratio range between: 1:3 and 1:55. Experimental standard deviation (σ) of ± 0.00786.

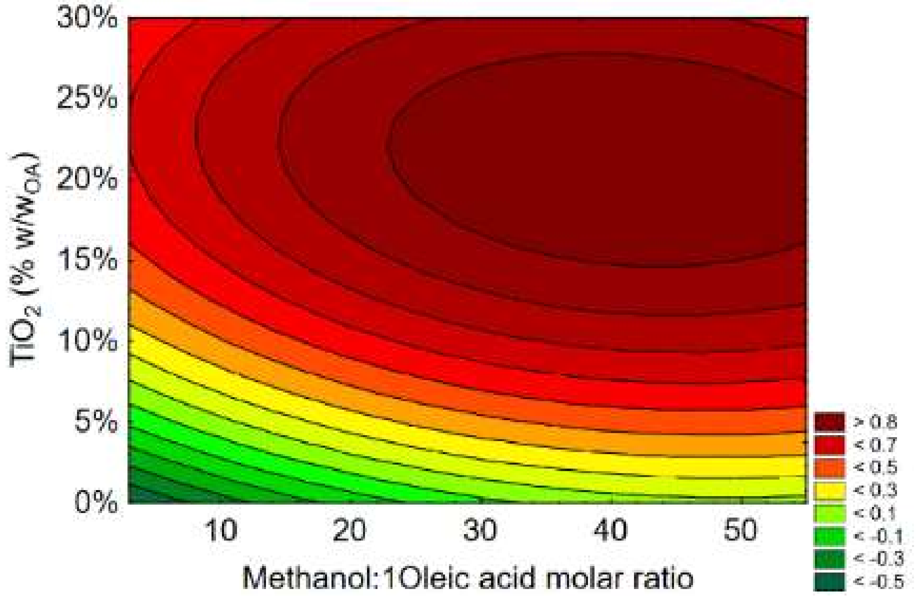

Figure 4. 9. Central composite rotational (CCR) experimental design of oleic acid conversion (%) with methanol to FAME using TiO_2 and UVA irradiation: Surface response contour plots of oleic acid conversion (%) for catalyst content-oleic acid:methanol molar ratio. Temperature: 55°C, TiO_2 content range between 1% and 30% (w/w_{OA}) and OA:MeOH molar ratio range between: 1:3 and 1:55. Experimental standard deviation (σ) of ± 0.00786.

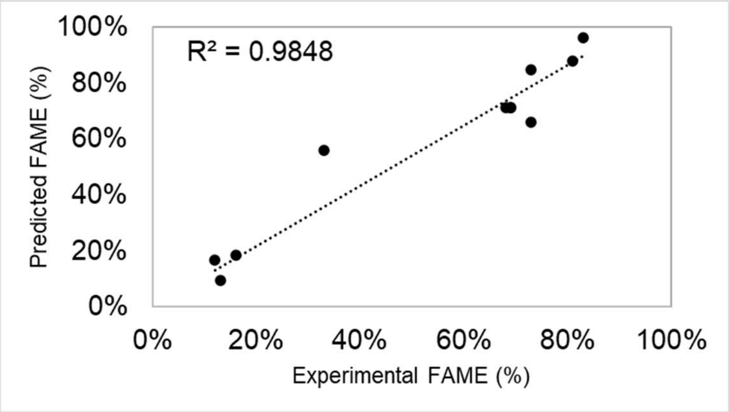

Figure 4. 10. Oleic acid conversion (%) obtained by the model (Equation 4. 10) and experimentally. FAME produced by oleic acid and methanol photoesterification.

$$FAME\ (\%) = -0.5815 + 0.0283 \cdot 7(OA{:}MeOH) + 8.7801 \cdot (Cat) - 0.000291 \cdot (OA{:}MeOH)^2 - 0.0094 \cdot (OA{:}MeOH) \cdot (Cat) - 20.2811 \cdot (Cat)^2 \qquad \text{Equation 4. 11}$$

Table 4. 6: *ANOVA for RSM obtained by CCR design for two variables [TiO_2 (w/w$_{OA}$)] and OA:MeOH molar ratio) for oleic acid and methanol photoesterification.*

	DF	SS	MS	F-value[a]	p-value
TiO_2	6	6066.27	1011.04	181.91	7.96E-5
OA:MeOH molar ratio	7	3052.07	436.01	78.45	4.07E-4
Model	13	12536.71	964.36	173.51	7.59E-5
Error	4	22.23	5.56		
Corrected total	17	12558.94			

[a]F_{crit}: 4.49.

To understand the impact of catalyst loading and alcohol content separately, both were evaluated by the mathematical model obtained from RSM (Equation 4. 11, and Figure 4. 11). The TiO_2 content showed a larger impact on FAME production than the OA:MeOH molar ratio. A high TiO_2 loading is required to increase the number of the active sites available by increasing the catalyst surface area, which was indeed observed until oleic acid conversion peaked at 20% (w/w$_{OA}$) of TiO_2. However, values higher than 20% w/w$_{OA}$ reduced oleic acid conversion. This reduction may be due to a decrease in the reaction medium's opacity and light scattering by the solid photocatalyst, hence reducing light incidence. Catalyst aggregation may have further reduced the catalyst surface area and hence photocatalytic efficiency. Despite the reaction stoichiometry of 1OA:1MeOH, a high alcohol concentration is needed to promote an efficient mix between the reactants (Bonet, Plesu, Ruiz, Iancu, & Llorens, 2014).

A lower concentration of methanol, e.g. 1OA:12MeOH, resulted in an increased presence of oleic acid close to the catalyst, forming a film that blocks the pores and reduces light irradiation (Figure 4. 5.b). At high concentrations of methanol such as 1OA:55MeOH, the formation of these passivating films becomes less likely (Figure 4. 5.c).

The high photoesterification efficiency observed for methanol was not retained for other alcohols, e.g. ethanol and n-propanol (Table 4. 7). This observation is in line with previous reports for other catalyst systems (Cardoso, Neves, & da Silva, 2009; Harun et al., 2018; M. v.d. Silva et al., 2015). Methanol has a partial charge greater than ethanol or propanol and thus, it is a better electron donor for oleic acid esterification (M. v.d. Silva et al., 2015). Consequently, the energy required to produce ethyl oleate or n-propyl oleate is higher than that of methyl oleate ($\Delta H°_{\text{methyl oleate}} \ll \Delta H°_{\text{ethyl oleate}}, \Delta H°_{\text{n-propyl oleate}}$ and $\Delta c_{p,L}/R^2_{\text{methyl oleate}} \ll \Delta c_{p,L}/R^2_{\text{ethyl oleate}}, \Delta c_{p,L}/R^2_{\text{propyl oleate}}$) (Guo et al., 2021; Moradi et al., 2021; S. M. Silva et al., 2020; M. v.d. Silva et al., 2015; Stacy et al., 2014). The pronounced differences in photoesterification efficiencies observed for the three alcohols may also be caused by RI (refractive index) differences, with higher RIs lowering the catalyst's capacity [RI_{MeOH}: 1.3165, RI_{EtOH}:1.3464, and $RI_{n\text{-}PrOH}$: 1.3704 (Craig, 1953)].

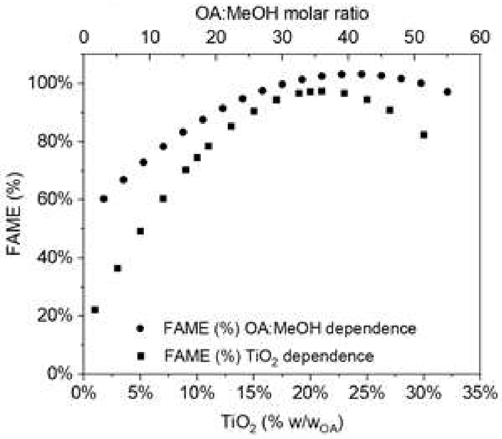

*Figure 4. 11***.** Predicted values of oleic acid conversion (%) considering % TiO_2 (w/w_{OA}) dependence (1OA:36MeOH molar ratio) and OA:MeOH molar ratio dependence [20% TiO_2 (w/w_{OA})], Temperature: 55°C.

Table 4. 7: *Oleic acid esterification by different catalysts and alcohols.*

Catalyst	Methanol	Ethanol	n-Propanol	Ref.
M-MMT K10 acid	70	40	35	(Harun et al., 2018)
$SnCl_2{\cdot}2H_2O$	77	68	36	(Cardoso et al., 2009)
TiO_2 + UVA[a]	97	21	6	This study

[a] Operational conditions: 55°C; 1OA:55MeOH and 20% (w/w_{OA}) of TiO_2.

Temperature relevance. The reaction temperature can have an impact on the reactants' miscibility and hence interfere with FAME yields. Temperature oscillations may also negatively impact on other operating conditions such as alcohol and catalyst content. Two distinct alcohol and catalyst loadings were thus investigated to evaluate the effect of temperature: PC1 [1:12 of OA:MeOH and 15% TiO_2 (w/w_{OA})] and PC2 [1:55 of OA:MeOH and 20% TiO_2 (w/w_{OA})]. For each PC condition, 5 tests were carried out (range: 25°C to 65°C; Table S4.1 of SI - APPENDIX C).

For both series, PC1 and PC2 operational conditions, higher conversions were obtained for higher temperatures (Figure 4. 12). Between 25°C and 55°C, an almost constant increase was noted, while a plateau and thus reaction equilibrium was reached between 55°C and 65°C. According to the thermodynamic properties obtained from this study (Section 4.3.7) and the literature (M. v.d. Silva et al., 2015), temperature weakly influences the esterification reaction. However, a higher temperature is required to obtain miscibility between free fatty acid and the alcohol, considering that alcohol has a higher affinity to itself than free fatty acid molecules (Bonet et al., 2014; Chandler, 2002; M. v.d. Silva et al., 2015). However, temperature alone is not sufficient to promote esterification. According to the blank tests (insert in Figure 4. 12) the reaction requires a catalyst to achieve a better oleic acid conversion.

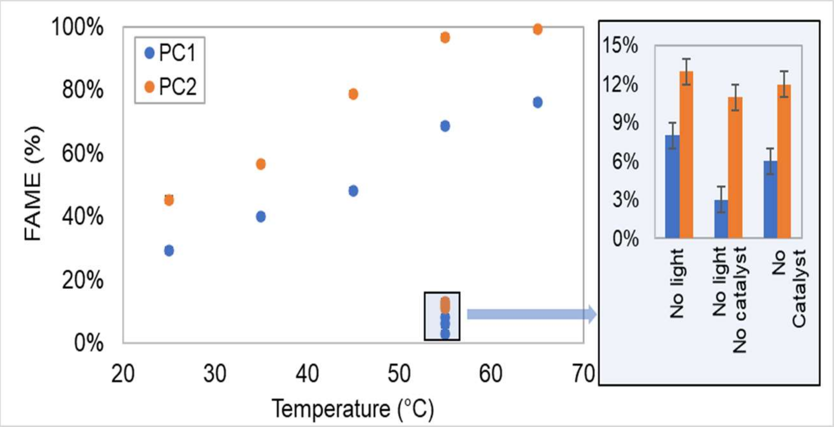

Figure 4. 12. Oleic acid conversion (%) with methanol to FAME. Photoesterification temperature analysis by PC1 (15% TiO_2 (w/w_{OA}) and 1OA:12MeOH), and PC2 (20% TiO_2 (w/w_{OA}) and 1OA:55MeOH). PC1 and PC2 enlargement: Blank tests conducted at 55°C considering the absence of light (UVA), light and catalyst (TiO_2), and catalyst (TiO_2), respectively [(σ) of ± 0.00786].

Relevance of individual operational conditions. The influence of the three independent variables (OA:MeOH, %TiO_2, and T) was analysed to understand their contribution to oleic acid conversion. A total of 33 experiments were performed (Table S 4. 1 of SI – APPENDIX C, including blank tests). According to these results (Table 4. 8), the correlation between the variables is consistent (p-value <0.0000 and an F-value of 27.891). Catalyst loading and temperature were identified as the more important variables (p-value <0.0002), in agreement with the literature for related reactions (Benyong Han et al., 2019; Foroutan, Mohammadi, & Ramavandi, 2021; Mohammad Fauzi & Saidina Amin, 2013; Prasertpong, Jaroenkhasemmeesuk, Regalbuto, Lipp, & Tippayawong, 2020; Rade et al., 2018).

Table 4. 8: *Oleic acid conversion (%) according to the dependent variables: TiO_2 content, OA:MeOH molar ratio, and temperature.*

	β*	SD of β*	B	SD of β	t (23)	p-value
Intercept			-55.5258	17.2989	-3.2098	0.0035
OA:MeOH	0.1612	0.1049	0.2514	0.1636	1.5359	0.1367
% TiO_2	0.7455	0.1061	2.9950	0.4262	7.0273	0.0000
T (°C)	0.4136	0.0969	1.2624	0.2958	4.2684	0.0002

R^2=0.76, F(3,26)=27.891, p_{value}<0.0000, and SD=15.052

4.3.4. Photocatalyst reuse

The reuse of photocatalyst after each recovery process resulted in a drop in conversion of 21% when compared with its first usage (Figure 4. 13). However, the conversion remained constant between subsequent reactions (C2 to C5). This finding suggests a reduction in the exposed catalyst's active sites. Besides a decrease in the contact area, residual oleic acid formed a passivating film on the catalyst's surface, thus blocking its pores and reducing the penetration of light. The catalyst's analysis and characterisation (discussed in Section 4.3.1) supports this interpretation. A decrease of pores and surface area was observed by N_2 physisorption and an increase of organic material impregnated on the catalyst was noted by FTIR and TGA. A similar behaviour was observed for Ni-doped ZnO nanocatalyst used for castor oil transesterification and its decrease in efficiency was associated with the deposition of organic material and a subsequent reduction in active sites (Baskar, Aberna Ebenezer Selvakumari, & Aiswarya, 2018; Guo et al., 2021).

Moreover, reductions in catalytic efficiencies are commonly observed, as shown in Table 4. 9. Nevertheless, the consistency in performances between 2 and 5 uses' cycles indicate that the catalyst retains its general stability and reactivity, thus making its reuse feasible and economical.

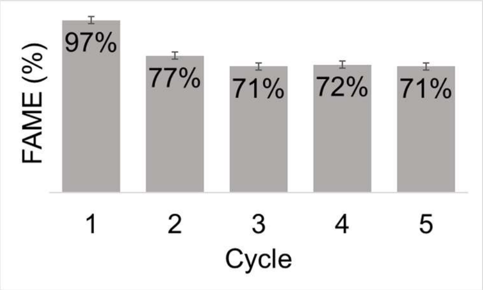

Figure 4. 13. Catalyst reuse. Operational conditions PC2: 55°C, 1OA mol:55MeOH mol, 20% TiO_2 (w/w_{OA}) [(σ) of ± 0.00786].

4.3.5. Photoesterification reaction mechanism

The accepted mechanism for oleic acid photoesterification with methanol in the presence of TiO_2 is depicted in Scheme 4. 1 (Ghani, Iqbal, Sadaf, Bhatti, & Asgher, 2020; Guo et al., 2021). TiO_2 excitation by photons (h^+) with sufficient energy to overcome its bandgap causes charge separation (Step 1) (Manique et al., 2016; Micic, Zhang, Cromack, Trifunac, & Thurnauer, 1993). Electrons (e^-) are promoted to the conduction band (CB), generating positive holes (h^+) in the valence band (VB) (Ohtani, 2011). Both species (h^+ and e^-) subsequently react with methanol (step 2) and oleic acid (step 3) adsorbed on the catalyst's surface. The hole (h^+) accepts an electron from the hydroxy-group, generating a methoxy radical ($CH_3O•$), while the electron (e^-) in the conduction band reacts with oleic acid, creating a carboxyl radical anion ($RCO_2^{-•}$). Both reactive intermediates combine and, after further reaction steps, form the ester and water (step 4). Alternative mechanisms have also been proposed (Karan et al., 2020; Manique et al., 2016).

4.3.6. Kinetics properties

Kinetic curves were obtained for all experiments, and a reaction time of 4 hours was found sufficient to reach equilibrium. For mathematical modelling, kinetic and equilibrium data obtained for PC1 [1OA mol:12MeOH mol, 15% TiO_2 (w/w_{OA})], and PC2 [1OA mol:55MeOH mol, 20% TiO_2 (w/ w_{OA})] within a temperature range of 25-65°C were considered. The kinetic results for photoesterification are shown in Figure 4. 14. At low temperatures (25 and 35°C) and methanol content (1OA:12MeOH of PC1), mixing is not efficient and after the first hour, reductions in conversions were observed. In particular, inefficient reagent ratios in combination with the hygroscopic nature of TiO_2 may favour water retention at the catalyst, thus favouring hydrolysis. At low temperature and high methanol content (all temperatures evaluated for 1OA: 55MeOH - PC2, Figure 4. 15), or at high temperature and low methanol content (45, 55, and

65°C for 1OA:12MeOH - PC1, Figure 4. 15) hydrolysis was successfully supressed. Hence, high temperatures and methanol contents are desirable to achieve a high esterification efficiency. Based on these overall findings, the kinetic mathematical model may result in a better accuracy when considering the backward reaction (hydrolysis). Five kinetic models were subsequently evaluated (Equation 4. 6 - 10), and their statistical analysis is shown in Table 4.10. The Langmuir-Hinshelwood (L-H) model achieved the best agreement with the experimental data (Figure 4. 15). This result highlights the importance of evaluating the heterogeneous catalytic reaction through models that consider the presence of active sites.

Table 4. 9: *Catalyst reuse for oleic acid and methanol photoesterification.*

Catalyst	FAME (%)	# cycles	FAME (%)	Decrease (%)[a]	Ref.
TiO_2 + UVA	98	5	71	28	This study
Fe3O4@PILPW	93	6	90	3	(Z. Wu et al., 2016)
HPA/ZIF(His.)	92	4	73	18	(Narenji-Sani et al., 2020)
LO (lanthanum oxide)	63	3	10	84	(Vieira et al., 2013)
SLO/HZSM-5	100	3	52	48	(Vieira et al., 2013)
SLO (sulphated lanthanum oxide)	98	3	28	71	(Vieira et al., 2013)
TiO_2/NP-800	87	6	70	20	(Essamlali et al., 2017)
$Zr(SO_4)_2$	98	4	41	57	(Senoymak Tarakcı & Ilgen, 2018)

[a]Decrease between first and last cycle.

Table 4. 10: *Kinetic models[a] statistical analysis applied to experimental kinetic data of oleic acid and methanol photoesterification.*

Model[a]	R^2	SD	p-value	F-test
HSE1HN	0.928	0.066	<0.0000	877.551
HSE1H1	0.939	0.061	<0.0000	1047.042
HSE1H2	0.931	0.065	<0.0000	1008.048
HSE2H2	0.480	0.122	<0.0000	62.878
L-H	0.997	0.026	<0.0000	4726.083

[a]Equation 4. 6 - 10. Kinetics data evaluated at time: 15, 30, 45, 60, 120, 180, and 240 minutes. For PC1 (1OA mol:12MeOH mol, 15% TiO_2 (w/w_{OA}) and PC2 [1OA mol:55MeOH mol, 20% TiO_2 (w/w_{OA})].

The L-H kinetic model was subsequently used to obtain kinetic parameters for PC1 and PC2 operational conditions at different temperatures (Figure 4. 16). The k_1 (esterification) and k_{-1} (hydrolysis) resulted in a $K_{eq}<1$ for low temperatures and $K_{eq}>1$ for high temperatures (Figure 4. 17). This confirms that the hydrolysis reaction is significant for the low-temperature process, but not dominant for high methanol content. However, a higher methanol content improves the esterification reaction according to K_{eq} (1OA:55MeOH molar ratio) ≫ K_{eq} (1OA:12MeOH molar ratio). K'_1 and K'_{-1} refer to oleic acid and FAME adsorption on the catalyst's active sites, respectively. According to the increase in reaction efficiency, K'_1 decreased and K'_{-1} increased, which indicates that oleic acid and FAME compete for adsorption on the catalyst. However, $K_{eq} \gg K'_1$ and K'_{-1} reveals that the reagent adsorption on the catalyst does not limit the reaction and it instead maintains its catalytic capacity. Moreover, the parameter (K) variation in the photochemical process suggests that the reaction does not have a rate-determining 'light-intensity limited' step (Ohtani, 2011). Thus, the energy from the catalyst's charge separation is enough to drive the reaction sufficiently.

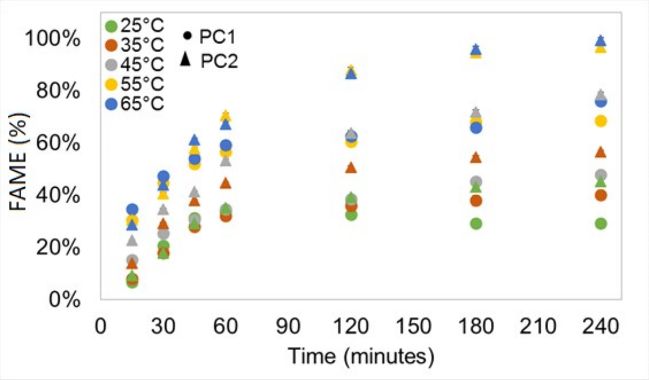

Figure 4. 14. Oleic acid and methanol photoesterification kinetic curves. Catalyst: TiO_2 irradiated by UVA. PC1 [1OA mol:12MeOH mol, 15% TiO_2 (w/w_{OA})] and PC2 [1OA mol:55MeOH mol, 20% TiO_2 (w/w_{OA})].

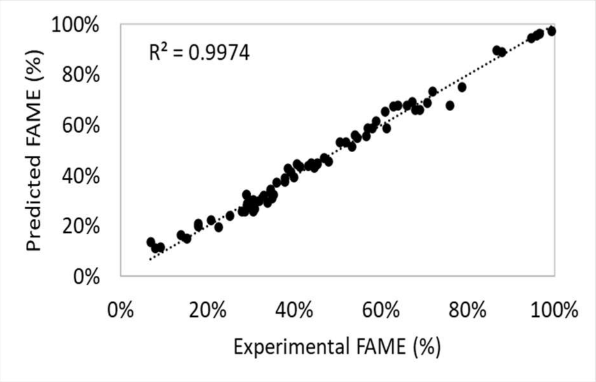

Figure 4. 15. Experimental and modelling data obtained by L-H kinetic model (Equation 4. 10*)* for FAME (x_{FAME}) obtained by oleic acid and methanol photoesterification. The x_{FAME} was evaluated at t: 15, 30, 45, 60, 120, 180 and 240 minutes for PC1 [1OA mol:12MeOH mol, 15% TiO_2 (w/w_{OA})] and PC2 [1OA mol:55MeOH mol, 20% TiO_2 (w/w_{OA})].

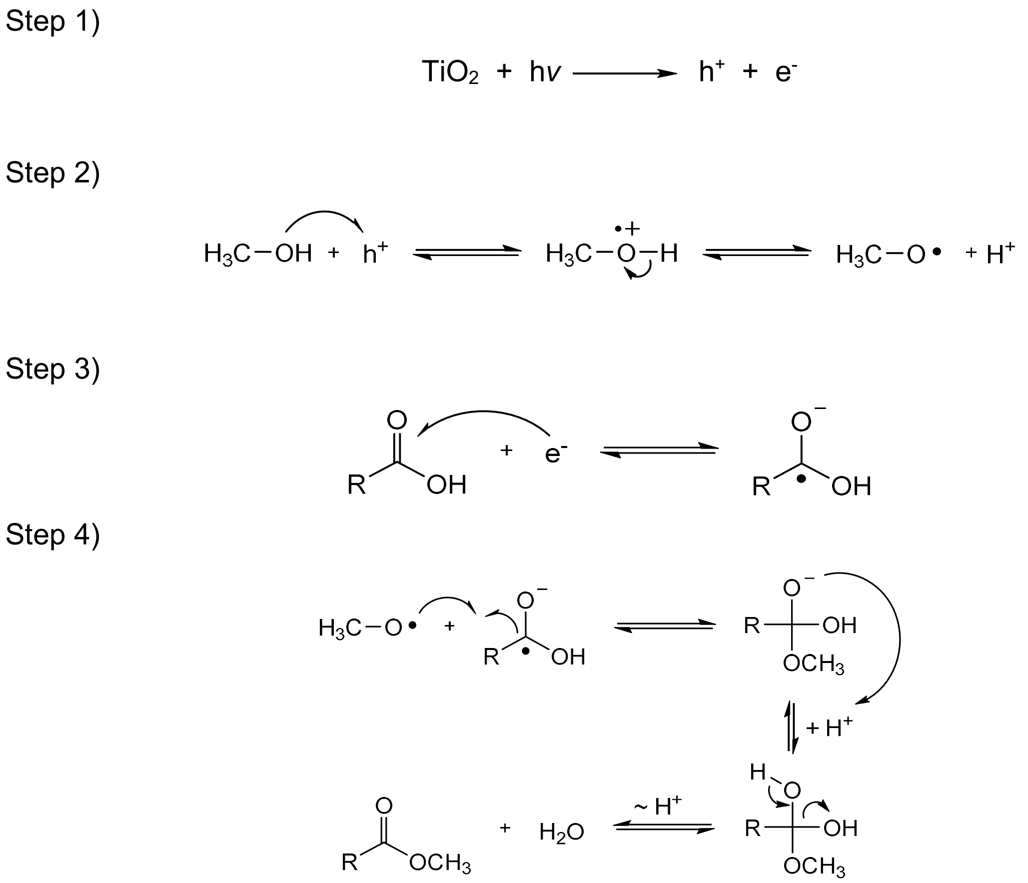

Scheme 4. 1. Proposed photoesterification mechanism for oleic acid and methanol (R = cis-$CH_3(CH_2)_7CH{=}CH(CH_2)_7$).

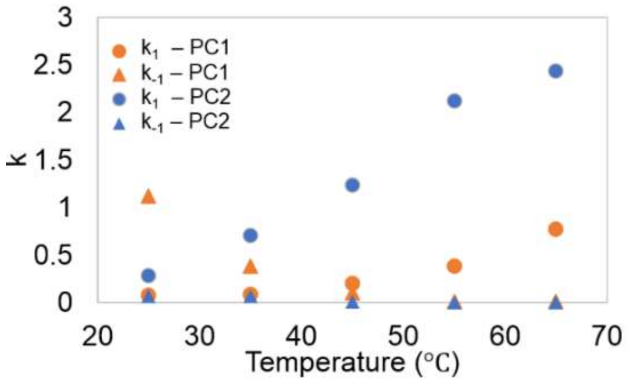

Figure 4. 16. Kinetic constants for the forward reaction (esterification, k_1) and for the backward reaction (hydrolysis, k_{-1}), obtained by the L-H kinetic model (Equation 4. 10). Two operational conditions were evaluated: PC1 (1OA mol:12MeOH mol, 15% TiO_2 (w/w_{OA}) and PC2 (1OA mol:55MeOH mol, 20% TiO_2 (w/w_{OA}).

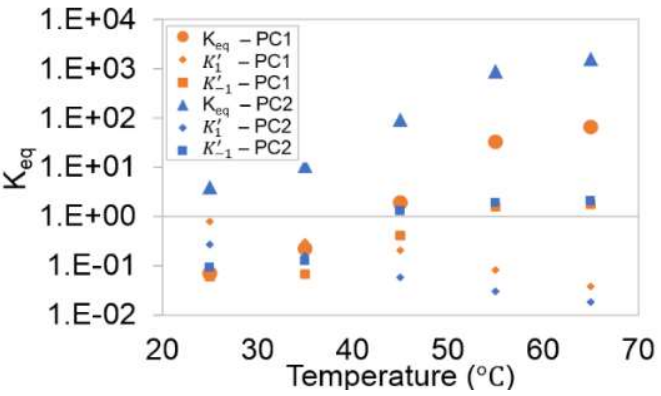

Figure 4. 17. Equilibrium constant for esterification/hydrolysis reactions (K_{eq}), equilibrium constant for oleic acid adsorption on active catalyst site (K'_1), and equilibrium constant for FAME adsorption on active catalyst site (K'_{-1}). Two operational conditions were evaluated: PC1 (1OA mol:12MeOH mol, 15% TiO_2 (w/w_{OA}) and PC2 (1OA mol:55MeOH mol, 20% TiO_2 (w/w_{OA}).

4.3.7. Thermodynamic properties

The thermodynamic properties of the oleic acid photoesterification with methanol were likewise determined. The Arrhenius and van't Hoff models (Equation 4. 2 and Equation 4. 3, details in S 4.5 of SI – APPENDIX D) were used to obtain E_a, A, ΔH, and ΔS (Table 4. 11). The energy required for operational conditions PC2 is lower than PC1, confirming that methanol content and temperature are significant parameters for improving the photoesterification efficiency. ΔH was determined as 15.609 kJ/mol for the 1OA:12MeOH and 13.748 kJ/mol for the 1OA:55MeOH molar ratio, respectively. This slight difference shows that a high methanol amount is predominantly required to mix the reagents. ΔH of the oleic acid/methanol photoesterification depends on each process analysed and according to the literature, it is possible to obtain values between 7 and 50 kJ/mol (Hassan & Vinjamur, 2013; Lapuerta, Rodríguez-Fernández, & Oliva, 2010; Osmont, Catoire, & Gökalp, 2007; M. v.d. Silva et al., 2015).

Furthermore, the positive values of ΔH and ΔS demonstrate that the reaction requires high temperatures. The ΔG (Equation 4. 5) behaviour is shown in Figure 4. 18. High temperatures and methanol content result in lower ΔG, favouring the esterification reaction. However, the methanol content (ΔG≈10 kJ/mol) interferes less than temperature (ΔG≈17 kJ/mol). Due to the positive value of ΔH and the negative value of ΔG, ΔS is a significant thermodynamic parameter, as known from the literature (Osmont et al., 2007). Therefore, the reagents' miscibility is relevant as maintained by a high content of methanol and/or a higher disorder caused by temperature increments. This behaviour supports literature findings (Bonet et al., 2014; M. v.d. Silva et al., 2015), where high alcohol contents and temperatures were required to mix the reagents properly and to achieve high esterification efficiencies. The Gibbs energy also reflects the catalyst behaviour, considering that after photoexcitation, the process is spontaneous (ΔG<0), mainly because of the exothermic natures of step 3 (ΔG <0) and step 4 (ΔGh <0) in Scheme 4. 1 (Ohtani, 2011). The ΔG<0 may result from systems where the reduction and oxidation steps do not need to be spatially or chemically separated (Ohtani, 2011).

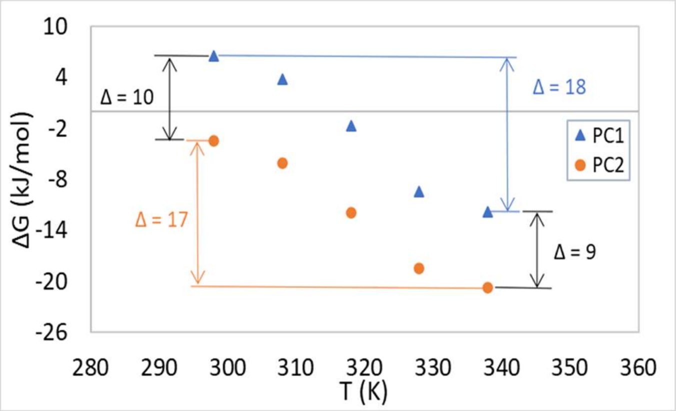

Figure 4. 18. Gibbs energy variation for oleic acid and methanol photoesterification. PC1: 1OA mol:12MeOH mol, 15% TiO_2 (w/w_{OA}). PC2: 1OA mol:55MeOH mol, 20% TiO_2 (w/w_{OA}).

Table 4. 11: *Thermodynamic properties for photoesterification obtained by PC1 and PC2 operational conditions at a temperature range between 25°C and 65°C by kinetic parameters obtained by the L-H kinetic model.*

	PC1[a]	**PC2[b]**
E_a (kJ/mol)	5.03	4.58
A (min^{-1})	4.02E+07	3.91E+07
ΔH (kJ/mol)	15.61	13.75
ΔS (kJ/mol.K)	0.50	0.47

[a]PC1: 1OA mol:12MeOH mol, 15% TiO_2 (w/w_{OA}); [b]PC2: 1OA mol:55MeOH mol, 20% TiO_2 (w/w_{OA}).

4.4. Conclusion

An optimised photoesterification process using TiO_2 and UVA irradiation with high efficiency to produce methyl oleate from oleic acid (conversion: 98%) was developed. Optimal conditions were obtained after catalyst pretreatment and with a loading of 20% wt/wt_{OA} and an oleic acid:alcohol molar ratio of 1:55 at 55ºC. The catalyst was reusable, proving its efficiency even after five cycles (FAME>70%). Kinetics modelling was carried out and thermodynamic properties were obtained. According to these, a temperature higher than 55ºC and excess of alcohol are required to reach a high conversion rate. Low temperatures and/or lower alcohol contents result in reduced conversions and/or reverse reactions (hydrolysis). The simple optimised process obtained in this study overcomes the difficulties frequently observed for FAME production by oleic acid esterification using thermal methods (high temperature, extreme pH, difficult catalyst reuse and recovery, large volumes of water, complex FAME purification). Future research will investigate potential applications of the developed process to produce biodiesel from other free fatty acids, crude oils and waste cooking oil, as well as solar operation (Oelgemöller, 2016) and process scale-up.

Acknowledgement

RAW wishes to thank the College of Science and Engineering at James Cook University for financial support (Competitive Research Training Grants 2021 and 2022). The authors thank Assoc.-Prof. George Vamvounis, Dr. Mark Robertson and Dr. Shane Askew (James Cook University) for technical support.

Chapter V

Biodiesel production from canola oil by TIO_2- photocatalysed transesterification

Submitted - *Fuel Journal*: Rosilene Andrea Welter[1,2], Harrson Silva Santana[2], Lucimara Gaziola de la Torre[2], Mark C. Barnes[1], Osvaldir Pereira Taranto[2], Michael Oelgemöller[1,3], Biodiesel Production from Canola Oil by TiO_2-Photocatalysed Transesterification. Available at SSRN: https://ssrn.com/abstract=4201382 or http://dx.doi.org/10.2139/ssrn.4201382.

Filiation: (1) College of Science and Engineering, James Cook University, Postcode Qld 4811, Townsville, Queensland, Australia; (2) School of Chemical Engineering, University of Campinas, Postcode 13083-852, Campinas, SP, Brazill; (3) Faculty of Chemistry and Biology, Hochschule Fresenius gGmbH-University of Applied Science, Postcode D-65510, Idstein, Germany.

Abstract

Fatty acid esters were produced by phototransesterification of canola oil using TiO_2 as a photocatalyst and UVA or sunlight as radiation sources. Conversions of approximately 73% (±1.41) and 19% to fatty acid methyl ester (FAME) were achieved with methanol (1 TGL (triglyceride) mol:55 MeOH mol, 20% TiO_2 $w/w_{TGL,}$ 65°C, 4 hours). Using ethanol resulted in a decreased conversion of 38% instead. Conventional acid- and alkali-catalysed methods were used to compare their reaction products, FAME, with that obtained by photocatalysis. The kinetic curves were established for temperatures between 25 and 65°C. Six different kinetic mathematical models were applied, and a second forward/fourth backward model showed the highest accuracy (R^2 of 0.996). This suggests that a homogeneous model is suitable for a heterogeneous process, with mass transfer to the active sites of the catalyst not being the rate-limiting step. The thermodynamic results ($\Delta G_{328.15K}$=29.98 kJ/mol, $\Delta G_{338.15K}$=-6.88 kJ/mol, ΔH=83.00 kJ/mol, and ΔS=0.26 kJ/mol.K) indicate that this endothermic reaction requires temperatures higher than 65°C to reach high conversions.

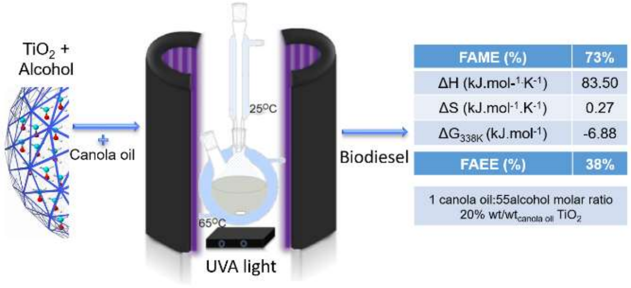

Figure 5. 1. Graphical abstract: - Biodiesel production from canola oil by TIO_2-photocatalysed transesterification.

Keywords

Biodiesel, canola oil, photocatalysis, phototransesterification, thermodynamic properties, titanium dioxide.

5.1. Introduction

Fossil fuels are the primary energy source for power and transportation, however, increasing energy demands have resulted in the depletion of natural oil reserves. In addition, the use of fossil fuels produces significant CO_2 emissions, exacerbating anthropogenic climate change. As an eco-friendly option, biodiesel is considered as a substitute for fossil fuels. The annual global biodiesel production consequently increased eight times between 2005 and 2020 to 46 billion litres (Ogunkunle & Ahmed, 2019). Biodiesel has several benefits such as being four times easier to degrade (A. Demirbaş, 2008), emitting 86% fewer greenhouse gases (Voegele, 2020), and its availability from renewable resources (e.g. crude vegetable oils, waste cooking oil (WCO), or animal fat - ASTM D6751–15, 2015). Canola oil is one of the most produced and consumed vegetable oils globally and represented 68% of the global biodiesel feedstock (D.-S. Kim, Hanifzadeh, & Kumar, 2018). Biodiesel is a mixture of long-chain fatty acid alkyl esters (FAAE) produced mainly by esterification, transesterification, or both. Transesterification, the most common reaction, occurs between triglycerides (TGL) and alcohols in the presence of a catalyst such as strong acids or alkalis, producing FAAE and glycerol. However, these conventional homogeneous methods demand extensive separation and purification processes that generate large amounts of waste (G. Berrebi et al., 1993). These issues may be circumvented by solid eco-friendly catalysts such as metal oxides, enzymes, zeolites, alumina, and the utilisation of waste materials (Alsharifi et al., 2017; Arzamendi et al., 2007; Calero et al., 2014; Corro et al., 2013; Wan Omar & Amin, 2011; Rosilene A. Welter, Santana, Torre, Robertson, Taranto, & Oelgemöller, 2022). Heterogeneous catalysts are commonly easier to separate and regenerate, safer and more practicable to handle, and less corrosive (Chouhan & Sarma, 2011; De & Boxi, 2020; Granados et al., 2007; Ma & Hanna, 1999).

One promising technology is the use of photoactivated catalysts such as titanium dioxide (TiO_2). TiO_2 is non-toxic, chemically stable, easy to handle, and recycable (Carp et al., 2004). Photocatalysis has been studied extensively for organic pollutant degradation e.g. dyes, pesticides, and pharmaceuticals (Kanakaraju et al., 2014; Konstantinou & Albanis, 2003; Rajeshwar et al., 2008), but much less for organic synthesis (N. Hoffmann, 2015). Importantly, it has recently been evaluated as an alternative for biodiesel synthesis by esterification and transesterification. For example, oleic acid and methanol photoesterification was achieved using TiO_2 and UVA-irradiation, resulting in 98% conversion (Rosilene A. Welter, Santana, Torre, Robertson, Taranto, & Oelgemöller, 2022). TiO_2 nanotubes and sunlight irradiation gave 91% conversion for WCO transesterification (Khaligh et al., 2021). TiO_2/g-C_3N_4 under sunlight irradiation resulted in a conversion of 90% for TGL from WCO (M. Khan et al., 2021). The attractive advantages of photocatalysis are its sustainable operation conditions in mild temperatures and pH-ranges, yielding higher-purity products that can be recovered easily, and the simple reuse of the catalyst. TiO_2-photocatalyis using natural sunlight has also be applied to the manufacturing of commodity chemicals or water treatment (Bahnemann, 2004; Oelgemöller, 2016).

The present study evaluated photoactivation of TiO_2 with UVA or sunlight for canola oil transesterification with methanol or ethanol. The aim was to provide essential experimental data to achieve the best operational conditions, to develop a robust process protocol, and to determine kinetic and thermodynamic properties. Despite their importance for developing cost-efficient and scalable processes, few studies have examined the kinetic and thermodynamic parameters thus far.

5.2. Methodology

5.2.1. Materials

Reagents and solvents were obtained from the following suppliers: canola oil (Brand: Woolworths), TiO_2 (P25: Aeroxide®, Evonik), methanol (HPLC grade, Fisher Chemical), chloroform D (99.8% atom D, $CDCl_3$, Aldrich), dichloromethane (DCM, AR, 99.5%, Univar), sulfuric acid (A.R., Univar), potassium hydroxide pellets (KOH, Univar), acetone (AR, 99.5%, Chemsupply), diethyl ether (AR, 99.5%, Univar), ethyl acetate (AR, 99.5%, Univar), ethanol (AR, 99.5%, Univar), 0.02 N potassium hydroxide in aqueous solution ($KOH_{aqueous}$, ±0.5%, Ace Chemical Company), sodium bicarbonate ($NaHCO_3$, AR, Univar), and anhydrous sodium sulfate (Na_2SO_4, AR, Univar). The reaction samples were filtered through a Hydraflon 0.22 µm, 35 mm syringe filter.

5.2.2. Canola oil transesterification

Canola oil and alcohol transesterification was examined using four different conditions: alkali-catalysis (KOH), acid-catalysis (H_2SO_4), UVA/TiO_2-photocatalysis and solar TiO_2-photocatalysis. The first two methods represent the most common thermal processes and were investigated to compare the biodiesels obtained with that from photocatalysis. An additional experiment was conducted using acid catalysis but with a shorter reaction time in order to examine the presence of possible intermediates, e.g. monoglycerol (MGL) and diglycerol (DGL).

5.2.3. Alkali catalyst

Anhydrous methanol (150 mL), canola oil (15 g), and KOH (1.5 g) were added to a round-bottom flask (250 mL). The mixture was stirred rapidly with a magnetic stirrer at 60°C for two hours. The mixture was then allowed to settle for 24 hours at room temperature. The product was purified using the following steps: (1) 600 mL of water was added; (2) the liquid phase was removed by rotary evaporation at 40°C (170 mbar for 60 minutes, 72 mbar for 60 minutes, and 30 mbar for 60 minutes); (3) for three consecutive times, 150 mL of ethyl acetate was added and mixed gently, allowed to settle for one hour in a separatory funnel, and the organic layer was separated; (4) 150 mL of diluted HCl 0.5% (v/v) solution was added, mixed, and the mixture was separated into two phases; (5) 150 mL of a saturated aqueous NaCl solution was added, mixed, and allowed to separate into phases; (6) the organic layer was separated and dried with anhydrous Na_2SO_4 for approximately five minutes; (7) filtered using a syringe filter (Hydraflon 0.22 µm, 35 mm); (8) the crude product was rotary evaporated at 40°C to remove any volatiles (170 mbar for 30 minutes, 72 mbar for 30 minutes, and 30 mbar for 60 minutes); (9) the samples were stored in glass vials at room temperature for further characterization.

5.2.4. Acid catalyst

Test one (complete conversion): Anhydrous methanol (150 mL), canola oil (15 g), and H_2SO_4 (1.5 g) were added to a round-bottom flask (250 mL), stirred rapidly with a magnetic stirrer at 60°C for five hours, and left to stand for 24 hours at room temperature. The product was purified using the following steps: (1) 600 mL of water was added; (2) the liquid phase was removed by rotary evaporation at 40°C (170 mbar for 60 minutes, 72 mbar for 60 minutes, and 30 mbar for 60 minutes); (3) for three consecutive times, 150 mL of ethyl acetate was added and mixed gently, allowed to settle for one hour in a separatory funnel, and separated; (4) 150 mL of a dilute $NaHCO_3$ solution was added and mixed to separate into two phases; (5) 150 mL of a saturated aqueous NaCl solution was added, mixed, and separated into phases; (6) anhydrous Na_2SO_4 was added to the organic layer and left to stand approximately five minutes; (7) filtered through a syringe filter (Hydraflon 0.22µm, 35 mm); (8) the mixture was rotary evaporated at 40°C to remove any volatiles (170 mbar for 30 minutes, 72 mbar for 30 minutes, and 30 mbar for 60 minutes); (9) the samples were stored in glass vials at room temperature for further characterization.

Test two (incomplete conversion): the same steps mentioned above were used; however, the reagents were mixed with a magnetic stirrer at 90°C for one hour instead of five hours, and purification was performed immediately.

.

5.2.5. UVA light irradiated TiO_2 catalyst

The catalyst pretreatment and operational conditions were adopted from the optimised photoesterification process developed by Welter (Rosilene A. Welter, Santana, Torre, Robertson, Taranto, & Oelgemöller, 2022). The light and water flow, and reaction heating (water bath) were turned on 30 minutes before the phototransesterification experiment. TiO_2 was added to methanol and mixed at the respective phototransesterification test temperature (25–65°C, Table S5.1 of SI – APPENDIX E). After stirring for 30 minutes, TiO_2 and MeOH (20% w/w_{TGL} of TiO_2, and 1 TGL mol:55 methanol mol, total volume of reactional medium: 100 mL) were loaded into the reactor (Figure 5. 2.a). with canola oil. The double jacketed two-necked round-bottom flask vessel (500 mL capacity) was manufactured using Pyrex glass (cut-off wavelength ≤290 nm). Irradiation was conducted in a Rayonet RPR-200 photochemical reactor (Southern New England Ultraviolet Company) equipped with 16 F8T5/BL fluorescent tubes (Ushio, 8W Black Light UVA T-5 G5 Base). The oil, methanol, and TiO_2 were mixed vigorously by magnetic stirring. During the kinetic studies, samples (<3 mL each) were withdrawn at set reaction times (15, 30, 45, 60, 120, 180, and 240 minutes). The reactions were stopped after presumably reaching equilibrium (240 minutes) and treated using the following steps: (1) filtered through a syringe filter (Hydraflon 0.22µm, 35 mm); (2) rota-evaporated at 40°C to remove water and alcohol (170 mbar for 15 minutes, 72 mbar for 30 minutes, and 30 mbar for 30 minutes); (3) left to stand for 20 hours to allow for glycerin separation; (4) stored in glass vials at room temperature; (5) conversion determined by ^1H-NMR as described in Section 5.2.7; (6) the final sample (240 minutes) was characterised further (Section 5.2.9). The best result was repeated three times, and the standard deviation was determined. Five blank tests were performed by keeping the operational conditions constant (65°C, 1 TGL mol:55 MeOH mol, and 20% w/w_{TGL} of TiO_2): Blank 1 (absence of catalyst); Blank 2 (absence of light with the reaction vessel wrapped in aluminium foil); Blank 3 (absence of catalyst and light with the reaction vessel wrapped in aluminium foil); Blank 4 (absence of stirring); Blank 5 (absence of catalyst pretreatment). FAEE was also produced, applying the best operational condition obtained previously for FAME, but using ethanol instead of methanol.

5.2.6. Concentrated solar/TiO_2-photocatalysis experiments

Considering the best operational conditions achieved with artificial UVA light (Section 5.2.5 and 5.4.1), the transesterification of canola oil was examined using natural sunlight instead of UVA light (Figure 5. 2.b). The apparatus utilised a spherical stainless steel dish (inner diameter of 44 cm, focal length of 16.13 cm) below the double-jacketed round-bottom reactor. The reaction was conducted on the ground outside the Molecular Genetic Laboratory Building on the James Cook University campus in Townsville (latitude – 19°33'S, longitude 146°76'E, elevation 37.2m above sea level) for 360 minutes, from 9:30 am to 3:30 pm (6th of January 2022), the period with the highest radiation. The sunlight irradiation measurements for Townsville were obtained from ARPANSA (ARPANSA, 2022) (Section S5.2 of SI – APPENDIX D).

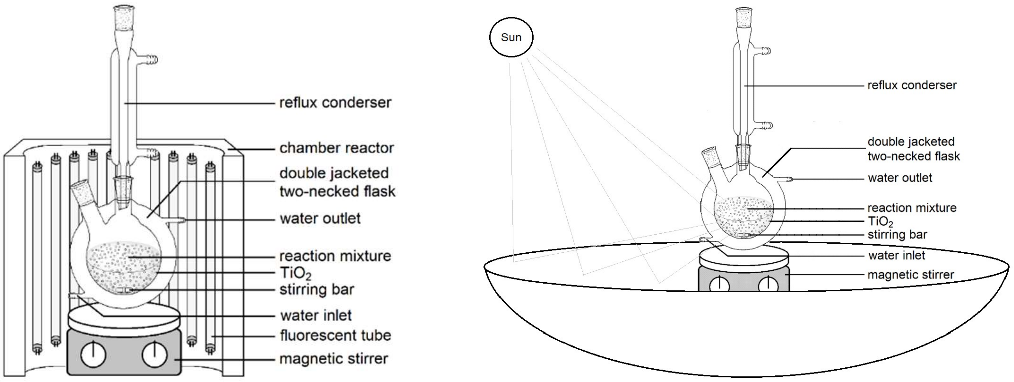

Figure 5. 2. a) UVA- and b) solar phototransesterification reactor schemes.

5.2.7. Reaction conversion determination

The biodiesel concentration was determined by ^{1}H-nuclear magnetic resonance (NMR) spectroscopy (*Bruker Ascend*™ *400 MHz* Spectrometer) by comparing the integration areas of baseline-separated signals using the MestReNova® software (Version 6.0.2-5476, Mestrelab Research S.L.®). The FAME amount (Equation 5. 1) was calculated by correlating the three methoxy protons (I_{Me}, approx. 3.6 ppm) with the two α-methylene protons of the oil

($I_{\alpha CH_2}$, approx. 2.3 ppm), as described by (Borah, Devi, Saikia, & Dhanapati Deka, 2018; Gelbard, Brès, Vargas, Vielfaure, & Schuchardt, 1995). The FAEE concentration was obtained similarly (Equation 5. 2), by correlating the glyceride CH_2 (I_{GL}) and ethoxy (I_{EE}) proton areas ($I_{GL + E.E.}$, overlapping peaks at 4.10–4.20) with the α-methylene protons area of the oil ($I_{\alpha CH_2}$, 2.3 ppm), as described by (Jaiswal, Tejo Prakash, & Prakash, 2016) (Section S5.3 of SI – APPENDIX D).

$$\% \mathrm{FAME} = 100\% \cdot \frac{2 \cdot \mathrm{I_{ME}}}{3 \cdot \mathrm{I_{\alpha CH_2}}}$$ Equation 5. 1

$$\% FAEE = 100\% \cdot \frac{I_{GL+EE} - I_{GL}}{I_{\alpha CH_2}}$$ Equation 5. 2

5.2.8. TiO_2 Catalyst

Recovery, reactivation and reuse. After each photochemical experiment, the catalyst was recovered and treated using the following steps: (1) filtered through a filter paper (Grade: MS 2 185 mm, MicroScience); (2) washed with acetone by mixing vigorously with magnetic stirring (500 rpm); (3) settled for 20 hours followed by decantation; (4) dried at 100°C for 24 hours; and (5) crushed. These steps represent the first stage of the recovery process (1 RP). This process was repeated three times (3 RP) to complete one reactivation cycle (1 C). The samples were stored in plastic vials at room temperature. The efficiency and reusability of the recovered TiO_2 was evaluated using the characterisation techniques described below and by conducting five subsequent photoreaction tests (1C to 5C).

Characterisation. TiO_2 was characterised before (pure), after use (0RP), after reactivation (1C), and after reuse (2C–5C) using the following analyses. Thermogravimetric analysis (TGA) and differential scanning calorimetry (DSC) (5°C/min, room temperature to 600°C, SDT650 equipment) were performed to determine the presence of organic material impregnated on the catalyst material. The data was subsequently analysed using the Trios® software (T.A. Instruments). Two samples were analysed in triplicates: one with the highest content (0RP) and one with the lowest content (5C) of organic material. The particle size, pore volume and size, and total surface area were determined using N_2 physisorption using the respective isotherms: Brunauer–Emmet–Teller (BET) and Barrett–Joyner–Halenda (BJH) methods (Quantachrome Instruments, 2009). The surface area was determined using the BET model (Equation 5. 3), correlating the surface coverage (ϴ), BET constant (c), pressure (p), and vapour pressure of the adsorptive bulk liquid phase (p_0). Pore volume and diameter were determined using the BJH model (Equation 5. 4), which is based on the Kelvin equation and correlates p, p_0, the gas/liquid surface tension (ϒ), molar volume of the adsorbate (M), gas constant (R), and temperature (T). The particle size (Equation 5. 5) was established by relating the surface area (S_{BET}) and the solid density (ρ, 4.2 g/mL for TiO_2) (Raj & Viswanathan, 2009).

$$\theta = \frac{cp}{(1 - p/p_0) \cdot \left(p_0 + p(c-1)\right)} \quad \text{Equation 5. 3}$$

$$ln \frac{p}{p_0} = \frac{-2\Upsilon M}{RT} \quad \text{Equation 5. 4}$$

$$D = \frac{6000}{S_{BET} \cdot \rho} \quad \text{Equation 5. 5}$$

Fourier transform infrared–attenuated total reflection (FTIR-ATR) spectroscopy was conducted at room temperature over the spectral range of 400–1000 cm^{-1} (Nicolet™ iS™ 5 FTIR Spectrometer coupled with an iD7 ATR accessory, ThermoFisher Scientific) to detect the presence of organic functional groups. The TiO_2 bandgap (E_g) was obtained by UV-Vis spectroscopy at room temperature over the spectral range of 200–1100 cm^{-1} (UV-1800, Shimadzu) using the Tauc method (Equation 5. 6) (Arunachalam, Dhanapandian, Manoharan, & Sivakumar, 2015; Kulak & Kiiliomin, 2018; Makuła, Pacia, & Macyk, 2018). The model correlates the absorption coefficient (α), photon energy ($h\nu$), a constant (B), and a factor (ϒ) that depends on the nature of the electron transition (0.5 for direct and 2.0 for indirect transition band gaps). For TiO_2, ϒ = 2 was considered (Makuła et al., 2018). The TiO_2 suspension was prepared by vigorously mixing 10^{-3} mg/L TiO_2 in methanol for four hours.

$$(\alpha \cdot h\nu)^{1/\gamma} = B \cdot \left(h\nu - E_g\right) \quad \text{Equation 5. 6}$$

The crystal structure and crystallite size were examined by powder X-ray diffraction (XRD, Siemens D5000 Diffractometer) using Cu Kα radiation (λ_{XRD} =0.154060 nm). The mean crystallite size was obtained by analysing the prominent peak observed in the XRD pattern for anatase (25.23° 2θ) and rutile (27.43° 2θ), respectively. The Scherrer equation (Equation 5. 7) was used to estimate the crystallite size according to:

$$D_C = \frac{K_{XRD} \cdot \lambda_{XRD}}{\beta_{XRD} \cdot \cos \theta_{XRD}} \qquad \text{Equation 5. 7}$$

Where K_{XRD}= 0.9 and λ_{XRD}=1.5406 Å

5.2.9. FAME characterisation

The FAME composition was analysed by gas chromatography (7890A Agilent Gas Chormatograph, Injector: 7683B Agilent). The analysis was carried out according to the EN14103:2011 methodology (McCurry, 2012) using an HP-5INNOWax capillary column (30 m × 0.25 mm x 0.25 μm film). Pure helium was used as the carrier gas (1 mL/min), 250°C was set as injector and detector temperature. The temperature program used was 60°C for two minutes, 10°C/min to 200°C, 5°C/min to 240°C, and holding at 240°C for seven minutes. FTIR-ATR spectroscopy was used to chemically analyse the oil and FAME. The acid value was determined by titration using a modified procedure (Du et al., 2022; EN 14104, 2003; Onu & Mbohwa, 2021) as follows. The organic sample (0.05 g) was diluted in a diethyl ether/ethanol solution (2:1, 25 mL) (v/v). Two drops of thymol blue indicator were added and the analyte was titrated using a 0.02N KOH aqueous standard solution. The acid value (A.V.) was calculated as described in Equation 5. 8, correlating the volume of the KOH solution used in the titration (S, mL), the volume of the KOH used in the blank titration (b, mL), the normality of KOH (N), and the sample mass (W, g):

$$AV = \frac{(Sb) \cdot N \cdot 56.1}{W} \qquad \text{Equation 5. 8}$$

TGA/DSC (SDT650 equipment) was used to determine the maximum combustion rate [$(dM/dT)_{max}$] (Lai et al., 2014; Wnorowska, Ciukaj, & Kalisz, 2021), mean combustion rate [$(dM/dT)_{mean}$] (Lai et al., 2014), burnout temperature (T_e) (J. J. Lu & Chen, 2015; Wnorowska et al., 2021), and ignition temperature (T_i) (N. Khan et al., 2021; J. J. Lu & Chen, 2015; Wnorowska et al., 2021). Air and nitrogen were used for operations. The temperature was increased from room temperature to 600°C at a heating rate of 10°C/min. The data were analysed using the Trios® software (T.A. instruments) and OriginPro 2021® (Learning Edition, OriginLab Corporation). The activation energy (E_a) was estimated using the Arrhenius model (Equation 5. 9) and expressed analytically according to the Coats–Redfern method (Equation 5. 10) (Cai & Bi, 2008; Kipcak, Senberber, Moroydor Derun, Tugrul, & Piskin, 2015; Yao, Wu, Lei, Guo, & Xu, 2008) by correlating the heating rate (β), gas constant (R, 8.314 J/mol.K), T (K) and mass loss according to the α parameter (Equation 5. 11), where W_o, W_{T_I} and W_f are the initial weight, weight at $T_{ignition}$ and final weight, respectively.

$$\ln(\mathrm{k}) = -\frac{\Delta \mathrm{E}}{\mathrm{R} \cdot \mathrm{T}} + \ln(A) \qquad \text{Equation 5. 9}$$

$$\log\left[\frac{-log(1-\alpha)}{T^2}\right] = \log\frac{A \cdot R}{\beta \cdot E_a}\left[1 - \frac{2 \cdot R \cdot T}{E_a}\right] - \frac{E_a}{2.303 \cdot R \cdot T} \qquad \text{Equation 5. 10}$$

$$\alpha = \frac{W_O - W_{T_I}}{W_O - W_f} \qquad \text{Equation 5. 11}$$

5.3. Kinetic and thermodynamic properties

Five kinetics experiments were conducted for canola oil and methanol phototransesterification with TiO$_2$ at different temperatures (range: 25–65°C, operational conditions described in operational conditions described in Section 5.2.5). Six kinetics models, and the proposed reaction conditions, were evaluated (Table 5.1). Five models considered a homogeneous system with complete miscibility between the reagents, and mass transfer effects were ignored. The differences between these models are the forward/backward reactions' orders. The first-order reversible model was found suitable for sunflower oil transesterification using ZnO as the catalyst (I. Lukić, Kesić, & Skala, 2014). The sixth model, Langmuir–Hinshelwood (L–H), considered a system with complete miscibility among reagents and a heterogeneous catalyst with homogeneous active sites. This model was applied satisfactory for oleic acid and methanol photoesterification using a heterogeneous catalyst (Rosilene A. Welter, Santana, Torre, Robertson, Taranto, & Oelgemöller, 2022), and is used frequently for photocatalysis with nanoparticle reactions (Ameh et al., 2013; Chaemchuen et al., 2020; Choo, 2018; Ezzati, 2018; Karan et al., 2020; Ould Brahim et al., 2021; Rajarshi Kar et al., 2012; S Khezrianjoo & HD Revanasiddappa, 2012; Tang & Huren An, 1995). Mathematical modelling was performed using the Matlab® software package, and the results were evaluated statistically (R^2, F-test, SD, β, t-value, and p-value) using the Statistica 7.0

software (StatSoft Inc.). Subsequently, the kinetic parameters (k_1, k_{-1}, E_a, and A), which are fundamental to understanding the reaction performance over time, were obtained. The activation energy (ΔE_a) and frequency factor (A) were determined using the Arrhenius model (Equation 5. 9). Likewise, the equilibrium constant (K_{eq}) and the thermodynamic properties (ΔH, ΔS, and ΔG) were determined. The enthalpy (ΔH) and entropy (ΔS) were determined using the van't Hoff model (Equation 5.12). The Gibb's free energy variation (ΔG) is dependent on temperature and was determined using two different models. Firstly, by correlating temperature and the equilibrium constant (K_{eq}) (Equation 5. 13) and secondly by correlating enthalpy, entropy and temperature (Equation 5. 14). Both results were compared and evaluated statistically (p-value and t-value).

$$\ln(\mathrm{K}) = -\frac{\Delta \mathrm{H}}{\mathrm{R} \cdot \mathrm{T}} + \frac{\Delta \mathrm{S}}{\mathrm{R}} \qquad \text{Equation 5. 12}$$

$$\Delta \mathrm{G} = -R \cdot T \cdot ln(K_{eq}) \qquad \text{Equation 5. 13}$$

$$\Delta \mathrm{G} = \Delta H - T \cdot \Delta S \qquad \text{Equation 5. 14}$$

Table 5. 1: *Kinetic models evaluated for canola oil and methanol phototransesterification.*

System	Assumptions	Model	Equation
Homogeneous	**F1B1** - FR: first order - BR: first order	$\frac{dx_{TGL}}{dt} = k_{-1} \cdot (1 - x_{TGL}) - k_1 \cdot x_{TGL}$	Equation 5. 15
	F1B2 - FR: pseudo-first order - BR: second order	$\frac{dx_{TGL}}{dt} = k_{-1} \cdot (1 - x_{TGL}) - k_1 \cdot C_{TGL_0} \cdot x_{TGL}^2$	Equation 5. 16
	F2B2 - FR: second order - B.R.: second order	$\frac{dx_{TGL}}{dt} = k_{-1} \cdot C_{TGL_0} \cdot (1 - x_{TGL})^2 - k_1 \cdot C_{TGL_0} \cdot x_{TGL}^2$	Equation 5. 17
	F1B3 - FR: first order - BR: third order	$\frac{dx_{TGL}}{dt} = k_1 \cdot (1 - x_{TGL}) \quad - k_{-1} \cdot C_{TGL_0}^2 \cdot x_{TGL}^3$	Equation 5. 18
	F2B4 - FR: second order - BR: fourth order	$\frac{dx_{TGL}}{dt} = k_1 \cdot C_{TGL_0} \cdot (1 - x_{TGL})^2 - k_{-1} \cdot C_{TGL_0}^3 \cdot x_{TGL}^4$	Equation 5. 19
Heterogeneous	**L-H kinetic model[a]** - FR: first order - BR: first order - FAME is bounding the catalyst capacity	$\frac{\mathrm{d}x_{TGL}}{\mathrm{dt}} = \mathrm{k}_{-1} \cdot \frac{\mathrm{K}_2' \cdot x_{TGL}}{1 + \mathrm{K}_2' \cdot \mathrm{C}_{TGL_0} \cdot x_{TGL}} - \mathrm{k}_1 \cdot \frac{\mathrm{K}_1' \cdot (1 - x_{TGL})}{1 + \mathrm{K}_1' \cdot \mathrm{C}_{TGL_0} \cdot (1 - x_{TGL})}$	Equation 5. 20

[a] L-H model details are shown in Section S5. 6 of SI – APPENDIX D; F: Forward reaction; B: Backward reaction.

5.4. Results and discussion

5.4.1. Canola oil transesterification

A series of transesterification reactions of canola oil and methanol using TiO_2 as the photocatalyst was conducted in a batch reactor at temperatures between 25 and 65°C. The influence of light (UVA vs. sunlight), TiO_2 content, and mixing was considered (Figure 5. 3). An approximately 73% (±1.41) conversion was achieved with a 1TGL:55MeOH molar ratio and 20% w/w_{TGL} at 65°C after four hours of UVA irradiation. The same operational conditions but using ethanol resulted in a lower conversion of 38%. Although triglycerides have a higher miscibility with ethanol than methanol, methanol reactions tend to achieve higher conversion rates due to its higher reactivity compared to longer-chain alcohols (Ayadi et al., 2021). For ethanol, its azeotropic effect, coupled with its larger molecular size led to its poorer performance compared to methanol, the latter also being a better electron donor (Ayadi et al., 2021; M. v.d. Silva et al., 2015). The biodiesel produced by photocatalysis was compared with that obtained by two conventional processes using acidic and alkaline conditions. Acid catalysis resulted in approximately 100% of FAME and FAEE by simultaneous esterification and transesterification. Esterification was confirmed by a reduction of the FFA content (Table 5.5). Alkali catalysis furnished 91% of FAME from transesterification instead. Significant esterification did not occur as shown by similar FFA contents before and after the reaction (Table 5.5). Compared with other studies (Table 5.2) the results obtained reveal that TiO_2, without further modification but with an adequate pretreatment and proper operational conditions, can effectively catalyse phototransesterification. Under the same operating conditions, FAME production in sunlight was less effective (19%) than with UVA light (approx. 73%). A lower conversion was expected as TiO_2 activation requires UVA light with a wavelength between 388 nm (anatase) and 410 (rutile) (Pawar, Topcu Sendoğdular, & Gouma, 2018), which represents only a small percentage of the sun's radiation (Kanakaraju, Motti, Glass, & Oelgemöller, 2016).

The blank tests (Figure 5. 3) revealed that favourable operating conditions are necessary to achieve high conversions. The test with TiO_2 without pre-treament resulted in a moderate conversion (30%) compared to the other parameters evaluated. In the absence of stirring, a poor conversion of just 17% was observed. In both cases, the drops in efficiency were caused by ineffective mass transfer.

Even under optimal operational conditions, the reuse of recovered TiO_2 caused a steady drop in its photocatalytic activity. However, a conversion of 36% was still maintained after a total of 5 cycles. Residual organic materials are known to form a passivating film on the catalyst's surface, thus blocking its pores and reducing light penetration (Rosilene A. Welter, Santana, Torre, Robertson, Taranto, & Oelgemöller, 2022). In fact, reductions in catalytic effectiveness are commonly observed during resuage studies (Table 5.3). According to (Gardy, Hassanpour, Lai, Ahmed, & Rehan, 2017), a drastic reduction in TiO_2-efficiency was caused by blockage of active sites. The organic material present in the catalyst was consequently analysed and will be discussed in Section 5.4.2.

After the first cycle, the global mass balance was calculated. The mass of organic material (canola oil and biodiesel) present in the reactional medium and retained inside the pores were considered. According to this, the final converions was estimated at 69%. However, the organic material retained inside the pores was not considered to have participated in the reaction, but only the free organic material. In this case, the nominal conversion of 73% (±1.41) is proposed.

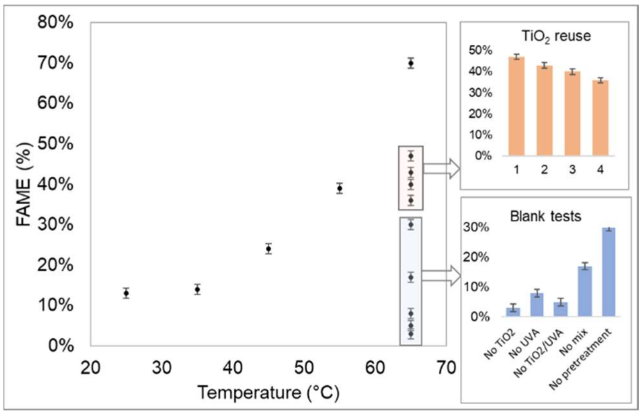

Figure 5. 3 – Canola oil conversion to FAME. Phototransesterification temperature analysis range: 25 - 65°C. Reused catalyst after recovery process (more detail in Section 5.2.8). Blank tests were conducted at 65°C considering the absence of light (UVA), catalyst (TiO_2), light and catalyst, and mixing, respectively [(σ) of ± 1.25]. Operational conditions: 1 TGL:55 MeOH molar ratio and 20% TiO_2 (w/w_{TGL}), batch reactor, and UVA light irradiation.

Table 5. 2: *Oil transesterification catalysed by oxides.*

	Catalyst	% (w/w_{TGL})	Alcohol	Molar ratio	T (°C)	Time (h)	FAME (%)	Ref.
Canola oil	TiO_2 + UVA	20	Methanol	55	65	4	73	This study
Canola oil	TiO_2 + sunlight	20	Methanol	55	65	6	19	This study
Canola oil	TiO_2 + UVA	20	Ethanol	55	65	4	38	This study
Canola oil	HSiW/Al_2O_3	3	Methanol	27	190	23	85	(Gaurav, Dumas, Mai, & Ng, 2019)
Canola oil	ZnO	12.5	Methanol	27	200	6	35	(Pugnet et al., 2010)
Canola oil	ZnAl/2O_4	12.5	Methanol	27	200	6	80	(Pugnet et al., 2010)
Palm oil	Cu+TiO_2	3	Methanol	20	45	45 minutes	91	(De & Boxi, 2020)
Soybean oil	$SnSO_4$	5	Ethanol	3.5	100	3	70	(Pereira, Portilho, Henriques, & Zotin, 2014)
Soybean oil	CaO	1.5	Methanol	9	70	3	80	(X. Chen et al., 2020)
Sunflower oil	CaO.ZnO	2	Methanol	10	70	4	95	(I. Lukić et al., 2013)
Sunflower oil	ZrO_2/La_2O_3	15	Methanol	50	200	8	89	(H. Sun et al., 2010)

Table 5. 3: *Solid catalyst reuse for FAME production by transesterification.*

Catalyst	Feedstock	FAME (%)	# cycles	FAME (%)	Decrease (%)[a]	Ref.
TiO_2 + UVA	Canola oil	73	5	36	37	This study
Ce/AC_{cs}-S	Chicken fat oil	93	5	90	3	(Shobhana-Gnanaserkhar et al., 2020)
HSiW/Al	Canola oil	39	4	38	1	(Gaurav et al., 2019)
$TiO_2/PrSO_3H$	Virgin oil+oleic acid	98	6	21	77	(Gardy et al., 2017)

[a]Decrease between first and last cycle.

5.4.2. TiO_2 characterisation

TiO_2 was characterised qualitatively and quantitatively at different stages of the phototransesterification process, and the results are listed in Table 5.4. FTIR-ATR spectroscopy (Figure S4.3 of SI – APPENDIX D) confirmed that canola oil and biodiesel are present within the catalyst material. TGA/DSC after the photoreactions (Figure 5.4, Section S5. 4 of SI – APPENDIX D) indicated that substantial amounts of organic material (42% w/w) were present within the TiO_2 after the reaction (0RP). A lower retaining value of 27% was obtained for oleic acid photoesterification with methanol (Rosilene A. Welter, Santana, Torre, Robertson, Taranto, & Oelgemöller, 2022). The difference between photoesterification and phototransesterification is attributed to the miscibility of oleic acid in methanol, which allowed for its rapid removal. During the reactivation process, FAME is removed easily compared to canola oil, hence the catalyst retained the feedstock stronger. The complete recovery and washing process (3RP) effectively removed 97% (±0.69) (w/w) of the organic material (18%±0.69) of FAME and 82%±0.69 of canola oil). After five complete photocatalytic cycles and subsequent reactivation (5C), 10%±0.69 (w/w) of organic material remained on the TiO_2 (2%±0.69 of FAME and 8%±0.69 of canola oil). Comparing the organic material retained between 1C and 5C confirmed that the reagent (canola oil) preferentially remained on the catalyst structure. This difference in retention negatively impacted on the catalyst's efficiency during reuse. Welter and co-workers (Rosilene A. Welter, Santana, Torre, Robertson, Taranto, & Oelgemöller, 2022) investigated the recovery process for the photoesterification of oleic acid with methanol. After five cycles, the particles obtained were slightly more agglomerated with sharper structures, with 20% less surface area and pore volume and a 15% smaller diameter. It was suggested that this aggregation blocks the active sites, hence reducing the catalytic activity and stability (Li et al., 2009). Therefore, pretreatment is essential as methanol reduces the attachment of other organic materials by the catalyst. This finding correlates with the phototransesterification efficiency achieved after pretreatment (73%) and without pretreatment (30%) of the photocatalyst (Figure 5.3, Section S5. 1 of SI – APPENDIX D).

The DTA results (Figure 5.5) revealed two main degradation areas. The first corresponding to FAME (110–280°C, Peaks 1.a and 1.b) and the second to canola oil (280–500°C, peaks 2.a and 2.b). Within both areas, peak splitting can be observed. This behaviour is expected because of the organic material distribution retained on the TiO_2 surface and inside its pores. External organic material is removed faster (1st peak), whereas organic material inside the pores is removed more slowly (2nd peak). N_2 physisorption and XRD analyses were performed for the pure catalyst, after use (0RP), after the recovery and washing process (1C) and after five uses (5C). Sample 0RP could not be analysed due to the high organic load present, as naturally expected in the absence of any washing process.

In line with the TGA results, N_2 physisorption showed a decrease in the surface area, pore volume, and diameter, indicating catalyst poisoning through the presence of organic material, hence obstructing the pores. Moreover, the increase in particle size suggests particle aggregation. These physical changes reduce the ease of light access to the catalyst and the number of active sites available, consequently reducing the catalyst's efficiency. The crystallite size was found to have an average of 22.64±0.29 nm (Figure 5.6), consisting of 91% of anatase and 9% of rutile. This composition remained unchanged after the subsequent photoreactions. The catalyst bandgap before use (pure TiO_2) agrees with the literature (3.2 eV). After the reaction and without a reactivation through washing process, the bandgap changed considerably (4.49 eV). However, the bandgap was only 2% higher after one reactivation process (1C) and 11% higher after five reactivation cycles (5C) than that of the native material (Section S5.6 of SI – APPENDIX D). Subsequently, the reduction in light absorption by the increased bandgap (Luttrell et al., 2015) and the amount of organic material adhered to the particles decrease the efficiency of the phototransesterification process.

Table 5. 4: *TiO_2 characterisation.*

		Pure	**0RP[b]**	**1C[b]**	**5C[b]**
Canola oil content	(% wt./wt.)	-	33%	1%	8%
FAME	(% wt./wt.)	-	9%	3%	2%
Pore volume	(cm^3/g)	0.74	-	0.52	0.45
Pore diameter	(nm)	3.52	-	3.52	3.06
Surface area	(m^2/g)	51.85[a]	-	42.78	38.23
Particle size	(nm)	27.55	-	33.37	37.37
Crystallite size	(nm)	22.23	-	22.87	22.82
Anatase	(%)	91%	-	92%	90%
Rutile	(%)	9%	-	8%	10%
Bandgap[c]	(eV)	3.22[d]	4.49	3.28	3.56

[a]Surface area standard value according to the manufacturer: 35-65 mg^2/g (Aeroxide, 2020); [b]TiO_2 after phototransesterification reaction (0RP), 1C: after 1 cycle of phototransesterification and 3RP, 5C: after 5 cycles of phototransesterification and 3RP; [c] Error: ±0.02; [d]Bandgap of pure TiO_2 (P25 Evonik) standard value according to the literature: 3.18 eV (Ishigaki et al., 2020).

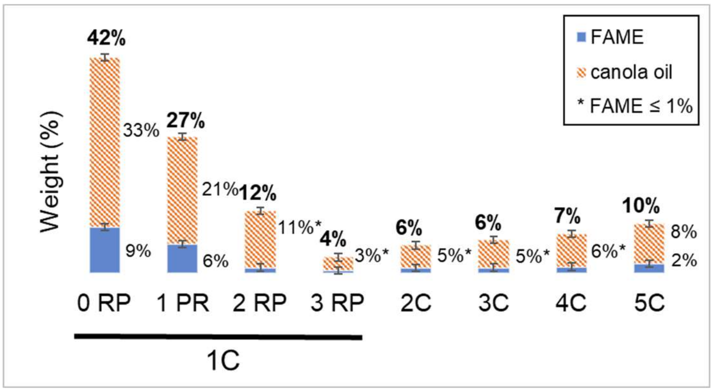

Figure 5. 4. Organic material found on TiO_2 after transesterifications of canola oil with methanol.

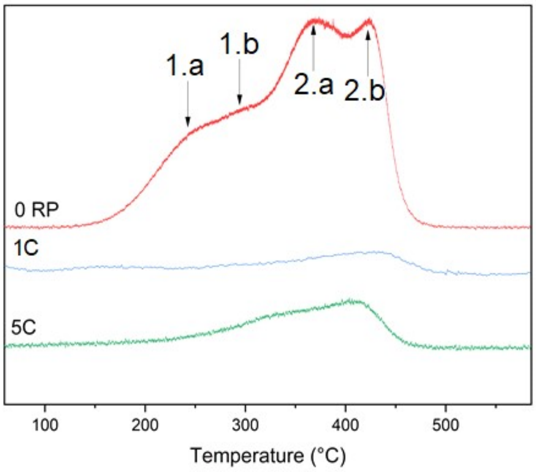

Figure 5. 5. DTA (range: R.T.to 600°C) of TiO_2 used for canola oil transesterification with methanol. Catalyst after use without reactivation process (0RP), after use and washing process (1C), and after use and reactivation for five cycles (5C). Details in Section 5.2.5. and 5.4.1, Peaks 1.a-b: FAME, Peaks 2.a-b:canola oil.

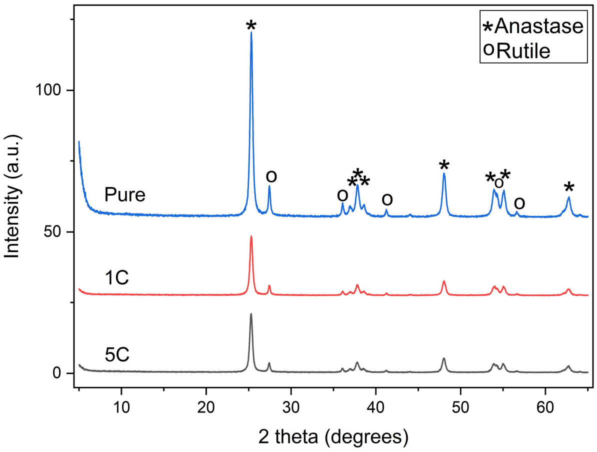

Figure 5. 6. XRD patterns of TiO_2 pure, after 1C (single use and washing process) and after 5C (after use and recovering the catalyst for five times).

5.4.3. FAME characterisation

Different analyses (Table 5.5) were conducted to characterise the feedstock (canola oil) and reaction products (FAME). The product composition obtained by photocatalysis was furthermore compared with that from traditional thermal methods (acid and alkali). TGL conversion to FAME was determined by ^{1}H-NMR spectroscopic analyses (Figure S5.3 and S5.4, S5.6 of SI – APPENDIX D) and monitored by FTIR-ATR spectroscopy (Figure S5.15 of SI – APPENDIX D). The FTIR-ATR spectra of canola oil and the various FAME products show significant similarities in their infrared regions (Table S5.7 of SI – APPENDIX D). The FFA content was determined by titration and was found to be 1.2% for canola oil. For the various FAMEs, the values were 0.2% from acid catalysis, 0.9% from alkali catalysis, and 0.6% for photocatalysis, respectively. Hence, partial esterification of FFA is suggested for acid catalysis, resulting in a decrease in %FFA and an increase in FAME conversion. By contrast, predominant transesterification is suggested for alkali catalysis as the FFA content did not significantly change. Photoesterification and phototransesterification both operate during TiO_2-photocatalysis, as also proposed in other studies (De & Boxi, 2020; Gardy et al., 2017; Khaligh et al., 2021; Mihankhah, Delnavaz, & Khaligh, 2018; Rosilene A. Welter, Santana, Torre, Robertson, Taranto, & Oelgemöller, 2022; Wen, Yu, Tu, Yan, & Dahlquist, 2010). The %FFA obtained by titration agrees with data from the literature (Caballero, 2003; Fereidoon Shahidi, 2005).

TGA (more details in Section S5.4 of SI – APPENDIX D) showed that canola oil has a degradation peak at 421°C (Figure S5.14 of SI – APPENDIX D). FAME was degraded at a lower temperature, showing a peak between 240 and 250°C. The product obtained by photocatalysis had two peaks corresponding to FAME and non-reacted oil, confirming incomplete conversion. The FAME degradation curves suggest that the products have high thermal stability. Products with low thermal stability tend to present an initial peak at 100–150°C, corresponding to volatile compounds (Mostafa & El-Gendy, 2017; Wnorowska et al., 2021). Different authors obtained similar results for FAME from soybean oil (Nicolau et al., 2018), babassu (Nicolau et al., 2018), and *Croton melagocarpus* oil (Kivevele, Mbarawa, Bereczky, Laza, & Madarasz, 2011), respectively.

Thermal parameters such as flash point, T_I, T_B, C_{max}, and E_a° were also determined. The flash point is the lowest temperature at which a vapour can ignite and flames spread across the remaining liquid (Abdelkhalik et al., 2018). This point is equivalent to the temperature where 17.5% of the weight is lost (Abdelkhalik et al., 2018) or where 74% of the boiling point temperature is reached (Mofijur et al., 2017). The ASTM 93 procedure states that the minimum value should be 120°C (Mofijur et al., 2017). A value of 160°C was obtained, which is similar to the literature (Encinar, Pardal, Sánchez, & Nogales, 2018). The ignition temperature (T_i) represents fuel stability during storage (N. Khan et al., 2021; B. K. Sharma, Rashid, Anwar, & Erhan, 2009) and the capacity of vapours to autocombust. The ignition temperature and burnout temperature (T_B, 95% of complete combustion) were similar for FAME products obtained by photocatalysis and traditional catalysis. The maximum combustion rate (C_{max}) revealed that the product from acid catalysis has the highest value with 2.24°C/min. In contrast, the product from photocatalysis showed the lowest value (1.49°C/min), suggesting that the presence of residual TGL may interfere with the thermoanalysis results. The activation energy ($E_a°$) for canola oil and FAME were found to be similar with 30.33 and 32.89 kJ/mol. This similarity indicates that additional energy is not required to further progress the reaction. System heat is essential mainly to increase mass transfer between the reactants, which is supported by the thermodynamic parameters discussed later and the literature (M. v.d. Silva et al., 2015; Rosilene A. Welter, Santana, Torre, Robertson, Taranto, & Oelgemöller, 2022).

Table 5. 5: *Characterisation of canola oil and FAME obtained by acid, alkali and photocatalysis.*

		Canola oil	**FAME**		
			Acid catalyst	**Photocatalyst**	**Alkali catalyst**
FAME	(% mol)	-	99	73 (±1.41)	91
FFA	(%)	1.2 (±0.2)	0.1 (±0.1)	0.4 (±0.2)	0.9 (±0.2)
Boiling point 1[a, b]	(°C)	-	254	246	251
	Mass loss (%)	-	99	75	95
Boiling point 2[a, c]	(°C)	421	-	400	400
	Mass loss (%)	99	-	23	3
Flash point[d]	(°C)	283	161	160	160
Ignition temperature (T_I)[c]	(°C)	383	217	216	215
Burnout temperature (T_B)[c]	(°C)	454	258	257	263
Maximum combustion rate (C_{max})[c]	$(dM/dt)_{max}$	1.81	2.24	1.49	1.9
$E_a°$	kJ/mol	30.33	30.17	30.33	32.89
A	-	0.13	0.25	0.15	0.21
R^2 of Ea_{TGA} linear model	-	0.981	0.982	0.981	0.966

[a]In accordance with ASTM D6751: minimum of 130°C; [b]Error: ±0.69; [c]n accordance with ASTM D7398: 100 – 615°C; [d]In accordance with ASTM 98: minimum of 120°C.

The composition of the different transesterification products was furthermore determined by gas chromatography (Table 5.6). In comparison with traditional methods (acid and alkali catalysts), transesterification by photocatalysis converts the C18:1-carbon chain (oleic acid) more readily than the C18:2 ones (linoleic and linolenic acids). This difference has been attributed to the larger number of double bonds in linoleic and linolenic acids (Hawash, Ebrahiem, & Farag, 2019), as this increases the energy required for reaction. This becomes noticeable when comparing the enthalpy of the two most common methyl esters, methyl oleate ($\Delta H°_{r,\ 298K}$=122 kJ/mol) and methyl linoleate ($\Delta H°_{r,\ 298K}$=245 kJ/mol) (Smith & Martell, 2004), respectively.

Table 5. 6: *FAME composition[a] obtained by canola oil-methanol transesterification using different catalysts.*

		Acid	Photocatalysis	Alkali
unreacted canola oil		9%	27%	1%
methyl palimatate	C16:0	4%	4%	5%
methyl stearate	C18:0	2%	2%	2%
methyl oleate (9)	C18:1	60%	70%	59%
methyl oleate (11)	C18:1	3%	3%	3%
methyl linoleate	C18:2	20%	14%	20%
methyl linolenate	C18:2	9%	5%	9%
methyl eicosonate	C20:1	1%	0%	0%
methyl eicosadienoate	C20:2	1%	1%	1%

[a]Obtained by G.C. spectra (Section S5.5 of SI – APPENDIX D).

5.4.4. Identification of intermediates MGL and DGL

The possible presence of reaction intermediates, e.g. monoglycerol (MGL) and diglycerol (DGL), was investigated experimentally and in comparison with literature data (Galvan, de Aguiar, Rohwedder, Borsato, & Killner, 2020; Nieva-Echevarría, Goicoechea, Manzanos, & Guillén, 2015). Analyses were conducted using the products obtained from acid and photocatalysis using shorter reaction times. Lower conversions of 15% to FAME were naturally observed for both methods and permit the possible presence of MGL and DGL. As would be expected, other studies have found the highest amounts of MGL and DGL at the beginning of the reaction, with correspondingly lower concentrations of FAME (Ferrão-Gonzales, Véras, Silva, Alvarez, & Moreau, 2011; Noureddini & Zhu, 1997). For example, Pugnet and co-workers (Pugnet et al., 2010) monitored the transesterification of rapeseed oil with methanol over six hours, but could detect small concentrations of MGL and DGL only within the first two hours of the reaction.

^{1}H-NMR analysis (Figure 5. 7) revealed that the crude products obtained from acid catalysis contained traces of MGL and DGL, in comparison with the low conversion of 15%. After prolonged reaction and hence at higher conversions, TGL was converted entirely to FAME for the acid-catalysed reaction, and no more intermediaries could be detected (99% of

FAME, (Figure 5. 8). In comparison, some trace amounts of intermediates (MGL and DGL) were detected in the photocatalysis product (Figure 5. 9). for higher conversion (73%) but not at lower conversion (15%, Figure 5.7). Noureddini and Zhu (Noureddini & Zhu, 1997) investigated the transesterification of soybean oil with methanol using KOH as the catalyst. The amounts of MGL and DGL found were negligible compared to FAME (Noureddini & Zhu, 1997). Likewise, Albuquerque Andrade and co-workers (Albuquerque Andrade et al., 2011) evaluated the transesterification of buriti oil and the isolated product composed of 94% FAME, 3.27% MGL, and 0.98% DGL, respectively. Ferrão-Gonzales et al. (Ferrão-Gonzales et al., 2011) assessed the presence of intermediates for the transesterification of rapeseed oil by *Candida antarctica* B lipase. Although the reaction was slow (10–24 hours), only trace concentrations of MGL and DGL were found (Ferrão-Gonzales et al., 2011). Hence, MGL and DGL may not represent significant components of the crude product, but their presence in trace amounts may still interfere with the reactant's miscibility (X. Chen et al., 2020). Triglycerides of fatty acids are only poorly miscible to insoluble in methanol. DGL and MGL may thus act as surfactants that improve the mixing between the oil and methanol. Chen and co-workers (X. Chen et al., 2020) performed the transesterification of soybean oil with methanol using CaO as a catalyst. The authors reported that oil and methanol quickly separated initially, but the separation rate decreased drastically after the addition of MGL and DGL.

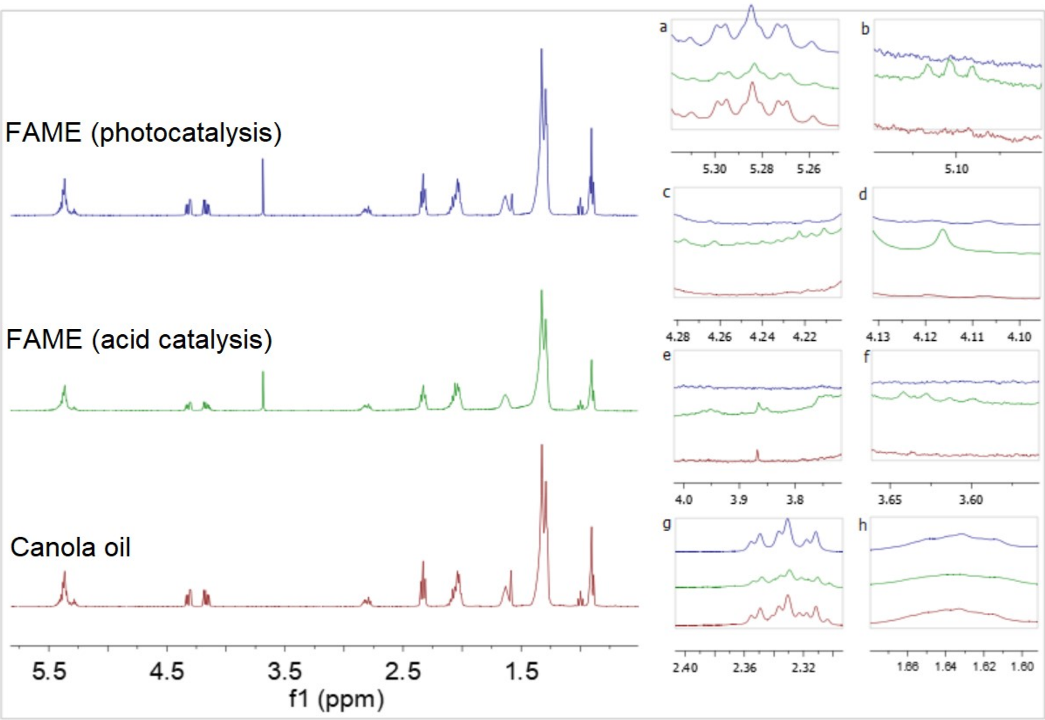

Figure 5. 7. ^{1}H-NMR spectra of canola oil and FAME obtained by acid catalysis and photocatalysis (FAME - 15% of purity). a-h: Main peaks of monoglycerides and diglycerides (Section S5.3 of SI – APPENDIX D).

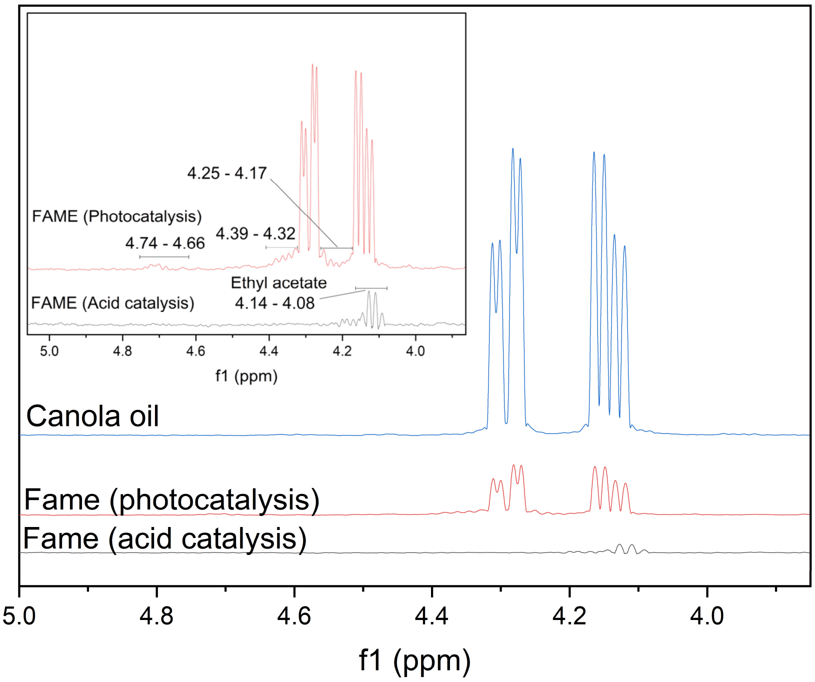

Figure 5. 8. ^{1}H-NMR spectra (Range: 4.40–4.00 ppm, CDCl$_3$) of canola oil and FAME obtained using acid catalysis and photocatalysis (73% of conversion). Highlight: residual ethyl acetate present in FAME obtained by acid catalysis.

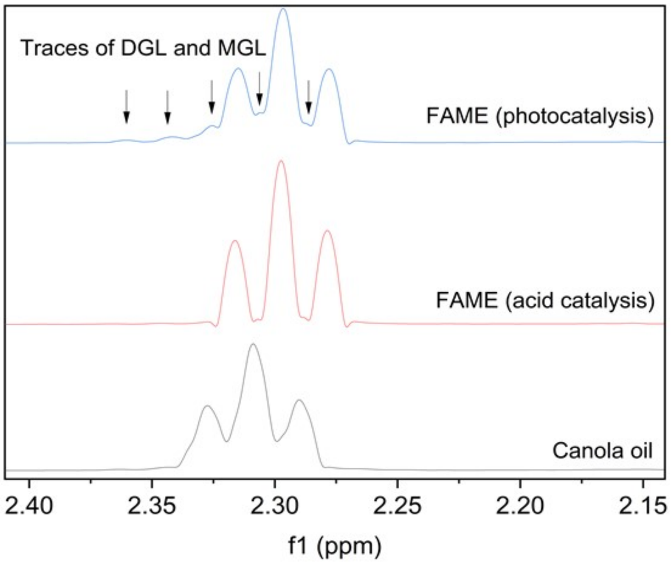

Figure 5. 9. ^{1}H-NMR spectra (Range: 2.40 – 2.25, CDCl$_3$) of canola oil and FAME obtained using acid catalysis and photocatalysis (73% of conversion).

5.4.5. *Photoreaction mechanism*

Photocatalysis may operate via transesterification of TGL and esterification of residual

FFA. However, the esterification was neglected from further discussions because of the small amounts of FFA in the feedstock (1.2%±0.2). Scheme 5. 1 shows the proposed mechanism for TGL (triolein) phototransesterification with methanol. TiO_2 excitation by photons (hv) with sufficient energy to overcome the bandgap causes charge separation (Step 1) (Manique et al., 2016; Micic et al., 1993). Electrons (e^-) are promoted to the conduction band (C.B.), generating positive holes (h^+) in the valence band (V.B.) (Ohtani, 2011). Both species (h^+ and e^-) react with methanol (step 2) or TGL (step 3) adsorbed on the catalyst's surface, generating a methoxy radical ($CH_3O\bullet$) and an ester radical anion ($RCO_2^{-\bullet}R'$). Subsequent radical combination and elimination yields the first intermediate, diglycerol (DGL, diolein), and one molecule of methyl oleate, RCO_2CH_3, (step 4). Successive transesterification of diglycerol results in monoglycerol (MGL, monoolein) and a second molecule of methyl oleate (steps 5 and 6). The monoglycerol is further converted by the same mechanism to the third methyl oleate molecule and glycerol (step 7). Similar mechanistic scenarios have been proposed for the TGL phototransesterification catalysed by TiO_2 supported on graphene (Borah et al., 2018) and for FFA photoesterification (Ghani et al., 2020; Guo et al., 2021; Rosilene A. Welter, Santana, Torre, Robertson, Taranto, & Oelgemöller, 2022). However, alternative phototransesterification mechanisms have likewise been proposed (Alsharifi et al., 2017; Yan, Salley, & Simon Ng, 2009).

Step 1)

$$TiO_2 + h \longrightarrow h^+ + e^-$$

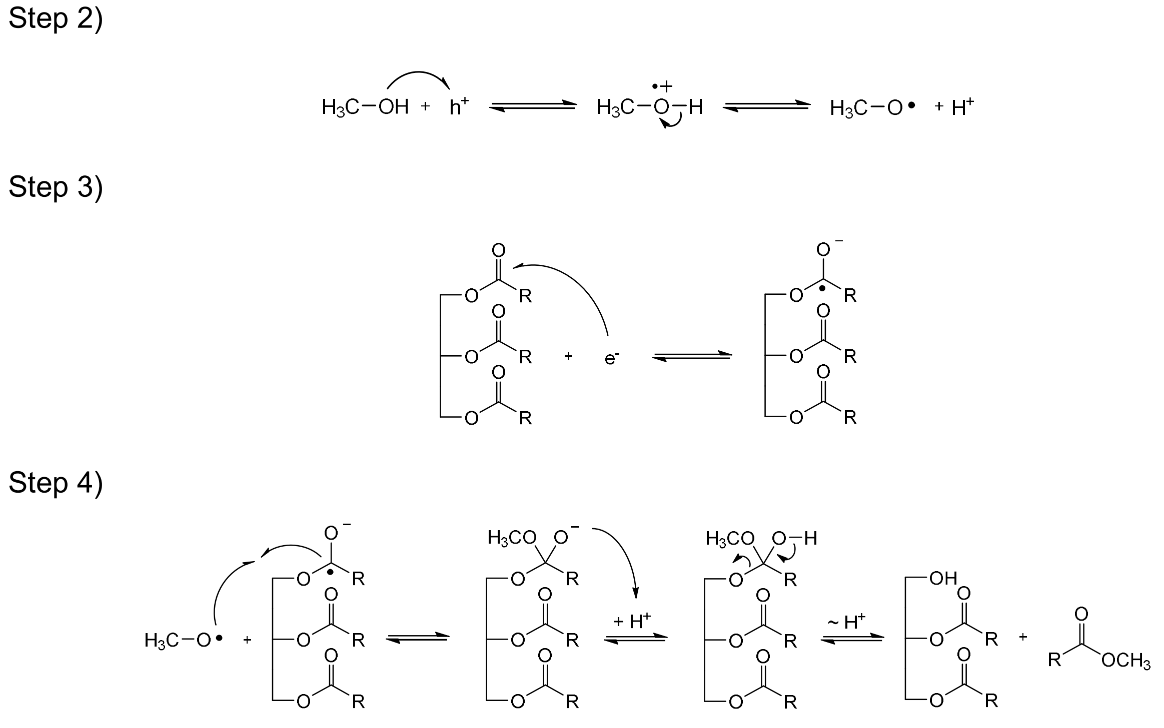

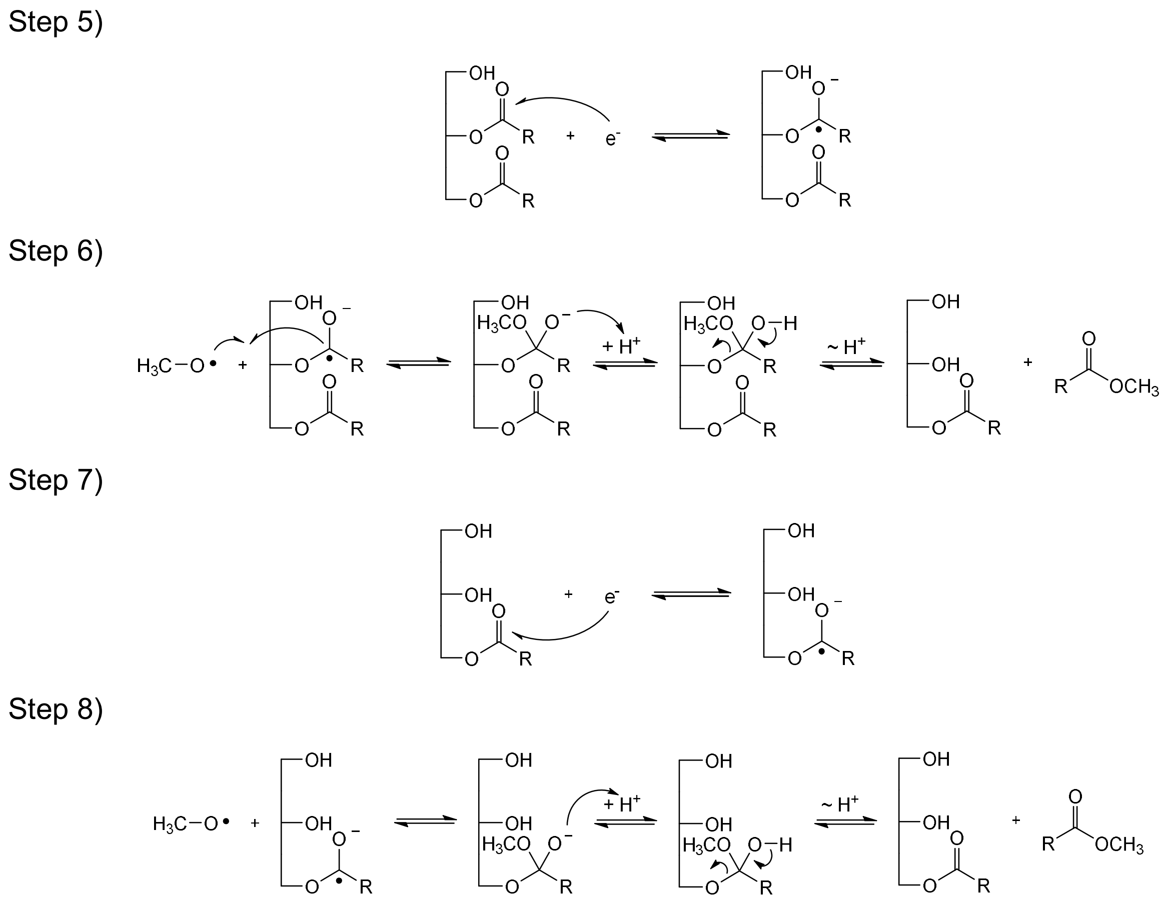

*Scheme 5. 1***.** Proposed phototransesterification mechanism for canola oil (TGL) and methanol photocatalysed by TiO_2 (R = cis-$CH_3(CH_2)_7CH{=}CH(CH_2)_7$).

5.4.6. Kinetics and thermodynamics properties

Kinetic curves were subsequently obtained for the phototransesterification of canola oil with methanol under UVA irradiation (Figure 5. 10, 1 mol TGL:55 mol MeOH, 20% w/w_{TGL} temperature range: 25 – 65°C, batch reactor, four hours). High temperatures was found desirable for achieving a high transesterification efficiency. The highest conversion of 73% (±1.41) was reached at 65°C. The gap between conversions achieved at 55°C and 65°C was approximately 33%. This sigificant difference can be attributed to the increased miscibility of the reagents and hence mass transfer at elevated temperatures. Six kinetic models were evaluated (Equations 5.15–20, Section 5. 6), and their statistical analyses are listed in Table 5.7. The F2B4 model, which considers the forward reaction as second-order and the backward reaction as fourth-order, provided the best fit with the experimental data (Figure 5.11). Both reaction constants (k_1 and k_{-1}) were consequently obtained using this model (Figure 5.11). The intermediates (MG and DG) were disregarded due to their neglectable concentrations, as discussed in Section 5.4.4. The solar phototransesterification conducted at 65°C showed a significantly lower conversion over time, most likely caused by the poor absorption of TiO_2 and the low amount of UV-radiation within the solar spectrum (Kanakaraju et al., 2016; Oelgemöller, 2016).

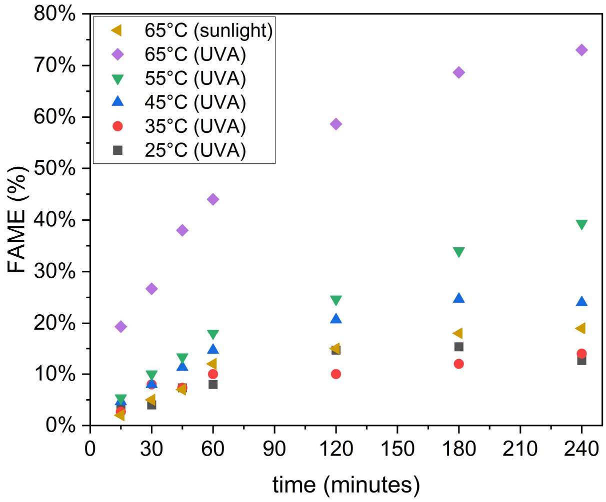

Figure 5. 10. Canola oil and methanol phototransesterification as a function of time. Catalyst: TiO_2 irradiated by UVA or sunlight (1 TGL mol:55 MeOH mol, 20% TiO_2 (w/w_{TGL}), Section S5.1 of SI – APPENDIX D).

Table 5. 7: *Kinetic model statistical analysis applied to the experimental kinetic data obtained for the phototransesterification of canola oil and considering FAME and feedstock kinetic curves.*

Model	R^2	F (1,38)	SD	β	t(38)	p
F1B1	0.971	5297	0.015	0.971	59.354	0.000
F1B2	0.995	7557	0.013	0.997	86.830	0.000
F2B2	0.972	5413	0.020	0.973	59.930	0.000
F1B3	0.972	5114	0.021	0.973	66.268	0.000
F2B4	**0.996**	**8969**	**0.012**	**0.998**	**97.700**	**0.000**
L-H	0.971	5778	0.021	0.970	60.029	0.000

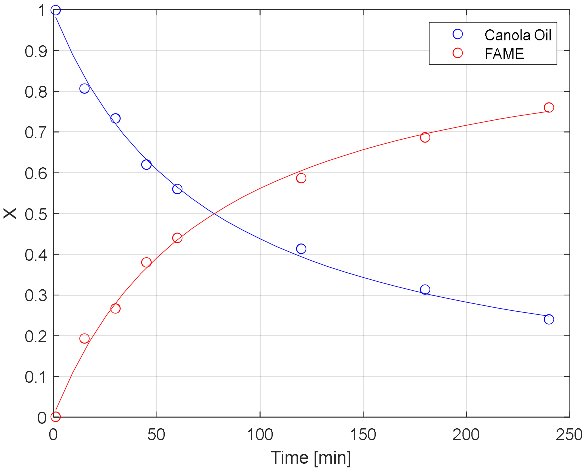

Figure 5. 11. Mathematical modelling of the F2B4 model applied for kinetic curves of phototransesterification of canola oil with methanol (1 TGL mol:55 MeOH mol, 20% w/w$_{TGL}$ of TiO$_2$, 65°C, TiO$_2$ irradiated by UVA).

The thermodynamic properties of the phototransesterification reaction were furthermore determined (Table 5.8). Although all of the models showed convergences higher than 0.95, only F2B4 (with the best accuracy) resulted in consistent data, as shown in (Table 5.8). Models that considered lower orders (first and second) resulted in negative values of E_a for the backward reaction. The F1B3 model gave a low convergence for enthalpy and entropy. Nevertheless, the F2B4 model produced higher convergence for all parameters, was considered the most satisfactory and was thus used for further discussion. The E_a value for the forward reaction (60.27 kJ/mol) can be considered small compared to the backward reaction (233.71 kJ/mol) and indicates the high efficiency of the catalyst (Encinar et al., 2018). The van't Hoff model (Equation 5. 12) was used to obtain ΔS and ΔH. The value of ΔH of 83.50 kJ/mol indicates the endothermic nature of the reaction, as observed by other authors (Gholipour Zanjani, Kamran Pirzaman, & Yazdanian, 2020). The increased conversion with increasing temperature also suggests an endothermic reaction. Moreover, the temperature increase improves the reagents' miscibility, resulting in higher conversion. For the oleic acid-methanol esterification, the temperature increase is more relevant for miscibility than for the reaction energy supply requirement (M. v.d. Silva et al., 2015; Rosilene A. Welter, Santana, Torre, Robertson, Taranto, & Oelgemöller, 2022). The ΔS of 0.27 kJ/mol.K (ΔS>0) indicates that the system's entropy is increasing, and the reaction tends to become irreversible (Gholipour Zanjani et al., 2020). ΔG (Figure 5.12) suggests that the reaction is favoured at higher temperatures, which is confirmed by the decrease in Gibbs energy with increasing temperature.

Table 5. 8: *Kinetic and thermodynamic parameters obtained by different mathematical models.*

Model	k_{-1}[a]	k_1[a]	K^1_{eq}	E_a[b] (kJ/moL)	A^4	E_a[c] (kJ/mol)	A[d]	ΔG[a. d] (kJ/mol)	ΔG[a, e] (kJ/mol)	ΔH (kJ/mol.K)	ΔS (kJ/mol)
F1B1	3.4E-03	1.1E-02	3.2E-01	26.88 (R^2: 0.709)	100.73 (R^2: 0.709)	-35.81 (R^2:0.740)	1.02E-8 (R^2: 0.740)	-3.24 (p_v:0.110)[f] (t_v: 1.795)	2.01 (p_v:0.110) (t_v: 1.795)	-62.68 (R^2: 0.863)	-0.19 (R^2: 0.863)
F1B2	9.7E-03	1.1E-02	8.8E-01	28.91 (R^2: 0.911)	1.8E+02 (R^2: 0.911)	-64.19 (R^2:0.715)	1.54E-12 (R^2: 0.715)	-5.67 (p_v:0.086) (t_v: 1.960)	-8.29 (p_v:0.086) (t_v: 1.960)	117.14 (R^2: 0.915)	0.37 (R^2: 0.915)
F2B2	3.1E-04	3.4E-02	9.0E-03	30.28 (R^2: 0.706)	1.00E+3 (R^2: 0.706)	-82.22 (R^2:0.764)	1.50E-16 (R^2: 0.764)	-13.23 (p_v:0.302) (t_v: 1.204)	9.37 (p_v:0.302) (t_v: 1.204)	-112.49 (R^2: 0.775)	-0.36 (R^2: 0.775)
F1B3	3.2E-02	3.3E-02	1.0E+00	60.29 (R^2: 0.840)	3.96E+7 (R^2: 0.840)	241.28 (R^2 0.321)	1.52E+12 (R^2: 0.321)	-0.08 (p_v:0.081) (t_v: 1.9987)	-14.97 p_v:0.081) (t_v: 1.9987)	123.65 (R^2: 0.447)	0.41 (R^2: 0.447)
F2B4	**3.1E-03**	**3.3E-02**	**9.3E-02**	**60.27** **(R^2: 0.839)**	**3.92E+07** **(R^2: 0.839)**	**233.71** **(R^2:0.791)**	**1.44E+18** **(R^2: 0.791)**	**-6.88** **(p_v:0.002)** **(t_v: 4.257)**	**-4.72** **(p_v:0.002)** **(t_v: 4.257)**	**83.50** **(R^2: 0.870)**	**0.27** **(R^2:0.870)**
L-H	6.0E-01	1.9E-02	2.7E+02	89.92 (R^2: 0.902)	3.50E-16 (R^2: 0.902)	-80.38 (R^2:0.839)	2.55E+13 (R^2: 0.839)	15.69 (p_v:0.947) (t_v: 0.069)	-11.25 (p_v:0.947) (t_v: 0.069)	175.58 (R^2=0.902)	0.55 (R^2=0.840)

[a]Temperature: 338.15K; [b]Forward; [c]Backward; [d]Van't Hoff model; [e]ΔG = f (ΔH,T,ΔS); [f]p_v: p-value, and t_v: t-valu

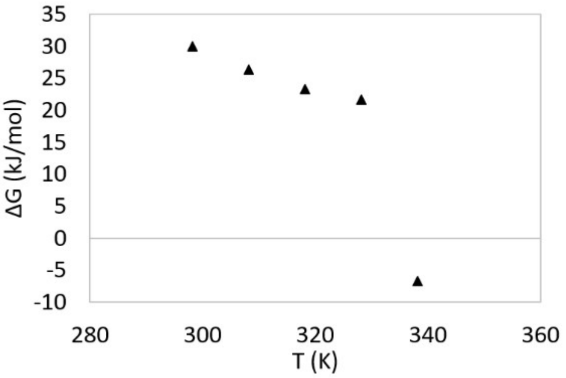

Figure 5. 12. Gibbs energy (ΔG) for canola oil and methanol transesterification catalysed by TiO_2 irradiated by UVA (1TGA mol:55MeOH mol, 20% TiO_2 (w/w$_{TGL}$, mathematical model: F2B4).

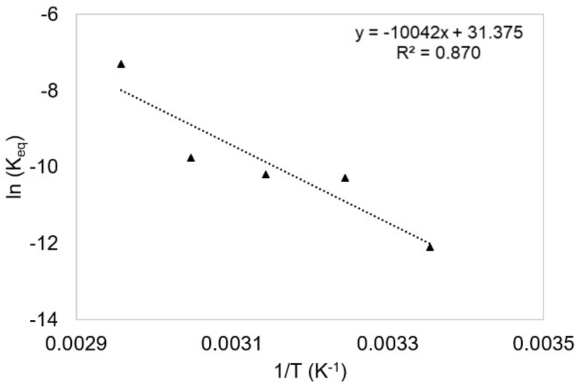

Figure 5. 13. Equilibrium constant for canola oil and methanol transesterification catalysed by TiO_2 irradiated by UVA. (1TGA mol:55MeOH mol, 20% TiO_2 (w/w$_{TGL}$, mathematical model: F2B4).

5.5. Conclusion

An eco-friendly transesterification process of canola oil with methanol (1 mol canola oil: 55 mol MeOH) to FAME was developed using photocatalysis (20% w/w$_{TGL}$ TiO_2 under UVA irradiation), resulting in a 73% (±1.41) conversion at 65°C under vigorous stirring. The photocatalytic process comprised of triglyceride transesterification with simultaneous free fatty acid esterification. The photocatalyst was reusable but with a notable decrease in efficiency for every cycle, which was linked to the presence of organic material within the photocatalytic material. The reaction could be conducted in natural sunlight, but a reduced efficiency with a conversion of just 19% was observed and attributed to the low UVA-content and poor absorption of the photocatalyst within the solar spectrum. Ethanol was evaluated as a substitute for methanol, but solely a moderate conversion of 38% was achieved because of its generally lower reactivity. Six kinetic models were applied to the experimental data and the one considering second-order forward/fourth-order backward reactions showed the best convergence between the predicted and experimental data. In addition, the thermodynamic properties were established. According to these parameters, a temperature higher than 65ºC is desired for the endothermic reaction to proceed and for the compounds to be miscible. The process developed shows that it is possible to overcome issues frequently observed in traditional homogeneous catalysis (high temperatures, extreme pHs, challenging catalyst handling, recovery and reuse, large volumes of waste and water, and complex product purifications). The scale-up of heterogeneous photocatalytic processes remains challenging because of significant photon and mass transfer limitations (van Gerven et al., 2007). Further studies will be conducted considering waste feedstocks with a high FFA content such as cooking oil (Corro et al., 2017; Khaligh et al., 2021), and scale-up using continuous-flow reactors (Donnelly & Baumann, 2021).

Acknowledgement

RAW wishes to thank the College of Science and Engineering at James Cook University for financial support (Competitive Research Training Grants 2021 and 2022). The authors thank Assoc.-Prof. George Vamvounis, Dr. Mark Robertson and Dr. Shane Askew (James Cook University) for technical support.

Chapter VI

TiO_2 photocatalysed biodiesel production through simultaneous esterification and transesterification of waste cooking oil

Submission (12/2022): Rosilene Andrea Welter[1,2], Harrson Silva Santana[2], Lucimara Gaziola de la Torre[2], Mark C. Barnes[1], Osvaldir Pereira Taranto[2], Michael Oelgemöller[1,3]. Biodiesel production focusing on heterogenous catalysts and eco-friendly routes, *ChemBioEng Rev*.

Filiation: (1) College of Science and Engineering, James Cook University, Postcode Qld 4811, Townsville, Queensland, Australia; (2) School of Chemical Engineering, University of Campinas, Postcode 13083-852, Campinas, SP, Brazil; (3) Faculty of Chemistry and Biology, Hochschule Fresenius gGmbH-University of Applied Sciences, Limburger Straße 2, Postcode D-65510, Idstein, Germany.

Abstract

Biodiesel was produced by simultaneous esterification and transesterification of waste cooking oil (WCO) using TiO_2 photocatalysis and UVA or natural sunlight irradiation. The highest overal conversion (82%±1.2) was achieved using methanol (UVA, 1 WCO mol:55 MeOH mol, 20% TiO_2 $w/w_{WCO,}$ and 65°C). The free fatty acid content present in the WCO (FFA, 10.9%±0.5) resulted in 89% conversion by esterification, while the triglycerides (TGL, 89%±1.9) resulted in 81% conversion by transesterification. Only 32% of global conversion was achieved by applying sunlight instead of UVA light. In addition, a conversion of 21% was achieved using ethanol instead of methanol with UVA light. The kinetic data were applied using five different kinetic modells, and the kinetic rate constants were determined. Subsequently, the thermodynamic properties were estimated ($\Delta G_{T<338.15K}>0$, $\Delta G_{338.15K}=-5.34$ kJ/mol, $\Delta H=92.58$ kJ/mol, and $\Delta S=0.29$ kJ/mol.K). The catalyst was recovered and reused for five cycles, and conversion decreased to 59% overall due to deposition of organic matterial onto and aggregation of the catalyst. This study nevertheless demonstrates the potential of biodiesel production by TiO_2 photocatalysis via simultaneous esterification and transesterification from a feedstock with a high FFA content such as WCO.

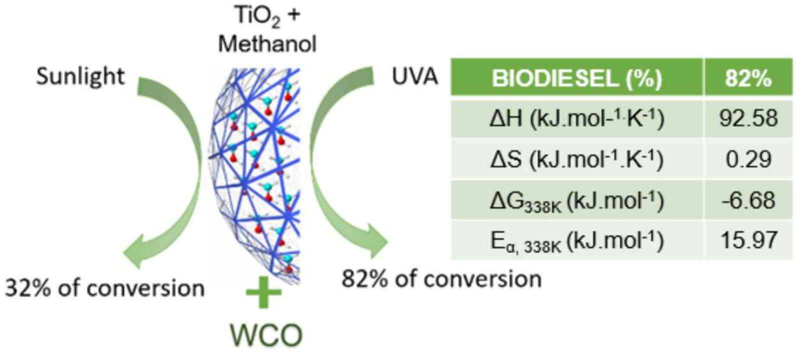

BIODIESEL (%)	82%
ΔH ($kJ.mol^{-1}.K^{-1}$)	92.58
ΔS ($kJ.mol^{-1}.K^{-1}$)	0.29
ΔG_{338K} ($kJ.mol^{-1}$)	-6.68
$E_{\alpha,\ 338K}$ ($kJ.mol^{-1}$)	15.97

Figure 6. 1. Graphical abstract: TiO_2 photocatalysed for biodiesel production from the simultaneous esterification and transesterification of waste cooking oil.

Keywords

Biodiesel, free fatty acid, photocatalysis, titanium dioxide, waste cooking oil.

6.1. Introduction

Biodiesel, an eco-friendly substitute to petrofuels, is produced globally on a large and growing scale. It has been added to petrodiesel (5–10%) to yield lower pollutant fuel. Biodiesel emits fewer greenhouse gases than petrodiesel (86% less) (Erin Voegele, 2020); it is free of aromatic compounds and sulfur (Esmaeili, 2022) and is produced predominantly from crude vegetable oils. Currently, more than 70% of biodiesel feedstock consists of edible vegetable oils, which are also used in the food industry (Oil World, 2022). The use of non-edible oils such as *Jatropha curcas* has been considered, but these raw materials also require farmland for production. Thus, the production from vegatable oils competes with edible oil raw material production and the food sector. As a cheaper and more sustainable approach, waste-cooking oil (WCO), which holds significant disposal problems, has been considered as a promising feedstock. As a result, the use of WCO for biodiesel production has seen a significant increase from 3% in 2007 to 11% in 2019 (Oil World, 2022).

Biodiesel production occurs through processes such as pyrolysis, esterification, and transesterification (Esmaeili, 2022), with the latter being the most common reaction. However, feedstocks with a high content of free fatty acids (FFA) such as WCO require pretreatment to remove these FFAs or use catalysts that promote triglyceride (TGL) transesterification and FFA esterification. A common process using strong homogeneous alkalis cannot be generally applied because it only catalyses the transesterification reaction, and the presence of water can result in saponification. The use of strong homogeneous acids represents an alternative. Strong acids, however, have disadvantages, such as their corrosiveness and hence complex handling, the need for product purification, the difficulty of catalyst recovery, or the generation of large volumes of waste (G. Berrebi et al., 1993). These issues can be minimised using heterogeneous catalysts for simultaneous esterification/transesterification reactions under mild operational conditions.

Different heterogeneous catalysts have been assessed, among these photoactivated metal oxides. Titanium dioxide (TiO_2) is one of the most common and cheapest metal oxides used in photocatalysis. TiO_2 is non-toxic, chemically stable, and easier to handle and recycle (Carp et al., 2004). Likewise, TiO_2-photocatalysis has been studied as a favourable methodology for various degradation and synthesis processes (Kanakaraju et al., 2014; Konstantinou & Albanis, 2003; Manique et al., 2016; Rajeshwar et al., 2008; R. A. Welter, Santana, de la Torre, Barnes, Taranto, & Olegemöller, 2022; Rosilene A. Welter, Santana, Torre, Robertson, Taranto, & Oelgemöller, 2022). TiO_2 has also been assessed as a promising photocatalyst for biodiesel production. For example, TiO_2 mediated photocatalysis resulted in a 96% conversion of oleic acid by photoesterification (Rosilene A. Welter, Santana, Torre, Robertson, Taranto, & Oelgemöller, 2022), and in a 73% conversion of canola oil by phototransesterification (R. A. Welter, Santana, de la Torre, Barnes, Taranto, & Oelgemöller, 2022). Khaligh et al. (Khaligh et al., 2021) achieved a 91% waste-cooking olive oil conversion using TiO_2 nanotubes as a photocatalyst. Khan et al. (M. Khan et al., 2021) reached 89% WCO conversion by transesterification using a TiO_2 composite with graphitic carbon nitride as the catalyst, even though the WCO required a pretreatment with sulphuric acid to initiate FFA esterification. However, simultaneous esterification/transesterification has not been evaluated for thermodynamic and physicochemical parameters. These parameters are crucial for achieving an optimised, cost-efficient and scalable process.

Therefore, this study developed a simultaneous WCO esterification/transesterification protocol for the production of biodiesel by collecting experimental data, postulating reaction mechanisms, establishing kinetic and thermodynamic analyses, and determining physicochemical properties of the reagents, products, and catalyst. In particular, TiO_2 photoactivated with UVA light or sunlight was evaluated as an eco-friendly catalyst at different reaction temperatures and with two alcohols.

6.2. Methodology

6.2.1. Materials

The reagents and solvents were obtained from the following suppliers: WCO (local restaurant, Townsville, Queensland, Australia), acetone (AR, 99.5%, Chemsupply), anhydrous sodium sulfate (Na_2SO_4, Univar), chloroform D (99.8% atom D, $CDCl_3$, Aldrich), dichloromethane (DCM, AR, 99.5%, Univar), diethyl ether (AR, 99.5%, Univar), ethanol (AR, 99.5%, Univar), ethyl acetate (AR, 99.5% Univar), potassium hydroxide pellets (KOH, Univar), methanol (HPLC grade, Fisher Chemical), sodium bicarbonate ($NaHCO_3$, Univar), sulphuric acid (AR, Univar), TiO_2 (P25: Aeroxide®, Evonik), and 0.02 N potassium hydroxide in aqueous solution (KOH aqueous, ±0.5%, Ace Chemical Company).

6.2.2. Simultaneous WCO esterification and transesterification

Biodiesel (fatty acid alkyl esters, FAAEs) production was investigated under three different conditions: acid-catalysis, UVA/TiO_2-photocatalysis and solar TiO_2-photocatalysis. Acid-catalysis represents the most common thermal process and was compared with that of photocatalysis. For both processes, two different alcohols were used: methanol to produce fatty acid methyl esters (FAMEs) and ethanol to produce fatty acid ethyl esters (FAEEs), respectively.

Acid catalyst process. Simultaneous esterification and transesterification was conducted using sulfuric acid (H_2SO_4). This conventional method was chosen to that provide reference biodiesel that could be compared with the product obtained from TiO_2-photocatalysis. The reactions were carried out in a round-bottom flask (500 mL) containing anhydrous alcohol (150 mL, methanol or ethanol), concentrated H_2SO_4 (1.5 g), and WCO (15 g), with vigorous mixing (magnetic stirrer, 500 rpm). The temperature was kept constant at 60°C for 5 h. After this period, stirring was continued for 24 h at room temperature. The product was purified using the following steps: (1) 600 mL of water were added; (2) the mixture was rotary evaporated (40°C, 170 mbar for 60 minutes, 72 mbar for 60 minutes, and 30 mbar for 60 minutes); (3) 150 mL of ethyl acetate was added; (4) the mixture was mixed gently; (5) phase separation was achieved in a separatory funnel after one hour (steps 3 to 5 were conducted three consecutive times); (6) 150 mL of a diluted $NaHCO_3$ solution were added; (7) the mixture was mixing gently; (8) after one hour of resting, phase separation was performed in a separatory funnel; (9) 150 mL of a saturated aqueous NaCl solution were added; (10) the mixture was mixed gently; (11) phase separation was conducted in a separatory funnel after resting for one hour; (12) the organic layer was separated, and dried over anhydrous Na_2SO_4 for approximately five minutes; (13) the liquid fraction was filtered through a syringe filter (Hydraflon 0.22µm, 35 mm); (14) the mixture was rotary evaporated at 40°C to remove any volatiles (170 mbar for 30 minutes, 72 mbar for 30 minutes, and 30 mbar for 60 minutes); and (15) the samples were stored in glass vials at room temperature for further characterisation.

TiO_2 photoirradiated process. The protocol applied to the synthesis of biodiesel from WCO and alcohols by photoactivated TiO_2 was developed previously for oleic acid esterification (Rosilene A. Welter, Santana, Torre, Robertson, Taranto, & Oelgemöller, 2022) and canola oil transesterification (R. A. Welter, Santana, de la Torre, Barnes, Taranto, & Oelgemöller, 2022). The protocol involved three stages: (1) catalyst pretreatment; (2) photoirradiation; and (3) organic product purification. Blank tests and experiments using illumination with sunlight instead of irradiation with UVA light were performed. (1) Catalyst pretreatment: TiO_2 was mixed (magnetic stirring at 500 rpm) with alcohol for 30 min at the same temperature used in the photoreaction. (2) Photoreaction: The pretreated TiO_2-alcohol mixture and WCO were loaded into a jacketed two-necked round-bottom flask vessel (500 mL capacity) manufactured from Pyrex glass (cut-off wavelength ≤290 nm (Figure S6.1 of SI – APPENDIX E) under mixing (magnetic stirring, 500 rpm). Irradiation was carried out in a Rayonet photochemcial chamber reactor (RPR-200, Southern New England Ultraviolet Company) equipped with fluorescent tubes (Ushio, 16 F8T5/BL, 8W Black Light UVA T-5 G5 Base). The system (light and water bath) was turned on 30 min prior to starting the reaction. Operational conditions: 20% w/w_{wco} of TiO_2, 1 WCO mol:55 MeOH mol, total volume of reaction medium: 100 mL, and temperatures of 25–65°C. Kinetics data: samples (<3 mL each) were withdrawn at set reaction times (15, 30, 45, 60, 120, 180, and 240 min). The reactions were conducted for 240 minutes, assuming that equilibrium was reached. Fatty acid ethyl ester (FAEE) was obtained accordingly at 65°C with ethanol instead of methanol. (3) Organic product purification: the reaction product was filtered through a syringe filter (Hydraflon 0.22μm, 35 mm), rotary-evaporated at 40°C to remove alcohol and water (170 mbar/15 minutes, 72 mbar/30 minutes, and 30 mbar/30 minutes), left to stand for 20 h to allow for glycerine separation and stored in glass vials at room temperature. The final samples (240 min) were characterised further (Section 6.2.4). The experiment at 65°C was repeated three times, and the standard deviation was determined.

Blank analysis: Five blank reactions were performed by keeping the operational conditions constant (65°C, 1 WCO mol:55 MeOH mol, and 20% w/w_{WCO} of TiO_2): Blank 1 (absence of catalyst); Blank 2 (absence of light with the reaction vessel wrapped in aluminium foil); Blank 3 (absence of catalyst and light with the reaction vessel wrapped in aluminium foil); Blank 4 (absence of stirring); and Blank 5 (absence of catalyst pretreatment).

Sunlight irradiation: an analogous process described for FAME above was performed at 65°C but applying natural sunlight instead of UVA light (Figure S6.2 of SI – APPENDIX E). A spherical stainless steel dish (inner diameter of 44 cm, focal length of 16.13 cm) was placed below the double-jacketed round-bottom reactor. The reaction was conducted on the ground outside the Molecular Genetic Laboratory Building on the James Cook University campus in Townsville (latitude – 19°33'S, longitude 146°76'E, elevation 37.2m above sea level) for 360 minutes, from 9:30 am to 3:30 pm (7th of January 2022), the time period with the strongest radiation. Sunlight irradiation measurements were obtained and monitored by ARPANSA (ARPANSA, 2022) (Section S6.3 of SI – APPENDIX E).

6.2.3. TiO_2 Catalyst

Recovery and reuse: After the reaction, organic materials (methanol, WCO, biodiesel, glyceride, and water) adhered to the catalyst (0RP), and thus a recovery process was required prior to its reuse. The recovery procedure was conducted according to the following steps: (1) the reaction mixture was filtered through a filter paper (Grade: MS 2 185 mm, MicroScience); (2) washed with acetone by mixing vigorously with magnetic stirring (500 rpm); (3) settled for 20 hours followed by decantation; (4) dried at 100°C for 24 hours; and (5) crushed. These steps represent the first stage of the recovery process (1 RP). This process was repeated three times (3 RP) to complete one reactivation cycle (1 C). The samples were stored in plastic vials at room temperature. The recovered and reused catalyst were evaluated according to their physicochemical properties (Section 6.2.3) and by conducting subsequent photoreactions. All these steps were followed 5 times (1C to 5C).

Characterisation: TiO_2 was characterised prior to use (pure), after the photoreaction without further treatment (0RP), after the recovery process (1C, Section 6.2.3), and after use and recovery for five times (5C).

Fourier transform infrared–attenuated total reflection (FTIR-ATR) spectroscopy: Functional group identifications were performed by FTIR-ATR coupled with an iD7 ATR accessory (Nicolet™ iS™ 5, room temperature, spectral range between 400 and 1000 cm^{-1}, ThermoFisher Scientific). Standard peaks are shown in the Supplementary material (Section S6.4 of SI – APPENDIX E).

Thermal gravimetric analysis (TGA) and differential scanning calorimetry (DSC): (5°C/min, temperature range: room temperature – 600°C, SDT650 equipment and Trios® software, TA instruments) were carried out to determine the presence of organic material impregnated within the catalyst. The data were analysed using the Trios® software (T.A. Instruments), and OriginPro® 2022.

UV-Vis: UV-Vis spectra (spectral range of 200 – 1100 cm^{-1}, UV-1800, room temperature, Shimadzu) were obtained using a TiO_2 suspension prepared by mixing (magnetic stirring) 10^{-3} mg/L TiO_2 in methanol for four hours. The catalyst bandgap (E_g) was determined by applying the spectra data to the Tauc model, $(\alpha \cdot h\nu)^{1/\Upsilon} = B \cdot (h\nu - E_g)$ (Tauc, Grigorovici, & Vancu, 1966), which correlates the absorption coefficient (α), photon energy ($h\nu$), a constant (B) with a factor (Υ=2 for TiO_2 (Makuła et al., 2018)).

6.2.4. Biodiesel characterisation

^{1}H-nuclear magnetic resonance (NMR) spectroscopy: used to determine the conversions to FAME and FAEE (*Bruker Ascend*TM *400 MHz* Spectrometer, MestReNova® software, Version 6.0.2-5476, Mestrelab Research S.L., and OriginPro® 2022, Section S6.5 of SI – VI). The conversion values are described as % biodiesel. The FAME amount ($\% \text{ FAME} = 100\% \cdot 2 \cdot I_{ME}/3 \cdot I_{\alpha CH_2}$) was calculated by correlating the three methoxy protons (I_{Me}, approx. 3.6 ppm) with the two α-methylene protons of the oil ($I_{\alpha CH_2}$, approx. 2.3 ppm), as described by (Borah et al., 2018; Gelbard et al., 1995). The FAEE concentration was obtained similarly ($\% \text{ FAEE} = 100\% \cdot (I_{GL+E} - I_{GL})/I_{\alpha CH_2}$) by correlating the glyceride CH_2 (I_{GL}) and ethoxy (I_{EE}) proton areas ($I_{GL + E.E.}$, overlapping peaks at 4.10–4.20 ppm) with the α-methylene protons area of the oil ($I_{\alpha CH_2}$, 2.3 ppm), as described by (Jaiswal et al., 2016).

Gas chromatography: used to evaluate the biodiesel composition according to the EN14103:2011 methodology (McCurry, 2012) (7890A Agilent Gas Chormatograph, Injector: 7683B Agilent, HP-5INNOWax capillary column, 30 m × 0.25 mm, 0.25 µm film). Pure helium was used as a carrier gas (1 mL/min), with a 250°C injector temperature and 250°C detector temperature; the temperature programme used was 60°C/2 minutes, 10°C/min to 200°C, 5°C/min to 240°C, and holding at 240°C/7 min. Compound identification was performed through standard retention times (Section S6.6 of SI – APPENDIX E).

FTIR-ATR spectroscopy analysed the oil and biodiesel qualitatively. Spectra deconvolution was delineated using OriginPro 202® (Learning Edition, OriginLab Corporation). Peak deconvolution analysis was performed by PeakDeconvolution.opx from OriginLab®, Straight Line as the baseline, Peak Resolution Enhancement Method: 2nd derivative Smooth Derivative Method:Quadratic Savitzki-Golay, 2nd order polynomial.

Acid values (AV): determined by titration. The samples (0.05 g) were diluted in a diethyl ether/ethanol solution (2:1 v/v, 25 mL) with two drops of thymol blue indicator and titrated using 0.02 N KOH aqueous standard solution. The AV was determined by correlating the volume of the KOH solution used in the titration (S, mL), the volume of the KOH used in the blank titration (b, mL), the normality of KOH (N), and the sample mass (W, g): $\mathrm{AV} = (\mathrm{Sb}) \cdot \mathrm{N} \cdot 56.1/\mathrm{W}$.

TGA and DSC: carried out through N_2 and air (temperature range: room temperature – 600°C, 5°C/min) used to determine the boiling point (dW/dT=0) and flash point (17.5% mass reduction), which indicates the lowest temperature the vapour could be ignited and the flame spread across the remaining liquid (Abdelkhalik et al., 2018), ignition temperature (T_i) which refers to the temperature where the vapours have the capacity for autocombustion (N. Khan et al., 2021; J. J. Lu & Chen, 2015; Wnorowska et al., 2021), burnout temperature (T_B, 95% of mass reduction) (J. J. Lu & Chen, 2015; Wnorowska et al., 2021), maximum combustion rate [C_{max}, (dW/dT)max=0] (Lai et al., 2014; Wnorowska et al., 2021), and mean combustion rate [C_{mean}, (dW/dT) mean at 50% of mass reduction] (Lai et al., 2014).

6.2.5. Kinetic and thermodynamic properties

Simultaneous esterification/transesterification reactions were conducted until equilibrium conditions were reached (4 h) over temperature range of 25 to 65°C (Section 6.2.2). Internal and external mass transfer limitations were neglected, and the reaction rates assumed that the reactions were limited kinetically (Section S6.9 of SI - APPENDIX E). Five kinetic models were applied (Table 6.1). Four models considered a homogeneous system (F1B1, F1B2, F2B2, and F2B4, Equations 6.7–10, respectively), whereas the fifth (Langmuir–Hinshelwood, L–H, Equation 6.8) considered the system heterogeneously involving a solid catalyst with homogeneous active sites and a system with complete miscibility among the reagents. Mathematical modelling was performed using the Matlab® software (algorithms applied: Lsqcurvefit, and 45ode). The predicted data were statistically compared to the experimental data (by R^2, F-test, Standard deviation, β, t-student, p-value). Moreover, through the kinetic rate constants (k_1 and k_{-1}), the equilibrium constant (K_{eq}) was determined. The activation energy (ΔE_a) and the frequency factor (A) were estimated using the Arrhenius model for both reactions (forward - Equation 5. 9.1, and backward – Equation 6.2). The effective activation energy (E_α, Equation 6. 3) was determined considering the isoconversional principles (Liavitskaya & Vyazovkin, 2016; Sbirrazzuoli, 2020). Subsequently, the thermodynamic properties were determined. The reaction enthalpy (ΔH_R) and entropy (ΔS) were estimated through linearisation of the Van't Hoff model (Equation 6.4) and Gibbs free energy variation (ΔG) by two equations. First correlating T and K_{eq} (Equation 6.5), and second, correlating ΔH_R, T, and ΔS (Equation 6.6), respectively.

$$\ln(k_1) = -\frac{\Delta E_{aF}}{\mathrm{R} \cdot \mathrm{T}} + \ln{(A_F)}$$

Equation 6. 1

$$\ln(k_{-1}) = -\frac{\Delta E_{aB}}{\mathrm{R} \cdot \mathrm{T}} + \ln{(A_B)}$$ Equation 6. 2

$$E\alpha = \frac{k_1 \cdot Ea_F + k_{-1} \cdot Ea_B}{k_1 + k_{-1}}$$ Equation 6. 3

$$\ln\left(K_{eq}\right) = -\frac{\Delta H_R}{\mathrm{R} \cdot \mathrm{T}} + \frac{\Delta \mathrm{S}}{\mathrm{R}}$$ Equation 6. 4

$$\Delta \mathrm{G}_1 = -R \cdot T \cdot ln\left(K_{eq}\right)$$ Equation 6. 5

$$\Delta \mathrm{G}_2 = \Delta H_R - \mathrm{T} \cdot \Delta \mathrm{S}$$ Equation 6. 6

Table 6. 1: *Kinetic models evaluated for WCO and methanol simultaneous esterification/transesterification photocatalysed by TiO_2.*

Assumptions	**Model**	**Equation**
Homogeneous system		
F1B1 - F: first-order - B: first-order	$\frac{dx_{wco}}{dt} = k_{-1} \cdot (1 - x_{wco}) - k_1 \cdot x_{wco}$	Equation 6. 7
F1B2 - F: pseudo-first-order - B.: second-order	$\frac{dx_{TGL}}{dt} = k_{-1} \cdot (1 - x_{TGL}) - k_1 \cdot C_{TGL_0} \cdot x_{TGL}^2$	Equation 6. 8
F2B2 - F: second-order - B: second-order	$\frac{dx_{wco}}{dt} = k_{-1} \cdot C_{wco_0} \cdot (1 - x_{wco})^2 - k_1 \cdot C_{wco_0} \cdot x_{wco}^2$	Equation 6. 9
F2B4 - F: Second-order - B: fourth-order	$\frac{dx_{TGL}}{dt} = k_1 \cdot C_{TGL_0} \cdot (1 - x_{TGL})^2 - k_{-1} \cdot C_{TGL_0}^3 \cdot x_{TGL}^4$	Equation 6. 10
Heterogeneous system		
L-H kinetic model[a] - F: first-order - B: first-order - FAME is bounding the catalyst capacity	$\frac{\mathrm{d}x_{wco}}{\mathrm{dt}} = \mathrm{k}_{-1} \cdot \frac{\mathrm{K}_2' \cdot x_{wco}}{1 + \mathrm{K}_2' \cdot \mathrm{C}_{\mathrm{wco}_0} \cdot x_{wco}} - \mathrm{k}_1 \cdot \frac{\mathrm{K}_1' \cdot (1 - x_{wco})}{1 + \mathrm{K}_1' \cdot \mathrm{C}_{\mathrm{wco}_0} \cdot (1 - x_{wco})}$	Equation 6. 11

[a] details of the model development can be found in Section S6. 8 of SI – APPENDIX E; F: Forward reaction; B: Backward reaction.

6.3. Results and discussion

6.3.1. WCO esterification/transesterification

A conversion of approximately 82% (±1.24%, Figure 6. 2) was achieved through simultaneous esterification and transesterification of WCO with methanol using TiO_2-photocatalysis (UVA light, batch reactor, vigorous stirring at 500 rpm, 4 h, 1WCO:55MeOH molar ratio, 20% w/w_{wco}, 65°C). Compared with other studies (Table 6. 2), this result indicates that photocatalysis can be applied to biodiesel production using a feedstock with a high FFA content (Table 6.3). A reduction of 37% between the first and fifth cycles was observed. Similar drops in efficiency were observed by other authors for solid catalysts and was associated with variations in the catalyst's physicochemical characteristics. In this study, the accumulation of organic material within the catalyst is impacting its efficiency, as described in the Section 6.3.5. Estimation of the FFA content (Table 6.4) suggested a final FFA content of 1.8%. Hhowever, a lower value of 1.2%±0.2 was determined, indicating that FFA esterification accounted for approximately 89% and was slightly more efficient than the transesterification with 81%. The influence of light, temperature, TiO_2 content, and stirring were likewise evaluated (Figure 6. 2, Section S6.7 of SI – APPENDIX E. A conversion of only 21% was achieved when applying the best operational conditions for UVA-irradiation to illumination with natural sunlight instead. TiO_2 is photoactivated by UVA-light between 315 and 400 nm. In contrast, sunlight only has a small fraction and low intensity of UVA (Kanakaraju et al., 2016), naturally resulting in reduced activation. Nevertheless, a noteable conversion was reached, indicating that the solar TiO_2-photocatalysed reaction is generally feasible. To achieve higher conversion, a larger exposure surface, a hybrid solar-lamp system, an optimised solar reactor design or concentration of sunlight may be applied (Oelgemöller, 2016).

Transfer of the best operational conditions (UVA irradiation) to ethanol resulted in a conversion of 38% compared to 83% when using methanol. A similar decrease was observed by other authors using different solid catalysts (Cardoso et al., 2009; Harun et al., 2018; Rosilene A. Welter, Santana, Torre, Robertson, Taranto, & Oelgemöller, 2022). Methanol is a better electron donor and has higher reactivity than other alcohols (Ayadi et al., 2021; M. v.d. Silva et al., 2015). Although the miscibility of WCO in methanol is lower than in ethanol, at high temperatures (65°C) and upon mixing, a homogeneous system is obtained for both alcohols, favouring mass transfer.

Five blank experiments were performed using the optimal operational conditions for FAME production. In the absence of TiO_2, UVA or both, conversions were found below 10%, confirming the need for irradiation and the presence of an efficient photocatalyst. The absence of vigorous stirring resulted in a decreased conversion of 25% due to a significant drop in mass transfer. The experimental run conducted without pretreatment resulted in a 34% conversion, compared to 83% with pretreatment. In the absence of pretreatment, the catalyst's pores are susceptible to absorption by other reagents, reducing its capacity to absorb light and subsequntly its efficiency. Catalyst reuse resulted in a 23% decrease in efficiency between the first (1C) and fifth (5C) run, which is explained by changes in the catalyst's characteristics, as discussed further in Section 6. 3. 5.

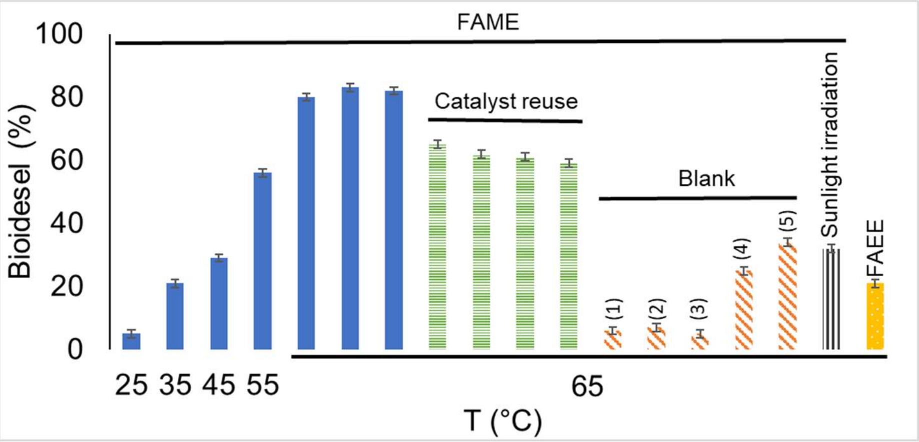

Figure 6. 2. WCO and alcohol simultaneous esterification/transesterification to produce biodiesel by TiO_2 under photoirradiation. Biodiesel (%) obtained using ^{1}H-NMR as described in Section 6.2.4. Regular tests: 🟦 1 WCO:55 MeOH molar ratio and 20% TiO_2 w/w$_{wco}$, UVA light irradiation. Blank tests, respectively: ▨ (1) absence of TiO_2; (2) absence of irradiation; (3), absence of TiO_2 and irradiation; (4) absence of reaction stirring; (5) absence of TiO_2 pretreatment. Operational conditions (if applicable): 1 WCO:55 MeOH molar ratio and 20% TiO_2 (w/w$_{wco}$), UVA light irradiation. Catalyst reuse: ▤ a total of 4 photoreactions developed subsequently with reused catalyst (2C – 5C). Sunlight: ▥ 1 WCO:55 MeOH molar ratio. 🟨 1 WCO:55 Ethanol molar ratio and 20% TiO_2 (w/w$_{wco}$), UVA light irradiation. Standard deviation (σ) ± 1.24 set by triplicate of the regular test at 65°C (FAME production).

\

Table 6. 2: *Biodiesel produced by WCO using oxides as the catalyst.*

Catalyst	% (w/w_{wco})	Alcohol	Molar ratio	T (°C)	Time (h)	FAME (%)	Ref.
CaO.ZnO	2	Methanol	10	70	60	95	(I. Lukić et al., 2013)
CuO/ZnO + UVA	5	Ethanol	9	65	120	93	(Guo et al., 2022)
ZnO-La_2O_3	2	Methanol	[a]	200	3	96	(Yan et al., 2009)
TiO_2	4	Methanol	10	120	4	91	(Mihankhah et al., 2018)
TiO_2/g-C_3N_4 + sunlight	2	Methanol	9	60	60	84	(M. Khan et al., 2021)
TiO_2/Graphene	1.5	Methanol	12	65	3	98	(Borah et al., 2018)
TiO_2-MgO	10	Methanol	30	160	6	92	(Wen et al., 2010)
TiO_2/$PrSO_3H$	1	Methanol	6	65	9	98	(Gardy et al., 2017)
TiO_2 + sunlight	nanotubes	Methanol	8	60	4	91	(Khaligh et al., 2021)
TiO_2 + sunlight	20	Methanol	55	65	6	32	This study
TiO_2 + UVA	20	Ethanol	55	65	4	21	This study
TiO_2 + UVA	**20**	**Methanol**	**55**	**65**	**4**	**82**[b]	**This study**
		Esterification				89	This study
		Transesterification				81	This study

[a]126g of oil and 180g of methanol; [b] 82% refers to the total conversion being 89% FFA esterification and 81% TGL transesterification.

Table 6. 3: *Efficiency of reused oxides as a catalyst for biodiesel production using WCO as a feedstock.*

Catalyst	FAME (%)	# cycles	FAME (%)	Decrease (%)[a]	Ref.
CuO/ZnO + UVA	93	6	80	13	(Guo et al., 2022)
SrO-ZnO/Al_2O_3	96	3	17	79	(Al-Saadi, Mathan, & He, 2020)
TiO_2/Graphene	98	3	79	19	(Borah et al., 2018)
TiO_2-MgO	92	5	81	11	(Wen et al., 2010)
TiO_2 + UVA	73	5	36	37	This study

[a]Decrease between first and last cycle.

6.3.2. FAME characterisation

The initial WCO and biodiesels produced were characterised as described in Table 6.4.

The FFA content was determined by titration for WCO (10.9%), FAME from acid catalysis (0.2%), and FAME from photocatalysis (1.2%). The FFA content in WCO agrees with the literature (range: 5–20%) (Hassani, Amini, Najafpour, & Rabiee, 2013; L. Liu, Liu, Tang, & Tan, 2014; Shah, Parikh, & Maheria, 2014). Similar results were established using FTIR-ATR spectral peak deconvolution (Figure 6. 3), considering the area under the peaks (Section S6.4 of SI – APPENDIX E). However, high accuracy between the results obtained by titration and FTIR-ATR peak deconvolution was only observed for the crude WCO. For FAME analyses, a reduced comparability between the two techniques was noted [FAME from photocatalysis: 1.5% (FTIR-ATR), 1.2 (Titration); FAME from acid catalysis: 1.1% (FTIR-ATR), 0.2 (Titration)]. Titration was found to be the more accurate methodology with a low standard deviation after triplicate analysis. In contrast, FTIR-ATR spectral deconvolutions of small peaks were strongly impacted by spectral noise. In particular, the main peak observed for FFA in the spectrum of FAME fluctuated at low concentrations. A large decrease in the FFA content was expected for acid catalysis as both, esterification and transesterification are operating under these conditions, and this was confirmed by titration. Transesterification by acid catalysis (99% conversion) was slightly more efficient than esterification (98% conversion). , both transformation likewise occur during photocatalysis (De & Boxi, 2020; Gardy et al., 2017; Khaligh et al., 2021; Mihankhah et al., 2018; Rosilene A. Welter, Santana, Torre, Robertson, Taranto, & Oelgemöller, 2022; Wen et al., 2010), however, esterification (89% conversion) was more efficient than transesterification (81% of conversion). Esterification requires less energy than transesterification and subsequently occurs more readily, resulting in a higher conversion rate. High conversions for esterification were also achieved for TiO_2-photocatalysis of oleic acid when irradiated with UVA-light (98% conversion) (Rosilene A. Welter, Santana, Torre, Robertson, Taranto, & Oelgemöller, 2022), supporting the efficiency of this methodology. In contrast, applying the same protocol to canola oil gave a conversion up to 73% (R. A. Welter, Santana, de la Torre, Barnes, Taranto, & Oelgemöller, 2022), indicating that the methodology is less efficient for transesterification than for esterification.

Crude WCO, FAME obtained using acid catalysis and FAME from photocatalysis were evaluated by thermoanalysis (Table 6. 4, Figure 6. 4). The WCO's boiling point peak was observed at 413°C and both FAMEs' at 230°C, respectively. Likewise, Ti temperatures of FAME obtained using acid catalysis and photocatalysis were 183°C and 181°C, respectively. Moreover, the volatile compounds' peak (100–150°C) was not observed. These three features suggest that the FAMEs obtained with both catalysts are thermostable (Mostafa & El-Gendy, 2017; Wnorowska et al., 2021). The flash points for FAME from both processes were similar with 190°C and 188°C, respectively, indicating the compatibility of both FAMEs, independent of the catalytic routes. The values of TB, C_{max}, and C_{mean} were slightly lower for FAME obtained by photocatalysis than from acid catalysis. However, the curves showed similar behaviours, suggesting that FAME from photocatalysis is thermically similar to the FAME generated from acid catalysis (considered as the standard).

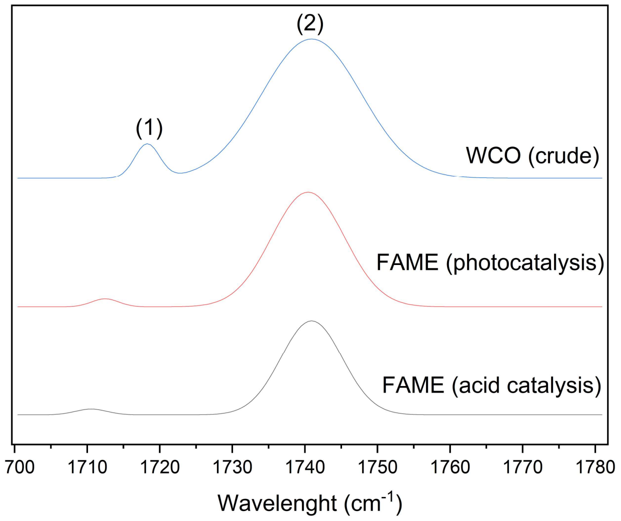

Figure 6. 3. FTIR – ATR spectra deconvoluted spectra of WCO crude and FAME from simultaneous esterification and transesterification using different catalysts: acid and TiO_2 under UVA irradiation. Deconvolution range: 1700–1780 cm^{-1}, peaks: (1) 1717 – COOH, free fatty acid, (2) 1740 – C=O, stretching ester (Section S6.4 of SI – VI).

Table 6. 4: *Characterisation of WCO and biodiesel obtained using acid catalysis and photocatalysis.*

		WCO	FAME	
			TiO_2+UVA	Acid
FAME	(% mol)	-	82 (±1.1%)	99
FFA	(%)	10.9 (±0.5)	1.2 (±0.2)	0.2 (±0.1)
Boiling point	(°C)	413	230	229
Ignition temperature (T_I)	(°C)	365	183	181
Flash point	(°C)	377	190	188
Burnout temperature (T_B)	(°C)	454	248	306
Maximum combustion rate (C_{max})	$(dW/dt)_{max}$	1.79	1.38	1.92
Mean combustion rate (C_{mean})	$(dW/dt)_{mean}$	0.75	0.49	0.99

The biodiesel composition produced by thermal acid catalysis and photocatalysis was likewise determined by gas chromatography (GC, Table 6. 5). According to these results, the reaction by photocatalysis tends to convert C18:1 (methyl oleate) and C19:1 (methyl nonadecanoate) carbon chains more efficiently and C18:2 (linoleic acid) less efficiently than the traditional acid catalysed method. C18:2 carries an additional double bond, which increases the energy required for the reaction (Hawash et al., 2019). For example, the reaction enthalpy of methyl oleate esterification (ΔH°_r, 298K=122 kJ/mol) is lower than that for methyl linoleate esterification (ΔH°_r, 298K=245 kJ/mol) (Smith & Martell, 2004). In addition, computational studies on canola oil methyl esters showed that methyl stearate (C19:0) is slightly more reactive than methyl oleate (C18:1) because of methyl oleate's double bond (Naik, Westbrook, Herbinet, Pitz, & Mehl, 2011). Thus, the energy required increases with the number of double bonds, and subsequently conversions decrease.

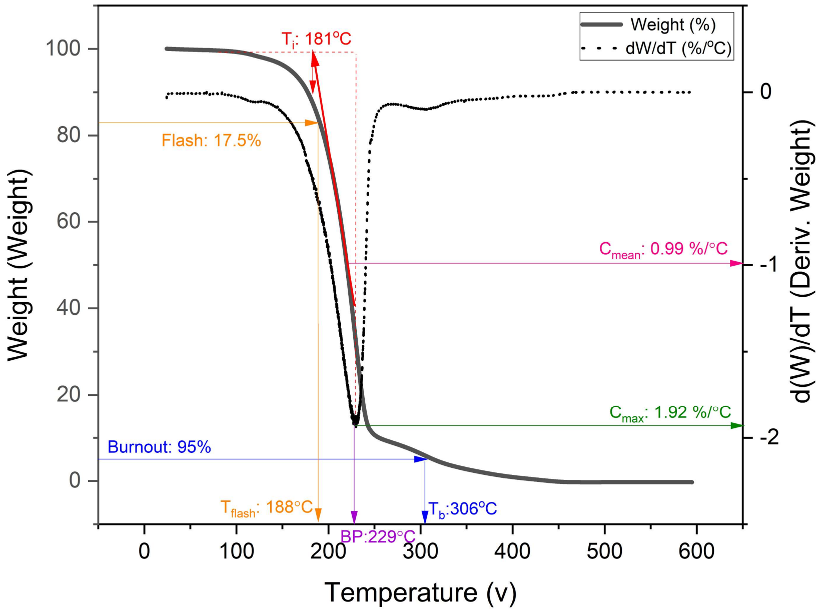

Figure 6. 4. TGA of biodiesel obtained using WCO and methanol catalysed by acid.

WCO conversions to biodiesel were furthermore determined by ^{1}H-NMR spectroscopy (Figure 6. 5, Sections S6.5 and S6.8 of SI – APPENDIX E) and confirmed by FTIR-ATR spectroscopy (Figure 6. 6). Biodiesel obtained from acid catalysis required several purification steps including extraction using ethyl acetate (Section 6.2.2), which could not be removed quantitatively. The presence of residual solvent somewhat confirms the general difficulty of removing contaminants when using traditional processes. In contrast, photocatalysis does not demand additional reagents or solvents for isolation or lengthy purification steps, thus minimizing waste production, and avoiding additional contaminants within the biodiesel product. The presence of reaction intermediates (MGL and DGL) was not observed, although some authors detected their presence in small quantities at the beginning of the reaction (Noureddini & Zhu, 1997; Pugnet et al., 2010; R. A. Welter, Santana, de la Torre, Barnes, Taranto, & Oelgemöller, 2022), suggesting that intermediate formation and consumption occur rapidly. However, MGL and DGL can improve the miscibility between oil and alcohol caused by their surfactant characteristics, consequently increasing the reaction efficiency (X. Chen et al., 2020).

Table 6. 5: *Biodiesel (FAME) composition (%) obtained using WCO and methanol transesterification using different catalysts* [a].

		TiO_2+UVA	**Acid**
methyl hexanoate	C6:0	0.1	0.1
methyl decanoate	C10:0	0.1	0.1
methyl mystarate	C14:0	0.5	0.5
methyl palmitate	C16:0	17.4	18.1
methyl palmitoleate	C16:1	0.4	0.4
methyl stearate	C18:0	2.9	3.0
methyl oleate	**C18:1**	**51.5**	**50.4**
methyl linoleate	**C18:2**	**21.0**	**25.0**
methyl linolenate	C18:3	1.4	1.1
methyl stearate	C19:0	3.6	0.5
methyl eicosonate	C20:1	0.5	0.7
methyl eicosadieonate	C20:2	0.7	0.0

[a]Obtained using GC (Section S6. 6 of SI – APPENDIX E).

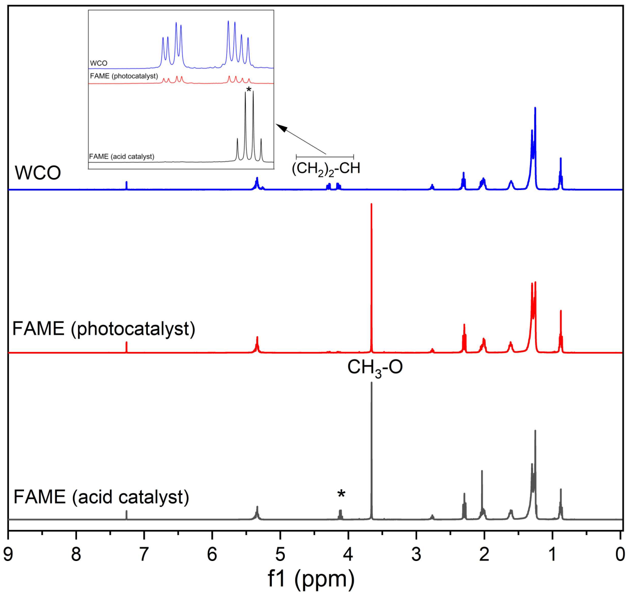

Figure 6. 5. 1H-NMR spectra (Range: 4.50 - 4.00 ppm) of WCO crude and FAME from simultaneous esterification and transesterification using different catalysts: acid and TiO_2

under UVA irradiation (*ethyl acetate present in the FAME obtained using acid catalysis, Section S6.5 of SI – APPENDIX E).

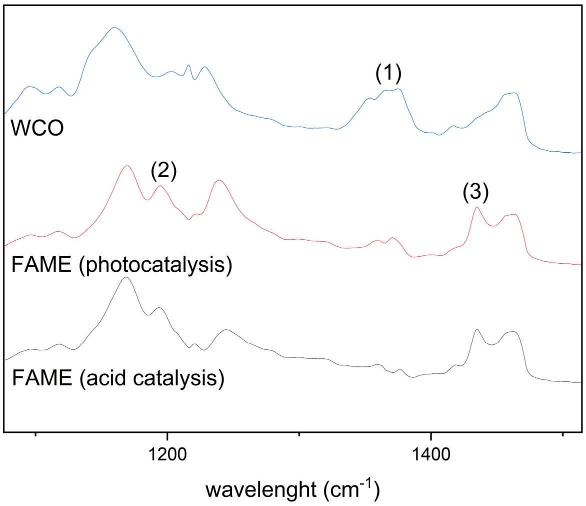

Figure 6. 6. FTIR – ATR spectra (Range: 1100 – 1300 cm^{-1}) of WCO crude and FAME from simultaneous esterification and transesterification using different catalysts: acid and TiO_2 under UVA irradiation. Peaks: (1) 1375.5 cm^{-1} - aliphatic C-H (for CH_2 and CH_3), (2) 1196 cm^{-1} - 0-CH_3 stretching, (3) 1434 cm^{-1} - CH_3 asymmetric bending (COO-CH_3) (Section S6.4 of SI – APPENDIX E).

6.3.3. Proposed photocatalysis mechanism

The proposed reaction mechanism for the generation of biodiesel involves parallel esterification of FFA and transesterification of TGL pathways (Figure 6. 7). Similar mechanisms were previously suggested for esterifications (Ghani et al., 2020; Guo et al., 2021; Rosilene A. Welter, Santana, Torre, Robertson, Taranto, & Oelgemöller, 2022) and transesterifications (Borah et al., 2018; R. A. Welter, Santana, de la Torre, Barnes, Taranto, & Oelgemöller, 2022) by TiO_2-photocatalysis. Irradiation of TiO_2 with UVA-light of sufficient energy to overcome its bandgap (3.2 eV, as described in Section 6.3.5), causes charge separation. Electrons (e^-) are promoted to the conduction band (CB), resulting in positive holes (h^+) in the valence band (VB) (Ohtani, 2011). The h^+ reacts with methanol, generating a methoxy radical ($CH_3O^\bullet$), while the e^- reacts with FFA or TGL, generating the corresponding carboxyl radical anion ($RCO_2^{-\bullet}H$ or $RCO_2^{-\bullet}R'$). Both radicals combine, generating FAME (biodiesel) via subsequent reaction steps. Esterification generates FAME and water via a single-step reaction pathway. In contrast, transesterification generates three FAME molecules and one glycerol through a three-step process, with the first and second step generating the intermediate monoglycerol and diglycerol, respectively.

$$TiO_2 + h \longrightarrow h^+ + e^-$$

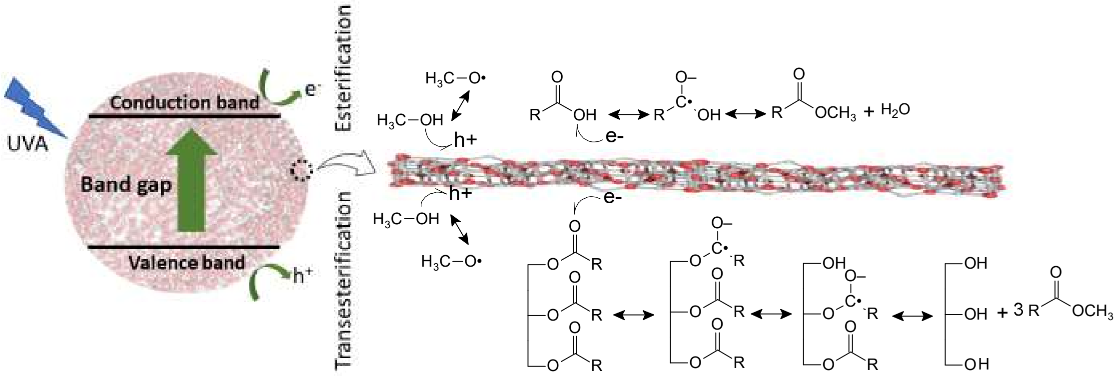

Figure 6. 7. Simultaneous esterification and transesterification of WCO and methanol catalysed by TiO_2 under UVA irradiation.

6.3.4. Identification of byproducts from parallel reactions

Different byproducts may have been produced in trace amounts, making their identification challenging. Methanol oxidation, for example, results in formaldehyde and subsequently formic acid (Figure 6. 8). Likewise, ester oxidation may generate a variety of compounds such as aldehydes, ketones, alkenes, and carboxylic acids (Bax, Hakka, Glaude, Herbinet, & Battin-Leclerc, 2010; Naik et al., 2011). Bak et al. (Bax et al., 2010) observed the presence of more than 30 compounds during thermal methyl oleate and methyl palmitate oxidation. Temperatures above 380°C resulted in larger amounts of 1-octane, 1-nonene, and methyl-5-hexenoate (Bax et al., 2010), which were not observed in FAME obtained by photocatalysis. In contrast, temperatures below this temperature generated larger quantities of methyl acrylate, acetaldehyde, 2-decenal, 2-undecenal, and $C_{19}H_{36}O_3$ isomers (Bax et al., 2010). Careful ^{1}H-NMR analysis of FAME obtained by photocatalysis indicated the possible presence of the following compounds in trace amounts: methyl acrylate, acetaldehyde, butyraldehyde, 2-undecenal, and 2-decenal (Figure 6. 9 and Figure 6. 10). These were identified based on representative signals, whereas others could not be assigned due to their overlap with more dominant signals. The blank experiments (Figure 6. 11 and Figure 6. 12) revealed that the reaction performed without TiO_2 pretreatment followed the same parallel reactions as those observed during the regular photocatalytic reaction. The other blanks containing TiO_2 also showed traces of 2-decenal and 2-undecenal, even without light or low FAME conversion. The blanks without TiO_2 did not result in any competing side-reactions.

Thus, the competing photooxidation pathways required the presence of TiO_2. However, because these compounds were detected solely in trace concentrations, it was impossible to quantify or correlate these with the concentration of the main product (FAME).

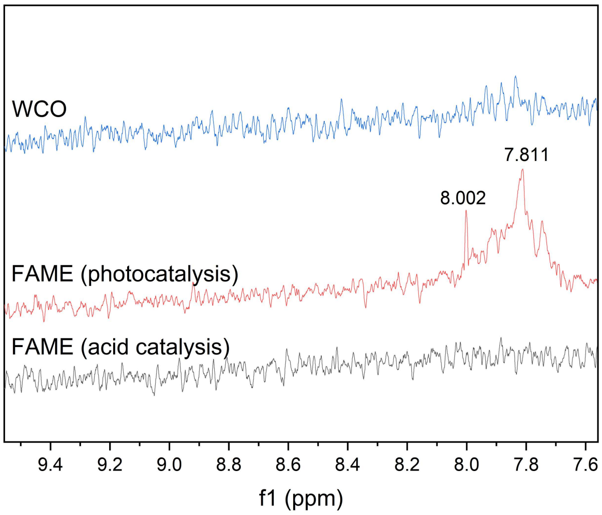

Figure 6. 8. Traces of formic acid (8.002 ppm) and 2-(hydroxymethyl) acrylic acid (7.811 ppm) from the parallel photo-oxidation reaction of esters.

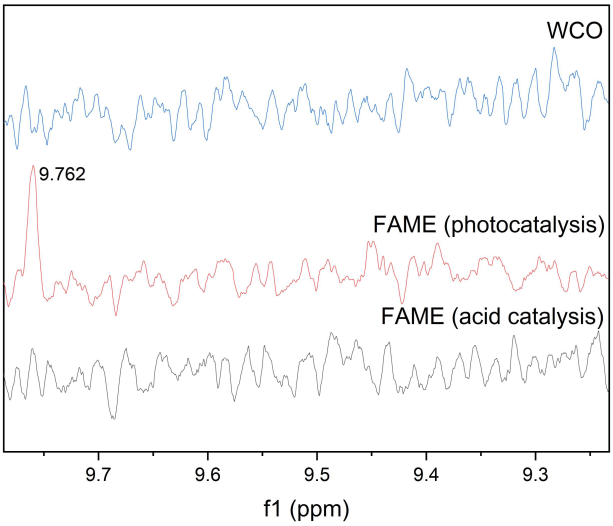

Figure 6. 9. Traces of products from the parallel photo-oxidation reaction of esters: Methyl acrylate, acrylic acid, 2-decenal, and 2-undecenal (9.762 ppm).

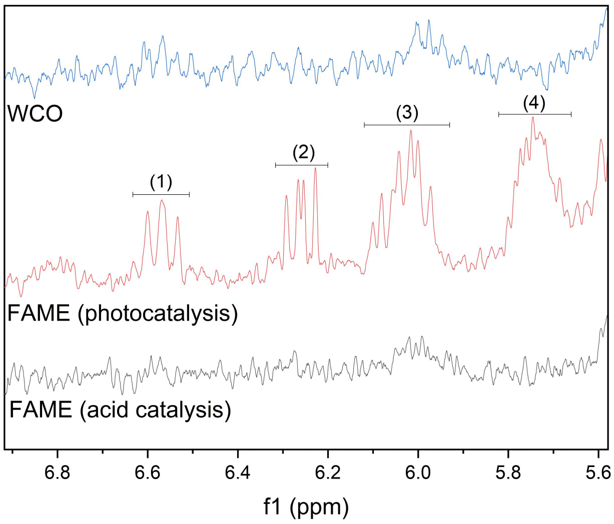

Figure 6. 10. Traces of products from the parallel photo-oxidation reaction of esters: (1) and (3- overlapping) 2-decenal and 2-undecenal. (2), (3 -overlapping), (4) methyl acrylate, and acrylic acid.

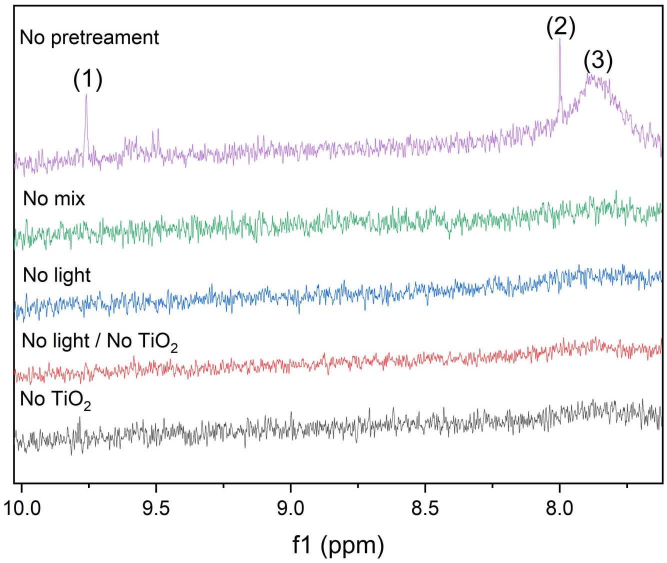

Figure 6. 11. Traces of products from the parallel photo-oxidation reaction of esters observed in the blank tests: (1) acetaldehyde, butyraldehyde, 2-decenal, 2-undecenal (2) formic acid, (3) 2-(hydroxymethyl) acrylic acid.

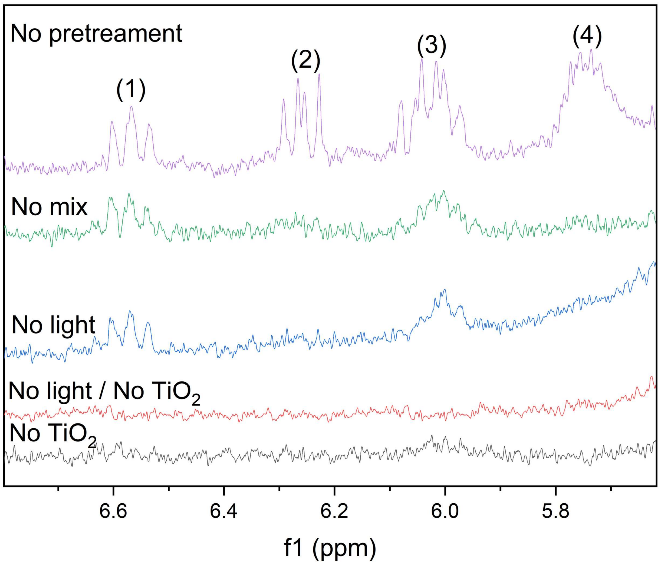

Figure 6. 12. Traces of products from parallel photo-oxidation reaction of esters observed in the blank tests: (1) and (3- overlapping) 2-decenal and 2-undecenal. (2), (3 -overlapping), (4) methyl acrylate, and acrylic acid.

6.3.5. *TiO$_2$ characterisation*

The catalyst (TiO$_2$) was characterised qualitatively and quantitatively before (TiO$_2$ pure), directly after the photoreaction (0RP), after the subsequent recovery process (1C), and after the reuse for five times (5C). FTIR-ATR spectroscopy (Figure 6. 13) revealed organic material within the catalyst material. The highest content was observed for 0RP; however, all samples contained more WCO than FAME. These results were confirmed by TGA (Figure 6. 14), where all samples gave higher degradation peaks for WCO than for FAME. The preferential presence of WCO on the catalyst was caused by the naturally higher concentration of WCO at the beginning of the reaction, and the miscibility of biodiesel methanol. The organic material retained on the catalyst conseqeuntly inhibits light access, thereby increasing the apparent bandgap of the catalyst and reducing light absorption (Luttrell et al., 2015) (Figure 6. 14). The organic material content between 0RP (after the photoreaction) and 1C (after the recovery process) dropped by 77% (0RP: 39% and 1C: 9%), and the apparent bandgap thus decreased by 72% (0RP: 4.62 eV and 1C: 3.31 eV). These results indicate the efficiency of the recovery process, as described previously for oleic acid and canola oil (R. A. Welter, Santana, de la Torre, Barnes, Taranto, & Oelgemöller, 2022; Rosilene A. Welter, Santana, Torre, Robertson, Taranto, & Oelgemöller, 2022). However, the organic material mass gradually increased from 9 to 12% between the first and fifth cycles (1C to 5C), and as a result, the apparent bandgap increased from 3.31 eV to 3.59 eV. These results suggest that the organic material reduces access to the active sites and forms a film on the catalyst, reducing light access and the catalyst's efficiency. This finding corresponds with the reduction in conversion from 83% (1C) to 59% (5C). The presence of the organic material also causes the formation of aggregates and reduces the surface area and porosity, as described elsewhere (R. A. Welter, Santana, de la Torre, Barnes, Taranto, & Oelgemöller, 2022; Rosilene A. Welter, Santana, Torre, Robertson, Taranto, & Oelgemöller, 2022).

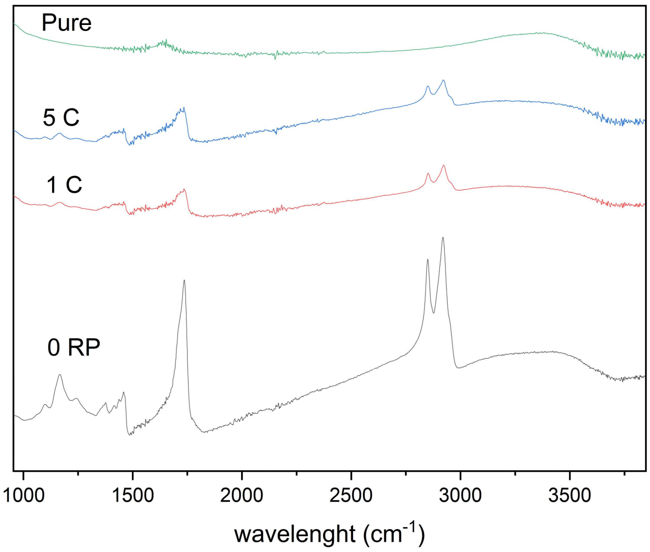

Figure 6. 13. FTIR-ATR of the catalyst TiO_2 pure, after photoreaction without the recovery process (0RP), after photoreaction and recovery process (1C), and after five cycles of the photoreaction and recovery process (5C).

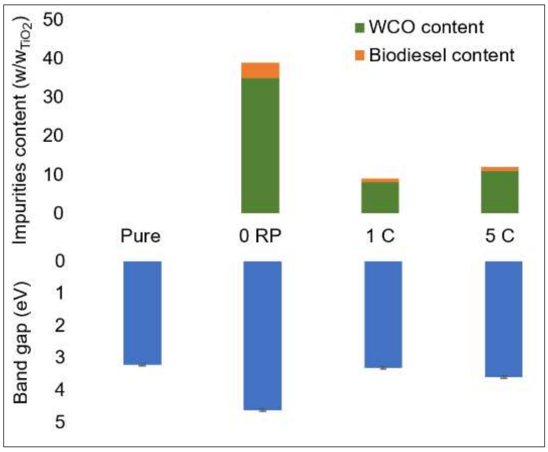

Figure 6. 14. Organic material within TiO_2 after photoreaction of WCO and methanol producing biodiesel and catalyst bandgap. Samples analysed: pure, after photoreaction without recovery process (0RP), after photoreaction and recovery process (1C), after five photoreactions and the recovery process (5C) (More details are found in Section 6.2.3). Bandgap analysis: Error: ±0.02. The standard bandgap of TiO_2 is 3.18 eV (Ishigaki et al., 2020).

6.3.6. *Kinetic modelling and thermodynamics properties*

The kinetic curves of WCO and methanol TiO_2-photocatalysis with UVA irradiation were plotted (Figure 6. 15) and assessed using mathematical modelling. Equilibrium state was reached within three and four hours for all experiments (UVA: 25-65°C; Sunlight: 65°C). In total, five models were applied (Table 6.1). Statistical analysis considered the data from both curves, FAME increase, and WCO decrease. All the models converged with R^2 >0.99 (Table 6. 6), indicating that they statistically agree with the experimental results. However, an evaluation of the kinetic data (Table 6. 7) showed that only the model that considers the forward reaction as second-order and backward reaction as fourth order (F2B4) resulted in consistent parameter values. This model showed higher convergence for higher conversions than lower conversions (R^2 = 0.996,Figure 6. 16).

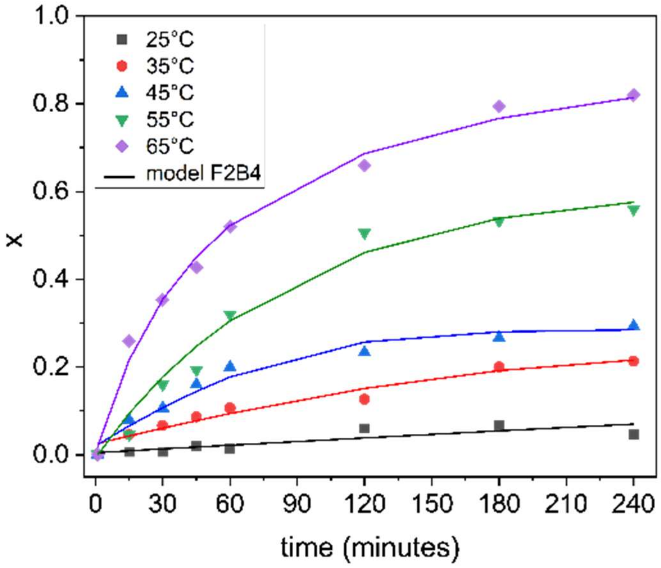

Figure 6. 15. WCO and methanol simultaneous esterification and transesterification kinetic curves to produce biodiesel. Catalyst: TiO_2 irradiated with UVA or sunlight (1 WCO mol:55 MeOH mol, 20% TiO_2 w/w_{wco}).

Table 6. 6: *Statistic analysis for the predicted and experimental data from simultaneous esterification and transesterification of WCO and methanol catalysed by TiO_2 and UVA irradiation.*

Model	R^2	F	SD	β	t	p
F1B1	0.990	4726	0.021	0,995	68.745	0.000
F1B2	0.997	15361	0.012	0.999	123.939	0.000
F2B2	0.996	5279	0.014	0.984	72.656	0.000
F2B4	**0.996**	**4386**	**0.021**	**0.996**	**66.229**	**0.000**
L-H	0.995	25161	0.019	0.997	158.62	0.000

Table 6. 7: *Kinetic and thermodynamic parameters obtained from different mathematical models.*

Model	$k_{-1}^{[a]}$	$k_1^{[a]}$	$K^{[a]}_{eq}$	$E_{a,\,B}$ (kJ/moL)	A_B	$E_{a,\,F}$ (kJ/mol)	A_F
F1B1	3.01E-03	1.34E-02	4.46E+00	−18.21 (R^2: 0.378)	6.14E-6 (R^2: 0.378)	62.99 (R^2: 0.963)	8.18E7 (R^2: 0.963)
F1B2	8.85E-03	1.24E-02	1.40E+00	−69.95 (R^2: 0.917)	8.12E+12 (R^2: 0.917)	44.03 (R^2: 0.886)	6.78E4 (R^2: 0.886)
F2B2	3.56E-10	4.66E-02	1.31E+08	68.13 (R^2: 0.973)	1.73E+9 (R^2: 0.973)	−288.64 (R^2: 0.525)	1.54E-51 (R^2: 0.525)
F2B4	1.73E+00	1.16E+01	6.68E+00	**223.71** **(R^2: 0.791)**	**8.50E+15** **(R^2: 0.791)**	**96.50** **(R^2: 0.990)**	**2.87E+30** **(R^2: 0.990)**
L-H	1.82E-03	1.16E+00	6.4E+02	−83.02 (R^2: 0.901)	1.41E15 (R^2: 0.901)	119.08 (R^2: 0.809)	1.15E+18 (R^2: 0.809)

[a]Temperature: 338.15K; F: Forward; B: Backward

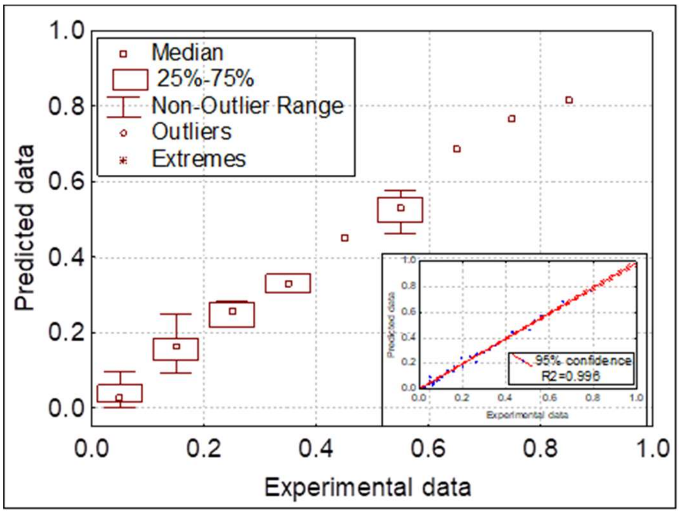

Figure 6. 16. Correlation between predicted (model F2B4) and experimental FAME conversion. ☐ 25%-75% = (-0.0089, 0.0078), I Non-Outlier Range= (-0.0335, 0.03), ■ Median = 0.0006, ● Outliers.

The thermodynamic data were determined after obtaining the kinetic data (Figure 6. 17). The values of E_a ($E_{a\ forward}$ of 96.55 kJ/mol and $E_{a\ backward}$ of 223.71 kJ/mol) and A ($A_{forward}$ of 2.87E+30 and $A_{backward}$ of 8.50E+15) were determined by the Arrhenius equation considering the F2B4 kinetic model results. The small E_a and higher A value indicate that the forward reaction is favoured. The effective E_α considering the entire process was obtained applying Equation 6. 3 and resulted in a linear decrease with increasing temperature (Figure 6. 17). The thermodynamic properties are described in Figure 6.18. ΔS (0.29 kJ/mol.K) and ΔH (92.58 kJ/mol) were determined using the Van't Hoff model (Equation 6. 4) and confirmed the endothermic nature of the reaction. ΔG was determined using two different equations and both produced consistent values (R^2 = 0.891), a decrease with increasing temperature, being negative at temperatures higher than 45°C. The analysis of all these parameters indicated an endothermic and irreversible process at temperatures higher than 45°C. Although the endothermic reaction requires higher temperatures to achieve higher conversion, it is also demanded to improve the miscibility between the WCO and methanol. Better miscibility between the phases is advantageous for higher mass transfer and increased conversion.

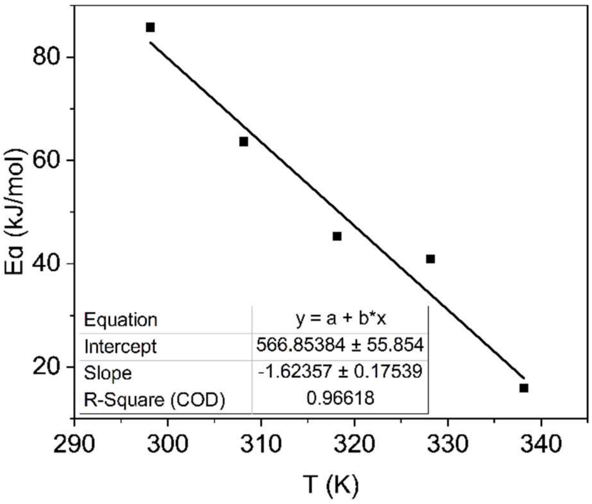

Figure 6. 17. Effective E_α of the reaction considering the F2B4 model.

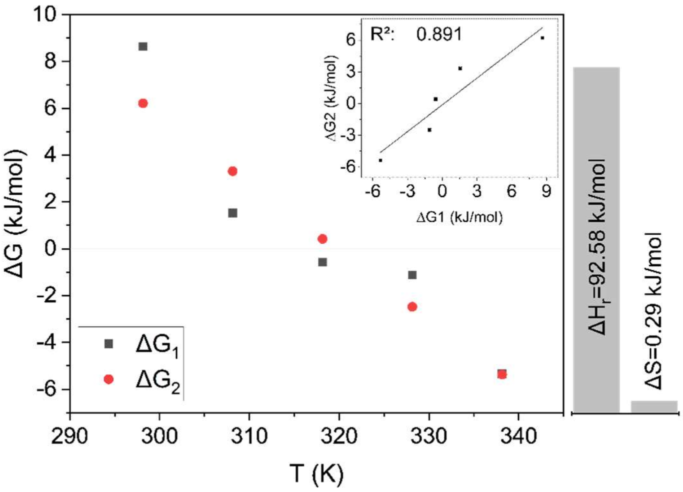

Figure 6. 18. Gibbs energy (ΔG) and equilibrium constant (K_{eq}) for WCO and methanol simultaneous esterification and transesterification catalysed by TiO_2 irradiated with UVA (1 WCO mol:55MeOH mol, 20% TiO_2 w/w_{WCO}).

6.4. Conclusion

Biodiesel was produced by TiO_2-photocatalysis from WCO and short-chain alcohols (methanol and ethanol) by simultaneous esterification and transesterification. Under the optimised operational conditions (1 mol WCO: 55 mol MeOH, 20% w/w_{wco} TiO_2, UVA irradiation, and 65°C), a conversion of 82% was achieved. Esterification resulted in a somewhat higher conversion (89%) than transesterification (81%). The developed process is thus suitable to produce biodiesel from feedstocks with high FFA content. The catalyst was reusable, and even after five cycles, a reasonable conversion 59% was achieved. Catalyst characterisation revealed the accumulation of organic material on the TiO_2-material, reducing the catalytic sites available and increasing the bandgap, and hence decreasing photocatalytic efficiency. Five different mathematical models were used to evaluate the experimental kinetic data. The model considering a second-order forward reaction and fourth-order backward reaction showed the best convergence with the predicted values (R^2: 0.996) and the kinetic and thermodynamic parameters. These parameters agreed with the observed behaviour, where the reaction was not efficient at temperatures below 45°C. Simultaneous esterification and transesterification enables the use of high FFA contents, which common problem with traditional thermal catalysts. Moreover, the use of heterogeneous photocatalysis can overcome many of the difficulties encountered using traditional homogeneous catalysts such as high temperature and extreme pH requirements, catalyst recovery and reuse challanges, low product purities that demand lenghty and resource-demanding purification steps, and specialized equipment needs due to the corrosive reaction conditions. While this study developed an efficient and eco-friendly process for the potential production of biodiesel, more aspects need to be evaluated, such as optimising catalyst reuse, scale-up, implementation of different feedstocks, and natural sunlight utilization.

Acknowledgement

RAW wishes to thank the College of Science and Engineering at James Cook University for financial support (Competitive Research Training Grants 2021 and 2022). The authors thank Assoc.-Prof. George Vamvounis, Dr. Mark Robertson and Dr. Shane Askew (James Cook University) for technical support.

Chapter VII
Conclusion

7.1 Conclusion

The main objective of this thesis was to evaluate eco-friendly optimised catalysts and processes to produce biodiesel. The most important results are reported in Chapters III – VI. There are eco-friendly catalysts and processes to produce biodiesel using different feedstock, such as waste cooking oil, with high efficiency. The conclusions of each chapter are presented to support this outcome.

In Chapter III, a lipase was immobilised, and the process was optimised. The lipases are the most common biocatalyst applied to biodiesel production by esterification and transesterification. The microbiocatalyst was developed through a double lipase immobilisation methodology. First, *Candida antarctica* lipase B was adsorbed onto TiO_2 nanoparticles ($CALB_{TiO_2}$), resulting in enzymatic activity of 189%, higher than that of the free enzyme. It was assumed that lipase was immobilised on the TiO_2 surface in a single layer through its hydrophilic amino acid scattering and forcing the exposure of the hydrophobic amino acids, where is found the active site. Second, $CALB_{TiO_2}$ was entrapped in calcium alginate microbeads [$(CALB_{TiO_2})_{EDTA\text{-}Ca}$]. The $(CALB_{TiO_2})_{EDTA\text{-}Ca}$ showed $REA_{t=0}$ of 232%, $REA_{t=24h}$ of 286%, and $REA_{t=30days}$ of 255%, clearly showing an improvement in the enzymatic activity and stability; and $REA_{\text{after resistant test}}$ of 289%, suggesting that that catalyst leaching did not occur. The improved microbiocatalyst obtained by double immobilisation offers a promising option for lipases immobilisation and, consequently, biodiesel production by esterification and transesterification under mild operational conditions.

Chapter IV reported the use of photocatalised TiO_2 to produce biodiesel by the esterification of oleic acid. An optimised photoesterification process using TiO_2 and UVA irradiation with high efficiency to produce methyl oleate (conversion: 98%) was developed. Optimal conditions were obtained after the study of catalyst pretreatment, and the operational conditions were analysed by statistical experimental design and methodology evaluations by the response surface. Subsequently, kinetics modelling was carried out, and the thermodynamic parameters were determined. According to this study, temperatures higher than 55ºC and an excess of alcohol are required to achieve a high conversion rate. Low temperatures and lower alcohol contents result in reduced conversions and reverse reactions (hydrolysis). The simple optimised process obtained in this study overcomes the difficulties frequently observed for FAME production by oleic acid esterification using thermal methods (high temperature, extreme pH, difficult catalyst reuse and recovery, large volumes of water, complex FAME purification).

Chapter V focused on the transesterification process of canola oil and methanol using photocatalysis. The optimised operational conditions (1 mol canola oil: 55 mol MeOH, 65°C 20% w/ w_{TGL}, TiO_2 under UVA irradiation), resulted in 73% conversion. The use of ethanol instead of methanol or sunlight instead of UVA irradiation resulted in poor efficiency. Although triglycerides have higher miscibility with ethanol than methanol, the methanol reaction tends to achieve higher conversion because it is more reactive than ethanol. The catalyst was reusable but the efficiency was reduced (36% after five cycles). The decrease occurred because of the presence of organic material (canola oil and biodiesel) in the catalyst, reducing the active sites available and preventing light access. The kinetic and thermodynamic parameters were determined. According to these parameters, a temperature higher than 65ºC is required for the endothermic reaction to proceed with high efficiency and for the compounds to be miscible. This process indicates that it is possible to overcome issues frequently observed in traditional homogeneous catalysis (high temperature, extreme pH, hardly catalyst handle, recovery and reuse, large volumes of waste and water, and complex product purification).

Chapter VI investigated biodiesel production from waste cooking oil via simultaneous esterification and transesterification using photoirradiated TiO_2. Under the optimised operational conditions (1 mol WCO: 55 mol MeOH, 20% w/w_{wco} TiO_2, UVA irradiation, and 65°C), it was possible to achieve 82% conversion during the first use of the catalyst and 59% after reusing it five times. The simultaneous esterification and transesterification reaction ensures that the high FFA content is not a problem because it frequently occurs with traditional catalysts. On the contrary, it is advantageous considering that conversion by esterification (89%) is higher than transesterification (81%). Catalyst characterisation revealed the accumulation of organic material in the TiO_2, reducing the catalytic sites available and increasing the bandgap. Both aspects resulted in a decreased photocatalyst efficiency. This decrease is frequently observed in solid catalysts. However, the use of a solid photocatalyst can circumvent some of the difficulties encountered using the traditional homogeneous catalysts, such as temperatures higher than 100°C, extreme pH, difficult to handle catalysts, recovering and reusing the product with low purity, many purification steps, large volumes of water and wastewater, unit operation equipment recovered with stainless steel, shorter useful lifetimes, and recurring maintenance. Thus, an efficient and eco-friendly process was developed in this study

7.2 Future studies

Future studies can be developed to solve some gaps observed in this thesis or even continues this study by optimising the process of producing biodiesel. The microbiocatalyst research (Chapter III) was developed at Unicamp – Brazil, and because of COVID-19, this study could not continue as predicted. Thus, the suggestions refer to the gaps observed in this study and the steps of the project that could not be developed:

- Study of the amino acids of the lipase after each immobilisation to understand the enzymatic mechanism better and, through that, develop a better mechanism for immobilisation
- Analyse the use of other metal oxides instead of TiO_2 and other lipases instead of *Candida antarctica* lipase.
- Application of the microbiocatalyst in biodiesel production and process optimisation.
- Economic evaluation and large-scale implementation.

The photocatalysis applied to biodiesel production (Chapter IV – VI) was developed at James Cook University – Australia. Although this part of the thesis was studied more extensively, some gaps and future studies are suggested below:

- Analyse the use of other metal oxides instead of TiO_2.
- Optimise the process using solar irradiation.
- Evaluate a better process to recover the catalyst to achieve higher conversion after its reuse.
- Evaluate the process using microreactors.
- Process scale-up considering the use of large reactors and microreactor numbering.
- An economic evaluation of the process on a large scale.

References

Abdelkhalik, A., Elsayed, H., Hassan, M., Nour, M., Shehata, A. B., & Helmy, M. (2018). Using thermal analysis techniques for identifying the flash point temperatures of some lubricant and base oils. *Egyptian Journal of Petroleum*, 27(1), 131–136. Retrieved 1 April 2022 from https://doi.org/10.1016/J.EJPE.2017.02.006

Abdulla Yusuf, H., Elkanzi, E. M., Hossain, S. M. Z., Alsaei, A. M., Alhindy, A. H., & Ebrahem, E. (2020). Design and performance assessment of an in-house fabricated microreactor for enzyme-catalysed biodiesel synthesis. *Arab Journal of Basic and Applied Sciences*, 27(1), 239–247. Retrieved from https://doi.org/10.1080/25765299.2020.1766789

Aboelazayem, O., Gadalla, M., & Saha, B. (2018). Biodiesel production from waste cooking oil via supercritical methanol: Optimisation and reactor simulation. *Renewable Energy*, 124, 144–154. Retrieved 11 November 2021 from https://doi.org/10.1016/j.renene.2017.06.076

Aeroxide. (2020). Product information: Aeroxide TiO_2 P25. Retrieved 12 November 2021, from https://products-re.evonik.com/www2/uploads/productfinder/AEROXIDE-TiO2-P-25-EN.pdf

Agarwal, M., Chauhan, G., Chaurasia, S. P., & Singh, K. (2012). Study of catalytic behavior of KOH as homogeneous and heterogeneous catalyst for biodiesel production. *Journal of the Taiwan Institute of Chemical Engineers*, 43(1), 89–94. Retrieved 6 July 2022 from https://doi.org/10.1016/J.JTICE.2011.06.003

Aghel, B., Mohadesi, M., Ansari, A., & Maleki, M. (2019). Pilot-scale production of biodiesel from waste cooking oil using kettle limescale as a heterogeneous catalyst. *Renewable Energy*, 142, 207–214. Retrieved 1 August 2022 from https://doi.org/10.1016/J.RENENE.2019.04.100

Ahmedzeki, N., & Jendeel, H. (2013). Heterogeneously catalyzed esterification reaction: experimental and modeling using Langmuir- Hinshelwood approach. *Iraqi Journal of Chemical and Petroleum Engineering*, 14(4), 45–52.

Ahsan, S. S., Gumus, A., & Erickson, D. (2013). Redox mediated photocatalytic water-splitting in optofluidic microreactors. *Lab Chip*, 13(3), 409–414. Retrieved from https://doi.org/10.1039/C2LC41129F

Akkarawatkhoosith, N., Tongtummachat, T., Kaewchada, A., & Jaree, A. (2021). Non-catalytic and glycerol-free biodiesel production from rice bran oil fatty acid distillate in a microreactor. *Energy Conversion and Management: X*, 11, 100096. Retrieved from https://doi.org/10.1016/j.ecmx.2021.100096

Albuquerque Andrade, R. D., Pozzebom, E., Faria, E. A., Dantas Filho, F., Suarez, P. A. Z., & Prado, A. G. S. do. (2011). Thermal behavior of diesel/biodiesel blends of biodiesel obtained from buriti oil. *Acta Scientiarum. Technology*, 34(2), 243. Retrieved from https://doi.org/10.4025/actascitechnol.v34i2.12797

Alenezi, R., Leeke, G. A., Winterbottom, J. M., Santos, R. C. D., & Khan, A. R. (2010). Esterification kinetics of free fatty acids with supercritical methanol for biodiesel production. *Energy Conversion and Management*, 51(5), 1055–1059. Retrieved 17 November 2021 from https://doi.org/10.1016/J.ENCONMAN.2009.12.009

Alhassan, F. H., Yunus, R., Rashid, U., Sirat, K., Islam, A., Lee, H. v., & Taufiq-Yap, Y. H. (2013). Production of biodiesel from mixed waste vegetable oils using Ferric hydrogen sulphate as an effective reusable heterogeneous solid acid catalyst. *Applied Catalysis A: General*, 456, 182–187. Retrieved 22 November 2021 from https://doi.org/10.1016/J.APCATA.2013.02.019

Ali, B., Yusup, S., Quitain, A. T., Alnarabiji, M. S., Kamil, R. N. M., & Kida, T. (2018). Synthesis of novel graphene oxide/bentonite bi-functional heterogeneous catalyst for one-pot esterification and transesterification reactions. *Energy Conversion and Management*, 171, 1801–1812. Retrieved 21 November 2021 from https://doi.org/10.1016/J.ENCONMAN.2018.06.082

Ali, M. A., Nouruddeen, Z., Muhamad, I., Latip, R., & Othman, N. H. (2013). Effect of microwave heating on the quality characteristics of canola oil in presence of palm olein. *Acta Scientiarum Polonorum. Technologia Alimentaria*, 12, 241–252.

Allain, F., Portha, J. F., Girot, E., Falk, L., Dandeu, A., & Coupard, V. (2016). Estimation of kinetic parameters and diffusion coefficients for the transesterification of triolein with methanol on a solid $ZnAl_2O_4$ catalyst. *Chemical Engineering Journal*, 283, 833–845. Retrieved 19 September 2022 from https://doi.org/10.1016/J.CEJ.2015.07.075

Alnoch, R. C., Santos, L. A. dos, de Almeida, J. M., Krieger, N., & Mateo, C. (2020). Recent trends in biomaterials for immobilization of lipases for application in non-conventional media. *Catalysts*, 10(6), 1–29. Retrieved from https://doi.org/10.3390/catal10060697

Al-Saadi, A., Mathan, B., & He, Y. (2020). Biodiesel production via simultaneous transesterification and esterification reactions over $SrO–ZnO/Al_2O_3$ as a bifunctional catalyst using high acidic waste cooking oil. *Chemical Engineering Research and Design*, 162, 238–248. Retrieved 19 November 2021 from https://doi.org/10.1016/j.cherd.2020.08.018

Alsharifi, M., Znad, H., Hena, S., & Ang, M. (2017). Biodiesel production from canola oil using novel Li/TiO_2 as a heterogeneous catalyst prepared via impregnation method. *Renewable Energy*, 114, 1077–1089. Retrieved 10 November 2021 from https://doi.org/10.1016/J.RENENE.2017.07.117

Alves, A. K. (2008). *Obtenção de micro e nanofibras de TiO_2 por electrospinning: caracterização de propriedades e atividade fotocatalítica*. Universidade Federal do Rio Grande do Sul, Porto Alegre.

Al-Zuhair, S. (2007). Production of biodiesel: Possibilities and challenges. *Biofuels, Bioproducts and Biorefining*, 1(1), 57–66. Retrieved 19 November 2021 from https://doi.org/10.1002/BBB.2

Ameh, C. U. , Jimoh, A. , Abdulkareem, A. S., & Otaru, A. J. (2013). Application of Langmuir-Hinshelwood model to bioregeneration of activated carbon contaminated with hydrocarbons. *IOSR Journal of Mathematics*, 6(2), 70–83.

Amore, K. M., & Leadbeater, N. E. (2007). Microwave-promoted esterification reactions: Optimization and scale-up. *Macromolecular Rapid Communications*, 28(4), 473–477. Retrieved 13 November 2021 from https://doi.org/10.1002/MARC.200600751

An, J., Li, G., Zhang, Y., Zhang, T., Liu, X., Gao, F., … Fan, H. (2020). Recent advances in enzyme-nanostructure biocatalysts with enhanced activity. *Catalysts*, 10(3), 338. Retrieved from https://doi.org/10.3390/catal10030338

Anastopoulos, G., Zannikou, Y., Stournas, S., & Kalligeros, S. (2009). Transesterification of vegetable oils with ethanol and characterization of the key fuel properties of ethyl esters. *Energies*, 2(2), 362–376. Retrieved from https://doi.org/10.3390/en20200362

Antonio, C., & Deam, R. T. (2007). Can "microwave effects" be explained by enhanced diffusion? *Phys. Chem. Chem. Phys.*, 9(23), 2976–2982. Retrieved from https://doi.org/10.1039/B617358F

Anwar, M. (2021). Biodiesel feedstocks selection strategies based on economic, technical, and sustainable aspects. *Fuel*, 283, 119204. Retrieved 7 September 2021 from https://doi.org/10.1016/J.FUEL.2020.119204

Arana-Peña, S., Rios, N. S., Carballares, D., Gonçalves, L. R. B., & Fernandez-Lafuente, R. (2021). Immobilization of lipases via interfacial activation on hydrophobic supports: Production of biocatalysts libraries by altering the immobilization conditions. *Catalysis Today*, 362, 130–140. Retrieved 7 February 2022 from https://doi.org/10.1016/J.CATTOD.2020.03.059

Aransiola, E. F., Ojumu, T. v., Oyekola, O. O., Madzimbamuto, T. F., & Ikhu-Omoregbe, D. I. O. (2014). A review of current technology for biodiesel production: State of the art. *Biomass and Bioenergy*, 61, 276–297. Retrieved 11 November 2021 from https://doi.org/10.1016/j.biombioe.2013.11.014

ARPANSA. (2022). Australian Radiation Protection and Nuclear Safety Agency. Retrieved 10 January 2022, from https://www.arpansa.gov.au/our-services/monitoring/ultraviolet-radiation-monitoring/ultraviolet-radiation-index

Arpigny, J. L., & Jaeger, K. E. (1999). Bacterial lipolytic enzymes: classification and properties.

The Biochemical Journal, 343(1), 177–183. Retrieved from https://pubmed.ncbi.nlm.nih.gov/10493927

Arunachalam, A., Dhanapandian, S., Manoharan, C., & Sivakumar, G. (2015). Physical properties of Zn doped TiO_2 thin films with spray pyrolysis technique and its effects in antibacterial activity. *Spectrochimica Acta Part A: Molecular and Biomolecular Spectroscopy*, 138, 105–112. Retrieved 30 March 2022 from https://doi.org/10.1016/J.SAA.2014.11.016

Arzamendi, G., Campo, I., Arguiñarena, E., Sánchez, M., Montes, M., & Gandía, L. M. (2007). Synthesis of biodiesel with heterogeneous NaOH/alumina catalysts: Comparison with homogeneous NaOH. *Chemical Engineering Journal*, 134(1–3), 123–130. Retrieved 10 November 2021 from https://doi.org/10.1016/J.CEJ.2007.03.049

ASTM D975. (2021, October 20). ASTM D975 - Standard, specification for biodiesel fuel blend stock (B100) for middle distillate fuels. *ASTM International*.

Ataman, E., Isvoranu, C., Knudsen, J., Schulte, K., Andersen, J. N., & Schnadt, J. (2011). Adsorption of L-cysteine on rutile TiO_2(110). *Surface Science*, 605(1–2), 179–186. Retrieved from https://doi.org/10.1016/J.SUSC.2010.10.017

Athar, M., Imdad, S., Zaidi, S., Yusuf, M., Kamyab, H., Jaromír Klemeš, J., & Chelliapan, S. (2022). Biodiesel production by single-step acid-catalysed transesterification of *Jatropha* oil under microwave heating with modelling and optimisation using response surface methodology. *Fuel*, 322, 124205. Retrieved 5 July 2022 from https://doi.org/10.1016/J.FUEL.2022.124205

Atitar, M. F., Bouziani, A., Dillert, R., el Azzouzi, M., & Bahnemann, D. W. (2018). Photocatalytic degradation of the herbicide imazapyr: do the initial degradation rates correlate with the adsorption kinetics and isotherms? *Catalysis Science Technology*, 8(4), 985–995. Retrieved from https://doi.org/10.1039/C7CY01903C

Avhad, M. R., & Marchetti, J. M. (2015). A review on recent advancement in catalytic materials for biodiesel production. *Renewable and Sustainable Energy Reviews*, 50, 696–718. Retrieved 21 July 2022 from https://doi.org/10.1016/J.RSER.2015.05.038

Ayadi, M., Saragih, F. N. A., Awad, S., Priadi, C., Abderrabba, M., Tazerout, M., & Andres, Y. (2021). Two steps methanolysis and ethanolysis of olive pomace oil using olive-pomace-based heterogeneous acid catalyst. *Fuel*, 296, 120678. Retrieved 28 February 2022 from https://doi.org/10.1016/J.FUEL.2021.120678

Azam, N. A. M., Uemura, Y., Kusakabe, K., & Bustam, M. A. (2016). Biodiesel production from palm oil using micro tube reactors: effects of catalyst concentration and residence time. *Procedia Engineering*, 148, 354–360. Retrieved 6 July 2022 from https://doi.org/10.1016/J.PROENG.2016.06.462

Azcan, N., & Danisman, A. (2008). Microwave assisted transesterification of rapeseed oil. *Fuel*, 87(10–11), 1781–1788. Retrieved 19 November 2021 from https://doi.org/10.1016/j.fuel.2007.12.004

Azcan, N., & Yilmaz, O. (2013). Microwave assisted transesterification of waste frying oil and concentrate methyl ester content of biodiesel by molecular distillation. *Fuel*, 104, 614–619. Retrieved 18 November 2021 from https://doi.org/10.1016/j.fuel.2012.06.084

Babajide, O., Petrik, L., Amigun, B., & Ameer, F. (2010). Low-Cost Feedstock Conversion to Biodiesel via Ultrasound Technology. *Energies*, 3(10), 1691–1703. Retrieved from https://doi.org/10.3390/en3101691

Badoei-dalfard, A., Tahami, A., & Karami, Z. (2022). Lipase immobilization on glutaraldehyde activated graphene oxide/chitosan/cellulose acetate electrospun nanofibrous membranes and its application on the synthesis of benzyl acetate. *Colloids and Surfaces B: Biointerfaces*, 209, 112151. Retrieved 3 December 2021 from https://doi.org/10.1016/J.COLSURFB.2021.112151

Baharfar, R., & Mohajer, S. (2016). Synthesis and characterization of immobilized lipase on Fe_3O_4 nanoparticles as nano biocatalyst for the synthesis of benzothiazepine and spirobenzothiazine chroman Derivatives. *Catalysis Letters*, 146(9), 1729–1742. Retrieved from https://doi.org/10.1007/s10562-016-1797-3

Bahnemann, D. (2004). Photocatalytic water treatment: solar energy applications. *Solar Energy*, 77(5), 445–459. Retrieved from https://doi.org/10.1016/j.solener.2004.03.031

Balbino, T. A., Serafin, J. M., Malfatti-Gasperini, A. A., de Oliveira, C. L. P., Cavalcanti, L. P., de Jesus, M. B., & de La Torre, L. G. (2016). Microfluidic assembly of pDNA/Cationic liposome lipoplexes with high pDNA loading for gene delivery. *Langmuir*, 32(7), 1799–1807. Retrieved from https://doi.org/10.1021/acs.langmuir.5b04177

Ballari, M. de los M., Brandi, R., Alfano, O., & Cassano, A. (2008). Mass transfer limitations in photocatalytic reactors employing titanium dioxide suspensions: II. External and internal particle constrains for the reaction. *Chemical Engineering Journal*, 136(2–3), 242–255. Retrieved 28 September 2022 from https://doi.org/10.1016/J.CEJ.2007.03.031

Bannatham, P., Banthaothook, C., Limtrakul, S., Vatanatham, T., Jaree, A., & Ramachandran, P. A. (2021). Two-Scale model for kinetics, design, and scale-up of biodiesel production. *Industrial & Engineering Chemistry Research*, 60(44), 15972–15988. Retrieved from https://doi.org/10.1021/acs.iecr.1c03009

Baroutian, S., Aroua, M. K., Raman, A. A. A., & Sulaiman, N. M. N. (2011). A packed bed membrane reactor for production of biodiesel using activated carbon supported catalyst. *Bioresource Technology*, 102(2), 1095–1102. Retrieved 6 July 2022 from https://doi.org/10.1016/J.BIORTECH.2010.08.076

Barros, H. R. de, Santos, M. C., Barbosa, L. R. S., Piovan, L., & Riegel-Vidotti, I. C. (2019). Physicochemical study of the interaction between gold nanoparticles and lipase from

Candida sp. (CALB): Insights into the nano-bio interface. *Journal of the Brazilian Chemical Society*, 30(10), 2231–2242. Retrieved from https://doi.org/10.21577/0103-5053.20190127

Baskar, G., Aberna Ebenezer Selvakumari, I., & Aiswarya, R. (2018). Biodiesel production from castor oil using heterogeneous Ni doped ZnO nanocatalyst. *Bioresource Technology*, 250, 793–798. Retrieved 18 March 2022 from https://doi.org/10.1016/J.BIORTECH.2017.12.010

Bassett, D. C., Håti, A. G., Melø, T. B., Stokke, B. T., & Sikorski, P. (2016). Competitive ligand exchange of crosslinking ions for ionotropic hydrogel formation. *Journal of Materials Chemistry B*, 4(37), 6175–6182. Retrieved from https://doi.org/10.1039/c6tb01812b

Bax, S., Hakka, M. H., Glaude, P.-A., Herbinet, O., & Battin-Leclerc, F. (2010). Experimental study of the oxidation of methyl oleate in a jet-stirred reactor. *Combustion and Flame*, 157(6), 1220–1229. Retrieved from https://doi.org/10.1016/j.combustflame.2009.12.008

Benyong Han, Fang Yin, Shiqing Liu, Xingling Zhao, Jing Liu, Changmei Wang, … Wudi Zhang. (2019). Optimization of oleic acid esterification for biodiesel production using Brønsted Acidic ionic liquid as a catalys. *Chiang Mai Journal Science*, 46(4), 714–726. Retrieved 2 January 2021 from http://cmuir.cmu.ac.th/handle/6653943832/66049

Bi, Y., Zhou, H., Jia, H., & Wei, P. (2017). A flow-through enzymatic microreactor immobilizing lipase based on layer-by-layer method for biosynthetic process: Catalyzing the transesterification of soybean oil for fatty acid methyl ester production. *Process Biochemistry*, 54, 73–80. Retrieved 8 July 2022 from https://doi.org/10.1016/J.PROCBIO.2016.12.008

Bilen, K., Ozyurt, O., Bakirci, K., Karsli, S., Erdogan, S., Yilmaz, M., & Comakli, O. (2008). Energy production, consumption, and environmental pollution for sustainable development: A case study in Turkey. *Renewable and Sustainable Energy Reviews*, 12(6), 1529–1561. Retrieved 10 November 2021 from https://doi.org/10.1016/J.RSER.2007.03.003

Billo, R. E., Oliver, C. R., Charoenwat, R., Dennis, B. H., Wilson, P. A., Priest, J. W., & Beardsley, H. (2015). A cellular manufacturing process for a full-scale biodiesel microreactor. *Journal of Manufacturing Systems*, 37, 409–416. Retrieved 22 November 2021 from https://doi.org/10.1016/j.jmsy.2014.07.004

Biodiesel Market. (2017). Markets and markets. Retrieved 9 November 2021, from https://www.marketsandmarkets.com/Market-Reports/Global-Biodiesel-Market-190.html

Biofuels. (2019). In *OECD-FAO AGRICULTURAL OUTLOOK 2019-2028* (pp. 204–216). Retrieved 9 November 2021 from https://www.fao.org/3/CA4076EN/CA4076EN_Chapter9_Biofuels.pdf

Bishop, G. W., Satterwhite, J. E., Bhakta, S., Kadimisetty, K., Gillette, K. M., Chen, E., &

Rusling, J. F. (2015). 3D-Printed fluidic devices for nanoparticle preparation and flow-injection amperometry using integrated prussian blue nanoparticle-modified electrodes. *Analytica Chemistry*, 87(10), 5437–5443. Retrieved from https://doi.org/10.1021/acs.analchem.5b00903

Bölük, S., & Sönmez, Ö. (2020). Microwave-assisted esterification of oleic acid using an ionic liquid catalyst. *Chemical Engineering and Technology*, 43(9), 1792–1801. Retrieved 13 November 2021 from https://doi.org/10.1002/CEAT.202000045

Bonet, J., Plesu, V., Ruiz, E. B., Iancu, P., & Llorens, J. (2014). Thermodynamic Study of Batch Reactor Biodiesel Synthesis. *Revista de Chimie*, 65(3), 358–361.

Borah, M. J., Devi, A., Saikia, R. A., & Dhanapati Deka. (2018). Biodiesel production from waste cooking oil catalyzed by in-situ decorated TiO_2 on reduced graphene oxide nanocomposite. *Energy*, 158, 881–889. Retrieved from https://doi.org/10.1016/j.energy.2018.06.079

Boro, J., Konwar, L. J., & Deka, D. (2014). Transesterification of non edible feedstock with lithium incorporated egg shell derived CaO for biodiesel production. *Fuel Processing Technology*, 122, 72–78. Retrieved 11 November 2021 from https://doi.org/10.1016/j.fuproc.2014.01.022

Borugadda, V. B., & Goud, V. v. (2012). Biodiesel production from renewable feedstocks: Status and opportunities. *Renewable and Sustainable Energy Reviews*, 16(7), 4763–4784. Retrieved 9 November 2021 from https://doi.org/10.1016/J.RSER.2012.04.010

Brandt, E. G., & Lyubartsev, A. P. (2015). Molecular dynamics simulations of adsorption of amino acid side chain analogues and a titanium binding peptide on the TiO_2 (100) Surface. *Journal of Physical Chemistry C*, 119(32), 18126–18139. Retrieved from https://doi.org/10.1021/acs.jpcc.5b02670

Brito, Y. C. (2008). *Esterificação e transesterificação em presença de complexos de titânio e zircônio*. Universidade Federal de Alagoas, Maceió.

Buchori, L., Istadi, I., Purwanto, P., Kurniawan, A., & Maulana, T. I. (2016). Preliminary Testing of Hybrid Catalytic-Plasma Reactor for Biodiesel Production Using Modified-Carbon Catalyst. *Bulletin of Chemical Reaction Engineering & Catalysis*, 11(1), 59–65. Retrieved from https://doi.org/10.9767/bcrec.11.1.416.59-65

Budžaki, S., Miljić, G., Tišma, M., Sundaram, S., & Hessel, V. (2017). Is there a future for enzymatic biodiesel industrial production in microreactors? *Applied Energy*, 201, 124–134. Retrieved 22 November 2021 from https://doi.org/10.1016/j.apenergy.2017.05.062

Caballero, B. (Ed.). (2003). *Encyclopedia of Food Sciences and Nutrition* (2nd ed.).

Cai, J., & Bi, L. (2008). Precision of the coats and Redfern method for the determination of the activation energy without neglecting the low-temperature end of the temperature integral. *Energy & Fuels*, 22(4), 2172–2174. Retrieved from https://doi.org/10.1021/ef8002125

Calderbank, P. H., & Moo-Young, M. B. (1961). The continuous phase heat and mass-transfer properties of dispersions. *Chemical Engineering Science*, 16(1–2), 39–54. Retrieved 28 September 2022 from https://doi.org/10.1016/0009-2509(61)87005-X

Calero, J., Luna, D., Sancho, E. D., Luna, C., Bautista, F. M., Romero, A. A., … Verdugo, C. (2014). Development of a new biodiesel that integrates glycerol, by using CaO as heterogeneous catalyst, in the partial methanolysis of sunflower oil. *Fuel*, 122, 94–102. Retrieved 11 November 2021 from https://doi.org/10.1016/j.fuel.2014.01.033

Cao, W., Han, H., & Zhang, J. (2005). Preparation of biodiesel from soybean oil using supercritical methanol and co-solvent. *Fuel*, 84(4), 347–351. Retrieved 11 November 2021 from https://doi.org/10.1016/j.fuel.2004.10.001

Cardoso, A. L., Neves, S. C. G., & da Silva, M. J. (2009). Kinetic study of alcoholysis of the fatty acids catalyzed by Tin Chloride(II): an alternative catalyst for biodiesel production. *Energy & Fuels*, 23(3), 1718–1722. Retrieved from https://doi.org/10.1021/ef800639h

Carlucci, C., Degennaro, L., & Luisi, R. (2019). Titanium dioxide as a catalyst in biodiesel production. *Catalysts*, 9(1), 75. Retrieved from https://doi.org/10.3390/catal9010075

Carp, O., Huisman, C. L., & Reller, A. (2004). Photoinduced reactivity of titanium dioxide. *Progress in Solid State Chemistry*, 32(1–2), 33–177. Retrieved 26 December 2021 from https://doi.org/10.1016/J.PROGSOLIDSTCHEM.2004.08.001

Cejudo-Sanches, J., Orrego, A. H., Jaime-Mendoza, A., Ghobadi, R., Moreno-Perez, S., Fernandez-Lorente, G., … Guisan, J. M. (2020). High stabilization of immobilized *Rhizomucor miehei* lipase by additional coating with hydrophilic crosslinked polymers: Poly-allylamine/Aldehyde–dextran. *Process Biochemistry*, 92, 156–163. Retrieved 3 December 2021 from https://doi.org/10.1016/J.PROCBIO.2020.02.026

Chaemchuen, S., Heynderickx, P. M., & Verpoort, F. (2020). Kinetic modeling of oleic acid esterification with UiO-66: from intrinsic experimental data to kinetics via elementary reaction steps. *Chemical Engineering Journal*, 394, 124816. Retrieved 2 November 2021 from https://doi.org/10.1016/J.CEJ.2020.124816

Chandler, D. (2002). Hydrophobicity: Two faces of water. *Nature*, 417(6888), 491. Retrieved 8 October 2021 from https://doi.org/10.1038/417491a

Chang, H.-M., Liao, H.-F., Lee, C.-C., & Shieh, C.-J. (2005). Optimized synthesis of lipase-catalyzed biodiesel by Novozym 435. *Journal of Chemical Technology & Biotechnology*, 80(3), 307–312. Retrieved from https://doi.org/10.1002/jctb.1166

Chaput, L., Marton, Z., Pineau, P., Domon, L., Tran, V., & Graber, M. (2012). Enhancing the enantioselectivity of CALB by substrate imprinting: A combined experimental and molecular dynamics simulation model study. *Journal of Molecular Catalysis B: Enzymatic*, 84, 55–61. Retrieved from https://doi.org/10.1016/j.molcatb.2012.04.017

Chen, K. S., Lin, Y. C., Hsu, K. H., & Wang, H. K. (2012). Improving biodiesel yields from waste cooking oil by using sodium methoxide and a microwave heating system. *Energy*, 38(1), 151–156. Retrieved 22 November 2021 from https://doi.org/10.1016/j.energy.2011.12.020

Chen, X., Li, Z., Chun, Y., Yang, F., Xu, H., & Wu, X. (2020). Effect of the formation of diglycerides/monoglycerides on the kinetic curve in oil transesterification with methanol catalyzed by calcium oxide. *ACS Omega*, 5(9), 4646–4656. Retrieved from https://doi.org/10.1021/acsomega.9b04431

Chiou, S. H., & Wu, W. T. (2004). Immobilization of *Candida rugosa lipase* on chitosan with activation of the hydroxyl groups. *Biomaterials*, 25(2), 197–204. Retrieved from https://doi.org/10.1016/S0142-9612(03)00482-4

Cho, H. J., Kim, S. H., Hong, S. W., & Yeo, Y.-K. (2012). A single step non-catalytic esterification of palm fatty acid distillate (PFAD) for biodiesel production. *Fuel*, 93, 373–380. Retrieved from https://doi.org/10.1016/j.fuel.2011.08.063

Choo, K. H. (2018). Modeling photocatalytic membrane reactors. In *Current trends and future developments on (bio-)membranes: photocatalytic membranes and photocatalytic membrane reactors - Chapter 10* (Vol. 1, pp. 297–316). Elsevier. Retrieved 6 October 2021 from https://doi.org/10.1016/B978-0-12-813549-5.00010-4

Chouhan, A. P. S., & Sarma, A. K. (2011). Modern heterogeneous catalysts for biodiesel production: A comprehensive review. *Renewable and Sustainable Energy Reviews*, 15(9), 4378–4399. Retrieved 19 November 2021 from https://doi.org/10.1016/J.RSER.2011.07.112

Chronopoulou, L., Kamel, G., Sparago, C., Bordi, F., Lupi, S., Diociaiuti, M., & Palocci, C. (2011). Structure–activity relationships of *Candida rugosa* lipase immobilized on polylactic acid nanoparticles. *Soft Matter*, 7(6), 2653–2662. Retrieved from https://doi.org/10.1039/c0sm00712a

Chueluecha, N., Kaewchada, A., & Jaree, A. (2017). Biodiesel synthesis using heterogeneous catalyst in a packed-microchannel. *Energy Conversion and Management*, 141, 145–154. Retrieved from https://doi.org/10.1016/j.enconman.2016.07.020

Clark, W. M., Medeiros, N. J., Boyd, D. J., & Snell, J. R. (2013). Biodiesel transesterification kinetics monitored by pH measurement. *Bioresource Technology*, 136, 771–774. Retrieved 21 July 2022 from https://doi.org/10.1016/J.BIORTECH.2013.03.089

Colmenares, J. C., & Luque, R. (2014). Heterogeneous photocatalytic nanomaterials: prospects and challenges in selective transformations of biomass-derived compounds. *Chemical Society Reviews*, 43(3), 765–778. Retrieved from https://doi.org/10.1039/C3CS60262A

Coltro, W. K. T., Piccin, E., Carrilho, E., Jesus, D. P., Silva, J. A. F., Silva, H. D. T., & Lago, C. L. (2007). Microssistemas de análise química. Introdução, tecnologias de fabricação, instrumentação e aplicaçoes. *Química Nova*, 30(8), 1986–2000. Retrieved from https://doi.org/https://doi.org/10.1590/S0100-40422007000800034

Conceição, M. M., Candeia, R. A., Silva, F. C., Bezerra, A. F., Fernandes, V. J., & Souza, A. G. (2007). Thermoanalytical characterization of castor oil biodiesel. *Renewable and Sustainable Energy Reviews*, 11(5), 964–975. Retrieved 11 November 2021 from https://doi.org/10.1016/j.rser.2005.10.001

Corro, G., Pal, U., & Tellez, N. (2013). Biodiesel production from Jatropha curcas crude oil using ZnO/SiO_2 photocatalyst for free fatty acids esterification. *Applied Catalysis B: Environmental*, 129, 39–47. Retrieved 7 September 2021 from https://doi.org/10.1016/J.APCATB.2012.09.004

Corro, G., Sánchez, N., Pal, U., Cebada, S., & Fierro, J. L. G. (2017). Solar-irradiation driven biodiesel production using Cr/SiO_2 photocatalyst exploiting cooperative interaction between Cr^{6+} and Cr^{3+} moieties. *Applied Catalysis B: Environmental*, 203, 43–52. Retrieved 7 September 2021 from https://doi.org/10.1016/J.APCATB.2016.10.005

Corro, G., Tellez, N., Bañuelos, F., & Mendoza, M. E. (2012). Biodiesel from *Jatropha curcas* oil using Zn for esterification step and solar radiation as energy source. *Fuel*, 97, 72–79.

Corro, G., Tellez, N., Jimenez, T., Tapia, A., Banuelos, F., & Vazquez-Cuchillo, O. (2011). Biodiesel from waste frying oil. Two step process using acidified SiO_2 for esterification step. *Catalysis Today*, 166(1), 116–122. Retrieved 6 October 2021 from https://doi.org/10.1016/J.CATTOD.2010.09.011

Courtenay Stanley Goss Phillips. (2021). alkaline earth metal summary. In *Britannica*. Retrieved 10 November 2021 from https://www.britannica.com/science/alkaline-earth-metal

Craig, B. M. (1953). Refractive indices of some saturated and monoethenoid fatty acids and methyl esters. *Canadian Journal of Chemistry*, 31(5), 499–504. Retrieved from https://doi.org/10.1139/v53-068

Cubas, A. L. V., Machado, M. M., Pinto, C. R. S. C., Moecke, E. H. S., & Dutra, A. R. A. (2016). Biodiesel production using fatty acids from food industry waste using corona discharge plasma technology. *Waste Management*, 47, 149–154. Retrieved 19 November 2021 from https://doi.org/https://doi.org/10.1016/j.wasman.2015.05.040

Cui, J., Zhao, Y., Liu, R., Zhong, C., & Jia, S. (2016). Surfactant-activated lipase hybrid nanoflowers with enhanced enzymatic performance. *Nature Publishing Group*, 6, 27928. Retrieved from https://doi.org/10.1038/srep27928

da S. Pereira, A., Fraga, J. L., Diniz, M. M., Fontes-Sant'ana, G. C., & Amaral, P. F. F. (2018). High catalytic activity of lipase from *yarrowia lipolytica* immobilized by microencapsulation. *International Journal of Molecular Sciences*, 19(11), 3393. Retrieved from https://doi.org/10.3390/ijms19113393 da Silva, M. G. C., Canevesi, R. L. S., Welter, R. A., Vieira, M. G. A., & da Silva, E. A. (2015). Chemical equilibrium of ion exchange in the binary mixture Cu^{2+} and Ca^{2+} in calcium alginate. *Adsorption*, 21(6–7), 445–458. Retrieved from https://doi.org/10.1007/s10450-015-9682-8

Dalla-Vecchia, R., Nascimento, M. da G., & Soldi, V. (2004). Aplicações sintéticas de lipases imobilizadas em polímeros. *Química Nova*, 27(4), 623–630. Retrieved from https://doi.org/10.1590/S0100-40422004000400017

De, A., & Boxi, S. S. (2020). Application of Cu impregnated TiO_2 as a heterogeneous nanocatalyst for the production of biodiesel from palm oil. *Fuel*, 265, 117019. Retrieved 4 March 2022 from https://doi.org/10.1016/J.FUEL.2020.117019

de Carvalho, B. G., Taketa, T. B., Garcia, B. B. M., Han, S. W., & de la Torre, L. G. (2021). Hybrid microgels produced via droplet microfluidics for sustainable delivery of hydrophobic and hydrophilic model nanocarriers. *Materials Science and Engineering: C*, 118, 111467. Retrieved 23 September 2021 from https://doi.org/10.1016/J.MSEC.2020.111467

Degirmenbasi, N., Boz, N., & Kalyon, D. M. (2014). Biofuel production via transesterification using sepiolite-supported alkaline catalysts. *Applied Catalysis B: Environmental*, 150–151, 147–156. Retrieved from https://doi.org/10.1016/j.apcatb.2013.12.013

Demirbaş, A. (2008). Biodegradability of biodiesel and petrodiesel fuels. *Energy Sources, Part A: Recovery, Utilization, and Environmental Effects*, 31(2), 169–174. Retrieved from https://doi.org/10.1080/15567030701521809

Demirbaş, Ayhan. (2002). Biodiesel from vegetable oils via transesterification in supercritical methanol. *Energy Conversion and Management*, 43(17), 2349–2356. Retrieved 11 November 2021 from https://doi.org/10.1016/S0196-8904(01)00170-4

Deshlahra, P., Pfeifer, K., Bernstein, G. H., & Wolf, E. E. (2011). CO adsorption and oxidation studies on nanofabricated model catalysts using multilayer enhanced IRAS technique. *Applied Catalysis A: General*, 391(1–2), 22–30. Retrieved from https://doi.org/10.1016/j.apcata.2010.07.026

Devanesan, M. G., Viruthagiri, T., & Sugumar, N. (2007). Transesterification of *Jatropha* oil using immobilized *Pseudomonas fluorescens*. *African Journal of Biotechnology*, 6(21), 2497–2501. Retrieved from https://doi.org/10.5897/AJB2007.000-2396

Deveci, I., Doğaç, Y. I., Teke, M., & Mercimek, B. (2015). Synthesis and characterization of chitosan/TiO_2 composite beads for improving stability of *Porcine Pancreatic* Lipase. *Applied Biochemistry and Biotechnology*, 175(2), 1052–1068. Retrieved from https://doi.org/10.1007/s12010-014-1321-4

Dharmsthiti, S., & Kuhasuntisuk, B. (1998). Lipase from *Pseudomonas aeruginosa* LP602: biochemical properties and application for wastewater treatment. *Journal of Industrial*

Microbiology & Biotechnology, 21, 75–80. Retrieved from https://doi.org/10.1038/sj.jim.2900563

di Serio, M., Casale, L., Tesser, R., & Santacesaria, E. (2010). New process for the production of glycerol tert-butyl ethers. *Energy and Fuels*, 24(9), 4668–4672. Retrieved 11 November 2021 from https://doi.org/10.1021/EF901230R

di Serio, M., Mallardo, S., Carotenuto, G., Tesser, R., & Santacesaria, E. (2012). Mg/Al hydrotalcite catalyst for biodiesel production in continuous packed bed reactors. *Catalysis Today*, 195(1), 54–58. Retrieved 10 November 2021 from https://doi.org/10.1016/J.CATTOD.2012.01.013

di Serio, M., Tesser, R., Pengmei, L., & Santacesaria, E. (2008). Heterogeneous catalysts for biodiesel production. *Energy and Fuels*, 22(1), 207–217. Retrieved 11 November 2021 from https://doi.org/10.1021/EF700250G

Dias, J. M., Alvim-Ferraz, M. C. M., & Almeida, M. F. (2008). Comparison of the performance of different homogeneous alkali catalysts during transesterification of waste and virgin oils and evaluation of biodiesel quality. *Fuel*, 87(17–18), 3572–3578. Retrieved 22 November 2021 from https://doi.org/10.1016/j.fuel.2008.06.014

Dimov, I. K., Garcia-Cordero, J. L., O'grady, J., Poulsen, C. R., Viguier, C., Kent, L., … O'kennedy, R. (2008). Integrated microfluidic tmRNA purification and real-time NASBA device for molecular diagnostics. *Lab on a Chip*, 8(12), 2071–2078.

Dimple Sharma. (n.d.). Used Cooking Oil : A hazard for health and environment. Retrieved 10 November 2022, from https://timesofindia.indiatimes.com/readersblog/tatsat/used-cooking-oil-a-hazard-for-health-and-environment-1228/

Domínguez, M. I., Centeno, M. A., Martínez T., M., Bobadilla, L. F., Laguna, Ó. H., & Odriozola, J. A. (2021). Current scenario and prospects in manufacture strategies for glass, quartz, polymers and metallic microreactors: A comprehensive review. *Chemical Engineering Research and Design*, 171, 13–35. Retrieved from https://doi.org/10.1016/j.cherd.2021.05.001

Donnelly, K., & Baumann, M. (2021). Scalability of photochemical reactions in continuous flow mode. *Journal of Flow Chemistry*, 11(3), 223–241. Retrieved from https://doi.org/10.1007/s41981-021-00168-z

Doran, P. M. (1995). Heterogeneous reactions. In Elsevier Science and Technology (Ed.), *Bioprocess Engineering Principals* (1st ed., pp. 297–331).

dos Santos, P. R. S., Voll, F. A. P., Ramos, L. P., & Corazza, M. L. (2017). Esterification of fatty acids with supercritical ethanol in a continuous tubular reactor. *The Journal of Supercritical Fluids*, 126, 25–36. Retrieved 17 November 2021 from https://doi.org/10.1016/J.SUPFLU.2017.03.002

Du, J., Yuan, R. kang, Hu, R. xue, Zhang, H. long, Qi, Y. tang, & Zhang, W. nong. (2022).

Biodiesel production from Momordica cochinchinensis (Lour.) Spreng seed oil. *Fuel*, 314, 123047. Retrieved 22 August 2022 from https://doi.org/10.1016/J.FUEL.2021.123047

Dumont, M. J., & Narine, S. S. (2007). Soapstock and deodorizer distillates from North American vegetable oils: Review on their characterization, extraction and utilization. *Food Research International*, 40(8), 957–974. Retrieved 16 December 2020 from https://doi.org/10.1016/j.foodres.2007.06.006

Dutra, L. da S., Costa Cerqueira Pinto, M., Cipolatti, E. P., Aguieiras, E. C. G., Manoel, E. A., Greco-Duarte, J., … Pinto, J. C. (2022). How the biodiesel from immobilized enzymes production is going on: An advanced bibliometric evaluation of global research. *Renewable and Sustainable Energy Reviews*, 153, 111765. Retrieved 17 November 2021 from https://doi.org/10.1016/J.RSER.2021.111765

eCycle. (2014). SO_2: conheça o dióxido de enxofre. Retrieved 6 July 2017, from http://www.ecycle.com.br/component/content/article/63/2409-dioxido-de-enxofre-e-um-dos-poluentes-do-ar-mais-perigosos.html

EIA. (2021). Diesel fuel explained Use of diesel. Retrieved 9 November 2021, from https://www.eia.gov/energyexplained/diesel-fuel/use-of-diesel.php

Elias, S., Rabiu, A. M., Okeleye, B. I., Okudoh, V., & Oyekola, O. (2020). Bifunctional heterogeneous catalyst for biodiesel production from waste vegetable oil. *Applied Sciences*, 10(9), 3153. Retrieved 22 November 2021 from https://doi.org/10.3390/app10093153

EN 14104. (2003). Fat and oil derivatives - Fatty Acid Methyl Esters (FAME) Determination of acid value. *European Standard*.

Encinar, J., Pardal, A., Sánchez, N., & Nogales, S. (2018). Biodiesel by transesterification of rapeseed oil using ultrasound: A kinetic study of base-catalysed reactions. *Energies*, 11(9), 2229. Retrieved from https://doi.org/10.3390/en11092229

Endalew, A. K., Kiros, Y., & Zanzi, R. (2011). Heterogeneous catalysis for biodiesel production from *Jatropha curcas* oil (JCO). *Energy*, 36(5), 2693–2700. Retrieved 11 November 2021 from https://doi.org/10.1016/j.energy.2011.02.010

Erin Voegele. (2020, November 13). NBB: Biodiesel can help meet USDA’s AIA goals. *Biodiesel Magazine*. Retrieved 23 January 2021 from https://biodieselmagazine.com/articles/2517256/nbb-biodiesel-can-help-meet-usdaundefineds-aia-goals

Escobar, J. C., Lora, E. S., Venturini, O. J., Yáñez, E. E., Castillo, E. F., & Almazan, O. (2009). Biofuels: Environment, technology and food security. *Renewable and Sustainable Energy Reviews*, 13(6–7), 1275–1287. Retrieved 10 November 2021 from https://doi.org/10.1016/J.RSER.2008.08.014

Eskandarloo, H., Badiei, A., Behnajady, M. A., & Ziarani, G. M. (2015). UV-LEDs assisted preparation of silver deposited TiO_2 catalyst bed inside microchannels as a high efficiency microphotoreactor for cleaning polluted water. *Chemical Engineering Journal*, 270, 158–167. Retrieved from https://doi.org/10.1016/j.cej.2015.01.117

Esmaeili, H. (2022). A critical review on the economic aspects and life cycle assessment of biodiesel production using heterogeneous nanocatalysts. *Fuel Processing Technology*, 230, 107224. Retrieved 19 April 2022 from https://doi.org/10.1016/J.FUPROC.2022.107224

Espindola, J. da S. (2010). *Produção fotocatalítica de hidrogênio a partir de soluções de etanol e água*. Universidade Federal do Rio Grande do Sul, Porto Alegre.

Essamlali, Y., Larzek, M., Essaid, B., & Zahouily, M. (2017). Natural phosphate supported titania as a novel solid acid catalyst for oleic acid Esterification. *Industrial & Engineering Chemistry Research*, 56(20), 5821–5832. Retrieved from https://doi.org/10.1021/acs.iecr.7b00607

Ezzati, R. (2018). Kinetics and thermodynamics of the esterification reaction according to the Langmuir-Hinshelwood mechanism. *Iranian Journal of Catalysis*, 8, 41–46.

Fang, Y., Al-Assaf, S., Philips, G. O., Nishinari, K., Funami, T., Williams, P. A., & Li, L. (2017). Multiple steps and critical behaviors of the binding of calcium to alginate. *The Journal of Physical Chemistry B*, 111(10), 2456–2462. Retrieved from https://doi.org/10.1021/jp0689870

Farooq, M., Ramli, A., & Subbarao, D. (2013). Biodiesel production from waste cooking oil using bifunctional heterogeneous solid catalysts. *Journal of Cleaner Production*, 59, 131–140. Retrieved 21 November 2021 from https://doi.org/10.1016/J.JCLEPRO.2013.06.015

Farra, R., Sheppard, N. F., McCabe, L., Neer, R. M., Anderson, J. M., Santini, J. T., … Langer, R. (2012). First-in-Human testing of a wirelessly controlled drug delivery microchip. *Science Translational Medicine*, 4(122), 122ra21. Retrieved from https://doi.org/10.1126/scitranslmed.3003276

Feng, J., Siu, V. S., Roelke, A., Mehta, V., Rhieu, S. Y., Palmore, G. T. R., & Pacifici, D. (2012). Nanoscale Plasmonic Interferometers for Multispectral, High-Throughput Biochemical Sensing. *Nano Letters*, 12(2), 602–609. Retrieved from https://doi.org/10.1021/nl203325s

Fereidoon Shahidi. (2005). *Bailey's Industrial Oil and Fat Products*. (F. Shahidi,Ed.) (6th ed., Vol. 1).

Fereidooni, L., Abbaspourrad, A., & Enayati, M. (2021). Electrolytic transesterification of waste frying oil using Na^+/zeolite–chitosan biocomposite for biodiesel production. *Waste Management*, 127, 48–62. Retrieved 19 November 2021 from https://doi.org/10.1016/j.wasman.2021.04.020

Fernández, C. M., Fiori, L., Ramos, M. J., Pérez, Á., & Rodríguez, J. F. (2015). Supercritical extraction and fractionation of *Jatropha curcas L.* oil for biodiesel production. *Journal of*

Supercritical Fluids, 97, 100–106. Retrieved 11 November 2021 from https://doi.org/10.1016/j.supflu.2014.11.010

Ferrão-Gonzales, A. D., Véras, I. C., Silva, F. A. L., Alvarez, H. M., & Moreau, V. H. (2011). Thermodynamic analysis of the kinetics reactions of the production of FAME and FAEE using Novozyme 435 as catalyst. *Fuel Processing Technology*, 92(5), 1007–1011. Retrieved 29 March 2022 from https://doi.org/10.1016/J.FUPROC.2010.12.023

Ferrari, A., Hunt, J., Stiegman, A., & Dudley, G. (2015). Microwave-assisted superheating and/or microwave-specific superboiling (nucleation-limited boiling) of liquids occurs under certain conditions but is mitigated by stirring. *Molecules*, 20(12), 21672–21680. Retrieved from https://doi.org/10.3390/molecules201219793

Flores, K. P., Omega, J. L. O., Cabatingan, L. K., Go, A. W., Agapay, R. C., & Ju, Y. H. (2019). Simultaneously carbonized and sulfonated sugarcane bagasse as solid acid catalyst for the esterification of oleic acid with methanol. *Renewable Energy*, 130, 510–523. Retrieved 15 October 2021 from https://doi.org/10.1016/J.RENENE.2018.06.093

Fonseca, J. M., Teleken, J. G., de Cinque Almeida, V., & da Silva, C. (2019). Biodiesel from waste frying oils: Methods of production and purification. *Energy Conversion and Management*, 184, 205–218. Retrieved 27 June 2022 from https://doi.org/10.1016/J.ENCONMAN.2019.01.061

Foresti, M. L., Valle, G., Bonetto, R., Ferreira, M. L., & Briand, L. E. (2010). FTIR, SEM and fractal dimension characterization of lipase B from *Candida antarctica* immobilized onto titania at selected conditions. *Applied Surface Science*, 256(6), 1624–1635. Retrieved 23 September 2021 from https://doi.org/10.1016/J.APSUSC.2009.09.083

Foroutan, R., Mohammadi, R., & Ramavandi, B. (2021). Waste glass catalyst for biodiesel production from waste chicken fat: Optimization by RSM and ANNs and toxicity assessment. *Fuel*, 291, 120151. Retrieved 2 November 2021 from https://doi.org/10.1016/J.FUEL.2021.120151

Fox, M. Anne., & Dulay, M. T. (1993). Heterogeneous photocatalysis. *Chemical Reviews*, 93(1), 341–357. Retrieved from https://doi.org/10.1021/cr00017a016

Freedman, B., Pryde, E. H., & Mounts, T. L. (1984). Variables affecting the yields of fatty esters from transesterified vegetable oils. *Journal of the American Oil Chemists Society*, 61(10), 1638–1643. Retrieved 19 November 2021 from https://doi.org/10.1007/BF02541649

Freedman, Bernard, Butterfield, R. O., & Pryde, E. H. (1986). Transesterification kinetics of soybean oil 1. *Journal of the American Oil Chemists' Society*, 63(10), 1375–1380. Retrieved 11 November 2021 from https://doi.org/10.1007/BF02679606

Fukuyama, T., Kasakado, T., Hyodo, M., & Ryu, I. (2022). Improved efficiency of photo-induced synthetic reactions enabled by advanced photo flow technologies. *Photochemical & Photobiological Sciences*, 21, 76–775. Retrieved from https://doi.org/10.1007/s43630-

021-00151-6

Fundueanu, G., Nastruzzi, C., Carpov, A., Desbrieres, J., & Rinaudo, M. (1999). Physico-chemical characterization of Ca-alginate microparticles produced with different methods. *Biomaterials*, 20(15), 1427–1435. Retrieved from https://doi.org/10.1016/S0142-9612(99)00050-2

G. Berrebi, P. Dufresne, & Y. Jacquier. (1993). Recycling of spent hydroprocessing catalysts: EURECAT technology. *Environmental Progress*, 12(2), 97–100. Retrieved from https://doi.org/10.1016/0921-3449(94)90032-9

Galvan, D., de Aguiar, L. M., Rohwedder, J. J. R., Borsato, D., & Killner, M. H. M. (2020). Online monitoring of transesterification reaction by medium-resolution benchtop ^{1}H-NMR and NIR spectroscopy. *Fuel Processing Technology*, 208, 106511. Retrieved from https://doi.org/10.1016/j.fuproc.2020.106511

Ganjalikhany, M. R., Ranjbar, B., Taghavi, A. H., & Moghadam, T. T. (2012). Functional motions of *Candida antarctica* lipase b: A survey through open-close conformations. *PLoS ONE*, 7(7). Retrieved from https://doi.org/10.1371/journal.pone.0040327

Gardy, J., Hassanpour, A., Lai, X., Ahmed, M. H., & Rehan, M. (2017). Biodiesel production from used cooking oil using a novel surface functionalised TiO_2 nano-catalyst. *Applied Catalysis B: Environmental*, 207, 297–310. Retrieved 14 March 2022 from https://doi.org/10.1016/J.APCATB.2017.01.080

Gaurav, A., Dumas, S., Mai, C. T. Q., & Ng, F. T. T. (2019). A kinetic model for a single step biodiesel production from a high free fatty acid (FFA) biodiesel feedstock over a solid heteropolyacid catalyst. *Green Energy and Environment*, 4(3), 328–341. Retrieved 19 November 2021 from https://doi.org/10.1016/j.gee.2019.03.004

Gelbard, G., Brès, O., Vargas, R. M., Vielfaure, R., & Schuchardt, U. F. (1995). ^{1}H Nuclear Magnetic Resonance determination of the yield of the transesterification of rapessed oil with methanol. *Journal of the American Oil Chemists' Society*, 72(10), 1239–1241. Retrieved from https://doi.org/10.1007/BF02540998

Ghanem, A., & Aboul-Enein, H. Y. (2005). Application of lipases in kinetic resolution of racemates. *Chirality*, 17(1), 1–15. Retrieved from https://doi.org/10.1002/chir.20089

Ghani, N., Iqbal, J., Sadaf, S., Bhatti, H. N., & Asgher, M. (2020). Comparison of photo-esterification capability of bismuth vanadate with reduced graphene oxide bismuth vanadate (RGO/$BiVO_4$) composite for biodiesel production from high free fatty acid containing non-edible oil. *ChemistrySelect*, 5(29), 9245–9253. Retrieved 6 October 2021 from https://doi.org/10.1002/SLCT.202001913

Ghazani, S. M., García-Llatas, G., & Marangoni, A. G. (2014). Micronutrient content of cold-pressed, hot-pressed, solvent extracted and RBD canola oil: Implications for nutrition and quality. *European Journal of Lipid Science and Technology*, 116(4), 380–387. Retrieved

10 September 2021 from https://doi.org/10.1002/EJLT.201300288

Gholipour Zanjani, N., Kamran Pirzaman, A., & Yazdanian, E. (2020). Biodiesel production in the presence of heterogeneous catalyst of alumina: Study of kinetics and thermodynamics. *International Journal of Chemical Kinetics*, 52(7), 472–484. Retrieved from https://doi.org/10.1002/kin.21363

Ghori, M. I., Iqbal, M. J., & Hameed, A. (2011). Characterization of a novel lipase from *bacillus sp.* Isolated from tannery wastes. *Brazilian Journal of Microbiology*, 42, 22–29. Retrieved from https://doi.org/10.1590/S1517-83822011000100003

Giacomelli, C. E., Avena, M. J., & Pauli, P. de. (1995). Aspartic acid adsorption onto TiO_2 particles surface. Experimental data and model calculations. *Langmuir*, 3483–3490. Retrieved from https://doi.org/10.1021/la00009a034

Goembira, F., Matsuura, K., & Saka, S. (2012). Biodiesel production from rapeseed oil by various supercritical carboxylate esters. *Fuel*, 97, 373–378. Retrieved 19 November 2021 from https://doi.org/10.1016/j.fuel.2012.02.051

Gojun, M., Šalić, A., & Zelić, B. (2021). Integrated microsystems for lipase-catalyzed biodiesel production and glycerol removal by extraction or ultrafiltration. *Renewable Energy*, 180, 213–221. Retrieved 10 December 2021 from https://doi.org/10.1016/J.RENENE.2021.08.064

Granados, M. L., Poves, M. D. Z., Alonso, D. M., Mariscal, R., Galisteo, F. C., Moreno-Tost, R., … Fierro, J. L. G. (2007). Biodiesel from sunflower oil by using activated calcium oxide. *Applied Catalysis B: Environmental*, 73(3–4), 317–326. Retrieved 4 March 2022 from https://doi.org/10.1016/J.APCATB.2006.12.017

Gruber, C. C., & Pleiss, J. (2012). Lipase B from *Candida antarctica* binds to hydrophobic substrate–water interfaces via hydrophobic anchors surrounding the active site entrance. *Journal of Molecular Catalysis B: Enzymatic*, 84, 48–54. Retrieved 24 September 2021 from https://doi.org/10.1016/J.MOLCATB.2012.05.012

Guan, G., Teshima, M., Sato, C., Mo Son, S., Faisal Irfan, M., Kusakabe, K., … Lin, T.-J. (2009). Two-phase flow behavior in microtube reactors during biodiesel production from waste cooking oil. *AIChE Journal*, 1383–1390. Retrieved from https://doi.org/10.1002/aic.12042

Guo, M., Jiang, W., Chen, C., Qu, S., Lu, J., Yi, W., & Ding, J. (2021). Process optimization of biodiesel production from waste cooking oil by esterification of free fatty acids using $La^{3+}/ZnO\text{-}TiO_2$ photocatalyst. *Energy Conversion and Management*, 229, 113745. Retrieved 7 September 2021 from https://doi.org/10.1016/J.ENCONMAN.2020.113745

Guo, M., Jiang, W., Ding, J., & Lu, J. (2022). Highly active and recyclable CuO/ZnO as photocatalyst for transesterification of waste cooking oil to biodiesel and the kinetics. *Fuel*, 315, 123254. Retrieved from https://doi.org/10.1016/j.fuel.2022.123254

Hanaor, D. A. H., & Sorrell, C. C. (2011). Review of the anatase to rutile phase transformation. *Journal of Materials Science*, 46(4), 855–874. Retrieved from https://doi.org/10.1007/s10853-010-5113-0

Handelsman, T., & Shoham, Y. (1994). Production and characterization of an extracellular thermostable lipase from a thermophilic *bacillus sp. The Journal of General and Applied Microbiology*, 40(5), 435–443. Retrieved 24 September 2021 from https://doi.org/10.2323/JGAM.40.435

Harun, F. W., Jihadi, N. 'Izzati M., Ramli, S., Hassan, N. R. A., & Zubir, 'Nur 'Atikah Mat. (2018). Esterification of oleic acid with alcohols over Cu-MMT K10 and Fe-MMT K10 as acid catalysts. *AIP Conference Proceedings*, 1972, 30025. Retrieved from https://doi.org/10.1063/1.5041246

Hassan, S. Z., & Vinjamur, M. (2013). Analysis of sensitivity of equilibrium constant to reaction conditions for esterification of fatty acids with alcohols. *Industrial & Engineering Chemistry Research*, 52(3), 1205–1215. Retrieved from https://doi.org/10.1021/ie301881g

Hassani, M., Amini, G., Najafpour, G., & Rabiee, S. M. (2013). A two-step catalytic production of biodiesel from waste cooking Oil. *International Journal of Engineering*, 26(6 (C)), 563–570. Retrieved from https://doi.org/10.5829/idosi.ije.2013.26.06c.01

Håti, A. G., Bassett, D. C., Ribe, J. M., Sikorski, P., Weitz, D. A., & Stokke, B. T. (2016). Versatile, cell and chip friendly method to gel alginate in microfluidic devices. *Lab on a Chip*, 16(19), 3718–3727. Retrieved from https://doi.org/10.1039/c6lc00769d

Hawash, S. A., Ebrahiem, E. E., & Farag, H. A. (2019). Kinetic study of the esterification of unsaturated free fatty acids. *Proceedings of the Institution of Civil Engineers - Energy*, 172(3), 105–114. Retrieved from https://doi.org/10.1680/jener.19.00006

Hayyan, A., Mjalli, F. S., Hashim, M. A., Hayyan, M., AlNashef, I. M., Al-Zahrani, S. M., & Al-Saadi, M. A. (2011). Ethanesulfonic acid-based esterification of industrial acidic crude palm oil for biodiesel production. *Bioresource Technology*, 102(20), 9564–9570. Retrieved from https://doi.org/10.1016/j.biortech.2011.07.074

He, Z., Li, Y., Zhang, Q., & Wang, H. (2010). Capillary microchannel-based microreactors with highly durable ZnO/TiO_2 nanorod arrays for rapid, high efficiency and continuous-flow photocatalysis. *Applied Catalysis B: Environmental*, 93(3–4), 376–382. Retrieved from https://doi.org/10.1016/j.apcatb.2009.10.011

Helmi, M., Tahvildari, K., Hemmati, A., Aberoomand azar, P., & Safekordi, A. (2021). Phosphomolybdic acid/graphene oxide as novel green catalyst using for biodiesel production from waste cooking oil via electrolysis method: Optimization using with response surface methodology (RSM). *Fuel*, 287, 119528. Retrieved 21 November 2022 from https://doi.org/10.1016/J.FUEL.2020.119528

Hernando, J., Leton, P., Matia, M. P., Novella, J. L., & Alvarez-Builla, J. (2007). Biodiesel and

FAME synthesis assisted by microwaves: Homogeneous batch and flow processes. *Fuel*, 86(10–11), 1641–1644. Retrieved 19 November 2021 from https://doi.org/10.1016/j.fuel.2006.11.003

Hincapié, G. M., Valange, S., Barrault, J., Moreno, J. A., & López, D. P. (2014). Effect of microwave-assisted system on transesterification of castor oil with ethanol. *Universitas Scientiarum*, 19(3), 193–200. Retrieved from https://doi.org/10.11144/Javeriana.SC19-3.emas

Ho, C. M. B., Ng, S. H., Li, K. H. H., & Yoon, Y.-J. (2015). 3D printed microfluidics for biological applications. *Lab on a Chip*, 15(18), 3627–3637. Retrieved from https://doi.org/10.1039/C5LC00685F

Hoffmann, M. R., Martin, S. T., Choi, W., & Bahnemann, D. W. (1995). Environmental applications of semiconductor photocatalysis. *Chemical Reviews*, 95(1), 69–96. Retrieved from https://doi.org/10.1021/cr00033a004

Hoffmann, N. (2015). Photocatalysis with TiO_2 applied to organic synthesis. *Australian Journal of Chemistry*, 68(11), 1621. Retrieved from https://doi.org/10.1071/CH15322

Hong, C., & Haiyun, W. (2010). Optimization of volatile fatty acid production with co-substrate of food wastes and dewatered excess sludge using response surface methodology. *Bioresource Technology*, 101(14), 5487–5493. Retrieved 8 October 2021 from https://doi.org/10.1016/J.BIORTECH.2010.02.013

Hong, I. K., Jeon, H., Kim, H., & Lee, S. B. (2016). Preparation of waste cooking oil based biodiesel using microwave irradiation energy. *Journal of Industrial and Engineering Chemistry*, 42, 107–112. Retrieved 5 July 2022 from https://doi.org/10.1016/J.JIEC.2016.07.035

Hosseini, S. M., Kim, S. M., Sayed, M., Younesi, H., Bahramifar, N., Park, J. H., & Pyo, S. H. (2019). Lipase-immobilized chitosan-crosslinked magnetic nanoparticle as a biocatalyst for ring opening esterification of itaconic anhydride. *Biochemical Engineering Journal*, 143, 141–150. Retrieved 24 September 2021 from https://doi.org/10.1016/J.BEJ.2018.12.022

Hou, C., Qi, Z., & Zhu, H. (2015). Preparation of core–shell magnetic polydopamine/alginate biocomposite for *Candida rugosa* lipase immobilization. *Colloids and Surfaces B: Biointerfaces*, 128, 544–551. Retrieved from https://doi.org/10.1016/j.colsurfb.2015.03.007

Hou, C., Wang, Y., Zhu, H., & Wei, H. (2016). Construction of enzyme immobilization system through metal-polyphenol assisted Fe_3O_4/chitosan hybrid microcapsules. *Chemical Engineering Journal*, 283, 397–403. Retrieved 1 December 2021 from https://doi.org/10.1016/J.CEJ.2015.07.067

Houas, A., Lachheb, H., Ksibi, M., Elaloui, E., Guillard, C., & Herrmann, J. M. (2001).

Photocatalytic degradation pathway of methylene blue in water. *Applied Catalysis B: Environmental*, 31(2), 145–157. Retrieved 25 October 2021 from https://doi.org/10.1016/S0926-3373(00)00276-9

Huang, Y. P., & Chang, J. I. (2010). Biodiesel production from residual oils recovered from spent bleaching earth. *Renewable Energy*, 35(1), 269–274. Retrieved 15 November 2021 from https://doi.org/10.1016/J.RENENE.2009.07.014

Huesing, N., Launay, B., Kickelbick, G., Gross, S., Armelao, L., Bottaro, G., … Kothleitner, G. (2003). Transition metal oxide-doped mesostructured silica films. *Applied Catalysis A: General*, 254(2), 297–310. Retrieved from https://doi.org/10.1016/S0926-860X(03)00475-7

Hussain, Z., & Kumar, R. (2018). Esterification of free fatty acids: experiments, kinetic modeling, simulation & optimization. *International Journal of Green Energy*, 15(11), 629–640. Retrieved from https://doi.org/10.1080/15435075.2018.1525736

IEA. (2020). International Energy Agency. Retrieved 9 November 2020, from https://www.iea.org/about

Ishigaki, T., Nakada, Y., Tarutani, N., Uchikoshi, T., Tsujimoto, Y., Isobe, M., … Hao, D. (2020). Enhanced visible-light photocatalytic activity of anatase-rutile mixed-phase nano-size powder given by high-temperature heat treatment. *Royal Society Open Science*, 7(1), 191539. Retrieved from https://doi.org/10.1098/rsos.191539

Jaiswal, S. K., Tejo Prakash, N., & Prakash, R. (2016). ^{1}H NMR based quantification of ethyl ester in biodiesel: A comparative study of product-dependent derivations. *Analytical Chemistry Letters*, 6(5), 518–525. Retrieved from https://doi.org/10.1080/22297928.2016.1246977

Jin, T., Wang, B., Zeng, J., Yang, C., Wang, Y., & Fang, T. (2015). Esterification of free fatty acids with supercritical methanol for biodiesel production and related kinetic study. *RSC Advances*, 5(64), 52072–52078. Retrieved from https://doi.org/10.1039/C5RA03709C

Johnson, A. K., Zawadzka, A. M., Deobald, L. A., Crawford, R. L., & Paszczynski, A. J. (2008). Novel method for immobilization of enzymes to magnetic nanoparticles. *Journal of Nanoparticle Research*, 10(6), 1009–1025. Retrieved 1 December 2021 from https://doi.org/10.1007/S11051-007-9332-5

Joyce, P., Kempson, I., & Prestidge, C. A. (2016). Orientating lipase molecules throught surface chemical control for enhanced activity: A QCM-D and ToF-SIM investigation. *Colloids and Surfaces B: Biointerfaces*, 173–181. Retrieved from https://doi.org/10.1016/j.colsurfb.2016.02.059

Kanakaraju, D., Glass, B. D., & Oelgemöller, M. (2014). Titanium dioxide photocatalysis for pharmaceutical wastewater treatment. *Environmetal Chemistry Letters* , 12, 27–47. Retrieved from https://doi.org/10.1007/s10311-013-0428-0

Kanakaraju, D., Motti, C. A., Glass, B. D., & Oelgemöller, M. (2016). Solar photolysis versus TiO_2-mediated solar photocatalysis: a kinetic study of the degradation of naproxen and diclofenac in various water matrices. *Environmental Science and Pollution Research*, 23(17), 17437–17448. Retrieved from https://doi.org/10.1007/s11356-016-6906-8

Kapoor, M., & Gupta, M. N. (2012). Lipase promiscuity and its biochemical applications. *Process Biochemistry*, 47(4), 555–569. Retrieved 23 June 2022 from https://doi.org/10.1016/J.PROCBIO.2012.01.011

Kappe, C. O. (2004). Controlled microwave heating in modern organic synthesis. *Angewandte Chemie - International Edition*, 43(46), 6250–6284. Retrieved 19 November 2021 from https://doi.org/10.1002/ANIE.200400655

Karan, P., Mukhopadhyay, P., & Chakraborty, R. (2020). Quartz halogen-ultrasonication integrated rotating reactor for efficient photocatalytic-thermocatalytic synthesis of glyceryl monocaprin: Kinetics of heterogeneous esterification. *Asia-Pacific Journal of Chemical Engineering*, 15(1), e2379. Retrieved from https://doi.org/10.1002/apj.2379

Karimi, M. (2016). Immobilization of lipase onto mesoporous magnetic nanoparticles for enzymatic synthesis of biodiesel. *Biocatalysis and Agricultural Biotechnology*, 8, 182–188. Retrieved 8 July 2022 from https://doi.org/10.1016/J.BCAB.2016.09.009

Kasirajan, R. (2021). Biodiesel production by two step process from an energy source of *Chrysophyllum albidum* oil using homogeneous catalyst. *South African Journal of Chemical Engineering*, 37, 161–166. Retrieved 6 July 2022 from https://doi.org/10.1016/J.SAJCE.2021.05.011

Kestenbaum, H., Lange de Oliveira, A., Schmidt, W., Schüth, F., Ehrfeld, W., Gebauer, K., … Züchner, H. (2002). Silver-catalyzed oxidation of ethylene to ethylene oxide in a microreaction system. *Industrial & Engineering Chemistry Research*, 41(4), 710–719. Retrieved from https://doi.org/10.1021/ie010306u

Khaligh, N. G., Mihankhah, T., Shahnavaz, Z., Zaharani, L., & Johan, M. R. (2021). Solar energy and TiO_2 nanotubes: Biodiesel production from waste cooking olive oil. *Environmental Progress & Sustainable Energy*, 40(2), e13537. Retrieved from https://doi.org/10.1002/ep.13537

Khan, M., Farah, H., Iqbal, N., Noor, T., Amjad, M. Z. bin, & Ejaz Bukhari, S. S. (2021). A TiO_2 composite with graphitic carbon nitride as a photocatalyst for biodiesel production from waste cooking oil. *RSC Advances*, 11(59), 37575–37583. Retrieved from https://doi.org/10.1039/D1RA07796A

Khan, N., Park, S. H., Kadima, L., Bourdeau, C., Calina, E., Edmunds, C. W., & Pursell, D. P. (2021). Locally sustainable biodiesel production from waste cooking oil and grease using a deep eutectic solvent: characterization, thermal properties, and blend Performance. *ACS Omega*, 6(13), 9204–9212. Retrieved from https://doi.org/10.1021/acsomega.1c00556

Kim, D., Choi, J., Kim, G. J., Seol, S. K., Ha, Y. C., Vijayan, M., … Park, S. S. (2011). Microwave-accelerated energy-efficient esterification of free fatty acid with a heterogeneous catalyst. *Bioresource Technology*, 102(3), 3639–3641. Retrieved 19 November 2021 from https://doi.org/10.1016/j.biortech.2010.11.067

Kim, D., Choi, J., Kim, G. J., Seol, S. K., & Jung, S. (2011). Accelerated esterification of free fatty acid using pulsed microwaves. *Bioresource Technology*, 102(14), 7229–7231. Retrieved 19 November 2021 from https://doi.org/10.1016/J.BIORTECH.2011.04.074

Kim, D.-S., Hanifzadeh, M., & Kumar, A. (2018). Trend of biodiesel feedstock and its impact on biodiesel emission characteristics. *Environmental Progress & Sustainable Energy*, 37(1), 7–19. Retrieved from https://doi.org/10.1002/ep.12800

Kipcak, A. S., Senberber, F. T., Moroydor Derun, E., Tugrul, N., & Piskin, S. (2015). Characterization and thermal dehydration kinetics of zinc borates synthesized from zinc sulfate and zinc chloride. *Research on Chemical Intermediates*, 41(11), 9129–9143. Retrieved from https://doi.org/10.1007/s11164-015-1952-2

Kiss, A. A., Dimian, A. C., & Rothenberg, G. (2008). Biodiesel by Catalytic Reactive Distillation Powered by Metal Oxides. *Energy & Fuels*, 22(1), 598–604. Retrieved from https://doi.org/10.1021/ef700265y

Kivevele, T. T., Mbarawa, M. M., Bereczky, A., Laza, T., & Madarasz, J. (2011). Impact of antioxidant additives on the oxidation stability of biodiesel produced from *Croton Megalocarpus* oil. *Fuel Processing Technology*, 92(6), 1244–1248. Retrieved 11 March 2022 from https://doi.org/10.1016/J.FUPROC.2011.02.009

Koelsch, M., Cassaignon, S., Guillemoles, J. F., & Jolivet, J. P. (2002). Comparison of optical and electrochemical properties of anatase and brookite TiO_2 synthesized by the sol–gel method. *Thin Solid Films*, 403, 312–319. Retrieved from https://doi.org/10.1016/S0040-6090(01)01509-7

Köhler, J., & Wünsch, B. (2007). The allosteric modulation of lipases and its possible biological relevance. *Theoretical Biology and Medical Modelling*, 4(1), 34. Retrieved from https://doi.org/10.1186/1742-4682-4-34

Kolet, M., Zerbib, D., Nakonechny, F., & Nisnevitch, M. (2020). Production of Biodiesel from Brown Grease. *Catalysts*, 10(10), 1189. Retrieved from https://doi.org/10.3390/catal10101189

Konstantinou, I. K., & Albanis, T. A. (2003). Photocatalytic transformation of pesticides in aqueous titanium dioxide suspensions using artificial and solar light: intermediates and degradation pathways. *Applied Catalysis B: Environmental*, 42(4), 319–335. Retrieved 25 October 2021 from https://doi.org/10.1016/S0926-3373(02)00266-7

Konwar, L. J., Boro, J., & Deka, D. (2014). Review on latest developments in biodiesel production using carbon-based catalysts. *Renewable and Sustainable Energy Reviews*, 29, 546–564. Retrieved 10 November 2021 from https://doi.org/10.1016/J.RSER.2013.09.003

Korkut, I., & Bayramoglu, M. (2018). Selection of catalyst and reaction conditions for ultrasound assisted biodiesel production from canola oil. *Renewable Energy*, 116, 543–551. Retrieved 21 November 2022 from https://doi.org/10.1016/J.RENENE.2017.10.010

Kosera, V. S., Cruz, T. M., Chaves, E. S., & Tiburtius, E. R. L. (2017). Triclosan degradation by heterogeneous photocatalysis using ZnO immobilized in biopolymer as catalyst. *Journal of Photochemistry and Photobiology A: Chemistry*, 344, 184–191. Retrieved 27 June 2022 from https://doi.org/10.1016/J.JPHOTOCHEM.2017.05.014

Kothe, V., Melfi, D. T., dos Santos, K. C., Corazza, M. L., & Ramos, L. P. (2020). Thermodynamic analysis, experimental and kinetic modeling of levulinic acid esterification with ethanol at supercritical conditions. *Fuel*, 260, 116376. Retrieved 17 November 2021 from https://doi.org/10.1016/J.FUEL.2019.116376

Kouzu, M., Fujimori, A., Suzuki, T., Koshi, K., & Moriyasu, H. (2017). Industrial feasibility of powdery CaO catalyst for production of biodiesel. *Fuel Processing Technology*, 165, 94–101. Retrieved from https://doi.org/10.1016/j.fuproc.2017.05.014

Kralj, J. G., Sahoo, H. R., & Jensen, K. F. (2007). Integrated continuous microfluidic liquid–liquid extraction. *Lab Chip*, 7(2), 256–263. Retrieved from https://doi.org/10.1039/B610888A

Kulak, A. I., & Kiiliomin, D. A. (2018). Double bond system formation in the process of thermocatalytic dehydration of polyvinyl alcohol. *Doklady of the National Academy of Sciences of Belarus*, 62(5), 569–575. Retrieved from https://doi.org/10.29235/1561-8323-2018-62-5-569-575

Kulkarni, M. G., & Dalai, A. K. (2006). Waste Cooking OilAn Economical Source for Biodiesel: A Review. *Industrial & Engineering Chemistry Research*, 45(9), 2901–2913. Retrieved from https://doi.org/10.1021/ie0510526

Kurtoglu, M. E., Longenbach, T., & Gogotsi, Y. (2011). Preventing Sodium Poisoning of Photocatalytic TiO_2 Films on Glass by Metal Doping. *International Journal of Applied Glass Science*, 2(2), 108–116. Retrieved from https://doi.org/10.1111/j.2041-1294.2011.00040.x

Kusdiana, D., & Saka, S. (2001). Kinetics of transesterification in rapeseed oil to biodiesel fuel as treated in supercritical methanol. *Fuel*, 80(5), 693–698. Retrieved 11 November 2021 from https://doi.org/10.1016/S0016-2361(00)00140-X

Kusdiana, Dadan, & Saka, S. (2004). Effects of water on biodiesel fuel production by supercritical methanol treatment. *Bioresource Technology*, 91(3), 289–295. Retrieved 11 November 2021 from https://doi.org/10.1016/S0960-8524(03)00201-3

Laane, C., & Verhaert, R. (1987). Photochemical, electrochemical, and hydrogen-driven enzymatic reductions in reversed micelles. *Israel Journal of Chemistry*, 28(1), 17–22. Retrieved from https://doi.org/10.1002/ijch.198800005

Lai, Y., Wang, B., Chen, X., Yuan, Y., Zhong, L., Qiao, X., … Wang, P. (2014). Thermogravimetric analysis of combustion characteristics of palm oil and rapeseed oil biodiesel. *Biotechnology*, 14(1), 9–15. Retrieved from https://doi.org/10.3923/biotech.2015.9.15

Lan, Z., Zhao, C., Guo, W., Guan, X., & Zhang, X. (2015). Optimization of culture medium for maximal production of spinosad using an artificial neural network - genetic algorithm modeling. *Journal of Molecular Microbiology and Biotechnology*, 25(4), 253–261. Retrieved from https://doi.org/10.1159/000381312

Lapuerta, M., Rodríguez-Fernández, J., & Oliva, F. (2010). Determination of enthalpy of formation of methyl and ethyl esters of fatty acids. *Chemistry and Physics of Lipids*, 163(2), 172–181. Retrieved from https://doi.org/10.1016/j.chemphyslip.2009.11.002

Laszlo, J. A., & Evans, K. O. (2007). Influence of self-assembled monolayer surface chemistry on *Candida antarctica* lipase B adsorption and specific activity. *Journal of Molecular Catalysis B: Enzymatic*, 48(3–4), 84–89. Retrieved 23 September 2021 from https://doi.org/10.1016/J.MOLCATB.2007.06.010

Laura Cassiday. (2018). *Comparison of fatty acid profiles*. Retrieved 15 November 2021 from https://www.informmagazine-digital.org/informmagazine/april_2018/MobilePagedArticle.action?articleId=1367747#articleId1367747

Lax, P. D. (2007). Computational fluid dynamics. *Journal of Scientific Computing*, 31(1–2), 185–193. Retrieved from https://doi.org/10.1007/s10915-006-9104-x

Leadbeater, N. E., & Stencel, L. M. (2006). Fast, easy preparation of biodiesel using microwave heating. *Energy and Fuels*, 20(5), 2281–2283. Retrieved 11 November 2021 from https://doi.org/10.1021/EF060163U

Lee, H. v., Juan, J. C., & Taufiq-Yap, Y. H. (2015). Preparation and application of binary acid-base CaO-La_2O_3 catalyst for biodiesel production. *Renewable Energy*, 74, 124–132. Retrieved 11 November 2021 from https://doi.org/10.1016/j.renene.2014.07.017

Leung, D. Y. C., Wu, X., & Leung, M. K. H. (2010). A review on biodiesel production using catalyzed transesterification. *Applied Energy*, 87(4), 1083–1095. Retrieved 10 November 2021 from https://doi.org/10.1016/J.APENERGY.2009.10.006

Li, G., Richter, C. P., Milot, R. L., Cai, L., Schmuttenmaer, C. A., Crabtree, R. H., … Batista, V. S. (2009). Synergistic effect between anatase and rutile TiO_2 nanoparticles in dye-sensitized solar cells. *Dalton Transactions*, 1(45), 10078–10085. Retrieved from https://doi.org/10.1039/B908686B

Liavitskaya, T., & Vyazovkin, S. (2016). Discovering the kinetics of thermal decomposition during continuous cooling. *Physical Chemistry Chemical Physics*, 18(47), 32021–32030. Retrieved from https://doi.org/10.1039/C6CP04507C

Lin, R., Ma, X., Fielitz, T. R., Obare, S. O., & Ofoli, R. Y. (2012). Facile hydrogenation of carbon-carbon double bonds using catalytic noble nanoparticles immobilized in microfluidic reactors. *Catalysis Communications*, 18, 168–175. Retrieved from https://doi.org/10.1016/j.catcom.2011.12.002

Liu, J., Chen, G., Yan, B., Yi, W., & Yao, J. (2022). Biodiesel production in a magnetically fluidized bed reactor using whole-cell biocatalysts immobilized within ferroferric oxide-polyvinyl alcohol composite beads. *Bioresource Technology*, 355, 127253. Retrieved 8 July 2022 from https://doi.org/10.1016/J.BIORTECH.2022.127253

Liu, L., Liu, Z., Tang, G., & Tan, W. (2014). Esterification of free fatty acids in waste cooking oil by heterogeneous catalysts. *Transactions of Tianjin University*, 20(4), 266–272. Retrieved from https://doi.org/10.1007/s12209-014-2242-6

Lokman, I. M., Goto, M., Rashid, U., & Taufiq-Yap, Y. H. (2016). Sub- and supercritical esterification of palm fatty acid distillate with carbohydrate-derived solid acid catalyst. *Chemical Engineering Journal*, 284, 872–878. Retrieved 17 November 2021 from https://doi.org/10.1016/J.CEJ.2015.08.102

Long, Y. D., Fang, Z., Su, T. C., & Yang, Q. (2014). Co-production of biodiesel and hydrogen from rapeseed and *Jatropha* oils with sodium silicate and Ni catalysts. *Applied Energy*, 113, 1819–1825. Retrieved 10 November 2021 from https://doi.org/10.1016/J.APENERGY.2012.12.076

Lotero, E., Liu, Y., Lopez, D. E., Suwannakarn, K., Bruce, D. A., & Goodwin, J. G. (2005). Synthesis of Biodiesel via Acid Catalysis. *Industrial & Engineering Chemistry Research*, 44(14), 5353–5363. Retrieved from https://doi.org/10.1021/ie049157g

Lu, H., Schmidt, M. A., & Jensen, K. F. (2001). Photochemical reactions and on-line UV detection in microfabricated reactors. *Lab on a Chip*, 1(1), 22–28. Retrieved from https://doi.org/10.1039/b104037p

Lu, J. J., & Chen, W. H. (2015). Investigation on the ignition and burnout temperatures of bamboo and sugarcane bagasse by thermogravimetric analysis. *Applied Energy*, 160, 49–57. Retrieved 11 March 2022 from https://doi.org/10.1016/J.APENERGY.2015.09.026

Lukić, I., Kesić, Ž., Maksimović, S., Zdujić, M., Liu, H., Krstić, J., & Skala, D. (2013). Kinetics of sunflower and used vegetable oil methanolysis catalyzed by CaO·ZnO. *Fuel*, 113, 367–378. Retrieved 25 February 2022 from https://doi.org/10.1016/J.FUEL.2013.05.093

Lukić, I., Kesić, Ž., & Skala, D. (2014). Kinetics of heterogeneous biodiesel synthesis using supported ZnO as catalyst. *Chemical Engineering & Technology*, 37(11), 1879–1884.

Retrieved from https://doi.org/10.1002/ceat.201300714

Lukić, M., & Vrsaljko, D. (2021). Effect of channel dimension on biodiesel yield in millireactors produced by stereolithography. *International Journal of Green Energy*, 18(2), 156–165. Retrieved from https://doi.org/10.1080/15435075.2020.1831513

Luttrell, T., Halpegamage, S., Tao, J., Kramer, A., Sutter, E., & Batzill, M. (2015). Why is anatase a better photocatalyst than rutile? - Model studies on epitaxial TiO_2 films. *Scientific Reports*, 4(1), 4043. Retrieved from https://doi.org/10.1038/srep04043

M. Canakci, & J. Van Gerpen. (2001). Biodiesel production from oils and fats with high free fatty acids. *Transactions of the ASAE*, 44(6), 1429–1436. Retrieved from https://doi.org/10.13031/2013.7010

Ma, F., & Hanna, M. A. (1999). Biodiesel production: A review. *Bioresource Technology*, 70(1), 1–15. Retrieved 11 November 2021 from https://doi.org/10.1016/S0960-8524(99)00025-5

Macario, A., Giordano, G., Onida, B., Cocina, D., Tagarelli, A., & Giuffrè, A. M. (2010). Biodiesel production process by homogeneous/heterogeneous catalytic system using an acid–base catalyst. *Applied Catalysis A: General*, 378(2), 160–168. Retrieved 21 November 2021 from https://doi.org/10.1016/J.APCATA.2010.02.016

Macrae, A. R., & Hammond, R. C. (1985). Present and future applications of lipases. *Biotechnology and Genetic Engineering Reviews*, 3(1), 193–217. Retrieved from https://doi.org/10.1080/02648725.1985.10647813

Makuła, P., Pacia, M., & Macyk, W. (2018). How to correctly determine the band gap energy of modified semiconductor photocatalysts based on UV–Vis spectra. *The Journal of Physical Chemistry Letters*, 9(23), 6814–6817. Retrieved from https://doi.org/10.1021/acs.jpclett.8b02892

Maneerung, T., Kawi, S., Dai, Y., & Wang, C.-H. (2016). Sustainable biodiesel production via transesterification of waste cooking oil by using CaO catalysts prepared from chicken manure. *Energy Conversion and Management*, 123, 487–497. Retrieved from https://doi.org/10.1016/j.enconman.2016.06.071

Manique, M. C., Silva, A. P., Alves, A. K., & Bergmann, C. P. (2016). Application of hydrothermally produced TiO_2 nanotubes in photocatalytic esterification of oleic acid. *Materials Science and Engineering: B*, 206, 17–21. Retrieved 7 September 2021 from https://doi.org/10.1016/J.MSEB.2016.01.001

Mansir, N., Teo, S. H., Mijan, N. A., & Taufiq-Yap, Y. H. (2021). Efficient reaction for biodiesel manufacturing using bi-functional oxide catalyst. *Catalysis Communications*, 149, 106201. Retrieved 22 November 2021 from https://doi.org/10.1016/J.CATCOM.2020.106201

Manuale, D. L., Torres, G. C., Vera, C. R., & Yori, J. C. (2015). Study of an energy-integrated biodiesel production process using supercritical methanol and a low-cost feedstock. *Fuel Processing Technology*, 140, 252–261. Retrieved 6 July 2022 from https://doi.org/10.1016/J.FUPROC.2015.08.026

Mardhiah, H. H., Ong, H. C., Masjuki, H. H., Lim, S., & Lee, H. v. (2017). A review on latest developments and future prospects of heterogeneous catalyst in biodiesel production from non-edible oils. *Renewable and Sustainable Energy Reviews*, 67, 1225–1236. Retrieved 10 November 2021 from https://doi.org/10.1016/J.RSER.2016.09.036

Mardhiah, H. H., Ong, H. C., Masjuki, H. H., Lim, S., & Pang, Y. L. (2017). Investigation of carbon-based solid acid catalyst from Jatropha curcas biomass in biodiesel production. *Energy Conversion and Management*, 144, 10–17. Retrieved 11 November 2021 from https://doi.org/10.1016/j.enconman.2017.04.038

Martínez Arias, E. L., Fazzio Martins, P., Jardini Munhoz, A. L., Gutierrez-Rivera, L., & Maciel Filho, R. (2012). Continuous synthesis and in situ monitoring of biodiesel production in different microfluidic devices. *Industrial & Engineering Chemistry Research*, 51(33), 10755–10767. Retrieved from https://doi.org/10.1021/ie300486v

Marton, Z., Léonard-Nevers, V., Syrén, P.-O., Bauer, C., Lamare, S., Hult, K., … Graber, M. (2010). Mutations in the stereospecificity pocket and at the entrance of the active site of *Candida Antarctica* lipase B enhancing enzyme enantioselectivity. *Journal of Molecular Catalysis B: Enzymatic*, 65(1–4), 11–17. Retrieved from https://doi.org/10.1016/j.molcatb.2010.01.007

Marulanda, V. F., Anitescu, G., & Tavlarides, L. L. (2010a). Biodiesel Fuels through a Continuous Flow Process of Chicken Fat Supercritical Transesterification. *Energy & Fuels*, 24(1), 253–260. Retrieved from https://doi.org/10.1021/ef900782v

Marulanda, V. F., Anitescu, G., & Tavlarides, L. L. (2010b). Investigations on supercritical transesterification of chicken fat for biodiesel production from low-cost lipid feedstocks. *The Journal of Supercritical Fluids*, 54(1), 53–60. Retrieved 6 July 2022 from https://doi.org/10.1016/J.SUPFLU.2010.04.001

Maser, J. (2001). Soft X-rays and extreme ultraviolet radiation: principles and application. *Microscopy and Microanalysis*, 7(6), 536. Retrieved 3 January 2022 from https://doi.org/10.1007/S10005-001-0023-1

Mazutis, L., Vasiliauskas, R., & Weitz, D. A. (2015). Microfluidic production of alginate hydrogel particles for antibody encapsulation and release. *Macromolecular Bioscience*, 15(12), 1641–1646. Retrieved from https://doi.org/10.1002/mabi.201500226

McCurry, J. D. (2012). *GC analysis of total fatty acid methyl esters (FAME) and methyl linolenate in biodiesel using the revised EN14103:2011 method*. *Agilent Technologies*.

McPherson, J. W., Kim, J., Shanware, A., Mogul, H., & Rodriguez, J. (2003). Trends in the ultimate breakdown strength of high dielectric-constant materials. *IEEE Transactions on*

Electron Devices, 50(8), 1771–1778. Retrieved from https://doi.org/10.1109/TED.2003.815141

Meher, L. C., Churamani, C. P., Arif, M., Ahmed, Z., & Naik, S. N. (2013). *Jatropha curcas* as a renewable source for bio-fuels - A review. *Renewable and Sustainable Energy Reviews*, 26, 397–407. Retrieved 11 November 2021 from https://doi.org/10.1016/j.rser.2013.05.065

Micic, O. I., Zhang, Y., Cromack, K. R., Trifunac, A. D., & Thurnauer, M. C. (1993). Trapped holes on titania colloids studied by electron paramagnetic resonance. *The Journal of Physical Chemistry*, 97(28), 7277–7283. Retrieved from https://doi.org/10.1021/j100130a026

Mihankhah, T., Delnavaz, M., & Khaligh, N. G. (2018). Application of TiO_2 nanoparticles for eco-friendly biodiesel production from waste olive oil. *International Journal of Green Energy*, 15(2), 69–75. Retrieved from https://doi.org/10.1080/15435075.2018.1423975

Milano, J., Ong, H. C., Masjuki, H. H., Silitonga, A. S., Chen, W.-H., Kusumo, F., … Sebayang, A. H. (2018). Optimization of biodiesel production by microwave irradiation-assisted transesterification for waste cooking oil-*Calophyllum* inophyllum oil via response surface methodology. *Energy Conversion and Management*, 158, 400–415. Retrieved from https://doi.org/10.1016/j.enconman.2017.12.027

Mo, Y., & Jensen, K. F. (2016). A miniature CSTR cascade for continuous flow of reactions containing solids. *Reaction Chemistry & Engineering*, 1(5), 501–507. Retrieved from https://doi.org/10.1039/C6RE00132G

Mofijur, M., Rasul, M. G., Hassan, N. M. S., Masjuki, H. H., Kalam, M. A., & Mahmudul, H. M. (2017). Assessment of physical, chemical, and tribological properties of different biodiesel fuels. In *Clean Energy for Sustainable Development - Chapter 14* (Vol. 1, pp. 441–463). Elsevier. Retrieved from https://doi.org/10.1016/B978-0-12-805423-9.00014-4

Mohadesi, M., Aghel, B., Maleki, M., & Ansari, A. (2019). Production of biodiesel from waste cooking oil using a homogeneous catalyst: Study of semi-industrial pilot of microreactor. *Renewable Energy*, 136, 677–682. Retrieved 7 September 2021 from https://doi.org/10.1016/J.RENENE.2019.01.039

Mohadesi, M., Aghel, B., Maleki, M., & Ansari, A. (2020a). Study of the transesterification of waste cooking oil for the production of biodiesel in a microreactor pilot: The effect of acetone as the co-solvent. *Fuel*, 273, 117736. Retrieved 27 June 2022 from https://doi.org/10.1016/J.FUEL.2020.117736

Mohadesi, M., Aghel, B., Maleki, M., & Ansari, A. (2020b). The use of KOH/Clinoptilolite catalyst in pilot of microreactor for biodiesel production from waste cooking oil. *Fuel*, 263, 116659. Retrieved 27 June 2022 from https://doi.org/10.1016/J.FUEL.2019.116659

Mohadesi, M., Gouran, A., & Dehghan Dehnavi, A. (2021). Biodiesel production using low cost material as high effective catalyst in a microreactor. *Energy*, 219, 119671. Retrieved 27 June 2022 from https://doi.org/10.1016/J.ENERGY.2020.119671

Mohammad Fauzi, A. H., & Saidina Amin, N. A. (2013). Optimization of oleic acid esterification catalyzed by ionic liquid for green biodiesel synthesis. *Energy Conversion and Management*, 76, 818–827. Retrieved 2 November 2021 from https://doi.org/10.1016/J.ENCONMAN.2013.08.029

Monti, S., & Walsh, T. R. (2010). Free energy calculations of the adsorption of amino acid analogues at the aqueous titania interface. *Journal of Physical Chemistry C*, 114(50), 22197–22206. Retrieved from https://doi.org/10.1021/jp107859q

Moradi, P., Saidi, M., & Najafabadi, A. T. (2021). Biodiesel production via esterification of oleic acid as a representative of free fatty acid using electrolysis technique as a novel approach: Non-catalytic and catalytic conversion. *Process Safety and Environmental Protection*, 147, 684–692. Retrieved 10 September 2021 from https://doi.org/10.1016/J.PSEP.2020.12.032

Mostafa Marzouk, N., Abo El Naga, A. O., Younis, S. A., Shaban, S. A., el Torgoman, A. M., & el Kady, F. Y. (2021). Process optimization of biodiesel production via esterification of oleic acid using sulfonated hierarchical mesoporous ZSM-5 as an efficient heterogeneous catalyst. *Journal of Environmental Chemical Engineering*, 9(2), 105035. Retrieved 13 October 2021 from https://doi.org/10.1016/J.JECE.2021.105035

Mostafa, S. S. M., & El-Gendy, N. S. (2017). Evaluation of fuel properties for microalgae *Spirulina platensis* bio-diesel and its blends with Egyptian petro-diesel. *Arabian Journal of Chemistry*, 10, S2040–S2050. Retrieved 11 March 2022 from https://doi.org/10.1016/J.ARABJC.2013.07.034

Motegh, M., van Ommen, J. R., Appel, P. W., & Kreutzer, M. T. (2014). Scale-up study of a multiphase photocatalytic reactor—degradation of cyanide in water over TiO_2. *Environmental Science & Technology*, 48(3), 1574–1581. Retrieved from https://doi.org/10.1021/es403378e

Mudunkotuwa, I. A., & Grassian, V. H. (2014). Histidine adsorption on TiO_2 nanoparticles: An integrated spectroscopic, thermodynamic, and molecular-based approach toward understanding Nano–Bio interactions. *Langmuir*, 30(29), 8751–8760. Retrieved from https://doi.org/10.1021/la500722n

Mukhopadhyay, A., Dasgupta, A. K., Chattopadhyay, D., & Chakrabarti, K. (2012). Improvement of thermostability and activity of *pectate lyase* in the presence of hydroxyapatite nanoparticles. *Bioresource Technology*, 116, 348–354. Retrieved 23 September 2021 from https://doi.org/10.1016/J.BIORTECH.2012.03.094

Naik, C. v., Westbrook, C. K., Herbinet, O., Pitz, W. J., & Mehl, M. (2011). Detailed chemical kinetic reaction mechanism for biodiesel components methyl stearate and methyl oleate.

Proceedings of the Combustion Institute, 33(1), 383–389. Retrieved 29 April 2022 from https://doi.org/10.1016/J.PROCI.2010.05.007

Narayan, R. C., & Madras, G. (2017). Esterification of sebacic acid in near-critical and supercritical methanol. *Industrial and Engineering Chemistry Research*, 56(10), 2641–2649. Retrieved 13 November 2021 from https://doi.org/10.1021/ACS.IECR.6B04769

Narenji-Sani, F., Tayebee, R., & Chahkandi, M. (2020). New task-specific and reusable ZIF-like grafted H6P2W18O62 catalyst for the effective esterification of free fatty acids. *ACS Omega*, 5(17), 9999–10010. Retrieved from https://doi.org/10.1021/acsomega.0c00358

Nasiri, R., Shamloo, A., Akbari, J., Tebon, P., R. Dokmeci, M., & Ahadian, S. (2020). Design and simulation of an integrated centrifugal microfluidic device for CTCs separation and cell Lysis. *Micromachines*, 11(7), 699. Retrieved from https://doi.org/10.3390/mi11070699

Neethirajan, S., Kobayashi, I., Nakajima, M., Wu, D., Nandagopal, S., & Lin, F. (2011). Microfluidics for food, agriculture and biosystems industries. *Lab on a Chip*, 11(9), 1574. Retrieved from https://doi.org/10.1039/c0lc00230e

Netto, C. G. C. M., Toma, H. E., & Andrade, L. H. (2013). Superparamagnetic nanoparticles as versatile carriers and supporting materials for enzymes. *Journal of Molecular Catalysis B: Enzymatic*, 85–86, 71–92. Retrieved 1 December 2021 from https://doi.org/10.1016/j.molcatb.2012.08.010

Nguyen, H. C., Wang, F. M., Dinh, K. K., Pham, T. T., Juan, H. Y., Nguyen, N. P., … Su, C. H. (2020). Microwave-assisted noncatalytic esterification of fatty acid for biodiesel production: A kinetic study. *Energies*, 13(9), 2167. Retrieved 13 November 2021 from https://doi.org/10.3390/EN13092167

Nicolau, C., Klein, A., Silva, C., Fiorucci, A., Stropa, J., Santos, E., … Simionatto, E. (2018). Thermal properties of the blends of methyl and ethyl esters prepared from babassu and soybean oils. *Journal of the Brazilian Chemical Society*, 29(8), 1672–1679. Retrieved from https://doi.org/10.21577/0103-5053.20180040

Nieva-Echevarría, B., Goicoechea, E., Manzanos, M. J., & Guillén, M. D. (2015). Usefulness of 1H NMR in assessing the extent of lipid digestion. *Food Chemistry*, 179, 182–190. Retrieved from https://doi.org/10.1016/j.foodchem.2015.01.104

Nigam, P. S., & Singh, A. (2011). Production of liquid biofuels from renewable resources. *Progress in Energy and Combustion Science*, 37(1), 52–68. Retrieved 11 November 2021 from https://doi.org/10.1016/j.pecs.2010.01.003

Noureddini, H., & Zhu, D. (1997). Kinetics of transesterification of soybean oil. *Journal of the American Oil Chemists' Society*, 74(11), 1457–1463. Retrieved from https://doi.org/10.1007/s11746-997-0254-2

Oelgemöller, M. (2016). Solar photochemical synthesis: from the beginnings of organic photochemistry to the solar manufacturing of commodity chemicals. *Chemical Reviews*, 116(17), 9664–9682. Retrieved from https://doi.org/10.1021/acs.chemrev.5b00720

Oelgemöller, M., Hoffmann, N., & Shvydkiv, O. (2014). From 'Lab & Light on a Chip' to Parallel Microflow Photochemistry. *Australian Journal of Chemistry*, 67(3), 337. Retrieved from https://doi.org/10.1071/CH13591

Ogunkunle, O., & Ahmed, N. A. (2019). A review of global current scenario of biodiesel adoption and combustion in vehicular diesel engines. *Energy Reports*, 5, 1560–1579. Retrieved 7 September 2021 from https://doi.org/10.1016/J.EGYR.2019.10.028

Ohtani, B. (2011). Photocatalysis by inorganic solid materials: Revisiting its definition, concepts, and experimental procedures. *Advances in Inorganic Chemistry*, 63, 395–430. Retrieved 20 October 2021 from https://doi.org/10.1016/B978-0-12-385904-4.00001-9

Oil World. (2022). Oil World. Retrieved 14 April 2022, from https://www.oilworld.biz/

Oliveira, A. F., Bastos, R. G., & de la Torre, L. G. (2019). *Bacillus subtilis* immobilization in alginate microfluidic-based microparticles aiming to improve lipase productivity. *Biochemical Engineering Journal*, 143, 110–120. Retrieved from https://doi.org/10.1016/j.bej.2018.12.014

Oliveira Palm, M., Luchetti Alves de Freitas Barbosa, S., Wilgen Gonçalves, M., Duarte, D. A., de Camargo Catapan, R., & Silva de Carvalho Pinto, C. R. (2022). Plasma-assisted catalytic route for transesterification reactions at room temperature. *Fuel*, 307, 121740. Retrieved 19 November 2021 from https://doi.org/10.1016/J.FUEL.2021.121740

Olutoye, M. A., & Hameed, B. H. (2011). Synthesis of fatty acid methyl ester from crude *jatropha* (*Jatropha curcas Linnaeus*) oil using aluminium oxide modified Mg-Zn heterogeneous catalyst. *Bioresource Technology*, 102(11), 6392–6398. Retrieved 11 November 2021 from https://doi.org/10.1016/j.biortech.2011.03.039

Omo Ibhadon, A., & Fitzpatrick, P. (2013). Heterogeneous photocatalysis: recent advances and applications. *Catalysts*, 3, 189–218. Retrieved from https://doi.org/10.3390/catal3010189

Ong, H. C., Tiong, Y. W., Goh, B. H. H., Gan, Y. Y., Mofijur, M., Fattah, I. M. R., … Mahlia, T. M. I. (2021). Recent advances in biodiesel production from agricultural products and microalgae using ionic liquids: Opportunities and challenges. *Energy Conversion and Management*, 228, 113647. Retrieved 9 November 2021 from https://doi.org/10.1016/J.ENCONMAN.2020.113647

Onu, P., & Mbohwa, C. (2021). New approach and prospects of agrowaste resources conversion for energy systems performance and development. *Agricultural Waste Diversity and Sustainability Issues*, 97–118. Retrieved 22 August 2022 from https://doi.org/10.1016/B978-0-323-85402-3.00007-3

Osmont, A., Catoire, L., & Gökalp, I. (2007). Thermochemistry of methyl and ethyl esters from vegetable oils. *International Journal of Chemical Kinetics*, 39(9), 481–491. Retrieved from https://doi.org/10.1002/kin.20264

Otero, C., Ballesteros, A., & Guisán, J. M. (1988). Immobilization/stabilization of lipase from *Candida rugosa*. *Applied Biochemistry and Biotechnology*, 19(2), 163–175. Retrieved from https://doi.org/10.1007/BF02921481

Ould Brahim, I., Belmedani, M., Hadoun, H., & Belgacem, A. (2021). The photocatalytic degradation kinetics of food dye in aqueous solution under UV/ZnO system. *Reaction Kinetics, Mechanisms and Catalysis*, 133(2), 1075–1095. Retrieved from https://doi.org/10.1007/s11144-021-02006-8

Pantaleone, S., Rimola, A., & Sodupe, M. (2017). Canonical, deprotonated, or zwitterionic? A Computational study on amino acid interaction with the TiO_2 (101) anatase surface. *Journal of Physical Chemistry C*, 121(26), 14156–14165. Retrieved from https://doi.org/10.1021/acs.jpcc.7b03305

Parandi, E., Safaripour, M., Abdellattif, M. H., Saidi, M., Bozorgian, A., Rashidi Nodeh, H., & Rezania, S. (2022). Biodiesel production from waste cooking oil using a novel biocatalyst of lipase enzyme immobilized magnetic nanocomposite. *Fuel*, 313, 123057. Retrieved 8 July 2022 from https://doi.org/10.1016/J.FUEL.2021.123057

Pászti, Z., & Guczi, L. (2009). Amino acid adsorption on hydrophilic TiO_2: A sum frequency generation vibrational spectroscopy study. *Vibrational Spectroscopy*, 50(1), 48–56. Retrieved from https://doi.org/10.1016/J.VIBSPEC.2008.07.014

Patel, A., & Brahmkhatri, V. (2013). Kinetic study of oleic acid esterification over 12-tungstophosphoric acid catalyst anchored to different mesoporous silica supports. *Fuel Processing Technology*, 113, 141–149. Retrieved 15 October 2021 from https://doi.org/10.1016/J.FUPROC.2013.03.022

Patil, P. D., Gude, V. G., & Deng, S. (2010). Transesterification of *camelina sativa* oil using supercritical and subcritical methanol with cosolvents. *Energy and Fuels*, 24(2), 746–751. Retrieved 13 November 2021 from https://doi.org/10.1021/EF900854H

Pavlović, S., Šelo, G., Marinković, D., Planinić, M., Tišma, M., & Stanković, M. (2021). Transesterification of sunflower oil over waste chicken eggshell-based catalyst in a microreactor: An optimization study. *Micromachines*, 12(2), 120. Retrieved from https://doi.org/10.3390/mi12020120

Pawar, M., Topcu Sendoğdular, S., & Gouma, P. (2018). A brief overview of TiO_2 photocatalyst for organic dye demediation: Case study of reaction mechanisms involved in Ce-TiO_2 photocatalysts system. *Journal of Nanomaterials*, 2018, 1–13. Retrieved from https://doi.org/10.1155/2018/5953609

Peirce, S., Tacias-Pascacio, V. G., Russo, M. E., Marzocchella, A., Virgen-Ortíz, J. J., & Fernandez-Lafuente, R. (2016). Stabilization of *Candida antarctica* Lipase B (CALB) immobilized on octyl agarose by treatment with polyethyleneimine (PEI). *Molecules*, 21(6), 751. Retrieved from https://doi.org/10.3390/molecules21060751

Perego, C., & Bosetti, A. (2011). Biomass to fuels: The role of zeolite and mesoporous materials. *Microporous and Mesoporous Materials*, 144(1–3), 28–39. Retrieved 10 November 2021 from https://doi.org/10.1016/J.MICROMESO.2010.11.034

Pereira, C. O., Portilho, M. F., Henriques, C. A., & Zotin, F. M. Z. (2014). $SnSO_4$ as catalyst for simultaneous transesterification and esterification of acid soybean oil. *Journal of the Brazilian Chemical Society*, 2409–2416. Retrieved from https://doi.org/10.5935/0103-5053.20140267

Pettibone, J. M., Cwiertny, D. M., Scherer, M., & Grassian, V. H. (2008). Adsorption of organic acids on TiO_2 nanoparticles: effects of pH, nanoparticle size, and nanoparticle aggregation. *Langmuir*, 24(13), 6659–6667. Retrieved from https://doi.org/10.1021/la7039916

Praneeth, N. V. S., & Paria, S. (2020). Clay-supported anisotropic Au-modified N,S-doped TiO_2 nanoparticles for enhanced photocatalytic dye degradation and esterification reactions. *New Journal of Chemistry*, 44(6), 2619–2629. Retrieved from https://doi.org/10.1039/C9NJ05306A

Prasanna Rani, K. N., Ramana Neeharika, T. S. V., Kumar, T. P., Satyavathi, B., & Sailu, C. (2016). Kinetics of non-catalytic esterification of free fatty acids present in *Jatropha* oil. *Journal of Oleo Science*, 65(5), 441–445. Retrieved from https://doi.org/10.5650/jos.ess15255

Prasertpong, P., Jaroenkhasemmeesuk, C., Regalbuto, J. R., Lipp, J., & Tippayawong, N. (2020). Optimization of process variables for esterification of bio-oil model compounds by a heteropolyacid catalyst. *Energy Reports*, 6, 1–9. Retrieved 2 November 2021 from https://doi.org/10.1016/J.EGYR.2019.11.026

Priecel, P., & Lopez-Sanchez, J. A. (2019). Advantages and limitations of microwave reactors: from chemical synthesis to the catalytic valorization of biobased chemicals. *ACS Sustainable Chemistry & Engineering*, 7(1), 3–21. Retrieved from https://doi.org/10.1021/acssuschemeng.8b03286

Pruszko, R. (2020). Biodiesel production. In *Bioenergy - Chapter 23* (Vol. 1, pp. 491–514). Academic Press. Retrieved 15 November 2021 from https://doi.org/10.1016/B978-0-12-815497-7.00023-3

Pugnet, V., Maury, S., Coupard, V., Dandeu, A., Quoineaud, A. A., Bonneau, J. L., & Tichit, D. (2010). Stability, activity and selectivity study of a zinc aluminate heterogeneous catalyst for the transesterification of vegetable oil in batch reactor. *Applied Catalysis A: General*, 374(1–2), 71–78. Retrieved 28 February 2022 from https://doi.org/10.1016/J.APCATA.2009.11.028

Qadeer, M. U., Ayoub, M., Komiyama, M., Khan Daulatzai, M. U., Mukhtar, A., Saqib, S., … Bokhari, A. (2021). Review of biodiesel synthesis technologies, current trends, yield influencing factors and economical analysis of supercritical process. *Journal of Cleaner Production*, 309, 127388. Retrieved 17 November 2021 from https://doi.org/10.1016/J.JCLEPRO.2021.127388

Qu, S., Chen, C., Guo, M., Jiang, W., Lu, J., Yi, W., & Ding, J. (2021). Microwave-assisted in-situ transesterification of Spirulina platensis to biodiesel using PEG/MgO/ZSM-5 magnetic catalyst. *Journal of Cleaner Production*, 311, 127490. Retrieved 6 July 2022 from https://doi.org/10.1016/J.JCLEPRO.2021.127490

Quantachrome Instruments. (2009). Gas sorption system operating manual. Boynton Beach: Quantachrome Instruments.

Rabiah Nizah, M. F., Taufiq-Yap, Y. H., Rashid, U., Teo, S. H., Shajaratun Nur, Z. A., & Islam, A. (2014). Production of biodiesel from non-edible *Jatropha curcas* oil via transesterification using Bi_2O_3-La_2O_3 catalyst. *Energy Conversion and Management*, 88, 1257–1262. Retrieved 11 November 2021 from https://doi.org/10.1016/j.enconman.2014.02.072

Rachman, S. A., Komariah, L. N., Andwikaputra, A. I., & Umbara, N. B. (2018). High conversion and yield of biodiesel using electrolysis method. *Journal of Physics: Conference Series*, 1095(1), 012040. Retrieved 19 November 2021 from https://doi.org/10.1088/1742-6596/1095/1/012040

Rade, L. L., Lemos, C. O. T., Barrozo, M. A. S., Ribas, R. M., Monteiro, R. S., & Hori, C. E. (2018). Optimization of continuous esterification of oleic acid with ethanol over niobic acid. *Renewable Energy*, 115, 208–216. Retrieved 2 November 2021 from https://doi.org/10.1016/J.RENENE.2017.08.035

Rafati, A., Tahvildari, K., & Nozari, M. (2019). Production of biodiesel by electrolysis method from waste cooking oil using heterogeneous MgO-NaOH nano catalyst. *Energy Sources, Part A: Recovery, Utilization, and Environmental Effects*, 41(9), 1062–1074. Retrieved from https://doi.org/10.1080/15567036.2018.1539139

Rahimi, M., Aghel, B., Alitabar, M., Sepahvand, A., & Ghasempour, H. R. (2014). Optimization of biodiesel production from soybean oil in a microreactor. *Energy Conversion and Management*, 79, 599–605. Retrieved 22 November 2021 from https://doi.org/10.1016/j.enconman.2013.12.065

Rahimi, M., Mohammadi, F., Basiri, M., Parsamoghadam, M. A., & Masahi, M. M. (2016). Transesterification of soybean oil in four-way micromixers for biodiesel production using a cosolvent. *Journal of the Taiwan Institute of Chemical Engineers*, 64, 203–210. Retrieved 5 January 2022 from https://doi.org/10.1016/J.JTICE.2016.04.023

Rahul Soosai, M., Moorthy, I. M. G., Varalakshmi, P., & Yonas, C. J. (2022). Integrated global optimization and process modelling for biodiesel production from non-edible silk-cotton seed oil by microwave-assisted transesterification with heterogenous calcium oxide catalyst. *Journal of Cleaner Production*, 367, 132946. Retrieved 6 July 2022 from https://doi.org/10.1016/J.JCLEPRO.2022.132946

Raj, K., & Viswanathan, B. (2009). Effect of surface area, pore volume and particle size of P25 titania on the phase transformation of anatase to rutile. *Indian Journal of Chemistry - Section A Inorganic, Physical, Theoretical and Analytical Chemistry*, 48, 1378–1382.

Rajarshi Kar, Oindrila Gupta, Kunal Mandol, & Sangita Bhattacharjee. (2012). Performance study on photocatalysis of phenol solution in a UV irradiated reactor. *Journal of Chemical Engineering & Process Technology*, 4(1), 1000143. Retrieved from https://doi.org/10.4172/2157-7048.1000143

Rajeshwar, K., Osugi, M. E., Chanmanee, W., Chenthamarakshan, C. R., Zanoni, M. V. B., Kajitvichyanukul, P., & Krishnan-Ayer, R. (2008). Heterogeneous photocatalytic treatment of organic dyes in air and aqueous media. *Journal of Photochemistry and Photobiology C: Photochemistry Reviews*, 9(4), 171–192. Retrieved 26 December 2021 from https://doi.org/10.1016/J.JPHOTOCHEMREV.2008.09.001

Ramachandran, K., Sivakumar, P., Suganya, T., & Renganathan, S. (2011). Production of biodiesel from mixed waste vegetable oil using an aluminium hydrogen sulphate as a heterogeneous acid catalyst. *Bioresource Technology*, 102(15), 7289–7293. Retrieved 10 November 2021 from https://doi.org/10.1016/J.BIORTECH.2011.04.100

Ramos, B., Ookawara, S., Matsushita, Y., & Yoshikawa, S. (2014). Low-cost polymeric photocatalytic microreactors: Catalyst deposition and performance for phenol degradation. *Journal of Environmental Chemical Engineering*, 2(3), 1487–1494. Retrieved from https://doi.org/10.1016/j.jece.2014.06.022

Razzaq, T., & Kappe, C. O. (2008). On the energy efficiency of microwave-assisted organic reactions. *ChemSusChem*, 1(1–2), 123–132. Retrieved 17 November 2021 from https://doi.org/10.1002/CSSC.200700036

Reetz, M. T., Zonta, A., Vijayakrishnan, V., & Schimossek, K. (1998). Entrapment of lipases in hydrophobic magnetite-containing sol-gel materials: magnetic separation of heterogeneous biocatalysts. *Journal of Molecular Catalysis A: Chemical*, 134(1–3), 251–258. Retrieved 1 December 2021 from https://doi.org/10.1016/S1381-1169(98)00043-0

Reis, P., Holmberg, K., Miller, R., Leser, M. E., Raab, T., & Watzke, H. J. (2009). Lipase reaction at interfaces as self-limiting processes. *C. R Chimie*, 163–170. Retrieved from https://doi.org/10.1016/j.crci.2008.04.018

Reyes-Coronado, D., Rodríguez-Gattorno, G., Espinosa-Pesqueira, M. E., Cab, C., de Coss, R. D., & Oskam, G. (2008). Phase-pure TiO_2 nanoparticles: anatase, brookite and rutile. *Nanotechnology*, 19(14), 145605. Retrieved from https://doi.org/https://doi.org/10.1088/0957-4484/19/14/145605

Roberge, D. M., Ducry, L., Bieler, N., Cretton, P., & Zimmermann, B. (2005). Microreactor technology: A revolution for the fine chemical and pharmaceutical industries? *Chemical Engineering & Technology*, 28(3), 318–323. Retrieved from https://doi.org/10.1002/ceat.200407128

Roddick-Lanzillota, A. D., Connor, P. A., & McQuillan, A. J. (1998). An In Situ infrared spectroscopic study of the adsorption of Lysine to TiO_2 from an aqueous solution. *Langmuir*, 6479–6484. Retrieved from https://doi.org/10.1021/la980425n

Roddick-Lanzilotta, A. D., & McQuillan, A. J. (2000). An in situ infrared spectroscopic study of glutamic acid and of aspartic acid adsorbed on TiO_2: Implications for the biocompatibility of titanium. *Journal of Colloid and Interface Science*, 227(1), 48–54. Retrieved from https://doi.org/10.1006/jcis.2000.6864

Rokni, K., Mostafaei, M., Dehghani Soufi, M., & Kahrizi, D. (2022). Microwave-assisted intensification of transesterification reaction for biodiesel production from camelina oil: Optimization by Box-Behnken Design. *Bioresource Technology Reports*, 17, 100928. Retrieved 6 July 2022 from https://doi.org/10.1016/J.BITEB.2021.100928

Roman, F. F., Ribeiro, A. E., Queiroz, A., Lenzi, G. G., Chaves, E. S., & Brito, P. (2019). Optimization and kinetic study of biodiesel production through esterification of oleic acid applying ionic liquids as catalysts. *Fuel*, 239, 1231–1239. Retrieved 13 October 2021 from https://doi.org/10.1016/J.FUEL.2018.11.087

Rosset, D. v., Wancura, J. H. C., Ugalde, G. A., Oliveira, J. V., Tres, M. v., Kuhn, R. C., & Jahn, S. L. (2019). Enzyme-catalyzed production of FAME by hydroesterification of soybean oil using the novel soluble Lipase NS 40116. *Applied Biochemistry and Biotechnology*, 188(4), 914–926. Retrieved 13 November 2021 from https://doi.org/10.1007/S12010-019-02966-7

S Khezrianjoo, & HD Revanasiddappa. (2012). Langmuir-Hinshelwood kinetic expression for the photocatalytic degradation of Metanil Yellow aqueous solutions by ZnO catalyst. *Chemical Sciences Journal*, 85, 1–7.

Sahar, Sadaf, S., Iqbal, J., Ullah, I., Bhatti, H. N., Nouren, S., … Iqbal, M. (2018). Biodiesel production from waste cooking oil: An efficient technique to convert waste into biodiesel. *Sustainable Cities and Society*, 41, 220–226. Retrieved from https://doi.org/10.1016/j.scs.2018.05.037

Saka, S., & Kusdiana, D. (2001). Biodiesel fuel from rapeseed oil as prepared in supercritical methanol. *Fuel*, 80(2), 225–231. Retrieved 19 November 2021 from https://doi.org/10.1016/S0016-2361(00)00083-1

Sakthivel, S., Halder, S., & Gupta, P. D. (2013). Optimisation of process variables for production of biodiesel in packed bed reactor using response surface methodology.

International Journal of Ambient Energy, 34(2), 83–91. Retrieved from https://doi.org/10.1080/01430750.2012.740422

Samat, M. H., Ali, A. M. M., Taib, M. F. M., Hassan, O. H., & Yahya, M. Z. A. (2016). Hubbard U calculations on optical properties of 3d transition metal oxide TiO_2. *Results in Physics*, 6, 891–896. Retrieved 1 August 2022 from https://doi.org/10.1016/J.RINP.2016.11.006

Sandesh Suresh, K., Suresh, P. V., & Kudre, T. G. (2019). Prospective ecofuel feedstocks for sustainable production. In *Advances in Eco-Fuels for a Sustainable Environment* (pp. 89–117). Woodhead Publishing. Retrieved 15 November 2021 from https://doi.org/10.1016/B978-0-08-102728-8.00004-8

Santacesaria, E., Vicente, G. M., di Serio, M., & Tesser, R. (2012). Main technologies in biodiesel production: State of the art and future challenges. *Catalysis Today*, 195(1), 2–13. Retrieved 10 November 2021 from https://doi.org/10.1016/J.CATTOD.2012.04.057

Santana, H. S., Lopes, M. G. M., Silva, J. L., & Taranto, O. P. (2018). Application of microfluidics in process intensification. *International Journal of Chemical Reactor Engineering*, 16(12). Retrieved from https://doi.org/doi:10.1515/ijcre-2018-0038

Santana, H. S., Sanchez, G. B., & Taranto, O. P. (2017). Evaporation of excess alcohol in biodiesel in a microchannel heat exchanger with Peltier module. *Chemical Engineering Research and Design*, 124, 20–28. Retrieved 27 June 2022 from https://doi.org/10.1016/J.CHERD.2017.05.022

Sbirrazzuoli, N. (2020). Interpretation and physical meaning of kinetic parameters obtained from isoconversional kinetic analysis of polymers. *Polymers*, 12(6), 1280. Retrieved from https://doi.org/10.3390/polym12061280

Schimpf, S., Lucas, M., Mohr, C., Rodemerck, U., Brückner, A., Radnik, J., … Claus, P. (2002). Supported gold nanoparticles: in-depth catalyst characterization and application in hydrogenation and oxidation reactions. *Catalysis Today*, 72(1–2), 63–78. Retrieved from https://doi.org/10.1016/S0920-5861(01)00479-5

Schmidt, M., & Steinemann, S. G. (1991). XPS studies of amino acids adsorbed on titanium dioxide surfaces. *Fresenius' Journal of Analytical Chemistry*, 341, 412–415. Retrieved from https://doi.org/10.1007/BF00321947

Senoymak Tarakcı, M. I., & Ilgen, O. (2018). Esterification of oleic acid with methanol using $Zr(SO_4)_2$ as a heterogeneous catalyst. *Chemical Engineering & Technology*, 41(4), 845–852. Retrieved from https://doi.org/10.1002/ceat.201700254

Serrano, D. C., Corazza, M. L., Mitchell, D. A., & Krieger, N. (2021). Performing under pressure: esterification activity of dry fermented solids in subcritical and supercritical CO_2. *Biotechnology Letters*, 43(2), 503–509. Retrieved 13 November 2021 from https://doi.org/10.1007/S10529-020-03029-2

Sert, E., & Atalay, F. S. (2010). Determination of adsorption and kinetic parameters for butanolacetic acid esterification system catalysed by Amberlyst 15. *Progress in Reaction Kinetics and Mechanism*, 35(3), 219–235. Retrieved from https://doi.org/10.3184/146867809X12583840521552

Sert, E., & Atalay, F. S. (2017). Application of green catalysts for the esterification of benzoic acid with different alcohols. *Celal Bayar Üniversitesi Fen Bilimleri Dergisi*, 907–912. Retrieved 13 November 2021 from https://doi.org/10.18466/CBAYARFBE.370364

Setvin, M., Shi, X., Hulva, J., Simschitz, T., Parkinson, G. S., Schmid, M., … Diebold, U. (2017). Methanol on anatase TiO_2 (101): mechanistic insights into photocatalysis. *ACS Catalysis*, 7(10), 7081–7091. Retrieved from https://doi.org/10.1021/acscatal.7b02003

Severson, K., Martín, M., & Grossmann, I. E. (2013). Optimal integration for biodiesel production using bioethanol. *AIChE Journal*, 59(3), 834–844. Retrieved from https://doi.org/10.1002/aic.13865

Shah, K. A., Parikh, J. K., & Maheria, K. C. (2014). Optimization studies and chemical kinetics of silica sulfuric acid-catalyzed biodiesel synthesis from waste cooking oil. *BioEnergy Research*, 7(1), 206–216. Retrieved from https://doi.org/10.1007/s12155-013-9363-y

Sharma, A., Kodgire, P., & Kachhwaha, S. S. (2019). Biodiesel production from waste cotton-seed cooking oil using microwave-assisted transesterification: Optimization and kinetic modeling. *Renewable and Sustainable Energy Reviews*, 116, 109394. Retrieved 6 July 2022 from https://doi.org/10.1016/J.RSER.2019.109394

Sharma, B. K., Rashid, U., Anwar, F., & Erhan, S. Z. (2009). Lubricant properties of Moringa oil using thermal and tribological techniques. *Journal of Thermal Analysis and Calorimetry*, 96(3), 999–1008. Retrieved from https://doi.org/10.1007/s10973-009-0066-8

Shchelokov, A., Palko, N., Potemkin, V., Grishina, M., Morozov, R., Korina, E., … Bol'Shakov, O. (2019). Adsorption of native amino acids on nanocrystalline TiO_2: physical chemistry, QSPR, and theoretical modeling. *Langmuir*, 35(2), 538–550. Retrieved from https://doi.org/10.1021/acs.langmuir.8b02007

Shobhana-Gnanaserkhar, Asikin-Mijan, N., AbdulKareem-Alsultan, G., Sivasangar-Seenivasagam, Izham, S. M., & Taufiq-Yap, Y. H. (2020). Biodiesel production via simultaneous esterification and transesterification of chicken fat oil by mesoporous sulfated Ce supported activated carbon. *Biomass and Bioenergy*, 141, 105714. Retrieved 25 February 2022 from https://doi.org/10.1016/J.BIOMBIOE.2020.105714

Shu, Q., Gao, J., Nawaz, Z., Liao, Y., Wang, D., & Wang, J. (2010). Synthesis of biodiesel from waste vegetable oil with large amounts of free fatty acids using a carbon-based solid acid catalyst. *Applied Energy*, 87(8), 2589–2596. Retrieved 10 November 2021 from https://doi.org/10.1016/J.APENERGY.2010.03.024

Shuai, W., Das, R. K., Naghdi, M., Brar, S. K., & Verma, M. (2017). A review on the important aspects of lipase immobilization on nanomaterials. *Biotechnology and Applied Biochemistry*, 64(4), 496–508. Retrieved from https://doi.org/10.1002/bab.1515

Sidik, S. M., Triwahyono, S., Jalil, A. A., Majid, Z. A., Salamun, N., Talib, N. B., & Abdullah, T. A. T. (2016). CO_2 reforming of CH_4 over Ni–Co/MSN for syngas production: Role of Co as a binder and optimization using RSM. *Chemical Engineering Journal*, 295, 1–10. Retrieved 25 November 2021 from https://doi.org/10.1016/J.CEJ.2016.03.041

Silva, G. S., Oliveira, P. C., Giordani, D. S., & Castro, H. F. de. (2011). Chitosan/siloxane hybrid polymer: synthesis, characterization and performance as a support for immobilizing enzyme. *Journal of the Brazilian Chemical Society*, 22(8), 1407–1417. Retrieved from https://doi.org/10.1590/S0103-50532011000800003

Silva, S. M., Peixoto, A. F., & Freire, C. (2020). Organosulfonic acid functionalized montmorillonites as solid catalysts for (trans) esterification of free fatty acids and (waste) oils. *Renewable Energy*, 146, 2416–2429. Retrieved 10 September 2021 from https://doi.org/10.1016/J.RENENE.2019.08.073

Silva, M. v.d., Hori, C. E., & Reis, M. H. M. (2015). Thermochemical data of the oleic acid esterification reaction: A quantum mechanics approach. *Fluid Phase Equilibria*, 406, 168–174. Retrieved 10 September 2021 from https://doi.org/10.1016/J.FLUID.2015.07.050

Singh, D., Sharma, D., Soni, S. L., Sharma, S., & Kumari, D. (2019). Chemical compositions, properties, and standards for different generation biodiesels: A review. *Fuel*, 253, 60–71. Retrieved 9 November 2021 from https://doi.org/10.1016/J.FUEL.2019.04.174

Singh, N. K., Singh, Y., & Sharma, A. (2022). Optimization of biodiesel synthesis from Jojoba oil via supercritical methanol: A response surface methodology approach coupled with genetic algorithm. *Biomass and Bioenergy*, 156, 106332. Retrieved 6 July 2022 from https://doi.org/10.1016/J.BIOMBIOE.2021.106332

Singh, N., Raj Kumar, & Sachan, P. K. (2013). Kinetic study of catalytic esterification of butyric acid and ethanol over Amberlyst 15. *ISRN Chemical Engineering*, 2013, 1–6. Retrieved from https://doi.org/10.1155/2013/520293

Sipponen, M. H., Farooq, M., Koivisto, J., Pellis, A., Seitsonen, J., & Österberg, M. (2018). Spatially confined lignin nanospheres for biocatalytic ester synthesis in aqueous media. *Nature Communications*, 9(1), 2300–2304. Retrieved from https://doi.org/10.1038/s41467-018-04715-6

Smith, R. M., & Martell, A. E. (2004). NIST Critically selected stability constants of methal complexes database. *NIST Standard Reference Database 46*. U.S. Department of Commerce Technology Administration.

Snellman, E. A., Sullivan, E. R., & Colwell, R. R. (2002). Purification and properties of the extracellular lipase, LipA, of *Acinetobacter sp.* RAG-1. *European Journal of Biochemistry*, 269(23), 5771–5779. Retrieved from https://doi.org/10.1046/j.1432-1033.2002.03235.x

Soltani, S., Khanian, N., Shean Yaw Choong, T., Asim, N., & Zhao, Y. (2021). Microwave-assisted hydrothermal synthesis of sulfonated TiO_2-GO core–shell solid spheres as heterogeneous esterification mesoporous catalyst for biodiesel production. *Energy Conversion and Management*, 238, 114165. Retrieved 6 July 2022 from https://doi.org/10.1016/J.ENCONMAN.2021.114165

Sootchiewcharn, N., Attanatho, L., & Reubroycharoen, P. (2015). Biodiesel production from refined palm oil using supercritical ethyl acetate in a microreactor. *Energy Procedia*, 79, 697–703. Retrieved 6 July 2022 from https://doi.org/10.1016/J.EGYPRO.2015.11.560

Sree, J. V., Chowdary, B. A., Kumar, K. S., Anbazhagan, M. P., & Subramanian, S. (2021). Optimization of the biodiesel production from waste cooking oil using homogeneous catalyst and heterogeneous catalysts. *Materials Today: Proceedings*, 46, 4900–4908. Retrieved 6 July 2022 from https://doi.org/10.1016/J.MATPR.2020.10.332

Stacy, C. J., Melick, C. A., & Cairncross, R. A. (2014). Esterification of free fatty acids to fatty acid alkyl esters in a bubble column reactor for use as biodiesel. *Fuel Processing Technology*, 124, 70–77. Retrieved 10 September 2021 from https://doi.org/10.1016/J.FUPROC.2014.02.003

Statistical Review of World Energy 2021. (2021). Retrieved 9 November 2021 from London: https://www.bp.com/content/dam/bp/business-sites/en/global/corporate/pdfs/energy-economics/statistical-review/bp-stats-review-2021-full-report.pdf

Stauch, B., Fisher, S. J., & Ciani, M. (2015). Open and closed conformations and protonation states of *Candida antarctica* Lipase B: atomic resolution native. *Journal of Lypid Research*, 2348–2358. Retrieved from https://doi.org/10.1194/jlr.M063388

Sturt, N. R. M., Vieira, S. S., & Moura, F. C. C. (2019). Catalytic activity of sulfated niobium oxide for oleic acid esterification. *Journal of Environmental Chemical Engineering*, 7(1), 102866. Retrieved 15 October 2021 from https://doi.org/10.1016/J.JECE.2018.102866

Sugimoto, A., Fukuyama, T., Sumino, Y., Takagi, M., & Ryu, I. (2009). Microflow photo-radical reaction using a compact light source: application to the Barton reaction leading to a key intermediate for myriceric acid A. *Tetrahedron*, 65(8), 1593–1598. Retrieved from https://doi.org/10.1016/j.tet.2008.12.063

Suhadolnik, L., Pohar, A., Likozar, B., & Čeh, M. (2016). Mechanism and kinetics of phenol photocatalytic, electrocatalytic and photoelectrocatalytic degradation in a TiO_2-nanotube fixed-bed microreactor. *Chemical Engineering Journal*, 303, 292–301. Retrieved from https://doi.org/10.1016/j.cej.2016.06.027

Sun, H., Ding, Y., Duan, J., Zhang, Q., Wang, Z., Lou, H., & Zheng, X. (2010). Transesterification of sunflower oil to biodiesel on ZrO_2 supported La_2O_3 catalyst. *Bioresource Technology*, 101(3), 953–958. Retrieved 11 November 2021 from https://doi.org/10.1016/j.biortech.2009.08.089

Sun, Z., Duan, X., Zhao, J., Wang, X., & Jiang, Z. (2015). Homogeneous borotungstic acid and heterogeneous micellar borotungstic acid catalysts for biodiesel production by esterification of free fatty acid. *Biomass and Bioenergy*, 76, 31–42. Retrieved 6 July 2022 from https://doi.org/10.1016/J.BIOMBIOE.2015.03.002

Supple, B., Howard-Hildige, R., Gonzalez-Gomez, E., & Leahy, J. J. (2002). The effect of steam treating waste cooking oil on the yield of methyl ester. *JAOCS, Journal of the American Oil Chemists' Society*, 79(2), 175–178. Retrieved 11 November 2021 from https://doi.org/10.1007/S11746-002-0454-1

Suthar, S., & Verma, R. (2018). Production of *Chlorella vulgaris* under varying nutrient and abiotic conditions: A potential microalga for bioenergy feedstock. *Process Safety and Environmental Protection*, 113, 141–148. Retrieved 19 November 2021 from https://doi.org/10.1016/j.psep.2017.09.018

Syazwani, O. N., Rashid, U., Mastuli, M. S., & Taufiq-Yap, Y. H. (2019). Esterification of palm fatty acid distillate (PFAD) to biodiesel using Bi-functional catalyst synthesized from waste angel wing shell (*Cyrtopleura costata*). *Renewable Energy*, 131, 187–196. Retrieved 21 November 2021 from https://doi.org/10.1016/J.RENENE.2018.07.031

Taghvaei, M., Jafari, S. M., Assadpoor, E., Nowrouzieh, S., & Alishah, O. (2014). Optimization of microwave-assisted extraction of cottonseed oil and evaluation of its oxidative stability and physicochemical properties. *Food Chemistry*, 160, 90–97. Retrieved 11 November 2021 from https://doi.org/10.1016/j.foodchem.2014.03.064

Takei, G., Kitamori, T., & Kim, H.-B. (2005). Photocatalytic redox-combined synthesis of l-pipecolinic acid with a titania-modified microchannel chip. *Catalysis Communications*, 6(5), 357–360. Retrieved from https://doi.org/10.1016/j.catcom.2005.02.010

Tamalampudi, S., Talukder, M. R., Hama, S., Numata, T., Kondo, A., & Fukuda, H. (2008). Enzymatic production of biodiesel from *Jatropha* oil: A comparative study of immobilized-whole cell and commercial lipases as a biocatalyst. *Biochemical Engineering Journal*, 39(1), 185–189. Retrieved 11 November 2021 from https://doi.org/10.1016/j.bej.2007.09.002

Tan, S. X., Lim, S., Ong, H. C., & Pang, Y. L. (2019). State of the art review on development of ultrasound-assisted catalytic transesterification process for biodiesel production. *Fuel*, 235, 886–907. Retrieved 15 December 2020 from https://doi.org/10.1016/j.fuel.2018.08.021

Tang, W. Z., & Huren An. (1995). UV/TiO_2 photocatalytic oxidation of commercial dyes in aqueous solutions. *Chemosphere*, 31(9), 4157–4170. Retrieved 25 October 2021 from https://doi.org/10.1016/0045-6535(95)80015-D

Tauc, J., Grigorovici, R., & Vancu, A. (1966). Optical properties and electronic structure of *Amorphous Germanium*. *Physica Status Solidi (b)*, 15(2), 627–637. Retrieved from https://doi.org/10.1002/pssb.19660150224

Ternel, C., Bouter, A., & Melgar, J. (2021). Life cycle assessment of mid-range passenger cars powered by liquid and gaseous biofuels: Comparison with greenhouse gas emissions of electric vehicles and forecast to 2030. *Transportation Research Part D: Transport and Environment*, 97, 102897. Retrieved 9 November 2021 from https://doi.org/10.1016/J.TRD.2021.102897

Terry, S. C., Jerman, J. H., & Angell, J. B. (1979). A gas chromatographic air analyzer fabricated on a silicon wafer. *IEEE Transactions on Electron Devices*, 26(12), 1880–1886. Retrieved from https://doi.org/10.1109/T-ED.1979.19791

Thanh, L. T., Okitsu, K., Boi, L. van, & Maeda, Y. (2012). Catalytic technologies for biodiesel fuel production and utilization of glycerol: A Review. *Catalysts*, 2(1), 191–222. Retrieved 9 November 2021 from https://doi.org/10.3390/catal2010191

Thitsartarn, W., & Kawi, S. (2011). An active and stable CaO–CeO_2 catalyst for transesterification of oil to biodiesel. *Green Chemistry*, 13(12), 3423–3430. Retrieved 11 November 2021 from https://doi.org/10.1039/C1GC15596B

Trodler, P., & Pleiss, J. (2008). Modeling structure and flexibility of *Candida antarctica* lipase B in organic solvents. *BMC Structural Biology*, 8, 9. Retrieved from https://doi.org/10.1186/1472-6807-8-9

UFOP. (2016). *REPORT ON GLOBAL MARKET SUPPLY*. Retrieved 9 November 2021 from Berlin: https://www.ufop.de/files/7814/9977/4144/UFOP_supply_report_20162017.pdf

UFOP. (2020). *REPORT ON GLOBAL MARKET SUPPLY*. Retrieved 9 November 2021 from Berlin: https://www.ufop.de/files/7216/1649/5848/UFOP_SupplyReport_2020-2021__120321.pdf#:~:text=The%20fourth%20UFOP%20Report%20on,are%20suffering%20famine%20or%20malnutrition.

Unker, S. A., Boucher, M. B., Hawley, K. R., Midgette, A. A., Stuart, J. D., & Parnas, R. S. (2010). Investigation into the relationship between the gravity vector and the flow vector to improve performance in two-phase continuous flow biodiesel reactor. *Bioresource Technology*, 101(19), 7389–7396. Retrieved 6 July 2022 from https://doi.org/10.1016/J.BIORTECH.2010.04.101

Uppenberg, J., Hansen, M. T., Patkar, S., & Jones, A. (1994). The sequence, crystal structure determination and refinement of two crystal forms of lipase B from *Candida antarctica*. *Structure*, 2(4), 293–308. Retrieved from https://doi.org/10.1016/s0969-2126(00)00031-9

Uppenberg, J., Öhrner, N., Norin, M., Hult, K., Kleywegt, G. J., Patkar, S., … Jones, A. T. (1995). Crystallographic and molecular-modeling studies of Lipases B from *Candida antarctica* reveal a stereospecificity pochet for secondary alcohols. *Biochemistry*, 34(51), 16838–16851. Retrieved from https://doi.org/10.1021/bi00051a035

van Gerpen, J. (2005). Biodiesel processing and production. *Fuel Processing Technology*, 86(10), 1097–1107. Retrieved 9 November 2021 from https://doi.org/10.1016/J.FUPROC.2004.11.005

van Gerven, T., Mul, G., Moulijn, J., & Stankiewicz, A. (2007). A review of intensification of photocatalytic processes. *Chemical Engineering and Processing: Process Intensification*, 46(9), 781–789. Retrieved from https://doi.org/10.1016/j.cep.2007.05.012

van Santen, R. A. (2009). Complementary structure sensitive and insensitive catalytic relationships. *Accounts of Chemical Research*, 42(1), 57–66. Retrieved from https://doi.org/10.1021/ar800022m

Veillette, M., Giroir-Fendler, A., Faucheux, N., & Heitz, M. (2017). Esterification of free fatty acids with methanol to biodiesel using heterogeneous catalysts: From model acid oil to microalgae lipids. *Chemical Engineering Journal*, 308, 101–109. Retrieved 3 November 2021 from https://doi.org/10.1016/J.CEJ.2016.07.061

Veljković, V. B., Stamenković, O. S., Todorović, Z. B., Lazić, M. L., & Skala, D. U. (2009). Kinetics of sunflower oil methanolysis catalyzed by calcium oxide. *Fuel*, 88(9), 1554–1562. Retrieved 11 November 2021 from https://doi.org/10.1016/j.fuel.2009.02.013

Verma, P., & Sharma, M. P. (2016). Review of process parameters for biodiesel production from different feedstocks. *Renewable and Sustainable Energy Reviews*, 62, 1063–1071. Retrieved 15 November 2021 from https://doi.org/10.1016/J.RSER.2016.04.054

Vieira, S. S., Magriotis, Z. M., Ribeiro, M. F., Graça, I., Fernandes, A., Lopes, J. M. F. M., … Saczk, A. A. (2015). Use of HZSM-5 modified with citric acid as acid heterogeneous catalyst for biodiesel production via esterification of oleic acid. *Microporous and Mesoporous Materials*, 201(C), 160–168. Retrieved 13 October 2021 from https://doi.org/10.1016/J.MICROMESO.2014.09.015

Vieira, S. S., Magriotis, Z. M., Santos, N. A. V., Saczk, A. A., Hori, C. E., & Arroyo, P. A. (2013). Biodiesel production by free fatty acid esterification using lanthanum (La^{3+}) and HZSM-5 based catalysts. *Bioresource Technology*, 133, 248–255. Retrieved 13 October 2021 from https://doi.org/10.1016/J.BIORTECH.2013.01.107

Viñambres, M., Filice, M., & Marciello, M. (2018). Modulation of the catalytic properties of lipase B from *Candida antarctica* by immobilization on tailor-made magnetic iron oxide nanoparticles: The key role of nanocarrier surface engineering. *Polymers*, 8(6), 615. Retrieved from https://doi.org/10.3390/polym10060615

Voegele, E. (2020, November 13). NBB: Biodiesel can help meet USDA's AIA goals. *Biodiesel Magazine*.

Vorontsov, A. v., Valdés, H., Smirniotis, P. G., & Paz, Y. (2020). Recent advancements in the understanding of the surface chemistry in TiO_2 photocatalysis. *Surfaces*, 3(1), 72–92. Retrieved 20 October 2021 from https://doi.org/10.3390/surfaces3010008

Wan Ghazali, W. N. M., Mamat, R., Masjuki, H. H., & Najafi, G. (2015). Effects of biodiesel from different feedstocks on engine performance and emissions: A review. *Renewable and Sustainable Energy Reviews*, 51, 585–602. Retrieved 15 November 2021 from https://doi.org/10.1016/J.RSER.2015.06.031

Wan Omar, W. N. N., & Amin, N. A. S. (2011). Biodiesel production from waste cooking oil over alkaline modified zirconia catalyst. *Fuel Processing Technology*, 92(12), 2397–2405. Retrieved 10 November 2021 from https://doi.org/10.1016/J.FUPROC.2011.08.009

Wan Omar, W. N. N., & Saidina Amin, N. A. (2011). Optimization of heterogeneous biodiesel production from waste cooking palm oil via response surface methodology. *Biomass and Bioenergy*, 35(3), 1329–1338. Retrieved 11 November 2021 from https://doi.org/10.1016/j.biombioe.2010.12.049

Wancura, J. H. C., Rosset, D. v., Mazutti, M. A., Ugalde, G. A., de Oliveira, J. V., Tres, M. v., & Jahn, S. L. (2019). Improving the soluble lipase–catalyzed biodiesel production through a two-step hydroesterification reaction system. *Applied Microbiology and Biotechnology*, 103(18), 7805–7817. Retrieved 13 November 2021 from https://doi.org/10.1007/S00253-019-10075-Y

Wang, A., Zhang, H., Li, H., & Yang, S. (2019). Efficient production of methyl oleate using a biomass-based solid polymeric catalyst with high acid density. *Advances in Polymer Technology*, 2019, 4041631. Retrieved from https://doi.org/10.1155/2019/4041631

Wang, L., & Yang, J. (2007). Transesterification of soybean oil with nano-MgO or not in supercritical and subcritical methanol. *Fuel*, 86(3), 328–333. Retrieved 11 November 2021 from https://doi.org/10.1016/j.fuel.2006.07.022

Wang, Y. T., Fang, Z., Yang, X. X., Yang, Y. T., Luo, J., Xu, K., & Bao, G. R. (2018). One-step production of biodiesel from *Jatropha* oils with high acid value at low temperature by magnetic acid-base amphoteric nanoparticles. *Chemical Engineering Journal*, 348, 929–939. Retrieved 21 November 2021 from https://doi.org/10.1016/J.CEJ.2018.05.039

Wang, Y. T., Fang, Z., Zhang, F., & Xue, B. J. (2015). One-step production of biodiesel from oils with high acid value by activated Mg–Al hydrotalcite nanoparticles. *Bioresource Technology*, 193, 84–89. Retrieved 21 November 2021 from https://doi.org/10.1016/J.BIORTECH.2015.06.059

Weisz, P. B., & Prater, C. D. (1954). Interpretation of Measurements in Experimental Catalysis (pp. 143–196). Retrieved from https://doi.org/10.1016/S0360-0564(08)60390-9

Welter, R. A., Santana, H. S., de la Torre, L., Barns, M. C., Taranto, O. P., & Oelgemöller, M. (2022). TiO_2 photocatalysed for biodiesel production from WCO simultaneous esterification and transesterification.

Welter, R. A., Santana, H. S., de la Torre, L. G., Barnes, M. C., Taranto, O. P., & Oelgemöller, M. (2022). Biodiesel production from canola oil photocatalysed by TiO_2. *Fuel*. Retrieved from https://doi.org/https://dx.doi.org/10.2139/ssrn.4201382

Welter, R. A., Santana, H. S., de la Torre, L. G., Barnes, M. C., Taranto, O. P., & Olegemöller, M. (2022). Biodiesel production focusing on heterogenous catalysts and eco-friendly routes. *ChemBioEng Reviews*.

Welter, R., Silva Jr., J., de Souza, M., Lopes, M., Taranto, O., & Santana, H. (2022). Are Microreactors the Future of Biodiesel Synthesis? In *The future of biodiesel* (1st ed., Vol. 1, pp. 47–82).

Welter, Rosilene A., Santana, H., Torre, L. G., Robertson, M., Taranto, O. P., & Oelgemöller, M. (2022). Methyl oleate synthesis by TiO_2 photocatalytic esterification of oleic acid: optimisation by response surface quadratic methodology, reaction kinetics and thermodynamics. *ChemPhotoChem*, 6(7), e202200007. Retrieved from https://doi.org/10.1002/cptc.202200007

Welter, Rosilene Andrea, Santana, H. S., Carvalho, B. G., Melani, N., Oelgemöller, M., de la Torre, L. G., & Taranto, O. P. (2022). Droplet microfluidics for double lipase immobilisation using TiO_2 and alginate microbeads. *Journal of Industrial and Engineering Chemistry*, 110, 576–586. Retrieved from https://doi.org/10.1016/j.jiec.2022.03.028

Wen, Z., Yu, X., Tu, S. T., Yan, J., & Dahlquist, E. (2009). Intensification of biodiesel synthesis using zigzag micro-channel reactors. *Bioresource Technology*, 100(12), 3054–3060. Retrieved 11 November 2021 from https://doi.org/10.1016/j.biortech.2009.01.022

Wen, Z., Yu, X., Tu, S. T., Yan, J., & Dahlquist, E. (2010). Biodiesel production from waste cooking oil catalyzed by TiO_2–MgO mixed oxides. *Bioresource Technology*, 101(24), 9570–9576. Retrieved 25 February 2022 from https://doi.org/10.1016/J.BIORTECH.2010.07.066

Wnorowska, J., Ciukaj, S., & Kalisz, S. (2021). Thermogravimetric analysis of solid biofuels with additive under air atmosphere. *Energies*, 14(8), 2257. Retrieved from https://doi.org/10.3390/en14082257

Wu, H., Gong, L. M., Guo, L., Zhang, L. Y., & Li, J. T. (2011). Effects of the free fatty acid content in yellow grease on performance, carcass characteristics, and serum lipids in broilers. *Poultry Science*, 90(9), 1992–1998. Retrieved 15 November 2021 from https://doi.org/10.3382/PS.2010-01298

Wu, Z., Chen, C., Wang, L., Wan, H., & Guan, G. (2016). Magnetic material grafted poly(phosphotungstate-based acidic ionic liquid) as efficient and recyclable catalyst for esterification of oleic acid. *Industrial & Engineering Chemistry Research*, 55(7), 1833–1842. Retrieved from https://doi.org/10.1021/acs.iecr.5b02906

Wulandari, P. P., Adiwibowo, M. T., Redjeki, A. S., Ibadurrohman, M., & Slamet. (2019). Synthesis of eco-friendly detergent based on crude palm oil and titania nanoparticles. *Asian Journal of Chemistry*, 31(10), 2394–2396. Retrieved from https://doi.org/10.14233/ajchem.2019.21984

Xie, W., Hu, L., & Yang, X. (2015). Basic ionic liquid supported on mesoporous SBA-15 silica as an efficient heterogeneous catalyst for biodiesel production. *Industrial and Engineering Chemistry Research*, 54(5), 1505–1512. Retrieved 15 December 2020 from https://doi.org/10.1021/ie5045007

Xie, W., & Ma, N. (2009). Immobilized lipase on Fe_3O_4 nanoparticles as biocatalyst for biodiesel production. *Energy & Fuels*, 23(3), 1347–1353. Retrieved from https://doi.org/10.1021/ef800648y

Xie, W., & Wang, J. (2012). Immobilized lipase on magnetic chitosan microspheres for transesterification of soybean oil. *Biomass and Bioenergy*, 36, 373–380. Retrieved 8 July 2022 from https://doi.org/10.1016/J.BIOMBIOE.2011.11.006

Xie, W., & Wang, J. (2014). Enzymatic production of biodiesel from soybean oil by using immobilized lipase on Fe_3O_4 /Poly(styrene-methacrylic acid) magnetic microsphere as a biocatalyst. *Energy & Fuels*, 28(4), 2624–2631. Retrieved from https://doi.org/10.1021/ef500131s

Xie, W., & Zang, X. (2017). Covalent immobilization of lipase onto aminopropyl-functionalized hydroxyapatite-encapsulated-γ-Fe_3O_4 nanoparticles: A magnetic biocatalyst for interesterification of soybean oil. *Food Chemistry*, 227, 397–403. Retrieved 1 December 2021 from https://doi.org/10.1016/j.foodchem.2017.01.082

Xie, W., & Zang, X. (2018). Lipase immobilized on ionic liquid-functionalized magnetic silica composites as a magnetic biocatalyst for production of trans -free plastic fats. *Food Chemistry*, 257, 15–22. Retrieved from https://doi.org/10.1016/j.foodchem.2018.03.010

Xie, W., & Zhao, L. (2014). Heterogeneous CaO–MoO_3–SBA-15 catalysts for biodiesel production from soybean oil. *Energy Conversion and Management*, 79, 34–42. Retrieved from https://doi.org/10.1016/j.enconman.2013.11.041

Xu, W., Zhou, J., Su, Z., Ou, Y., & You, Z. (2016). Microwave catalytic effect: a new exact reason for microwave-driven heterogeneous gas-phase catalytic reactions. *Catalysis Science & Technology*, 6(3), 698–702. Retrieved from https://doi.org/10.1039/C5CY01802A

Yan, S., Salley, S. O., & Simon Ng, K. Y. (2009). Simultaneous transesterification and esterification of unrefined or waste oils over ZnO-La_2O_3 catalysts. *Applied Catalysis A: General*, 353(2), 203–212. Retrieved 25 February 2022 from https://doi.org/10.1016/J.APCATA.2008.10.053

Yang, D., Li, Y., Liu, X., Cao, Y., Gao, Y., Shen, Y. R., & Liu, W.-T. (2018). Facet-specific interaction between methanol and TiO_2 probed by sum-frequency vibrational spectroscopy. *Proceedings of the National Academy of Sciences*, 115(17), E3888. Retrieved from https://doi.org/10.1073/pnas.1802741115

Yao, F., Wu, Q., Lei, Y., Guo, W., & Xu, Y. (2008). Thermal decomposition kinetics of natural fibers: Activation energy with dynamic thermogravimetric analysis. *Polymer Degradation and Stability*, 93(1), 90–98. Retrieved 15 March 2022 from https://doi.org/10.1016/J.POLYMDEGRADSTAB.2007.10.012

Yebo, L. (2016). Bioenergy: Principles and Applications–Yebo Li, Samir Kumar Khanal–Google Books.

Zahan, K. A., & Kano, M. (2018). Biodiesel production from palm oil, its by-products, and mill effluent: A Review. *Energies*, 11(8), 2132. Retrieved from https://doi.org/10.3390/en11082132

Zaks, A., & Klibanov, A. M. (1985). Enzyme-catalyzed processes in organic solvents. *Proceedings of the National Academy of Sciences*, 82(10), 3192–3196. Retrieved from https://doi.org/10.1073/pnas.82.10.3192

Zdarta, J., Klapiszewski, L., Jedrzak, A., Nowicki, M., Moszynski, D., & Jesionowski, T. (2016). Lipase B from *Candida antarctica* immobilized on a silica-lignin matrix as a stable and reusable biocatalytic system. *Catalysts*, 7(12), 14. Retrieved from https://doi.org/10.3390/catal7010014

Zhang, B., Li, P., Zhang, H., Wang, H., Li, X., Tian, L., … Zhang, Q. (2016). Preparation of lipase/$Zn_3(PO_4)_2$ hybrid nanoflower and its catalytic performance as an immobilized enzyme. *Chemical Engineering Journal*, 291, 287–297. Retrieved from https://doi.org/10.1016/J.CEJ.2016.01.104

Zhang, S., Shang, W., Yang, X., Zhang, S., Zhang, X., & Chen, J. (2013). Immobilization of lipase using alginate hydrogel beads and enzymatic evaluation in hydrolysis of p-nitrophenol butyrate. *Bulletin of the Korean Chemical Society*, 34(9), 2741–2746. Retrieved from https://doi.org/10.5012/bkcs.2013.34.9.2741

Zhang, X., Hayward, D. O., & Mingos, D. M. P. (1999). Apparent equilibrium shifts and hot-spot formation for catalytic reactions induced by microwave dielectric heating. *Chemical Communications*, (11), 975–976. Retrieved from https://doi.org/10.1039/a901245a

Zhang, Y., Dubé, M. A., McLean, D. D., & Kates, M. (2003). Biodiesel production from waste cooking oil: 1. Process design and technological assessment. *Bioresource Technology*, 89(1), 1–16. Retrieved 19 November 2021 from https://doi.org/10.1016/S0960-8524(03)00040-3

Zhen, B., Li, H., Jiao, Q., Li, Y., Wu, Q., & Zhang, Y. (2012). $SiW_{12}O_{40}$-based ionic liquid catalysts: catalytic esterification of oleic acid for biodiesel production. *Industrial & Engineering Chemistry Research*, 51, 10374–10380. Retrieved 10 September 2021 from https://doi.org/10.1021/ie301453c

Zhou, W., Zhou, X., Zhuang, W., Lin, R., Zhao, Y., Ge, L., … Ying, H. (2021). Toward controlled geometric structure and surface property heterogeneities of TiO_2 for lipase immobilization. *Process Biochemistry*, 110, 118–128. Retrieved 3 December 2021 from https://doi.org/10.1016/J.PROCBIO.2021.08.004

Zisis, T., Freddolino, P. L., Turunen, P., van Teeseling, M. C. F., Rowan, A. E., & Blank, K. G. (2015). Interfacianl activation of *Candida antarctica* lipase B: combined evidence from experiment and simulation. *Biochemistry*, 54(38), 5969–5979. Retrieved from https://doi.org/10.1021/acs.biochem.5b00586

Zulfiqar, A., Mumtaz, M. W., Mukhtar, H., Najeeb, J., Irfan, A., Akram, S., … Nabi, G. (2021). Lipase-PDA-TiO_2 NPs: An emphatic nano-biocatalyst for optimized biodiesel production from *Jatropha curcas* oil. *Renewable Energy*, 169, 1026–1037. Retrieved 8 July 2022 from https://doi.org/10.1016/J.RENENE.2020.12.135

APPENDIX A

General information

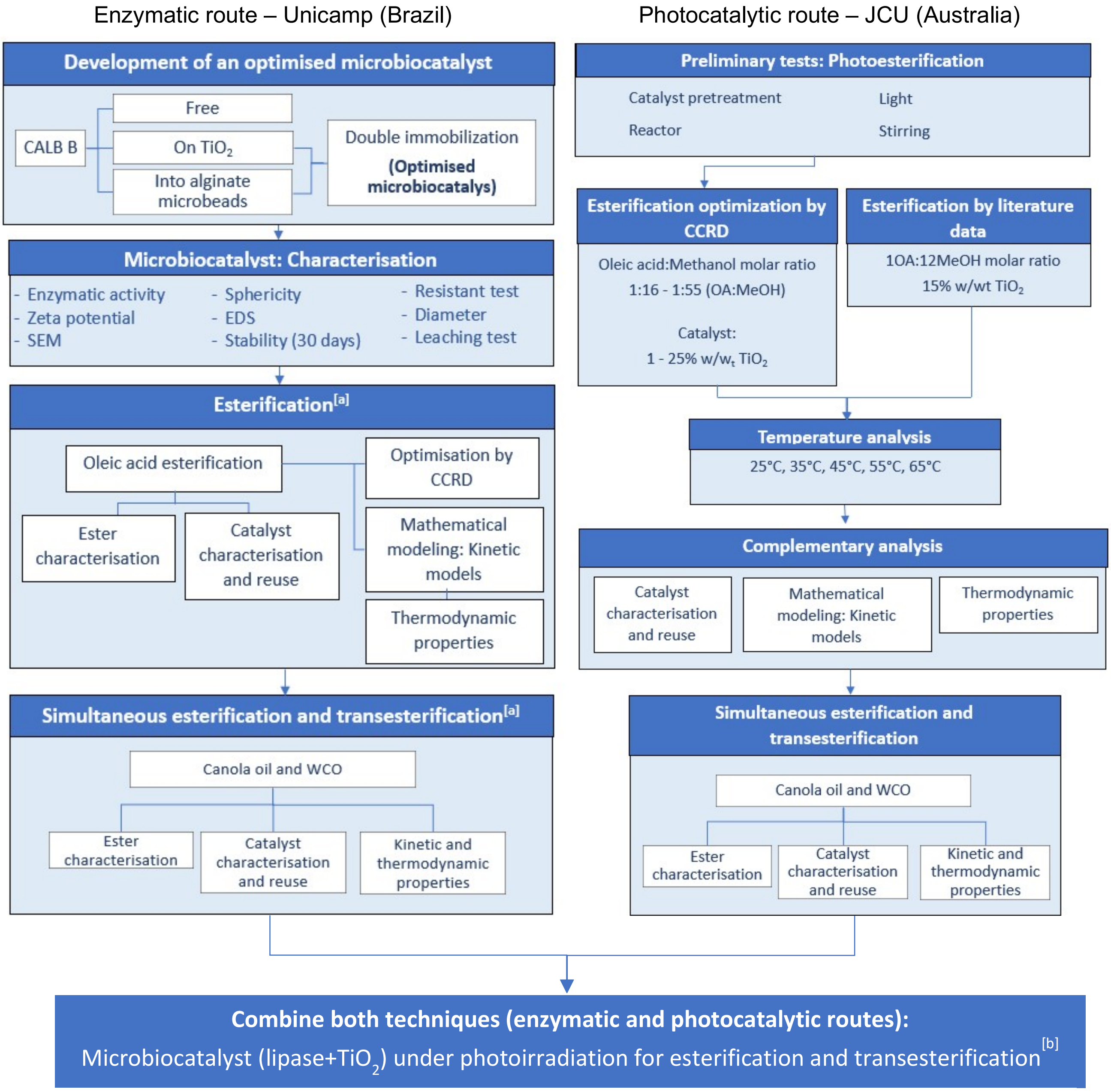

[a] Could not be done because of COVID outbreak; [a, b] Suggestion for future studies.

Figure S2. 1. General Steps developed in Brazil (enzymatic catalysis) and Australia (photocatalysis) and future studies suggestions.

APPENDIX B

Supplementary information for chapter III
Droplet microfluidics for double lipase immobilisation using TiO_2 and alginate microbeads

S3.1. Calb oriented immobilisation

The enzyme can be bound to the support by chemical or physical immobilisation. Chemical immobilisation interferes directly with the enzyme's chemical characteristics and consequently its catalyst capacity. The covalent link and hydrogen bond are the most common chemical immobilisation methods, which can be made using hydrophobic or hydrophilic materials. Lipases are more attracted to hydrophobic than hydrophilic material (Joyce et al., 2016),. In the presence of hydrophobic support, the enzyme can be linked in multiple layers by the hydrophobic residues; however, the active site is not available for reaction. Hence, a better immobilisation is possible, although it shows lower catalyst activity (Joyce et al., 2016; Reis et al., 2009; Tan et al., 2019). Contrarily, in the presence of hydrophilic support, the hydrophilic chain enzyme residues are linked by one layer around the support material. This mechanism keeps the hydrophobic residues free and the active site available for the medium reaction, resulting in a higher catalyst activity (Joyce et al., 2016), and a monolayer connection with stronger activation (Laszlo & Evans, 2007).

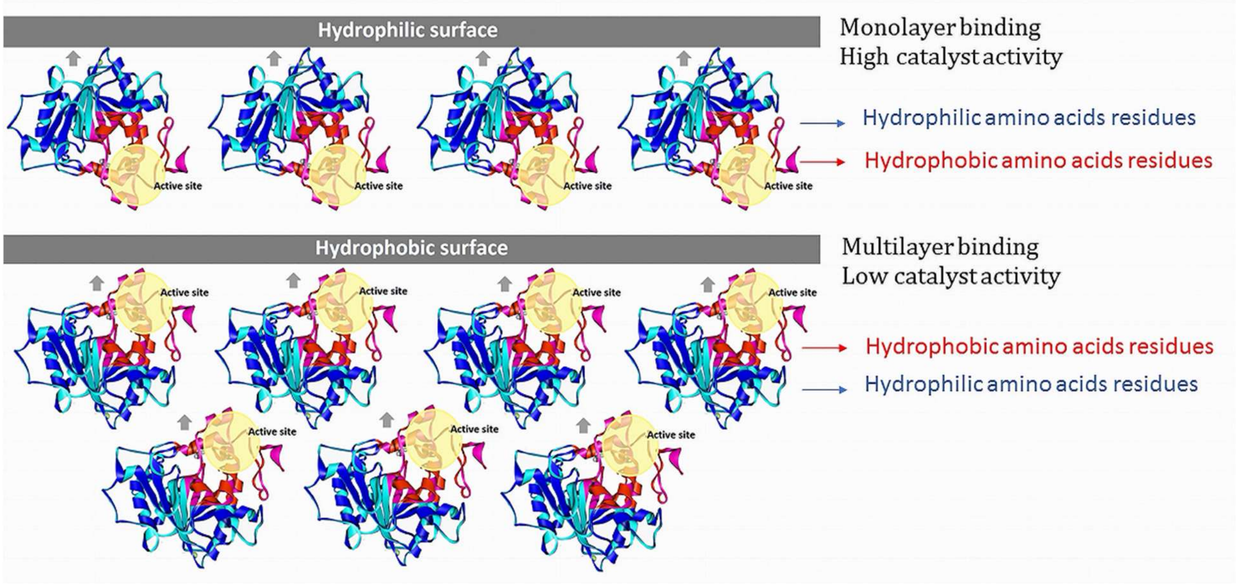

Figure S3. 1. CALB immobilised on (a) hydrophilic surface and (b) hydrophobic surface.

CALB is a globular α/β protein, has 33kD of molecular weight, approximate dimension of 30 Å x 40 Å x 50 Å, with a surface area of 12043 Å^2. CALB is formed by 317 amino acids residues distributed in two distinct parts: hydrophilic, with a surface area of 6071 Å^2, and hydrophobic, with a surface area of 5972 Å^2 (Trodler & Pleiss, 2008). Inside the hydrophobic part is the active site. The active site is composed of the triad Ser105-Asp187-His224 (Uppenberg et al., 1994), which is inserted in a hydrophobic channel measuring 10 Å × 4 Å of width and 12 Å of depth (Uppenberg et al., 1994). This channel is protected by a double lid formed by a short α helix, α5 (141 – 147, acyl side (Uppenberg et al., 1995), a long α helix, α10 (280 – 288, alcohol side (Uppenberg et al., 1995), and a loop region, Ile189 (Uppenberg et al., 1994). These mobile helixes adopt different conformations and may be responsible for the enzyme stereospecificity and open/close the active site's lids (Chaput et al., 2012; Ganjalikhany et al., 2012; Marton et al., 2010; Trodler & Pleiss, 2008; Uppenberg et al., 1994; Zisis et al., 2015). The enzyme residues movements occur according to the surrounding elements' hydrophobicity. The other three amino acids are directly responsible for CALB enantioselectivity: Thr42, Ser47, and Trp104 (Uppenberg et al., 1995). Each amino acids have different characteristics that interfere with their linking capacity; for CALB structure, at pH 6.7 and 25°C, we defined the essential amino acids connected to $TiO_2.(H_2O)_n$ surface:

Asp →Gln → Lys → Met → Pro → Ser

These binding relation has been based on experimental and model data, study of pH, temperature physical and chemical enzymatic structure, considering that pH of 6.7. At this pH, TiO_2 has a negative surface charge and amino acids near-neutral surface charge. Amino acids at neutral surface charge are almost organised by the zwitterionic form (Ataman et al., 2011; Brandt & Lyubartsev, 2015; Giacomelli, Avena, & Pauli, 1995; Monti & Walsh, 2010; Mudunkotuwa & Grassian, 2014; Pantaleone, Rimola, & Sodupe, 2017; Pászti & Guczi, 2009; Roddick-Lanzillota, Connor, & McQuillan, 1998; Roddick-Lanzilotta & McQuillan, 2000; Schmidt & Steinemann, 1991; Shchelokov et al., 2019). These six crucial amino acids are almost found in the external enzyme chain, hence, available for contact $TiO_2.(H_2O)_n$ nanoparticles as described below in Table S3.1. The most important CALB's amino acids binding to $TiO_2.(H_2O)_n$.

Table S3. 1: *The most important CALB's amino acids binding to* $TiO_2.(H_2O)_n$.

Amino acid	Total N° of amino acids (CALB)	N° of amino acids binding to $TiO_2.(H_2O)_n$	Position	Binding
Aspartic acid	**14**	**5**	D6, D17, D257, D265, D296	ionic binding, receiving H^+ atoms from water
Glutamine	**18**	**6**	Q11, Q58, Q175, Q247, Q270, Q291	hydrogen bond, receiving H^+ atoms from H_2O, or donating H^+ atoms to TiO_2
Lysine	**9**	**7**	K13, K32, K98, K124, K271, K290, K308	ionic binding, donating O^- atoms from TiO_2
Methionine	**4**	**1**	Met298	donating atoms to $TiO_2.(H_2O)_n$, receiving atoms from water, S acting as metal ions ligand
Proline	**30**	**10**	P12, P27, P33, P119, P178, P260, P268, P295, P299, P303	ionic binding, donating O^- atoms from TiO_2
Serine	**31**	**14**	S3, S5, S10, S14, S26, S28, S29, S31, S94, S120, S123, S243, S250, S312	ionic binding, receiving H^+ atoms from water

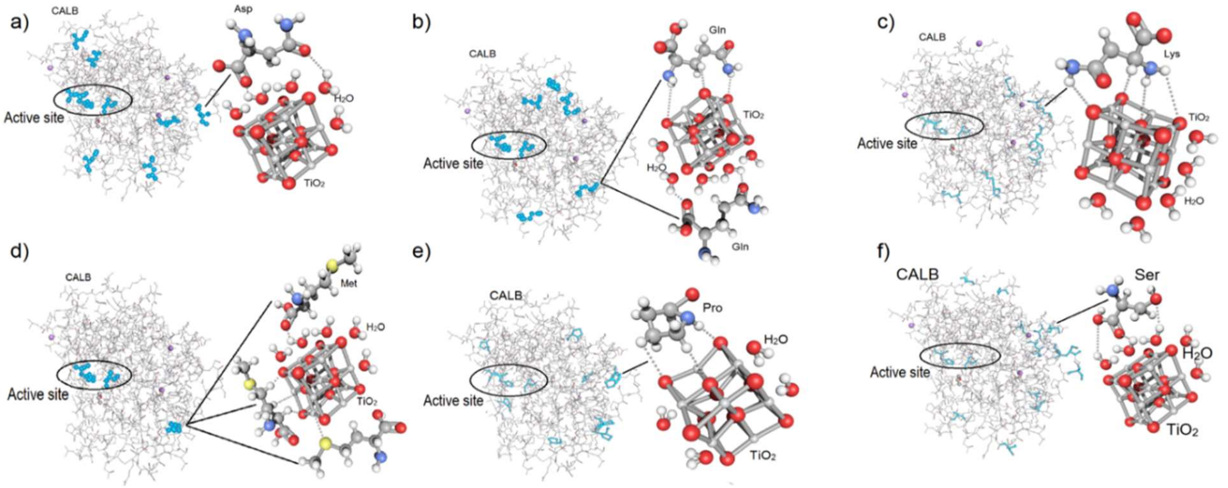

Figure S3. 2. The most important CALB's amino acids binding to $TiO_2.(H_2O)_n$; (a) Asp, (b) Gln, (c) Lys, (d) Met, (e) Pro, (f) Ser). Enzyme structure: 5A71 (STAUCH et al., 2015). Chemical structures developed by: Chemdoodle®, design developed by: Sketchup Pro 2021® and PhotoPad Professional v. 6.59®.

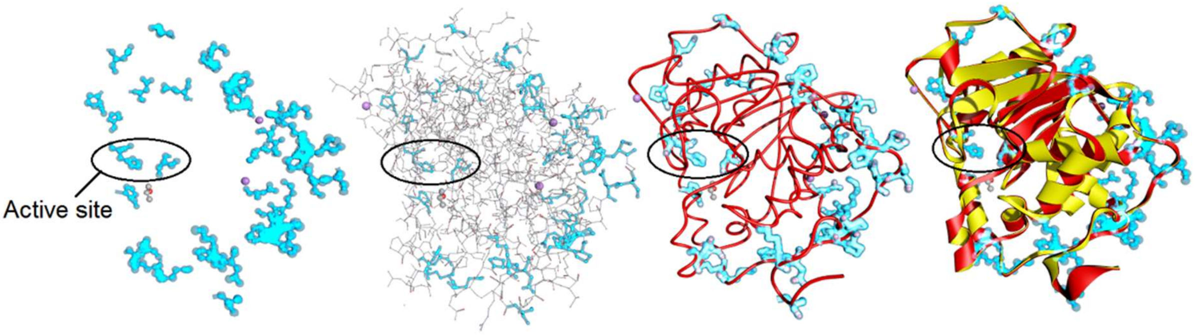

Figure S3. 3. CALB structure: Active site (inside the circle) and amino acids bonded to $TiO_2.(H_2O)_n$ (blue colour). Enzyme structure: 5A71 (STAUCH et al., 2015). Chemical structures developed by: Chemdoodle®, design developed by: Sketchup Pro 2021® and PhotoPad Professional v. 6.59®.

However, the external enzyme chain is formed mainly by hydrophilic amino acids, interspersed by hydrophobic amino acids (Panel S3. 1). These hydrophilic amino acids (His, Arg, Asn, Thr, Cys, Glu) can link to TiO_2 as well (Ataman et al., 2011; Giacomelli et al., 1995; Mudunkotuwa & Grassian, 2014; Pászti & Guczi, 2009; Roddick-Lanzillota et al., 1998; Roddick-Lanzilotta & McQuillan, 2000; Schmidt & Steinemann, 1991).

LPSGSDPAFSQPKSVLDAGLTCQGASPSSVSKPILLVPGTGTTGPQSFDSNWIPLSTQLGYTPCWISP
PPFMLNDTQVNTEYMVNAITALYAGSGNNKLPVLTWSQGGLVAQWGLTFFPSIRSKVDRLMAFAPDY
KGTVLAGPLDALAVSAPSVWQQTTGSALTTALRNAGGLTQIVPTTNLYSATDEIVQPQVSNSPLDSSY
LFNGKNVQAQAVCGPLFVIDHAGSLTSQFSYVVGRSALRSTTGQARSADYGITDCNPLPANDLTPEQ
KVAAAALLAPAAAAIVAGPKQNCEPDLMPYARPFAVGKRTCSGIVTP

*Six main amino acids available to $TiO_2.(H_2O)_n$ binding / Lids: α5 and α10 / active site / Hydrophilic amino acis / More flexible residues.

Panel S3. 1. Amino acids available to $TiO_2.(H_2O)$ binding.

S3.2. CLEX via DMT

One of the most promising gelling processes used in microscale is the competitive internal crosslinking ion exchange (CLEX) developed by Bassett et al. (2016). In this method, the biopolymer is added into two different aqueous solutions containing chelated ions. According to the difference in the equilibrium binding constant between them when the two solutions are combined (Table S3.2), the competitive displacement induces the interaction between a specific ion and the biopolymer chain resulting in the hydrogel matrix formation.

Adding other components can interfere with the alginate gelation efficiency. TiO_2 added to stream DS2 (Zn^{2+}-EDDA) prevents the gelation (mechanism described in Figure S3. 4). May because TiO_2 are attracted to Zn^{2+} blocking its crosslinking and binding with the EDTA. Without Zn^{2+}-EDTA binding, Ca^{2+} is not released and is free to bind with alginate**.** The alginate can not be gelling without the presence of ionic calcium.

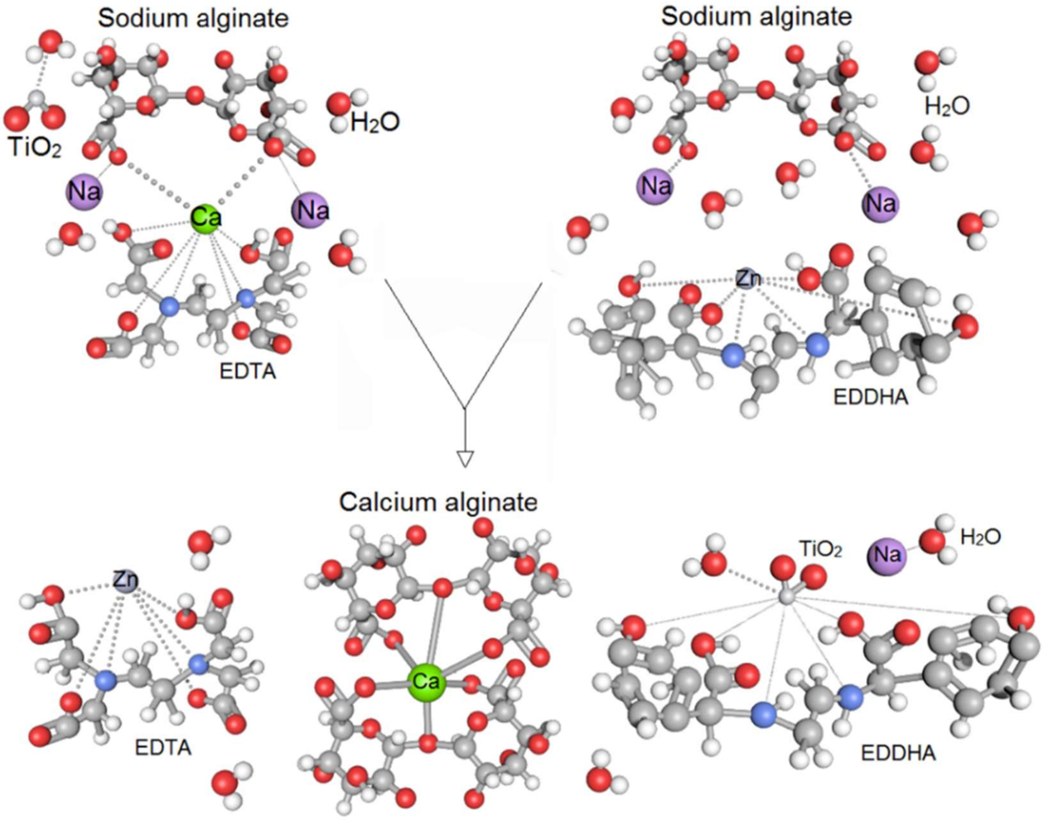

Figure S3. 4. CLEX mechanism. Chemical structures developed by: Chemdoodle®, design developed by: Sketchup Pro 2021® and PhotoPad Professional v. 6.59®.

Table S3. 2: *Log K values of cations and chelates (25°C).*

	Alginate	EDTA	EDDA
Ca^{2+}	~4.00 (Fang et al., 2017)	10.60 (Smith & Martell, 2004)	2.90 (Smith & Martell, 2004)
Zn^{2+}	~2.27 (Smith & Martell, 2004)	16.00 (Smith & Martell, 2004)	11.10 (Smith & Martell, 2004)

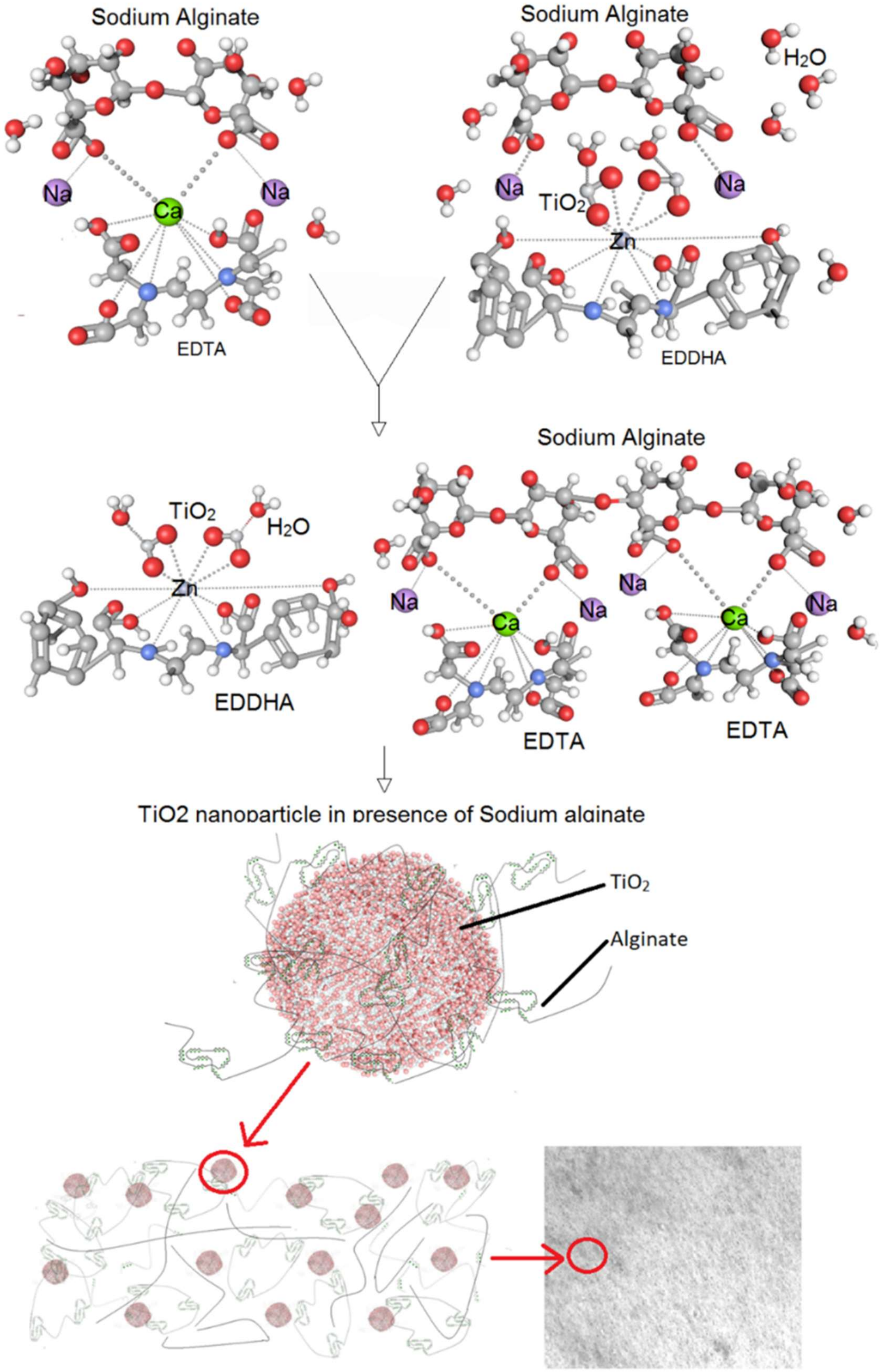

Figure S3. 5. CLEX mechanism developed with TiO_2 nanoparticles added in the stream DS2 (Zn^{2+}-EDDA) Chemical structures developed by: Chemdoodle®, design developed by: Sketchup Pro 2021® and PhotoPad Professional v. 6.59®.

S3.3. Enzymatic activity

The table below (Table S3.3) shows the enzymatic activity and the respective Relative enzymatic activity (REA), which is considered a percentage of free enzyme enzymatic activity when time equals zero.

Table S3. 3: *Enzymatic activity and REA (%) of CALB.*

CLEX via DMT compounds	**REA (%)**	**U/mg**	**SD**
CALB$_{\text{Free}}$ + Sodium alginate	111%	0.901	±0.0495
CALB$_{\text{Free}}$ + Calcium chloride	126%	1.023	±0.0709
CALB$_{\text{Free}}$ + EDTA	106%	0.861	±0.0301
CALB$_{\text{Free}}$ + EDDA	70%	0.568	±0.0219
CALB$_{\text{Free, t=0}}$	100%	0.812	±0.0583
CALB$_{\text{Free, t=30 days}}$	84%	0.682	±0.0351
CALB immobilised			
CALB$_{\text{EDTA, t=0}}$	121%	0.982	±0.0254
CALB$_{\text{EDTA, t=30 minutes}}$	127%	1.029	±0.0399
CALB$_{\text{EDDA, t=0}}$	110%	0.896	±0.0292
CALB$_{\text{EDDA, t=30 minutes}}$	80%	0.652	±0.0260
CALB$_{\text{CaCl2, t=0}}$	112%	0.912	±0.1170
CALB$_{\text{CaCl2, t=30 minutes}}$	138%	1.121	±0.0237
CALB$_{\text{TiO2, t=0}}$	289%	2.343	±0.0467
CALB$_{\text{TiO2, t=30 days}}$	287%	2.330	±0.0981
[CALB]$_{\text{EDTA-Ca, t=0}}$	100%	0.810	±0.1759
[CALB]$_{\text{EDTA-Ca, t=24 h}}$	90%	0.731	±0.0219
[CALB]$_{\text{EDTA-Ca, t=48 h}}$	85%	0.690	±0.0591
[CALB]$_{\text{EDTA-Ca, after resistant test}}$	42%	0.341	±0.0134
[CALB]$_{\text{EDDA-Zn, t=0}}$	82%	0.666	±0.0492
[CALB]$_{\text{EDDA-Zn, t=24 h}}$	67%	0.544	±0.0337
[CALB$_{\text{TiO2}}$]$_{\text{EDTA-Ca, t=0}}$	232%	1.884	±0.1437
[CALB$_{\text{TiO2}}$]$_{\text{EDTA-Ca, t=24 h}}$	286%	2.322	±0.0556
[CALB$_{\text{TiO2}}$]$_{\text{EDTA-Ca, t=48 h}}$	291%	2.363	±0.0937
[CALB$_{\text{TiO2}}$]$_{\text{EDTA-Ca, after resistant test}}$	289%	2.347	±0.0789
[CALB$_{\text{TiO2}}$]$_{\text{EDTA-Ca, t=30 days}}$	263%	2.136	±0.0637
[CALB$_{\text{TiO2}}$]$_{\text{EDDA-Zn, t=0}}$	96%	0.780	±0.0494
[CALB$_{\text{TiO2}}$]$_{\text{EDDA-Zn, t=24 h}}$	127%	1.031	±0.0483
Suspension			
[CALB]$_{\text{EDTA-Ca, t=0}}$	0%	0.000	±0.0010
[CALB]$_{\text{EDTA-Ca, t=24 h}}$	0%	0.000	±0.0010
[CALB]$_{\text{EDTA-Ca, t=48 h}}$	5%	0.041	±0.0081
[CALB]$_{\text{EDTA-Ca, after resistant test}}$	6%	0.049	±0.0114
[CALB$_{\text{TiO2}}$]$_{\text{EDTA-Ca, t=0}}$	0%	0.000	±0.0010
[CALB$_{\text{TiO2}}$]$_{\text{EDTA-Ca, t=24 h}}$	0%	0.000	±0.0010
[CALB$_{\text{TiO2}}$]$_{\text{EDTA-Ca, t=48 h}}$	1%	0.008	±0.0010
[CALB$_{\text{TiO2}}$]$_{\text{EDTA-Ca, after resistant test}}$	1%	0.008	±0.0011
[CALB$_{\text{TiO2}}$]$_{\text{EDTA-Ca, t=30 days}}$	2%	0.016	±0.0124

S3.4. Scanning electron microscope

$CALB_{Free}$, TiO_2, $CALB_{TiO2}$, $(CALB_{TiO2})_{EDTA\text{-}Ca}$, and alginate microbeads without catalyst were analysed by scanning electron microscope (SEM). Comparing the images (Figure S3. 6), it is possible to observe that CALB is immobilised onto TiO_2, and both $(CALB_{TiO2})$ are entrapped into alginate microbeads.

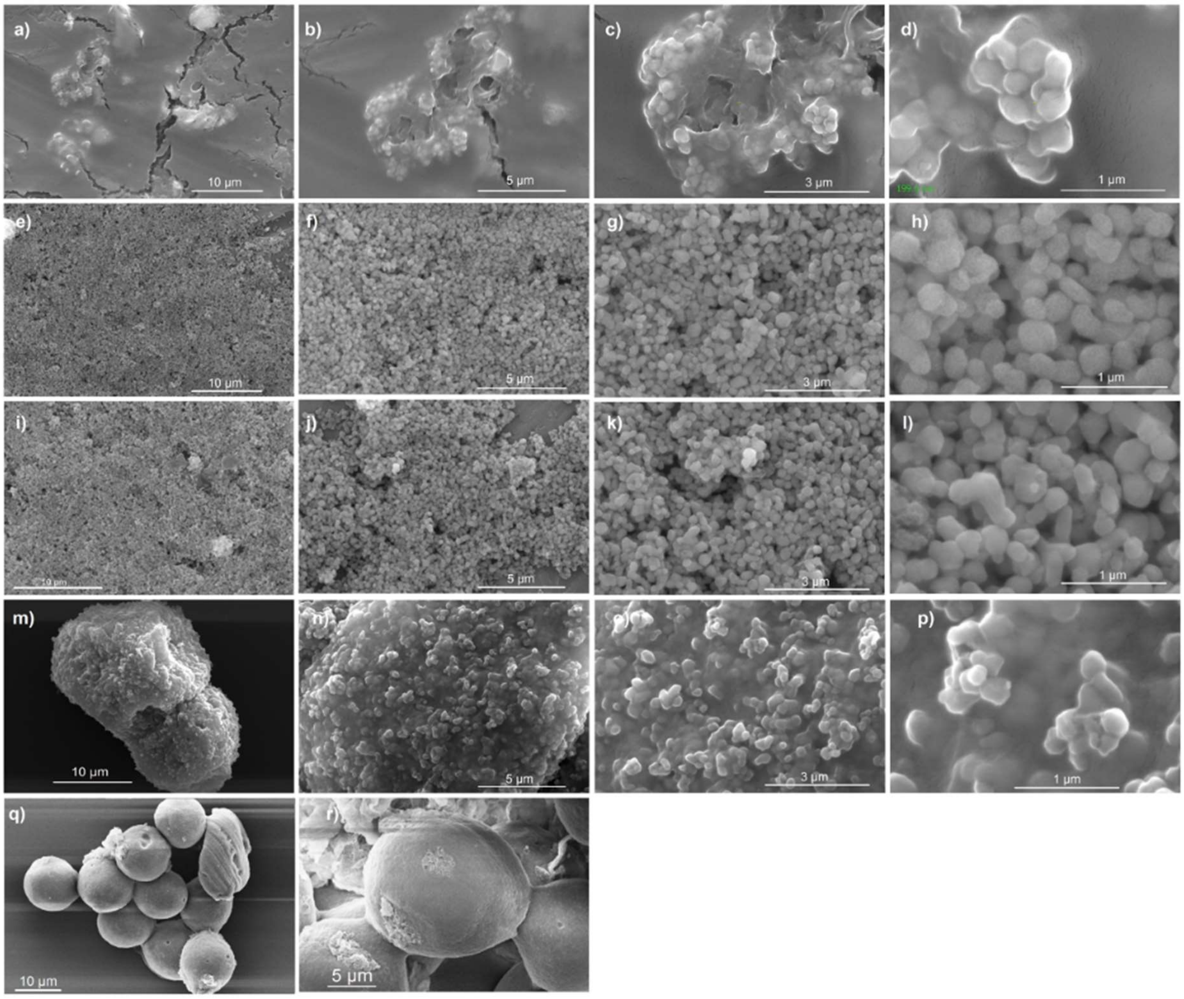

Figure S3. 6. SEM images of (a – d) CALB in native form, (e - h) TiO_2 nanoparticles, (i – l) CALB immobilised onto TiO_2, (m – p) CALB immobilised onto TiO_2 entrapped into calcium alginate microbeads obtained by CLEX via DMT, (q – r) Calcium alginate microbeads obtained by CLEX via DMT without catalyst. The calibration bar represents 10 µm, 5 µm, 3 µm and 1 µm, respectively.

APPENDIX C

Supplementary information for chapter IV

Methyl oleate synthesis by TiO_2-photocatalytic esterification of oleic acid: optimisation by response surface quadratic methodology, reaction kinetics and thermodynamics

S4.1 Photoesterification experimental design

Table S4. 1: *Oleic acid and methanol photoesterification: experimental kinetic planning.*

Entry	Coded Variables		Real Variables			
	x1	x2	FFA:MeOH	TiO_2 (% w/w_{OA})		
Pretreatment					**Reagent mixed with TiO_2[a]**	**Mixing time (minutes)**
1	1.41	1.41	01:55	20	FFA	30
2	1.41	1.41	01:55	20	FFA + MeOH	30
3	1.41	1.41	01:55	20	MeOH	5
4	1.41	1.41	01:55	20	MeOH	30
5	1.41	1.41	01:55	20	MeOH	60
CCR experimental design						
6	-1	-1	01:16	5	MeOH	30
7	1	-1	01:42	5	MeOH	30
8	-1	1	01:16	15	MeOH	30
9	1	1	01:42	15	MeOH	30
10	-1.41	0	01:03	10	MeOH	30
11	1.41	0	01:55	10	MeOH	30
12	0	-1.41	01:29	1	MeOH	30
13	0	1.41	01:29	20	MeOH	30
14	0	0	01:29	10	MeOH	30
15	0	0	01:29	10	MeOH	30
16	0	0	01:29	10	MeOH	30
Complementary tests						
17	[c]	[c]	01:12	15	MeOH	30
18	[c]	[c]	01:12	15	MeOH	30
19	[c]	[c]	01:12	15	MeOH	30
20	1.41	[d]	01:55	25	MeOH	30
21	1.41	[d]	01:55	30	MeOH	30
22	1.41	1.41	01:55	20	MeOH	30
23	1.41	1.41	01:55	20	MeOH	30
24	1.41	1.41	01:55	20	MeOH	30

Optimisation model validation						
25	[e]	1.41	01:36	20	MeOH	30
26	[e]	1.41	01:45	20	MeOH	30
Blank tests						**Test**
27	1.41	X	01:55	0	[f]	B1
28	1.41	1.41	01:55	20	[f]	B2
28	1.41	X	01:55	0	[f]	B3
Temperature analysis						**Temperature (°C)**
29	[b]	[b]	01:12	15	[f]	25
30	[b]	[b]	01:12	15	[f]	35
31	[b]	[b]	01:12	15	[f]	45
32	[b]	[b]	01:12	15	[f]	55
33	[b]	[b]	01:12	15	[f]	65
34	1.41[c]	1.41[c]	01:55	20	[f]	25
35	1.41[c]	1.41[c]	01:55	20	[f]	35
36	1.41[c]	1.41[c]	01:55	20	[f]	45
37	1.41[c]	1.41[c]	01:55	20	[f]	55
38	1.41[c]	1.41[c]	01:55	20	[f]	65
TiO_2 reuse						**Cycle**
39	1.41	1.41	01:55	20	[f]	1C
40	1.41	1.41	01:55	20	[f]	2C
41	1.41	1.41	01:55	20	[f]	3C
42	1.41	1.41	01:55	20	[f]	4C
43	1.41	1.41	01:55	20	[f]	5C
Use of different alcohols						**Alcohol**
44	1.41	1.41	01:55	20	[f]	Ethanol
45	1.41	1.41	01:55	20	[f]	n-Propanol

[a] reagent used in the same proportion of the respective photoesterification tests; [b]PC1: operational condition 1 obtained from the literature (Manique et al., 2016); [c]PC2: operational condition 2 obtained by the best experimental photoesterification result; [d]Additional run. As the point 1.41 of TiO_2 showed a higher conversion, a higher concentration of catalyst was analysed; [e]Values obtained by optimisation model; [f]Catalyst pretreatment: TiO_2 mixed to MeOH for 30 minutes.

S4.2 Mathematical modelling

The photoesterification reaction between oleic acid and methanol is described by Equation S4. 2.

$$\mathrm{FFA} + \mathrm{MeOH} \underset{k_{-1}}{\overset{k_1}{\rightleftarrows}} \mathrm{FAME} + \mathrm{H_2O}$$

Equation S4. 1

For the reaction rate (Equation S4. 2), the following assumptions are made:

- Pseudo-first order for the forward reaction (esterification), considering reversible reaction.
- First-order for the backward reaction (hydrolysis).
- Both processes are dependent on the coverage fractions of catalyst sites occupied by FFA and FAME (Θ_{FAME} and Θ_{FFA}).

$$r = -\frac{d[FFA]}{dt} = k_{-1} \cdot \theta_{FAME} - k_1 \cdot \theta_{FFA} \qquad \text{Equation S4. 2}$$

Θ_{FAME} and Θ_{FFA} are frequently described by the Langmuir-Hinshelwood mechanism (LH). This model considers the reactant adsorption on the active catalyst site. It is the most common kinetic model to explain the heterogeneous catalytic process (Vorontsov, Valdés, Smirniotis, & Paz, 2020) for FFA in the presence of a heterogeneous catalyst. FFA adsorption (forward reaction) and desorption (backward reaction) are described by Equation S4. 3. The model is frequently applied by considering first-order kinetics (Atitar, Bouziani, Dillert, el Azzouzi, & Bahnemann, 2018; Ezzati, 2018; Houas et al., 2001; Konstantinou & Albanis, 2003; Tang & Huren An, 1995; Vorontsov et al., 2020) even for the esterification process using a heterogeneous catalyst (Ahmedzeki & Jendeel, 2013; Ezzati, 2018; Sert & Atalay, 2010).

$$FFA + Ti \underset{k'_{-1}}{\overset{k'_1}{\rightleftarrows}} FFA\,Ti \qquad \text{Equation S4. 3}$$

For the reaction rate, the following assumptions are made:

- Forward reaction (adsorption): first order.
- The FFA concentration is the limiting reactant.
- Reversible reaction.
- Backward reaction (desorption): first order.
- All of the active sites on the catalyst surface are the same.

$$k'_1 \cdot [\mathrm{FFA}] \cdot (1 - \theta_{\mathrm{FFA}}) = k'_{-1} \cdot \theta_{\mathrm{FFA}}$$ Equation S4. 4

At equilibrium, it is considered that: $r'_1 = r'_{-1}$

$$\therefore\ \theta_{\mathrm{FFA}} = \frac{k'_1 \cdot [\mathrm{FFA}]}{k'_{-1} + k'_1 \cdot [\mathrm{FFA}]} = \frac{K'_1 \cdot [\mathrm{FFA}]}{1 + K'_1 \cdot [\mathrm{FFA}]}$$ Equation S4. 5

r'_1 = FFA on Ti adsorption rate

r'_{-1}= FFA on Ti desorption rate

[FFA] = free fatty acid concentration (limiting parameter)

Θ_{FFA} = active site occupied by FFA

A similar mechanism was considered for hydrolysis (Equation S4. 8).

$$\mathrm{FAME} + \mathrm{Ti} \underset{k'_{-2}}{\overset{k'_2}{\rightleftarrows}} \mathrm{FAME\ Ti}$$ Equation S4. 6

$$\therefore\ \theta_{\mathrm{FAME}} = \frac{k'_2 \cdot [\mathrm{FAME}]}{k'_{-2} + k'_2 \cdot [\mathrm{FAME}]} = \frac{K'_2 \cdot [\mathrm{FAME}]}{1 + K'_2 \cdot [\mathrm{FAME}]}$$ Equation S4. 7

Therefore, substituting Equation S4. 8 and Equation S4. 9 into Equation S4. 2 gives:

$$-\frac{d[\mathrm{FFA}]}{dt} = k_{-1} \cdot \frac{K'_2 \cdot [\mathrm{FAME}]}{1 + K'_2 \cdot [\mathrm{FAME}]} - k_1 \cdot \frac{K'_1 \cdot [\mathrm{FFA}]}{1 + K'_1 \cdot [\mathrm{FFA}]}$$ Equation S4. 8

Considering that $[\mathrm{FFA}] = C_{\mathrm{FFA}_0} \cdot (1 - x)$, where x(t) is the FFA fraction at time t, Equation S4.10 becomes:

$$-C_{\mathrm{FFA}_0} \frac{dx}{dt} = k_{-1} \cdot \frac{K'_2 \cdot C_{\mathrm{FFA}_0} \cdot x}{1 + K'_2 \cdot C_{\mathrm{FFA}_0} \cdot x} - k_1 \cdot \frac{K'_1 \cdot C_{\mathrm{FFA}_0} \cdot (1 - x)}{1 + C_{\mathrm{FFA}_0} \cdot (1 - x)}$$ Equation S4. 9

$$\therefore\ \frac{dx}{dt} = k_1 \cdot \frac{K'_1 \cdot (1 - x)}{1 + K'_1 \cdot C_{\mathrm{FFA}_0} \cdot (1 - x)} - k_{-1} \cdot \frac{K'_2 \cdot x}{1 + K'_2 \cdot x \cdot C_{\mathrm{FFA}_0}}$$ Equation S4. 10

Considering the contour conditions:

$t=0 \rightarrow x=0;$

$t=t_{eq} \rightarrow x=x_{eq};$

$$\frac{dx}{dt} = 0 \quad \rightarrow \quad x = x_{eq}$$

S4.3. Catalyst characterization

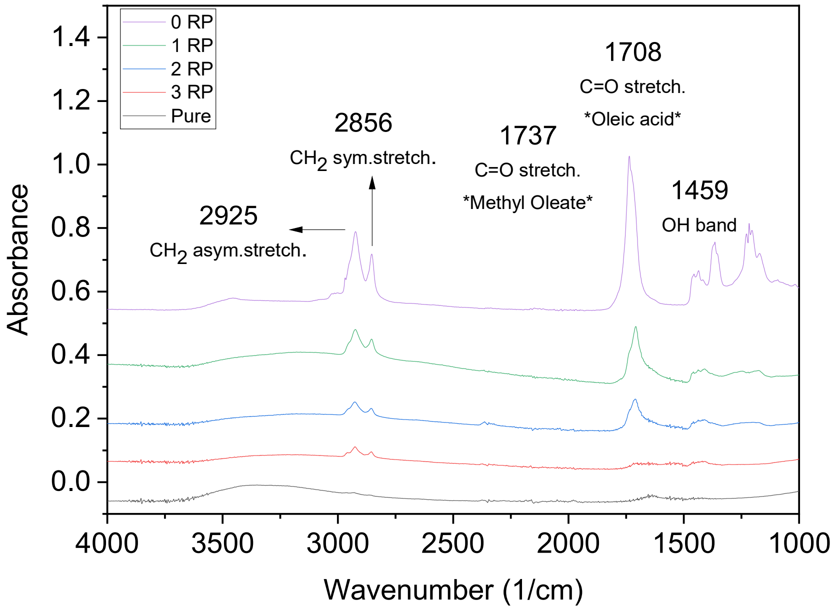

Figure S4. 1. FTIR spectra of TiO_2 during the recovery process: pure, after photoesterification PC2, after 1 RP, 2 RP and 3 RP (1 cycle).

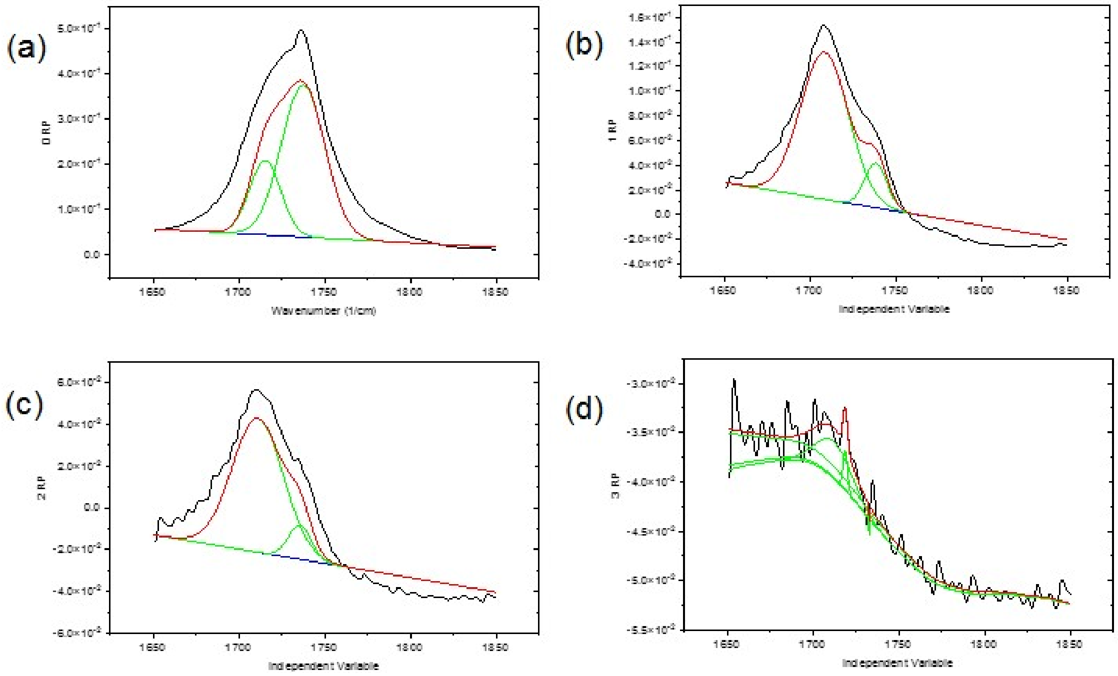

Figure S4. 2. TiO_2 FTIR spectra deconvolution of peaks: $C_{18}=O_{19}$ of organic material (methyl oleate and oleic acid) present in TiO_2: (a) after photoesterification; (b) after 1 RP; (c) after 2 RP; (d) after 3 RP (CPR); which completes the 1st cycle (C1). Deconvolution curves obtained by PeakDeconvolution.opx for OriginLab®.

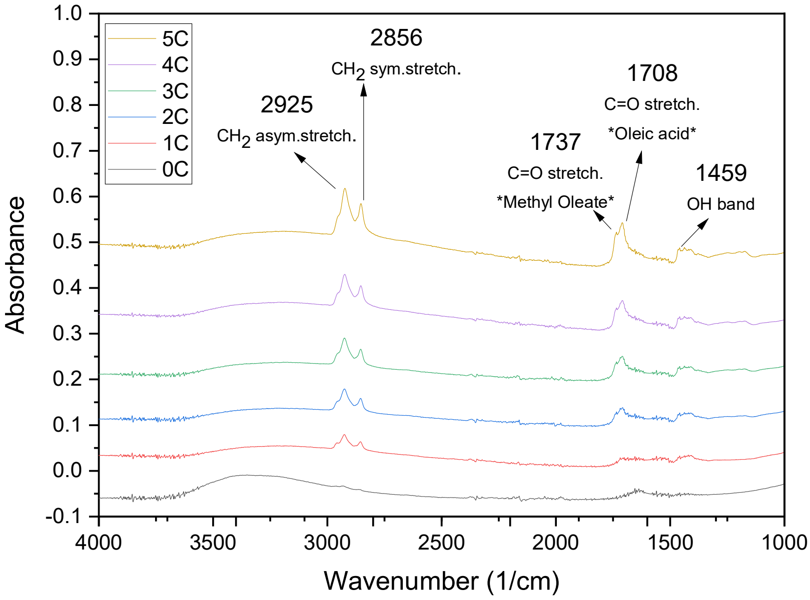

Figure S4. 3. FTIR spectra of TiO_2 of the catalyst in reuse process: pure, after 1cycle (photoesterification and CRP), 2 cycles, 3 cycles, 4 cycles and 5 cycles.

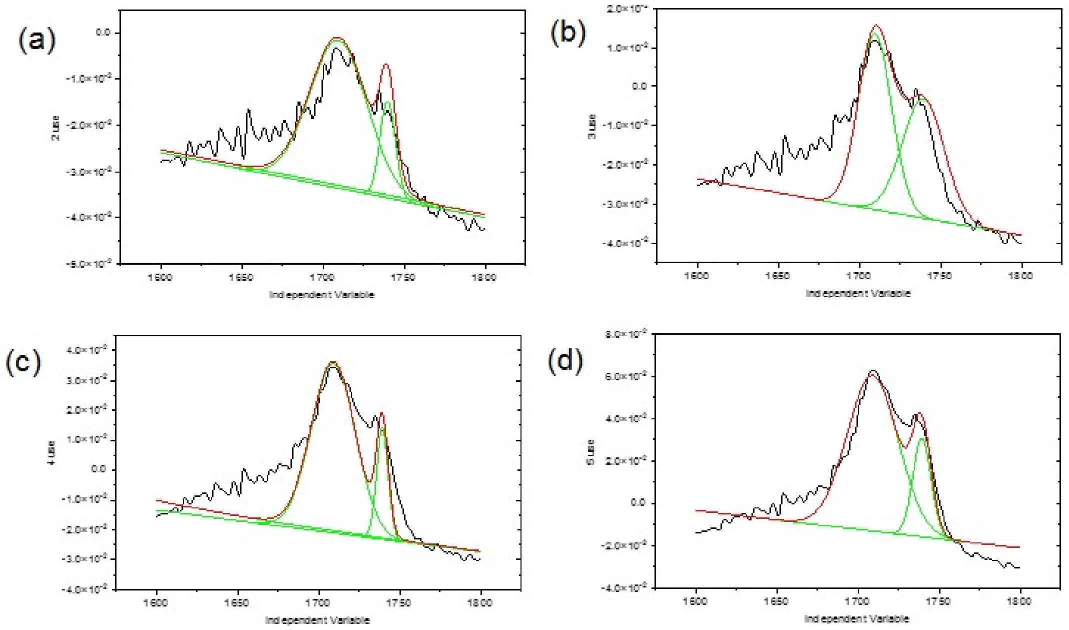

Figure S4. 4. TiO_2 FTIR spectra deconvolution of peaks: $C_{18}=O_{19}$ of organic material (methyl oleate and oleic acid) present in TiO_2: (a – d) 2C to 5C, respectively. Deconvolution curves obtained by PeakDeconvolution.opx for OriginLab®.

Table S4. 2: *TiO_2 characterisation by FTIR deconvolution and TGA analysis.*

	FTIR				**TGA**			
Beginning X	2785.56065	1572.0032	**Peak deconvolution**		**Weight lost**	**MO**	**Moisture**	**Proportion MO/AO**
Ending X	2982.54944	1839.215						
Sample	**MO**	**MO and AO**	**MO**	**OA**	**RT - 600**	**110 - 600**	**RT - 110**	
Pure	0.224	0.063	0	0	2.71%	1.44%	1.27%	0%
0 RP	14.799	28.314	10.698	3.772	29.29%	28.77%	0.53%	284%
1 RP	6.294	11.247	0.584	4.169	11.24%	10.53%	0.71%	14%
2 RP	3.134	6.414	0.275	2.392	6.36%	5.77%	0.59%	11%
1C[a]	2.191	0.583	~0	~0	4.21%	3.69%	0.52%	~0
2C	3.666	2.152	0.251	1.415	6.40%	5.78%	0.62%	15%
3C	4.593	3.007	0.199	1.169	6.79%	6.21%	0.59%	15%
4C	5.442	3.718	0.337	1.923	7.74%	7.07%	0.67%	15%
5C	8.162	5.603	0.654	2.894	10.95%	10.31%	0.64%	18%

[a] Represents 1 complete cycle, after photoesterificaiton and entire recovery process.

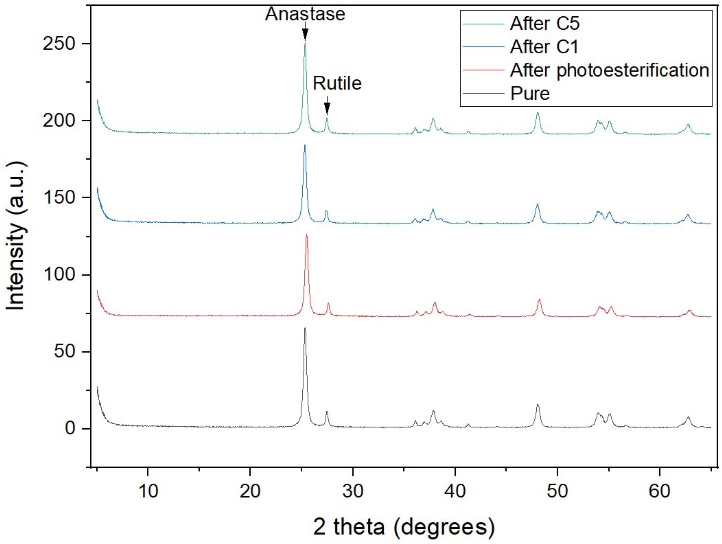

Figure S4. 5. XRD of TiO_2: pure, after photoesterification, after 1 cycle of photoesterification and recovery process (C1), after 5 cycles of photoesterification and recovery process (C5). The prominent peak of anatase (25.33°) and rutile (27.42°) are highlighted.

Table S4. 3: *Atomic (%) of TiO_2 pure, after photoesterification, recovery, and reuse obtained by EDS.*

Element	**TiO_2 pure**	**PC1[a]**	**PC2[b]**	**After C1[c, d]**	**After C5[e]**
C	19.13	30.08	13.75	15.26	18.39
O	66.67	66.67	66.67	66.67	66.67
Ti	14.20	3.26	19.58	17.97	14.94
Total:	100.00	100.00	100.00	100.00	100.00

[a]Photoesterification operational conditions 1 (PC1): 15% TiO_2 (w w_{OA}) irradiated by UVA light, 1OA:12MeOH molar ratio, 55°C, batch reactor; [b]Photoesterification operational conditions 1 (PC1): 20% TiO_2 (w w_{OA}) irradiated by UVA light, 1OA:55MeOH molar ratio, 55°C, batch reactor; [c]After 1 cycle (C1): photoesterification by PC2 and a complete recovery process; [d]Presence of Si traces; [e]After 5 cycles (C5): five times of photoesterifications by PC2 and complete recovery process.

S4.4 Fame characterisation

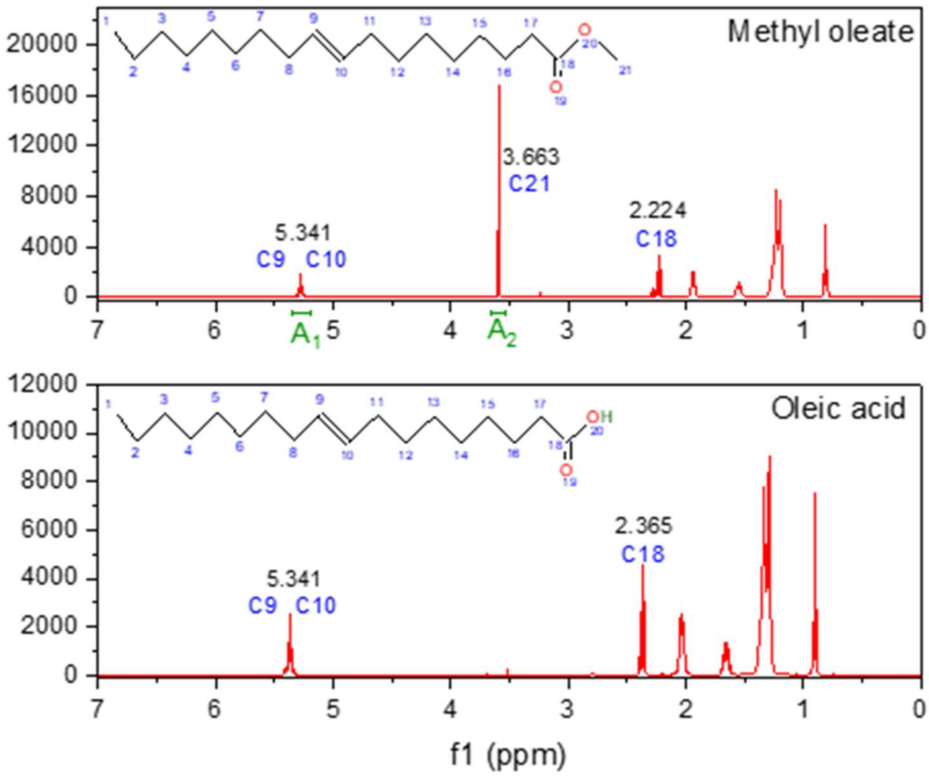

Figure S4. 6. ^{1}H-NMR of methyl oleate and oleic acid, respectively. The molecular structures were obtained by ACD/ChemSketch® (Advanced Chemistry Development Inc.).

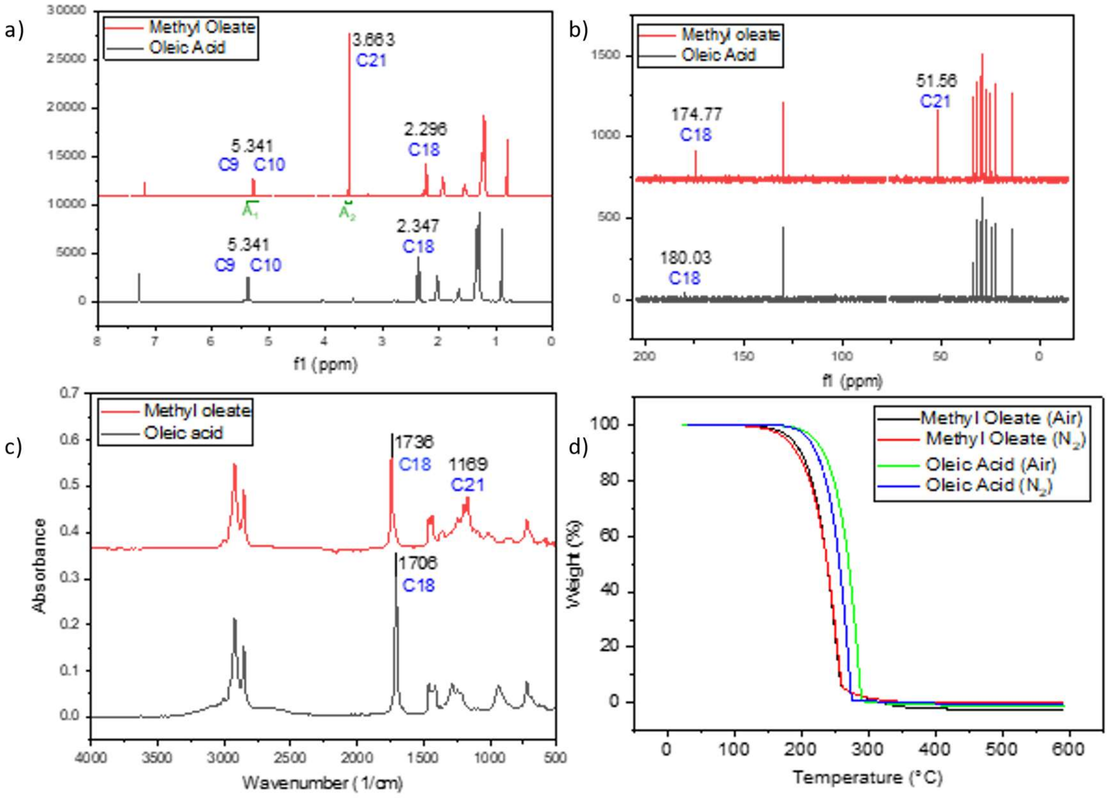

Figure S4. 7. FFA and FAME (photoesterification product) analysis by: (a) ^{1}H-NMR. (b) ^{13}C-NMR, (c) FTIR ATR, (d) TGA.

S4.5 Kinetic and thermodynamic properties

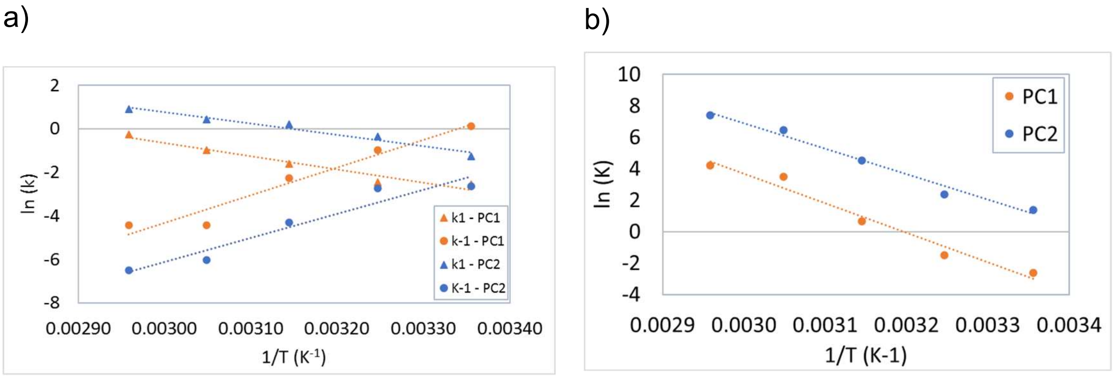

*Figure S4. 8***.** Thermodynamic analysis: (a) Arrhenius diagram for PC1 and PC2 operational conditions, (b) van 't Hoff diagram for PC1 and PC2 [PC1: 1 OA:12 MeOH molar ratio and 15%TiO_2 (w/w_{OA}) and PC2: 1 OA:55 MeOH molar ratio 20% TiO_2 (w/w_{OA})].

APPENDIX D

Supplementary information for Chapter V

Biodiesel production from canola oil by TIO_2- photocatalysed transesterification

S.5.1 Phototransesterification

Table S5.1 summarises the transesterification reactions of canola oil with alcohols.

Table S5. 1: *Transesterification/esterification of canola oil by different catalytic methods.*

Test #	Feedstock	Alcohol	Catalyst	T (°C)	Biodiesel (%)
1	Canola oil	Methanol	KOH	120	91
2	Canola oil	Methanol	H_2SO_4 - 4 hrs	120	99
3	Canola oil	Methanol	H_2SO_4 - 1 hrs	120	19
3	Canola oil	Methanol	TiO_2 + sunlight	65	19
4	Canola oil	Methanol	TiO_2 + UVA (replicate 1)	65	73
5	Canola oil	Methanol	TiO_2 + UVA (replicate 2)	65	73
6	Canola oil	Methanol	TiO_2 + UVA (replicate 3) (C1)	65	71
7	Canola oil	Methanol	TiO_2 + UVA	55	39
8	Canola oil	Methanol	TiO_2 + UVA	45	24
9	Canola oil	Methanol	TiO_2 + UVA	35	14
10	Canola oil	Methanol	TiO_2 + UVA	25	13
11 (Blank 1)	Canola oil	Methanol	UVA (without TiO_2)	65	3
12 (Blank 2)	Canola oil	Methanol	TiO_2 (without UVA)	65	8
13 (Blank 3)	Canola oil	Methanol	Without TiO_2 and UVA	65	5
14 (Blank 4)	Canola oil	Methanol	TiO_2 + UVA (without mix)	65	17
15 (Blank 5)	Canola oil	Methanol	No pretreatment	65	30
15	Canola oil	Methanol	TiO_2 (reuse) + UVA (C2)	65	47
16	Canola oil	Methanol	TiO_2 (reuse) + UVA (C3)	65	43
17	Canola oil	Methanol	TiO_2 (reuse) + UVA (C4)	65	40
18	Canola oil	Methanol	TiO_2 (reuse) + UVA (C5)	65	36
19	Canola oil	Ethanol	TiO_2 + UVA	65	38

S.5.2 Photoesterification by sunlight

The sunlight irradiation measurements were obtained and monitored by Arpansa (ARPANSA, 2022), and the data are shown below for the day of solar exposure.

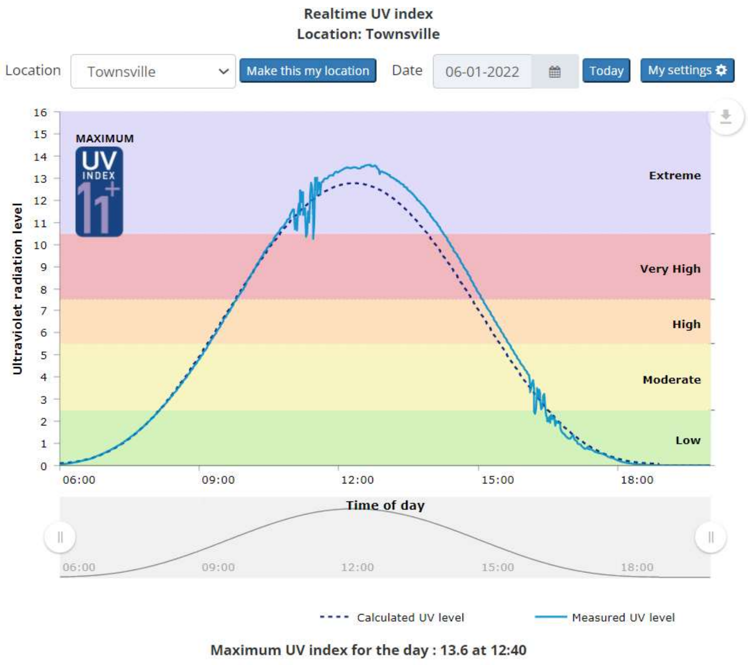
Realtime UV index
Location: Townsville

Location: Townsville

Date: 06-01-2022

Maximum UV index for the day : 13.6 at 12:40

Figure S5. 1. UV radiation level on the 6th of January 2022, at James Cook University, Townsville (Geographic coordinate: -19.325598727686298, 146.75950750865223).

S.5.3 ^{1}H-NMR

Table S5. 2: *^{1}H-NMR chemical shifts for the main protons of canola oil (Solvent: $CDCl_3$).*

Shift δ (ppm)	Multiplicity	Assignments
0.91 – 0.77	Doublet of Triplet	Terminal CH_3
0.92 - 0.99	Triplet	Terminal CH_3 in Fatty Acid Chain
1.13 - 1.42	Multiplet	CH_2 groups in Fatty Acid Chain
1.47 - 1.69	Unresolved Multiplet	$C\underline{H}_2CH_2CO_2$ **(5)**
1.86 - 2.13	Multiplet	$C\underline{H}_2CH_2CH=$
2.21 - 2.39	Triplet	CH_2CO_2 **(4)**
2.65 - 2.88	Multiplet	$C\underline{H}_2CH=$
4.2	Doublet of Doublet	$OC\underline{H}_2CH$ **(2 & 3)**
5.24	Triplet of Triplets	CHO **(1)**
5.27 - 5.44	Multiplet	CH=CH

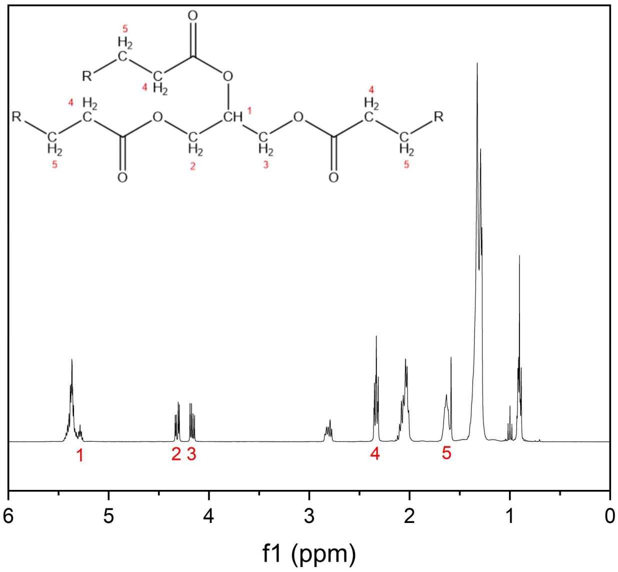

Figure S5. 2. ^{1}H NMR spectrum (400 MHz, $CDCl_3$) of canola oil (R = cis-$CH_3(CH_2)_7CH{=}CH(CH_2)_5$).

Table S5. 3: *^{1}H NMR chemical shifts for the main protons of methyl oleate[a] (Solvent: $CDCl_3$).*

Shift δ (ppm)	Multiplicity	Assignments
0.85	Triplet of Doublets	Terminal CH_3 in Fatty Acid Chain
0.94	Triplet	Terminal CH_3 in Fatty Acid Chain
1.07 - 1.40	Multiplet	CH_2 in Fatty Acid Chain
1.47 - 1.66	Multiplet	Ester β Carbon **(3)**
1.87 - 2.10	Multiplet	Olefin β Carbon in Fatty Acid Chain
2.26	Triplet	Ester α Carbon **(2)**
2.75	Doublet of Triplets	Olefin α Carbon in Fatty Acid Chain
3.63	Singlet	Methyl Ester **(1)**
5.25 - 5.37	Multiplet	Olefins in Fatty Acid Chain

[a]Contains traces of residual ethyl acetate, methanol and acetone.

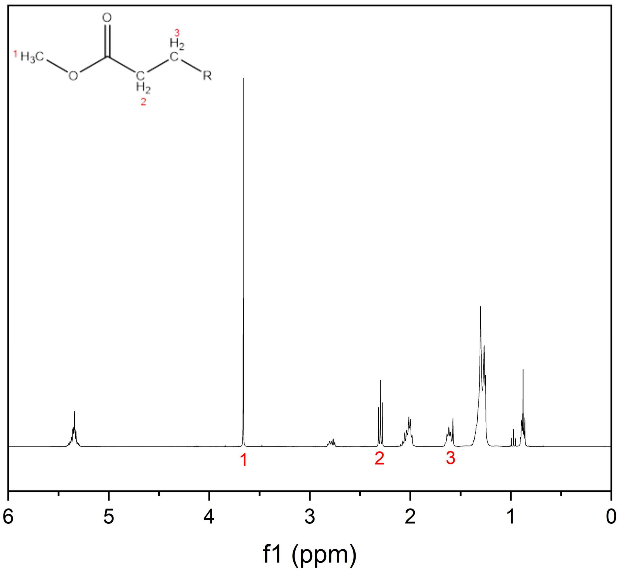

Figure S5. 3. ^{1}H NMR spectrum (400 MHz, $CDCl_3$) of methyl oleate from canola oil (R = cis-$CH_3(CH_2)_7CH=CH(CH_2)_5$).

Table S5. 4: *^{1}H NMR chemical shifts for the main protons of ethyl oleate*[a] *(Solvent: $CDCl_3$).*

Shift δ (ppm)	**Multiplicity**	**Assignments**
0.85	Triplet of Doublets	Terminal CH_3 in Fatty Acid Chain
0.94	Triplet	Terminal CH_3 in Fatty Acid Chain
1.07 - 1.40	Multiplet	CH_2 in Fatty Acid Chain
1.47 - 1.66	Multiplet	Ester β Carbon **(4)**
1.87 - 2.10	Multiplet	Olefin β Carbon in Fatty Acid Chain
2.26	Triplet	Ester α Carbon **(3)**
2.75	Doublet of Triplets	Olefin α Carbon in Fatty Acid Chain
4.10 - 4.15	Quartet	Ethyl Ester **(1,2)**
5.25 - 5.37	Multiplet	Olefins in Fatty Acid Chain

[a]Contains traces of residual ethyl acetate, methanol and acetone.

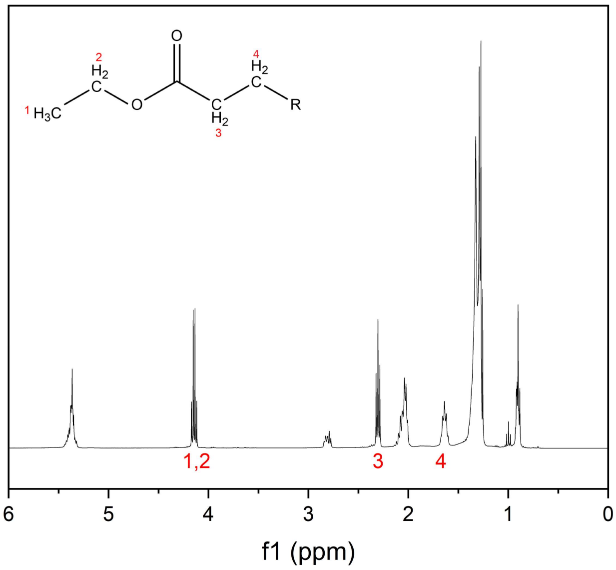

Figure S5. 4. ^{1}H NMR spectrum (400 MHz, $CDCl_3$) of ethyl oleate from canola oil (R = cis-$CH_3(CH_2)_7CH=CH(CH_2)_5$).

Table S5. 5: *Reported ^{1}H NMR chemical shifts for the main protons of key-intermediaries, diglycerides and monoglycerides of canola oil and methanol transesterification (Solvent: $CDCl_3$)* (Galvan et al., 2020; Nieva-Echevarría et al., 2015).

Shift δ (ppm)	Multiplicity	Assignments
0.88	Triplet	Saturated, monounsaturated ω-9 and/or ω-7 acyl groups and FA
0.89	Triplet	Unsaturated ω-6 acyl groups and FA
0.97	Triplet	Unsaturated ω-3 acyl groups and FA
1.19–1.42	Multiplet	Acyl groups and FA
1.61	Multiplet	Acyl groups in TG, except for DHA, EPA and ARA acyl groups
1.62	Multiplet	Acyl groups in 1,2-DG, except for DHA, EPA and ARA acyl groups
1.63	Multiplet	Acyl groups in 1,3-DG, 1-MG and FA, except for DHA, EPA and ARA acyl groups
1.64	Multiplet	Acyl groups in 2-MG, except for DHA, EPA and ARA acyl groups
1.69	Multiplet	EPA and ARA acyl groups in TG
1.72	Multiplet	EPA and ARA acids
1.92–2.15	Multiplet	Acyl groups and FA, except for –CH2– of DHA acyl group in β-position in relation to carbonyl group
2.26–2.36	Duplet	Acyl groups in TG, except for DHA acyl groups
2.33	Multiplet	Acyl groups in 1,2-DG, except for DHA acyl groups
2.35	Triplet	Acyl groups in 1,3-DG, 1-MG and FA, except for DHA acyl groups
2.38	Triplet	Acyl groups in 2-MG, except for DHA acyl groups
2.37–2.41	Multiplet	DHA acyl groups in TG
2.39–2.44	Multiplet	DHA acid
2.77	Triplet	Diunsaturated ω-6 acyl groups and FA
2.77–2.90	Multiplet	Polyunsaturated ω-6 and ω-3 acyl groups and FA
3.65	Triplet of double	Glyceryl group in 1-MG
3.73	Multiplet	Glyceryl group in 1,2-DG
3.84	Multiplet	Glyceryl group in 2-MG
3.94	Multiplet	Glyceryl group in 1-MG
4.05–4.21	Multiplet	Glyceryl group in 1,3-DG
4.18	Triplet of double	Glyceryl group in 1-MG
4.22	Quartet of double	Glyceryl group in TG
4.28	Triplet of double	Glyceryl group in 1,2-DG
4.93	Multiplet	Glyceryl group in 2-MG
5.08	Multiplet	Glyceryl group in 1,2-DG
5.27	Multiplet	Glyceryl group in TG
5.28–5.46	Multiplet	Acyl groups and FA

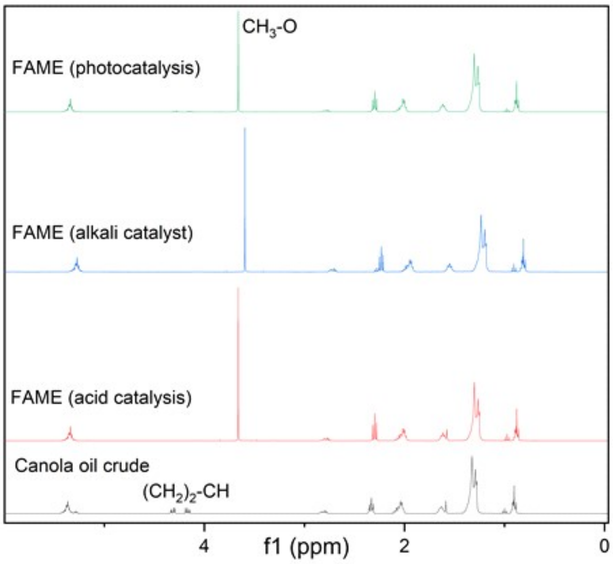

Figure S5. 5. ^{1}H-NMR spectra (400 MHz, $CDCl_3$) of crude canola oil and the products obtained by its transesterification with methanol using different catalysts: acid, alkali, and TiO_2/UVA irradiation.

S.5.4 Thermogravimetric analysis

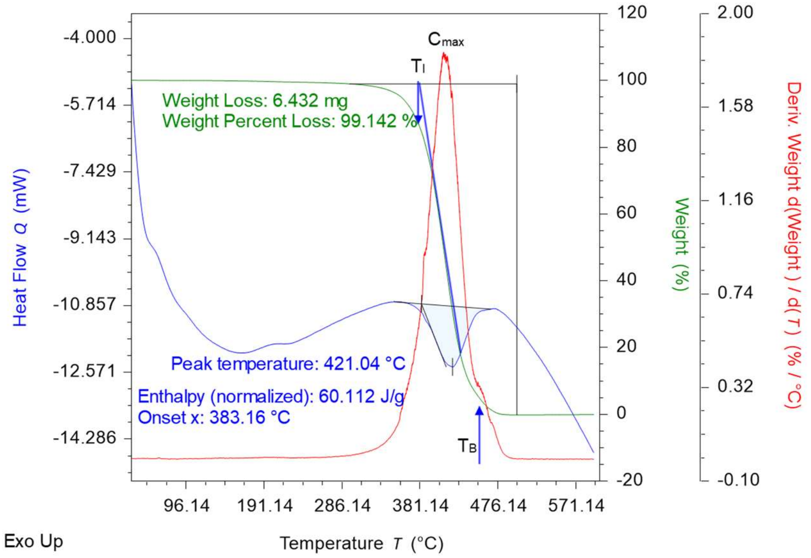

Figure S5. 6. TGA, DTA and DSC of canola oil.

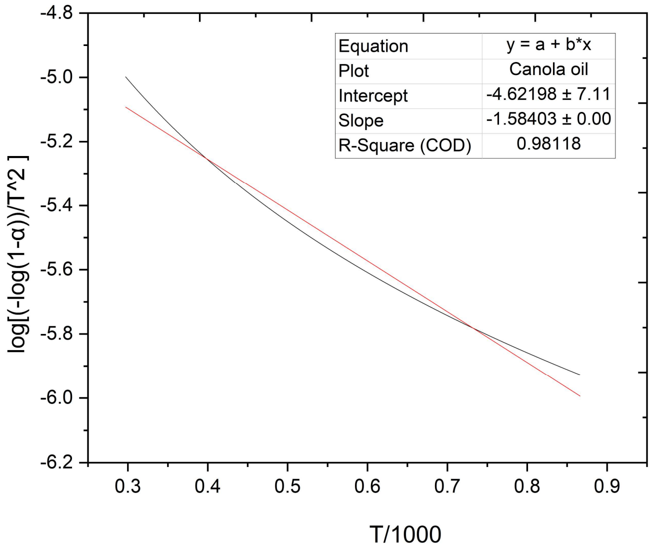

Figure S5. 7. Arrhenius model linearized using the Coats–Redfern method for the thermographic analysis of canola oil.

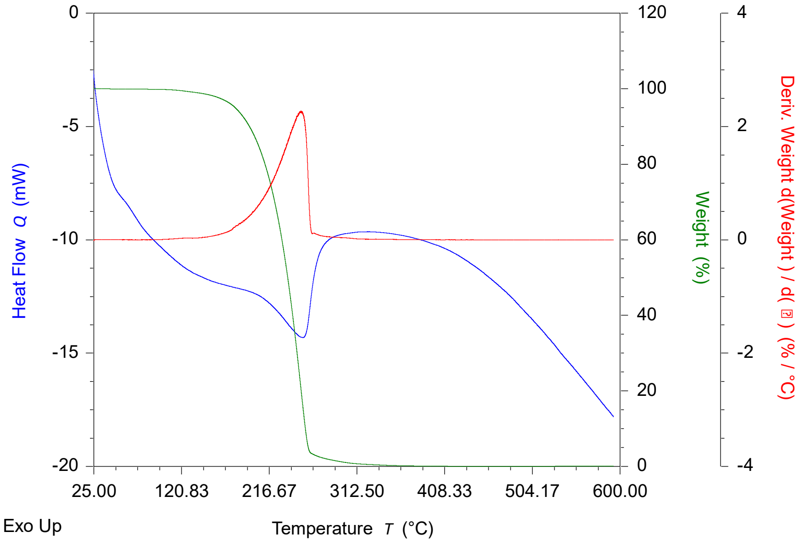

Figure S5. 8. TGA, DTA and DSC of FAME obtained using an acid catalyst.

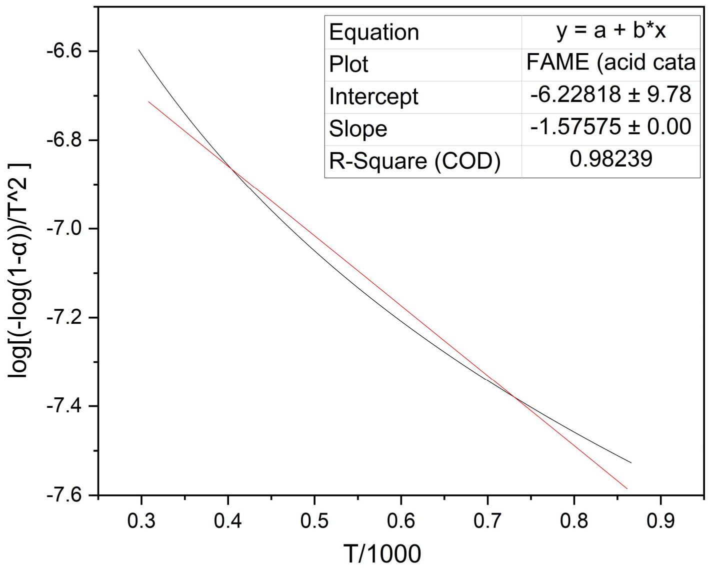

Figure S5. 9. Arrhenius model linearized by the Coats–Redfern method for the thermographic analysis of canola oil transesterification by acid catalysis.

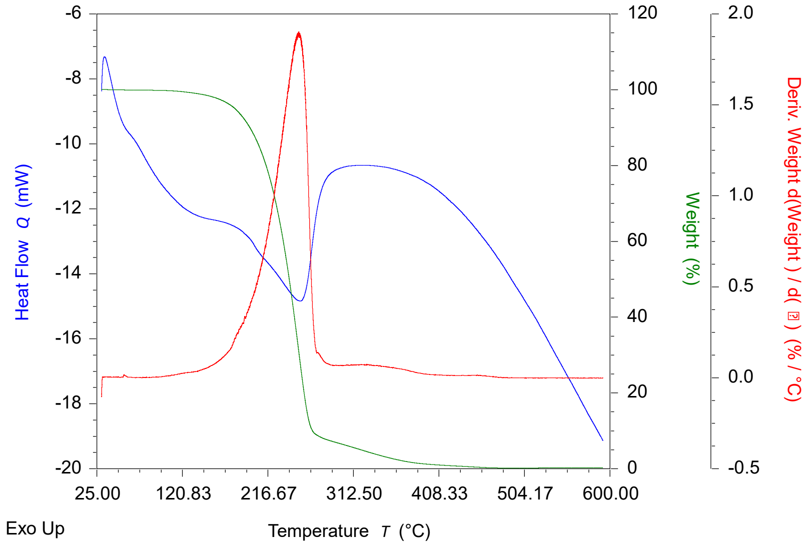

Figure S5. 10. TGA, DTA and DSC of FAME obtained using an alkali catalyst.

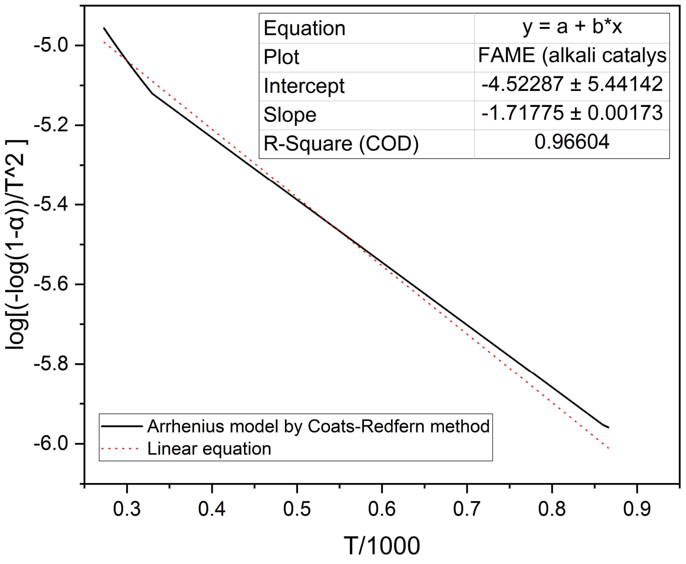

Figure S5. 11. Arrhenius model linearized by the Coats–Redfern method for the thermographic analysis of canola oil transesterification by alkali catalysis.

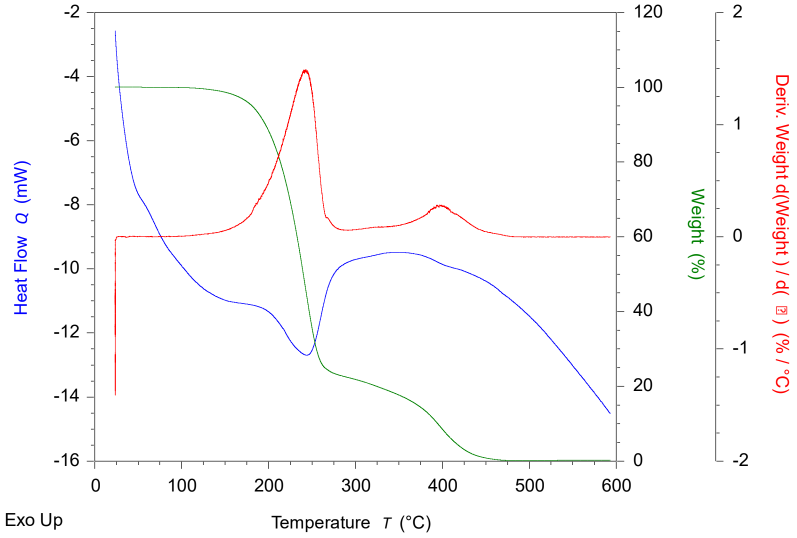

Figure S5. 12. TGA, DTA and DSC of FAME obtained by photocatalysis.

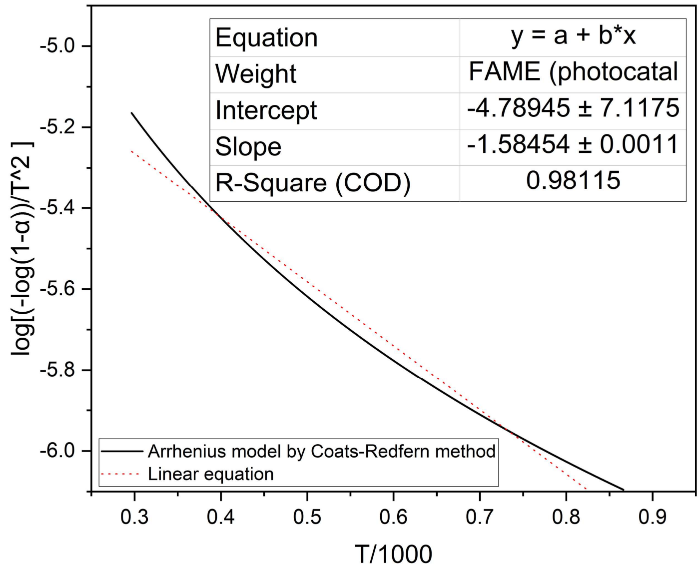

Figure S5. 13. Arrhenius model linearized by Coats–Redfern method for the thermographic analysis of canola oil transesterification by photocatalysis.

Table S5. 6: *Thermogravimetric analysis of canola oil and biodiesel obtained by different catalysis methods.*

			FAME by different catalysts		
		Canola oil	**Acid**	**Alkali**	**TiO_2+UVA**
T_I	(°C)	383	217	215	206
T_B	(°C)	454	258	263	257
Wo	mg	6.488	6.662	6.624	5.536
Wl	mg	5.645	4.997	5.266	4.706
Wf	mg	0	0	0	0
α	-	0.13	0.25	0.205	0.15
Slope	-	-1.584	-1.576	-1.718	-1.584
Ea_{TGA}	kJ/mol	-30.32	-30.17	-32.89	-30.33

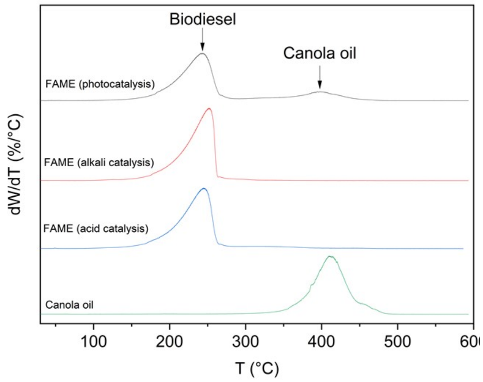

Figure S5. 14. DTA of canola oil and FAME obtained by transesterification catalysed by acid (99% purity), alkali (91% purity), and TiO_2 irradiated with UVA (73% of purity).

S.5.5 FTIR-ATR spectroscopy and GC analysis

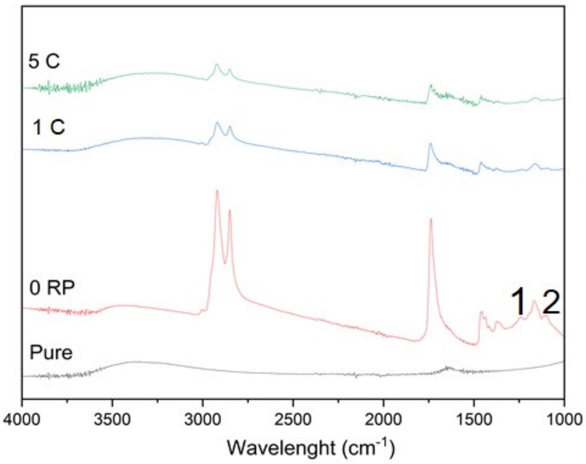

Figure S5. 15. FTIR-ATR spectra (10000 – 400 cm^{-1}) of pure TiO_2 used for canola oil and methanol transesterification under UVA irradiation (0 RP), after C1 (transesterification and recovery process), and after C5 (five reuses of transesterification and recovery process). Peak 1: characteristic of biodiesel, peak 2: characteristic of canola oil.

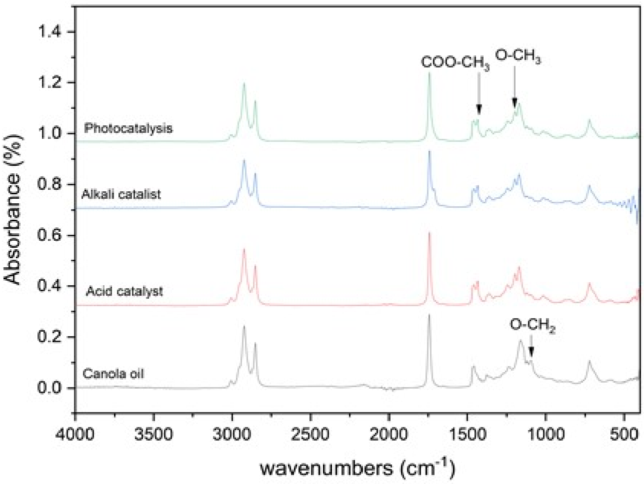

Figure S5. 16. FTIR-ATR spectra of canola oil and the crude products obtained by its transesterification in the presence of methanol using different catalysts: acid, alkali and TiO_2 under UVA irradiation.

Table S5. 7: *Characteristics bands of canola oil and related fatty acid methyl esters by FTIR-ATR spectroscopy.*

Canola oil		**FAME**	
band position (cm^{-1})	**assignments**	**band position (cm^{-1})**	**assignments**
3006.5	C=C-H stretching	3011.1	C=C-H stretching
2916.5	Aliphatic C-H stretching	2919.7	Aliphatic C-H stretching
2852.9	Aliphatic C-H stretching	2852.9	Aliphatic C-H stretching
1741.8	C=O stretching (ester)	1738.6	C=O stretching (ester)
1462.2	Aliphatic C-H (for CH_2 and CH_3)	1462.7	Aliphatic C-H (for CH_2 and CH_3)
1375.5	Aliphatic C-H (for CH_2 and CH_3)	-	-
-	-	1434.2	CH_3 asymmetric bending (COO-CH_3)
-	-	1196.2	0-CH3 stretching
1159.6	C-O-C symmetric stretching	1168.7	C-O-C symmetric stretching
1092.7	O-CH_2 asymmetric stretching	-	-
720.2	Aliphatic C-H out of plane bending (for CH_2>4)	724.1	Aliphatic C-H out of plane bending (for CH_2>4)

Table S5. 8:*Characteristics and retention times of FAME by GC spectroscopy according to the EN14103:2011 methodology* (McCurry, 2012).

#	Compound		RT (min)
1	Methyl hexanoate	C6:0	6.031
2	Methyl myristate	C14:0	15.878
3	Methyl myristoleate	14:1	16.275
4	Methyl palmitate	C16:1	17.996
5	Methyl palmitoleate	C16:1	17.996
6	Methyl stearate	C18:0	20.332
7	Methyl oleate (1)	C18:1	20.617
8	Methyl oleate (2)	C18:1	20.697
9	Methyl linoleate	C18:2	21.205
10	Methyl linolenate	C18:3	22.052
11	Methyl arachidate	C20:2	22.857
12	Methyl eicosonate	C20:1	24.166
13	Methyl eicosadienoate	C20:2	23.808
14	Methyl arachidonate	C20:4	24.551
15	Methyl eicosatrienoate	C20:3	24.730
16	Methyl behenate and methyl eicosapentanoenoate	C22:0 C20:5	25.582
17	Methyl erucate	C22:1	26.031
18	Methyl lignocerate	C24:0	29.574
19	Methyl noervonate	C24:1	30.203
20	Methyl docosahexaenoate	C22:6	30.365

S.5.6 TiO₂ bandgap

UV-Vis of TiO_2 pure, after use (0 RP), after use and recovery process (1C), after use and recovery five times (5C).

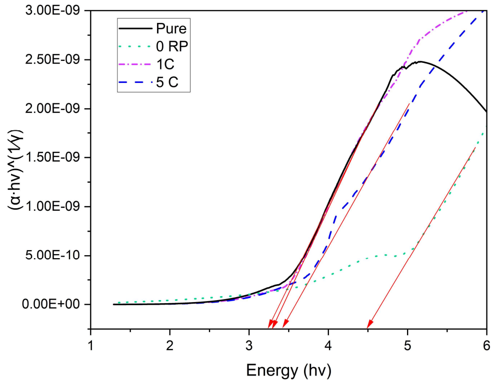

Figure S5. 17. Estimated bandgap of TiO_2 pure, after use (0 RP), after recovery process (1C), and after reuse five times (5C).

S.5.7 Mathematical modelling: L-H kinetic model

The phototransesterification reaction between TGL of canola oil and methanol is described by Equation S5.1.

$$\mathrm{TGL} + 3\,\mathrm{MeOH} \underset{k_{-1}}{\overset{k_1}{\rightleftarrows}} \mathrm{FAME} + \mathrm{GLY}$$ Equation S*5.* 1

For the reaction rate (Equation S5. 2), the following assumptions are made:

- Pseudo-first order for the forward reaction, considering a reversible reaction.
- First-order for the backward reaction.
- Both processes are dependent on the coverage fractions of the catalyst sites occupied by TGL and FAME (Θ_{FAME} and Θ_{TGL}).

$$r = -\frac{d[TGL]}{dt} = k_{-1} \cdot \theta_{FAME} - k_1 \cdot \theta_{TGL}$$ Equation S*5.* 2

Θ_{FAME} and Θ_{TGL} are described by the Langmuir–Hinshelwood mechanism (L–H). This model considers the reactant adsorption on the active catalyst site. It is the most common kinetic model for explaining the heterogeneous catalytic process (Vorontsov et al., 2020) for TGL in the presence of a heterogeneous catalyst. TGL adsorption (forward reaction) and desorption (backward reaction) are described using Equation S5. 3. The model is frequently applied by considering first-order kinetics (Atitar et al., 2018; Ezzati, 2018; Houas et al., 2001; Konstantinou & Albanis, 2003; Tang & Huren An, 1995; Vorontsov et al., 2020) even for the transesterification process using a heterogeneous catalyst (Ahmedzeki & Jendeel, 2013; Ezzati, 2018; Sert & Atalay, 2010).

$$\mathrm{TGL} + \mathrm{Ti} \underset{\mathrm{k}'_{-1}}{\overset{\mathrm{k}'_1}{\rightleftarrows}} \mathrm{TGL\ \ Ti}$$ Equation S5. 3

For the reaction rate, the following assumptions are made:

- Forward reaction (adsorption): first order.
- The TGL concentration is the limiting reactant.
- Reversible reaction.
- Backward reaction (desorption): first order.
- All the active sites on the catalyst surface are the same.

$$\mathrm{r}'_1 = \mathrm{k}'_1 \cdot [TGL] \cdot (1 - \theta_{TGL})$$ Equation S5. 4

$$\mathrm{r}'_{-1} = \mathrm{k}'_{-1} \cdot \theta_{TGL}$$ Equation S*5.* 5

$$\mathrm{k}'_1 \cdot [TGL] \cdot (1 - \theta_{TGL}) = \mathrm{k}'_{-1} \cdot \theta_{TGL}$$ Equation S*5.* 6

At equilibrium, $\mathrm{r}'_1 = \mathrm{r}'_{-1}$

$$\therefore\ \theta_{\mathrm{TGL}} = \frac{\mathrm{k}'_1 \cdot [TGL]}{\mathrm{k}'_{-1} + \mathrm{k}'_1 \cdot [TGL]} = \frac{\mathrm{K}'_1 \cdot [TGL]}{1 + \mathrm{K}'_1 \cdot [TGL]}$$ Equation S*5.* 7

r'_1 = TGL on the Ti adsorption rate

r'_{-1}= TGL on the Ti desorption rate

[TGL] = triglyceride concentration (limiting parameter)

Θ_{TGL} = active site occupied by TGL

A similar mechanism was considered for hydrolysis (Equation S5. 8).

$$\mathrm{FAME} + \mathrm{Ti} \underset{k'_{-2}}{\overset{k'_2}{\rightleftarrows}} \mathrm{FAME\ Ti}$$

Equation S5. 8

$$\therefore\ \theta_{\mathrm{FAME}} = \frac{k'_2 \cdot [\mathrm{FAME}]}{k'_{-2} + k'_2 \cdot [\mathrm{FAME}]} = \frac{K'_2 \cdot [\mathrm{FAME}]}{1 + K'_2 \cdot [\mathrm{FAME}]}$$

Equation S5. 9

Therefore, substituting Equation S5. 8 and Equation S5. 9 into Equation S5.2 gives the Equation S5. 10:

$$-\frac{d[\mathrm{TGL}]}{dt} = k_{-1} \cdot \frac{K'_2 \cdot [\mathrm{FAME}]}{1 + K'_2 \cdot [\mathrm{FAME}]} - k_1 \cdot \frac{K'_1 \cdot [\mathrm{TGL}]}{1 + K'_1 \cdot [\mathrm{TGL}]}$$

Equation S5.10

Considering that $[TGL] = C_{TGL_0} \cdot (1 - x)$, where x(t) is the TGL fraction at time t, Equation S5.10 becomes:

$$-C_{TGL_0} \frac{dx}{dt} = k_{-1} \cdot \frac{K'_2 \cdot C_{TGL_0} \cdot x}{1 + K'_2 \cdot C_{TGL_0} \cdot x} - k_1 \cdot \frac{K'_1 \cdot C_{TGL_0} \cdot (1 - x)}{1 + C_{TGL_0} \cdot (1 - x)}$$

Equation S5.11

$$\therefore\ \frac{dx}{dt} = k_1 \cdot \frac{K'_1 \cdot (1 - x)}{1 + K'_1 \cdot C_{TGL_0} \cdot (1 - x)} - k_{-1} \cdot \frac{K'_2 \cdot x}{1 + K'_2 \cdot x \cdot C_{TGL_0}}$$

Equation S5.12

Considering the contour conditions:

t=0 → x=0;

$t=t_{eq} \rightarrow x=x_{eq}$;

$$\frac{dx}{dt} = 0 \quad \rightarrow \quad x = x_{eq}$$

APPENDIX E

Supplementary information for chapter VI

TiO_2 photocatalysed for biodiesel production from the simultaneous esterification and transesterification of waste cooking oil

S.6.1 Traditional acid catalysis for biodiesel production

Test one (complete conversion): Anhydrous methanol (150 mL), canola oil (15 g), and H_2SO_4 (1.5 g) were added to a round-bottom flask (250 mL), stirred rapidly with a magnetic stirrer at 60°C for five hours, and left to stand for 24 hours at room temperature. The product was purified using the following steps: (1) 600 mL of water was added; (2) the liquid phase was removed by rotary evaporation at 40°C (170 mbar for 60 minutes, 72 mbar for 60 minutes, and 30 mbar for 60 minutes); (3) for three consecutive times, 150 mL of ethyl acetate was added and mixed gently, allowed to settle for one hour in a separatory funnel, and separated; (4) 150 mL of a dilute $NaHCO_3$ solution was added and mixed to separate into two phases; (5) 150 mL of a saturated aqueous NaCl solution was added, mixed, and separated into phases; (6) anhydrous Na_2SO_4 was added to the organic layer and left to stand approximately five minutes; (7) filtered through a syringe filter (Hydraflon 0.22μm, 35 mm); (8) the mixture was rotary evaporated at 40°C to remove any volatiles (170 mbar for 30 minutes, 72 mbar for 30 minutes, and 30 mbar for 60 minutes); (9) the samples were stored in glass vials at room temperature for further characterisation.

Test two (incomplete conversion): the same steps mentioned above were used; however, the reagents were mixed with a magnetic stirrer at 60°C for one hour instead of five hours, and purification was performed immediately.

S.6.2 Photoreactor scheme

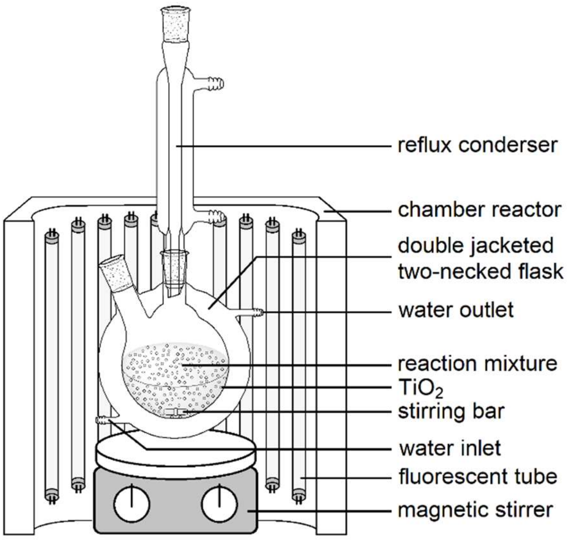

Figure S6. 1. Phototransesterification/photoesterification reactor scheme.

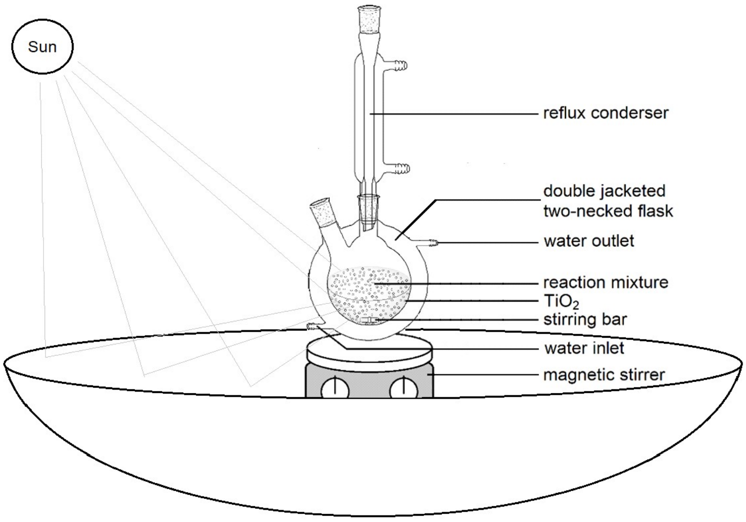

Figure S6. 2. Photoreactor (sunlight irradiation) scheme (Stainless stell, inner diameter of 44 cm, focal length of 16.13 cm).

S.6.3 Photoesterification by sunlight

The sunlight irradiation measurements were obtained and monitored by Arpansa (ARPANSA, 2022) and shown below for the day the test was developed.

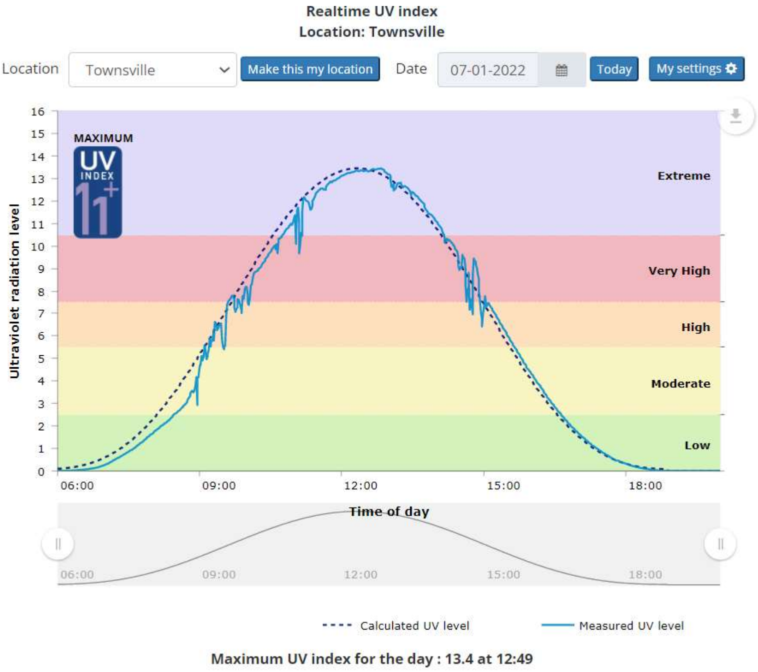

Location: Townsville

Date: 07-01-2022

Maximum UV index for the day : 13.4 at 12:49

Figure S6. 3. UV radiation level on January 06, 2022 in James Cook University, Townsville (Geographic coordinates: -19.325598727686298, 146.75950750865223).

S.6.4 **FTIR analysis**

Table S6. 1: *Characteristic bands of vegetable oil and related fatty acid methyl esters by FTIR-ATR spectroscopy* (Degirmenbasi, Boz, & Kalyon, 2014).

Vegetable oil		**FAME**	
band position (cm^{-1})	**Assignments**	**band position (cm^{-1})**	**assignments**
720.2	Aliphatic C-H out of plane bending (for CH_2>4)	724.1	Aliphatic C-H out of plane bending (for CH_2>4)
1092.7	O-CH_2 asymmetric stretching	-	-
1159.6	C-O-C symmetric stretching	1168.7	C-O-C symmetric stretching
-	-	1196.2	0-CH3 stretching
1375.5	Aliphatic C-H (for CH_2 and CH_3)	-	-
-	-	1434.2	CH_3 asymmetric bending (COO-CH_3)
1462.2	Aliphatic C-H (for CH_2 and CH_3)	1462.7	Aliphatic C-H (for CH_2 and CH_3)
1741.8	C=O stretching (ester)	1738.6	C=O stretching (ester)
2852.9	Aliphatic C-H stretching	2852.9	Aliphatic C-H stretching
2916.5	Aliphatic C-H stretching	2919.7	Aliphatic C-H stretching
3006.5	C=C-H stretching	3011.1	C=C-H stretching

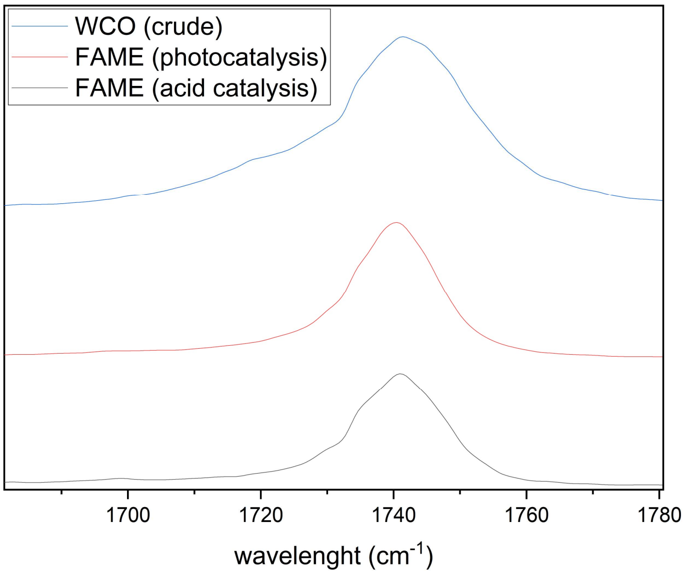

Figure S6. 4. FTIR-ATR of WCO crude, and crude products obtained by its simultaneous esterification and transesterification in presence of methanol using different catalysts: acid and TiO_2 under UVA irradiation (Range: 1800 – 1780 cm^{-1}).

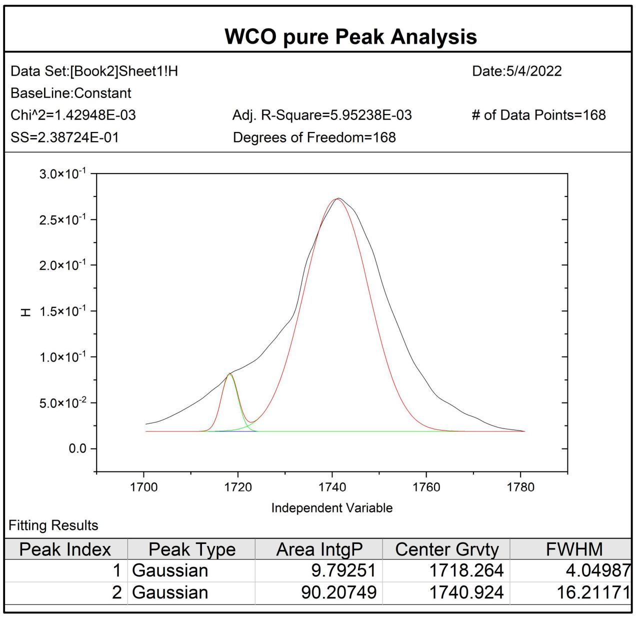

WCO pure Peak Analysis

Data Set:[Book2]Sheet1!H Date:5/4/2022
BaseLine:Constant
Chi^2=1.42948E-03 Adj. R-Square=5.95238E-03 # of Data Points=168
SS=2.38724E-01 Degrees of Freedom=168

Fitting Results

Peak Index	Peak Type	Area IntgP	Center Grvty	FWHM
1	Gaussian	9.79251	1718.264	4.04987
2	Gaussian	90.20749	1740.924	16.21171

Figure S6. 5. FTIR-ATR spectrum of WCO pure. Deconvolution of the peaks in a range between 1700 and 1780 cm^{-1}.

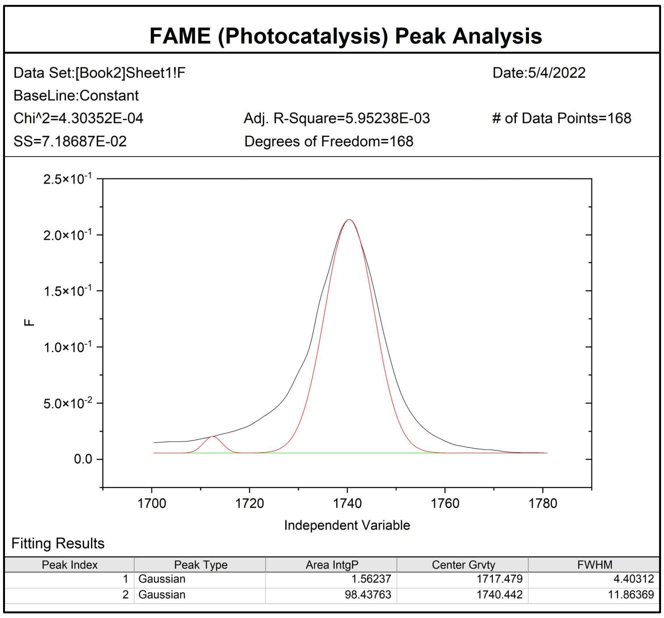

FAME (Photocatalysis) Peak Analysis

Data Set:[Book2]Sheet1!F
Date:5/4/2022
BaseLine:Constant
Chi^2=4.30352E-04
Adj. R-Square=5.95238E-03
# of Data Points=168
SS=7.18687E-02
Degrees of Freedom=168

Fitting Results

Peak Index	Peak Type	Area IntgP	Center Grvty	FWHM
1	Gaussian	1.56237	1717.479	4.40312
2	Gaussian	98.43763	1740.442	11.86369

Figure S6. 6. FTIR-ATR spectrum of biodiesel obtained by photocatalysis. Deconvolution of the peaks in a range between 1700 and 1780 cm^{-1}.

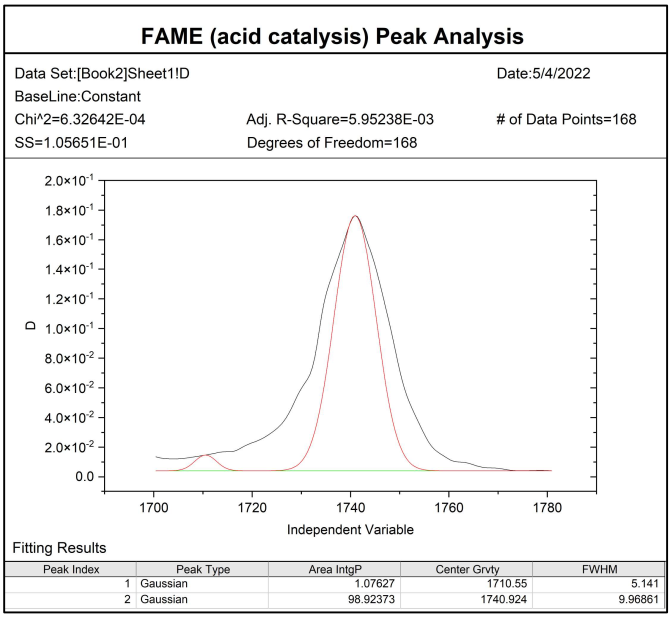

FAME (acid catalysis) Peak Analysis

Data Set:[Book2]Sheet1!D
Date:5/4/2022
BaseLine:Constant
Chi^2=6.32642E-04
Adj. R-Square=5.95238E-03
# of Data Points=168
SS=1.05651E-01
Degrees of Freedom=168

Fitting Results

Peak Index	Peak Type	Area IntgP	Center Grvty	FWHM
1	Gaussian	1.07627	1710.55	5.141
2	Gaussian	98.92373	1740.924	9.96861

Figure S6. 7. FTIR-ATR spectrum of biodiesel obtained by acid catalysis. Deconvolution of the peaks in a range between 1700 and 1780 cm^{-1}.

S.6.5 ^{1}H-NMR

Table S6. 2: *^{1}H-NMR chemical shifts for the main protons of WCO (400 MHz, $CDCl_3$).*

Shift δ (ppm)	Multiplicity	Assignments
0.91 – 0.77	Doublet of Triplet	Terminal CH_3
0.92 - 0.99	Triplet	Terminal CH_3 in Fatty Acid Chain
1.13 - 1.42	Multiplet	CH_2 groups in Fatty Acid Chain
1.47 - 1.69	Unresolved Multiplet	$CH_2CH_2CO_2$ **(5)**
1.86 - 2.13	Multiplet	$CH_2CH_2CH=$
2.21 - 2.39	Triplet	CH_2CO_2 **(4)**
2.65 - 2.88	Multiplet	$CH_2CH=$
4.2	Doublet of Doublet	OCH_2CH **(2 & 3)**
5.24	Triplet of Triplets	CHO **(1)**
5.27 - 5.44	Multiplet	CH=CH

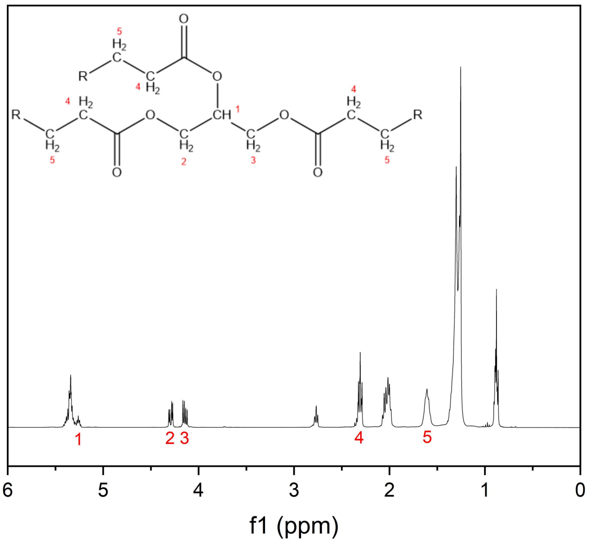

Figure S6. 8. ^{1}H NMR spectrum (400 MHz, $CDCl_3$) of WCO (R = cis-$CH_3(CH_2)_7CH=CH(CH_2)_5$).

Table S6. 3: *^{1}H-NMR chemical shifts for the main protons of FAME from WCO (400 MHz, $CDCl_3$).*

Shift δ (ppm)	**Multiplicity**	**Assignments**
0.85	Triplet of Doublets	Terminal CH_3 in Fatty Acid Chain
0.94	Triplet	Terminal CH_3 in Fatty Acid Chain
1.07 - 1.40	Multiplet	CH_2 in Fatty Acid Chain
1.47 - 1.66	Multiplet	Ester β Carbon **(3)**
1.87 - 2.10	Multiplet	Olefin β Carbon in Fatty Acid Chain
2.26	Triplet	Ester α Carbon **(2)**
2.75	Doublet of Triplets	Olefin α Carbon in Fatty Acid Chain
3.63	Singlet	Methyl Ester **(1)**
5.25 - 5.37	Multiplet	Olefins in Fatty Acid Chain

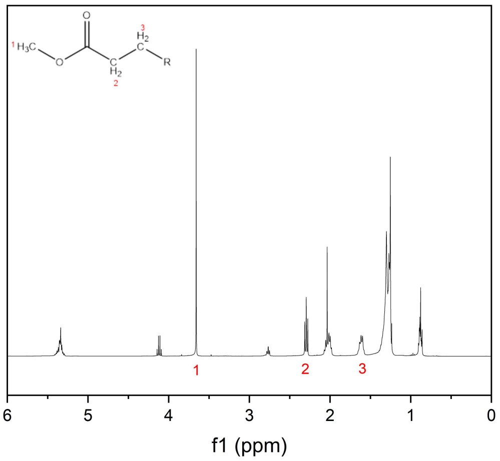

Figure S6. 9. ^{1}H NMR spectrum (400 MHz, $CDCl_3$) of methyl oleate from canola oil (R = cis-$CH_3(CH_2)_7CH{=}CH(CH_2)_5$).

Table S6. 4: *^{1}H-NMR chemical shifts for the main protons of ethyl oleate[a] (400 MHz, $CDCl_3$).*

Shift δ (ppm)	**Multiplicity**	**Assignments**
0.85	Triplet of Doublets	Terminal CH_3 in Fatty Acid Chain
0.94	Triplet	Terminal CH_3 in Fatty Acid Chain
1.07 - 1.40	Multiplet	CH_2 in Fatty Acid Chain
1.47 - 1.66	Multiplet	Ester β Carbon **(3)**
1.87 - 2.10	Multiplet	Olefin β Carbon in Fatty Acid Chain
2.26	Triplet	Ester α Carbon **(2)**
2.75	Doublet of Triplets	Olefin α Carbon in Fatty Acid Chain
3.63	Singlet	Methyl Ester **(1)**
5.25 - 5.37	Multiplet	Olefins in Fatty Acid Chain

Table S6. 5: *^{1}H NMR shift (ppm) for the main protons of FAEE from WCO.*

Shift δ (ppm)	Spin-Spin Splitting	Assignments
5.37 – 5.25	Multiplet	Olefins in Fatty Acid Chain
4.11	Quartet	Residual ethyl acetate
4.15 – 4.10	Quartet	Ethyl Ester **(1,2)**
3.69	Quartet	Residual methanol
3.44	Singlet	Residual ethanol (CH_2)
2.75	Doublet of Triplets	Olefin α Carbon in Fatty Acid Chain
2.61	Singlet	Residual ethanol (OH)
2.26	Triplet	Ester α Carbon **(3)**
2.17	Singlet	Residual Acetone
2.10 – 1.87	Multiplet	Olefin β Carbon in Fatty Acid Chain
1.66 – 1.47	Multiplet	Ester β Carbon **(4)**
1.40 – 1.07	Multiplet	CH_2 in Fatty Acid Chain
1.26	Triplet	Residual ethanol (CH_3)
0.94	Triplet	Terminal CH_3 in Fatty Acid Chain
0.85	Triplet of Doublets	Terminal CH_3 in Fatty Acid Chain

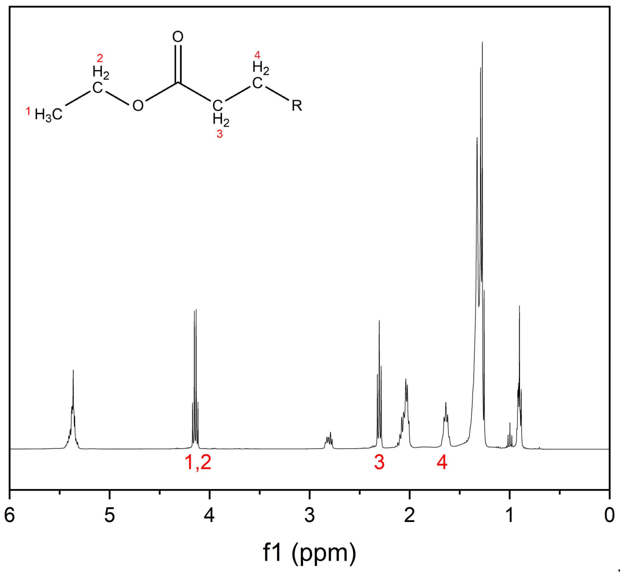

Figure S6. 10. ^{1}H-NMR spectrum (400 MHz, $CDCl_3$) of ethyl oleate from canola oil (R = cis-$CH_3(CH_2)_7CH{=}CH(CH_2)_5$).

FAME (Equation 5. 1) was obtained correlating the methoxy protons (I_{Me}, 3.6 ppm) and oil α-methylene protons ($I_{\alpha CH_2}$, 2.3 ppm) (Borah et al., 2018; Gelbard et al., 1995). The FAEE was obtained similarly (Equation 6. 2), but correlating the FAEE ethoxy protons and glyceride CH_2 sn-

1 and sn-3 ($I_{TGA + EE}$, overlapping peaks at 4.10 – 4.20) and oil α-methylene protons ($I_{\alpha CH2}$, 2.3 ppm) (Jaiswal et al., 2016).

$$\% FAME = 100\% \cdot \frac{2 \cdot I_{ME}}{3 \cdot I_{\alpha CH_2}}$$ Equation S6. 1

$$\% FAEE = 100\% \cdot \frac{I_{TGA+EE} - I_{TGA}}{I_{\alpha CH_2}}$$ Equation S6. 2

Table S6. 6: *Reported ^{1}H-NMR chemical shifts for the main protons of key-intermediaries, diglycerides and monoglycerides of canola oil and methanol transesterification (400 MHz, $CDCl_3$)* (Galvan et al., 2020; Nieva-Echevarría et al., 2015).

Shift δ (ppm)	Spin-Spin Splitting	Assignments
0.88	Triplet	Saturated, monounsaturated ω-9 and/or ω-7 acyl groups and FA
0.89	Triplet	Unsaturated ω-6 acyl groups and FA
0.97	Triplet	Unsaturated ω-3 acyl groups and FA
1.19–1.42	Multiplet	Acyl groups and FA
1.61	Multiplet	Acyl groups in TG, except for DHA, EPA and ARA acyl groups
1.62	Multiplet	Acyl groups in 1,2-DG, except for DHA, EPA and ARA acyl groups
1.63	Multiplet	Acyl groups in 1,3-DG, 1-MG and FA, except for DHA, EPA and ARA acyl groups
1.64	Multiplet	Acyl groups in 2-MG, except for DHA, EPA and ARA acyl groups
1.69	Multiplet	EPA and ARA acyl groups in TG
1.72	Multiplet	EPA and ARA acids
1.92–2.15	Multiplet	Acyl groups and FA, except for –CH2– of DHA acyl group in β-position in relation to the carbonyl group
2.26–2.36	Duplet	Acyl groups in TG, except for DHA acyl groups
2.33	Multiplet	Acyl groups in 1,2-DG, except for DHA acyl groups

Shift δ (ppm)	Spin-Spin Splitting	Assignments
2.35	Triplet	Acyl groups in 1,3-DG, 1-MG and FA, except for DHA acyl groups
2.38	Triplet	Acyl groups in 2-MG, except for DHA acyl groups
2.37–2.41	Multiplet	DHA acyl groups in TG
2.39–2.44	Multiplet	DHA acid
2.77	Triplet	Diunsaturated ω-6 acyl groups and FA
2.77–2.90	Multiplet	Polyunsaturated ω-6 and ω-3 acyl groups and FA
3.65	Triplet of double	Glyceryl group in 1-MG
3.73	Multiplet	Glyceryl group in 1,2-DG
3.84	Multiplet	Glyceryl group in 2-MG
3.94	Multiplet	Glyceryl group in 1-MG
4.05–4.21	Multiplet	Glyceryl group in 1,3-DG
4.18	Triplet of double	Glyceryl group in 1-MG
4.22	Quartet of double	Glyceryl group in TG
4.28	Triplet of double	Glyceryl group in 1,2-DG
4.93	Multiplet	Glyceryl group in 2-MG
5.08	Multiplet	Glyceryl group in 1,2-DG
5.27	Multiplet	Glyceryl group in TG
5.28–5.46	Multiplet	Acyl groups and FA

S.6.6 GC analysis

Table S6. 7: *Retention times of FAME by GC spectroscopy according to the EN14103:2011 methodology* (McCurry, 2012).

#	Compound		RT (min)
1	Methyl hexanoate	C6:0	6.031
2	Methyl myristate	C14:0	15.878
3	Methyl myristoleate	14:1	16.275
4	Methyl palmitate	C16:1	17.996
5	Methyl palmitolate	C16:1	17.996
6	Methyl stearate	C18:0	20.332
7	Methyl oleate (1)	C18:1	20.617
8	Methyl oleate (2)	C18:1	20.697
9	Methyl linoleate	C18:2	21.205
10	Methyl linolenate	C18:3	22.052
11	Methyl arachidate	C20:2	22.857
12	Methyl eicosonate	C20:1	24.166
13	Methyl eicosadienoate	C20:2	23.808
14	Methyl arachidonate	C20:4	24.551
15	Methyl eicosatrienoate	C20:3	24.730
16	Methyl behenate and methyl eicosapentanoenoate	C22:0 C20:5	25.582
17	Methyl erucate	C22:1	26.031
18	Methyl lignocerate	C24:0	29.574
19	Methyl noervonate	C24:1	30.203
20	Methyl docosahexaenoate	C22:6	30.365

S.6.7 FFA content by titration

A 0.05 g organic sample was diluted in 25 mL of a diethyl ether/ethanol solution (2:1) (v/v). Two drops of thymol blue indicator were added and titrated using a 0.02N KOH aqueous standard solution. The acid value (AV, Equation S6. 3) was determined by correlating the volume of the KOH used in the titration (S, mL), used in the blank titration (b, mL), normality of KOH (N), and sample mass (W, g):

$$AV = \frac{(Sb) \cdot N \cdot 56.1}{W}$$ Equation S6. 3

S.6.8 Mathematical modelling: Langmuir- *Hinshelwood mechanism (L–H) mathematical model*

- Pseudo-first order for the forward reaction (transesterification), considering a reversible reaction.
- First-order for the backward reaction (methanolysis).
- Both processes are dependent on the coverage fractions of the catalyst sites occupied by WCO and FAME (Θ_{FAME} and Θ_{WCO}).

$$\mathrm{r} = -\frac{\mathrm{d}[WCO]}{\mathrm{dt}} = \mathrm{k}_{-1} \cdot \theta_{\mathrm{FAME}} - \mathrm{k}_1 \cdot \theta_{WCO}$$ Equation S6. 4

Θ_{FAME} and Θ_{WCO} are described by the L–H mechanism. This model considers the reactant adsorption on the active catalyst site. It is the most common kinetic model to explain the heterogeneous catalytic process (Vorontsov et al., 2020) for WCO in the presence of a heterogeneous catalyst. WCO adsorption (forward reaction) and desorption (backward reaction) are described using Equation S6. 5. The model is applied frequently by considering first-order kinetics (Atitar et al., 2018; Ezzati, 2018; Houas et al., 2001; Konstantinou & Albanis, 2003; Tang & Huren An, 1995; Vorontsov et al., 2020) even for the transesterification process using a heterogeneous catalyst (Ahmedzeki & Jendeel, 2013; Ezzati, 2018; Sert & Atalay, 2010).

$$\mathrm{WCO} + \mathrm{Ti} \underset{\mathrm{k}'_{-1}}{\overset{\mathrm{k}'_1}{\rightleftarrows}} \mathrm{WCO\ \ Ti}$$ Equation S6. 5

For the reaction rate, the following assumptions are made:

- Forward reaction (adsorption): first order.
- The FFA concentration is the limiting reactant.
- Reversible reaction.
- Backward reaction (desorption): first order.
- All of the active sites on the catalyst surface are the same.

$$\mathrm{r}'_1 = \mathrm{k}'_1 \cdot [TGL] \cdot (1 - \theta_{TGL})$$ Equation S6. 6

$$\mathrm{r}'_{-1} = \mathrm{k}'_{-1} \cdot \theta_{TGL}$$ Equation S6. 7

$$\mathrm{k}'_1 \cdot [TGL] \cdot (1 - \theta_{TGL}) = \mathrm{k}'_{-1} \cdot \theta_{TGL}$$ Equation S6. 8

At equilibrium, it is considered that: $\mathrm{r}'_1 = \mathrm{r}'_{-1}$

$$\therefore\ \theta_{\mathrm{FFA}} = \frac{\mathrm{k}'_1 \cdot [TGL]}{\mathrm{k}'_{-1} + \mathrm{k}'_1 \cdot [TGL]} = \frac{\mathrm{K}'_1 \cdot [TGL]}{1 + \mathrm{K}'_1 \cdot [TGL]}$$ Equation S6. 9

r'_1 = WCO on the Ti adsorption rate

r'_{-1}= WCO on the Ti desorption rate

[WCO] = WCO concentration (limiting parameter)

Θ_{WCO} = active site occupied by WCO

A similar mechanism was considered for hydrolysis (Equation S6. 9).

$$\mathrm{FAME} + \mathrm{Ti} \underset{\mathrm{k}'_{-2}}{\overset{\mathrm{k}'_2}{\rightleftarrows}} \mathrm{FAME\ Ti}$$ Equation S6. 10

$$\therefore\ \theta_{\mathrm{FAME}} = \frac{\mathrm{k}'_2 \cdot [\mathrm{FAME}]}{\mathrm{k}'_{-2} + \mathrm{k}'_2 \cdot [\mathrm{FAME}]} = \frac{\mathrm{K}'_2 \cdot [\mathrm{FAME}]}{1 + \mathrm{K}'_2 \cdot [\mathrm{FAME}]}$$ Equation S6. 11

Therefore, substituting Equations S6. 9 and S6. 10 into Equation 2 gives:

$$-\frac{\mathrm{d[WCO]}}{\mathrm{dt}} = \mathrm{k}_{-1} \cdot \frac{\mathrm{K}'_2 \cdot [\mathrm{FAME}]}{1 + \mathrm{K}'_2 \cdot [\mathrm{FAME}]} - \mathrm{k}_1 \cdot \frac{\mathrm{K}'_1 \cdot [WCO]}{1 + \mathrm{K}'_1 \cdot [WCO]}$$ Equation S6. 12

Considering that $[WCO] = \mathrm{C}_{WCO_0} \cdot (1 - \mathrm{x})$, where x(t) is the FFA fraction at time t, Equation S6.11 becomes:

$$-\mathrm{C}_{WCO_0} \frac{\mathrm{dx}}{\mathrm{dt}} = \mathrm{k}_{-1} \cdot \frac{\mathrm{K}'_2 \cdot \mathrm{C}_{WCO_0} \cdot \mathrm{x}}{1 + \mathrm{K}'_2 \cdot \mathrm{C}_{WCO_0} \cdot \mathrm{x}} - \mathrm{k}_1 \cdot \frac{\mathrm{K}'_1 \cdot \mathrm{C}_{WCO_0} \cdot (1 - \mathrm{x})}{1 + \mathrm{C}_{WCO_0} \cdot (1 - \mathrm{x})}$$ Equation S6. 13

$$\therefore\ \frac{\mathrm{dx}}{\mathrm{dt}} = \mathrm{k}_1 \cdot \frac{\mathrm{K}'_1 \cdot (1 - \mathrm{x})}{1 + \mathrm{K}'_1 \cdot \mathrm{C}_{WCO_0} \cdot (1 - \mathrm{x})} - \mathrm{k}_{-1} \cdot \frac{\mathrm{K}'_2 \cdot \mathrm{x}}{1 + \mathrm{K}'_2 \cdot \mathrm{x} \cdot \mathrm{C}_{WCO_0}}$$ Equation S6. 14

Considering the contour conditions:

$t=0 \rightarrow x=0$, $t=t_{eq} \rightarrow x=x_{eq}$;

$$\frac{\mathrm{dx}}{\mathrm{dt}} = 0 \quad \rightarrow \quad \mathrm{x} = \mathrm{x_{eq}}$$

S.6.9 Analysis of mass transfer limitations

Internal mass transfer limitations

The internal mass transfer limitations were evaluated by Weisz–Prater criterion (CWP). The Weisz-Prater criterion (CWP) was determined for the forward and backward reactions to assess the interference of the internal mass transfer resistances. The C_{WP} (Equation S6.15) correlates the respective rate constants, catalyst density (ρc), pellet radius (r_C, 13.78 nm) (R. A. Welter, Santana, de la Torre, Barnes, Taranto, & Oelgemöller, 2022), and effective diffusivity (D_e) (Doran, 1995; Weisz & Prater, 1954). The D_e value was obtained by an estimation considering only triolein as TGL, and methanol (Allain et al., 2016) (D_{AB}) and correlating with the particle porosity (φ) by Equation S6.16. According to Table S6. 8, all values of C_{WP} are lower than 0.3, indicating that the internal mass transfer limitations are insignificant (Doran, 1995; Weisz & Prater, 1954).

$$C_{WP} = \frac{k' \cdot \rho_C {r_c}^2}{D_e} \qquad \text{Equation S6.15}$$

Where:

$$D_e = \varphi^2 \cdot D_{AB} \qquad \text{Equation S6.16}$$

Table S6. 8: *Weisz-Prater criteria (C_{WP}).*

T (K)	$C_{WP, Forward}$	$C_{WP, Backward}$
298.15	3.77E-29	4.94E-21
308.15	1.91E-22	2.02E-21
318.15	1.53E-21	1.46E-21
328.15	7.77E-22	5.74E-22
338.15	9.53E-22	1.60E-22

External mass transfer limitations

The external mass transfer coefficient (k_s) was determined by Calderbank and Moo-Young empirical correlation (Calderbank & Moo-Young, 1961) as described by Equation S6.17. The equation correlate de particle diameter (d_p), diffusion coefficient ($D_{A,mix}$), catalyst density (ρ_P), fluid density (ρ_F), gravity (g), and viscosity (μ).

$$\frac{k_s d_p}{D_{A,mix}} = 2.0 + 0.31\left[\frac{d_p^3(\rho_P - \rho_F)g}{\mu D_{A,mix}}\right]^{1/3} \qquad \text{Equation S6.17}$$

The value obtained was equal 1.24914E+12 cm/s. Indicating that external mass transfer does not limit the reaction. This value is in accordance whit the ones obtained previously by Ballari et al. (Ballari, Brandi, Alfano, & Cassano, 2008). They analysed the external mass transfer coefficient for TiO_2 with different sizes and observed an inverse correlation between d_p and k_s. According to their study reducing the particle size the k_s tends to infinite and the reaction is controlled kinetically. By this value is possible to calculate Ω which corelates the concentration at the reaction medium, and onto the particle surface (Equation S6.18). According to Table S6. 9, small values were obtained indicating the external mass transfer can be negleted.

$$\Omega = \frac{V_\mathrm{P}}{S_\mathrm{x}} \frac{r_\mathrm{A,obs}}{k_\mathrm{S}\, C_\mathrm{Ab}}$$ Equation S6.17

Table S6. 9: *Coeffiient Ω for the forward and backward reactions.*

T (K)	$\Omega_{\mathrm{Forward}}$	$\Omega_{\mathrm{Backward}}$
298.15	3.61E-30	4.73E-22
308.15	1.83E-23	1.93E-22
318.15	1.46E-22	1.40E-22
328.15	7.43E-23	5.49E-23
338.15	9.12E-23	1.53E-23